



# Reactive transport of dichloromethane and micropollutants in laboratory aquifers

Maria de Lourdes Prieto-Espinoza

## ► To cite this version:

Maria de Lourdes Prieto-Espinoza. Reactive transport of dichloromethane and micropollutants in laboratory aquifers. Earth Sciences. Université de Strasbourg, 2022. English. NNT : 2022STRAH005 . tel-03888162

**HAL Id: tel-03888162**

**<https://theses.hal.science/tel-03888162>**

Submitted on 7 Dec 2022

**HAL** is a multi-disciplinary open access archive for the deposit and dissemination of scientific research documents, whether they are published or not. The documents may come from teaching and research institutions in France or abroad, or from public or private research centers.

L'archive ouverte pluridisciplinaire **HAL**, est destinée au dépôt et à la diffusion de documents scientifiques de niveau recherche, publiés ou non, émanant des établissements d'enseignement et de recherche français ou étrangers, des laboratoires publics ou privés.

**ÉCOLE DOCTORALE des Sciences de la Terre et de l'Environnement (ED 413)**

**Institut Terre et Environnement de Strasbourg (ITES)**

**UMR 7063 / Unistra, CNRS, ENGEEES**

# THÈSE présentée par :

**Maria de Lourdes PRIETO ESPINOZA**

soutenue le : **29 Avril 2022**

pour obtenir le grade de : **Docteur de l'Université de Strasbourg**

Discipline/ Spécialité : Hydrologie

**Reactive transport of dichloromethane and  
micropollutants in laboratory aquifers**

**THÈSE dirigée par :**

**M. Imfeld Gwenaël  
M. Weill Sylvain**

Directeur de recherche, CNRS, Université de Strasbourg, France  
Chargée de Recherche, HDR, ENGEEES, Université de Strasbourg, France

**RAPPORTEURS :**

**M. Hunkeler Daniel  
Mme. Passeport Elodie**

Professeur, Université Neuchâtel, Suisse  
Professeure, Université de Toronto, Canada

**AUTRES MEMBRES DU JURY :**

**M. Höhener Patrick  
Mme. Muller Emilie**

Professeur, Université d'Aix-Marseille, France  
Chargée de Recherche, HDR, GMGM, Université de Strasbourg, France

---





**"Groundwater: Making the invisible visible"**

*This is the theme of the World Water Day 2022 proposed by the UN-Water. It is certainly delightful to present this PhD thesis in the context of groundwater protection against anthropogenic contamination.*



## Acknowledgements

This research was funded by the EC2CO-BIOHEFECT program (CNRS-INSU), the École Nationale du Génie de l'Eau et de l'Environnement de Strasbourg (ENGEE, France) and the doctoral school Earth and Environmental Sciences (ED 413) of the University of Strasbourg. I am grateful to all the people involved for supporting this research project. I would like to also thank the jury members for accepting evaluating this PhD thesis: Patrick Höhener, Daniel Hunkeler, Emilie Muller and Elodie Passeport.

I would like to express my gratitude to my PhD advisors Gwenaël Imfeld and Sylvain Weill. Thank you for believing in me and for your support throughout the last three years. I appreciated your time for the scientific questions and discussions, and for providing all the tools to carry out this thesis. I have learnt so much from you, from a personal and professional level. I am grateful with Benjamin Belfort and François Lehmann from the TrHyCOs group for the planning and mounting of the laboratory aquifers, for your expertise in operating and monitoring the experiments, for our discussions and for providing me access to your laboratory. My great gratitude goes to Raphaël di Chiara who I admire for his expertise in numerical modeling, and for learning so much throughout our numerous discussions.

My gratitude also goes to Stéphane Vuilleumier for granting me access to the GMGM laboratory for hydrochemical measurements, and for the always pleasant discussions with you. I also thank Carmen Lázaro Sanchez for helping in DNA sampling and extractions from DCM contaminated groundwater. I want to also acknowledge Jérémy Masbou for the development of Cl-isotope analysis of DCM, for the fruitful discussions and for your analytical assistance throughout the PhD. I thank to all the members of the BISE group, who warmly welcomed me all these years. Particularly, Sylvain Payraudeau, Benoît Guyot, Eric Pernin, Sophie Glangloff and Colin Fournet for your assistance in the laboratory. I want to also thank those colleagues who I had fruitful discussions with: Adrian Borreca, Guillaume Drouin, Boris Droz, Tetyana Gylevska, Felix Kögler, Tobias Junginger, Paula Perez, Roch Sungthong and Lou Weidenfeld. I also acknowledge the intern students who participated in this thesis project.

My warm thoughts and gratitude goes to my dear friends who kept the mood positive and the

---

motivation up, and with whom lots of fun moments were shared. Tobias, my dear officemate, I thank you for cheering me up around the office with your homemade muffins, my chocolate bars, the daily music and cheerful notes. My cheerful lab friends: Sara, Tetyana, Mouna, Felix, Adrian, Daniel, Patricia, Paula, Jessica, Jordi, Lou, Oscar, David and many more. Thanks for the endless coffees at work and soirées.

I want to thank my little family of expatriates who supported me the most. Your friendship was a big source of companionship during this time: Daniel, Gilberto, Carmen and Pierre-Oliver. So many laughs and so much love shared that made things smoother between PhD stories, lock-downs and curfews! Especially PO, thank you for your great patience in listening to me and reminding me of what matters most. *Recuerden; subir y bajar, la montaña, nos abrazamos.* Y para aquellos que no importando en donde esté, su apoyo y amor lo siento incondicional. Gracias familia Prieto-Espinoza: mamá, papá, hermano. Gracias por soportarme tanto, y por creer en mí. Se los digo cada domingo, pero como no hay tantas oportunidades para escribirlo públicamente, entonces les digo: los amo por siempre.

## Abstract

Groundwater quality is of increasing concern due to the ubiquitous release of many substances in subsurface environments. Although biodegradation is a major process for the removal of organic contaminants in aquifers, the interplay of dynamic hydrogeochemical conditions, bacterial diversity and contaminant dissipation is yet poorly understood. An integrative approach is required to understand the reactive transport and factors affecting the degradation of both industrial contaminants and micropollutants. In this study, we examined the reactive transport of dichloromethane (DCM) and a micropollutant mixture in two laboratory aquifers under near-natural settings. An integrative approach was used to examine reactive transport processes, including high-resolution hydrochemical monitoring, compound-specific isotope analysis of multiple elements (ME-CSIA), biomolecular markers (16S rRNA gene sequencing) and numerical modeling. First, degradation of DCM – a volatile and toxic industrial solvent frequently detected in multi-contaminated aquifers – was examined in laboratory aquifers fed with anoxic contaminated groundwater under steady-state and transient (i.e., water table fluctuating) conditions. DCM degradation was more pronounced under water table fluctuations (95%) compared to steady-state conditions (42%). Based on C and Cl isotope composition, two distinct DCM degradation pathways were observed under the two flow regimes, correlating with the increase of potentially associated DCM degraders (*Peptococcaceae* family). Second, a multi-phase reactive transport model was developed to predict DCM dissipation, accounting for water table fluctuations and the associated transport processes. Four distinct bacterial populations potentially involved in distinct DCM degradation pathways were implemented following Michaelis-Menten kinetics and pathway-specific reaction rates associated with distinct isotope fractionation. Additionally, DOC was considered as a carbon source for non-DCM degraders further serving as supplier of CO<sub>2</sub> for DCM fermentative pathways. Model results highlighted complex relationships among bacterial populations and dynamic hydrochemical conditions, and underscored concomitant DCM degradation across the fluctuation zone. Third, the dissipation of a micropollutant mixture (i.e., atrazine, terbutryn, S-metolachlor, metalaxyl, metformin and caffeine) was examined in laboratory aquifers mimicking stream-groundwater interactions to an

---

adjacent shallow aquifer under steady-state conditions and varying (short- and long-term) exposure periods. Biodegradation capacity of the laboratory aquifers was mainly demonstrated for caffeine (up to 90%) and metformin (14%), while the persistence of the remaining micropollutant mixture suggested risks to long-term groundwater contamination. Varying micropollutant exposures over time revealed changes in bacterial community composition, indicating the selective pressure of micropollutants. Results from a conceptual model further evidenced substrate concentration dependence on micropollutant biodegradation. Overall, this study demonstrated that dynamic environmental conditions may exert a powerful control on pollutants biodegradation. In the future, integrative approaches accounting for dynamic hydrogeological and biogeochemical conditions may improve the assessment of natural attenuation of organic pollutants in groundwater.

**Keywords:** groundwater contamination, hydrogeochemical dynamics, ME-CSIA, bacterial dynamics, numerical modeling

## Résumé en Français

La qualité des eaux souterraines est un sujet sociétal de première importance en raison de la libération constante de nombreuses substances dans les milieux souterrains. Les aquifères du monde entier sont vulnérables aux applications extensives de produits chimiques naturels et synthétiques qui peuvent être persistants et toxiques pour la vie aquatique et la santé humaine. Les principaux contaminants des eaux souterraines sont les polluants organiques, qui sont couramment utilisés dans des contextes agricoles, urbains et/ou industriels. Cette classe de polluants comprend notamment (i) les contaminants industriels historiques tels que les composés organiques volatils chlorés (COV-CL), et (ii) les contaminants émergents, tels que les pesticides et les produits pharmaceutiques. L'identification de leurs sources potentielles et la compréhension des mécanismes de transport réactif de ces molécules sont donc essentielles pour prédire correctement le devenir des contaminants les aquifères et définir des stratégies de remédiation.

L'atténuation des concentrations de polluants organiques dans le milieu souterrain résulte de plusieurs processus de transformation abiotiques et/ou biotiques impliquant des réactions chimiques et/ou biologiques. Les processus de dégradation reflètent la véritable élimination des contaminants, par opposition aux processus physiques tels que la dispersion, la sorption ou la volatilisation qui ne causent pas de dégradation à proprement parlé. En plus des méthodes conventionnelles – comme la quantification des concentrations de contaminants et des produits de transformation – l'analyse isotopique composé spécifique (CSIA) s'est avérée être un outil efficace pour l'étude de ces processus. La CSIA repose sur les changements dans les rapports d'isotopes stables d'un contaminant subissant une réaction de dégradation. La CSIA peut aider à (i) évaluer l'étendue des processus de dégradation in situ, (ii) identifier les sources de contaminants, (iii) prouver l'occurrence de la dégradation indépendamment des processus non destructifs, et (iv) distinguer les voies et mécanismes de dégradation abiotiques et biotiques sous-jacents. De plus, la combinaison d'approches biomoléculaires (par exemple, le séquençage Illumina) et de la CSIA s'est avérée avantageuse pour évaluer la biodégradation des polluants, fournissant une preuve plus fiable de l'étendue et des voies de biodégradation des polluants sur les sites contaminés.



---

Bien que la biodégradation soit largement reconnue comme le principal processus d'élimination des polluants organiques dans les aquifères, les interactions entre les conditions hydrogéochimiques, la diversité microbienne et la dissipation des contaminants dans les aquifères sont encore mal comprises. En effet, le transport réactif des contaminants dans les milieux poreux implique des interactions complexes entre plusieurs processus relatifs au flux d'eau et de gaz, au transport d'éléments, aux réactions chimiques et aux activités microbiennes. Ces processus ont lieu dans des systèmes dynamiques, où les conditions hydrogéologiques et biogéochimiques peuvent évoluer rapidement. Cela peut notamment être le cas quand des fluctuations de la nappe phréatique et/ou des échanges avec les eaux de surface se produisent. L'impact des conditions dynamiques n'est souvent pas bien pris en compte lors de l'interprétation du devenir et du transport des contaminants dans les aquifères. Le développement et l'application de modèles de transport réactif (MTRs) représentent une opportunité unique pour mieux comprendre les processus physiques et chimiques gouvernant le transport et le devenir des polluants organiques dans les eaux souterraines. Les MTRs peuvent inclure dans les formalismes mathématiques les interactions complexes des processus physiques et chimiques et leurs dynamiques. À ce jour, peu d'études se sont concentrées sur l'étude de l'impact de l'évolution spatio-temporelle des conditions environnementales sur la biodégradation des polluants, qui nécessite une approche intégrative. En raison de la complexité des conditions de terrain, la mise en place d'expériences dans des aquifères de laboratoire semble pertinente car elle permet d'approcher la dégradation in situ des polluants organiques dans les eaux souterraines et facilite les calculs de bilan de masse dans des systèmes raisonnablement contrôlés.

Dans ce contexte, cette thèse vise à améliorer la compréhension de l'impact des conditions environnementales dynamiques sur l'atténuation naturelle des polluants organiques dans les aquifères. Une approche intégrative comprenant des mesures de concentration, des analyses hydrochimiques, des approches biomoléculaires, des analyses isotopiques spécifiques (CSIA) et de la modélisation du transport réactif a été utilisée pour étudier le transport réactif de deux classes de polluants organiques : i) le dichlorométhane (DCM), molécule cible pour les contaminants industriels chlorés historiques, et ii) un mélange de micropolluants représentatif que l'on peut retrouver en condition réelle après une contamination diffuse provenant d'application saisonnière de pesticides et/ou à la suite de rejets de station de traitement des eaux usées. Les résultats et les perspectives de ce projet de thèse peuvent répondre aux questions de recherche suivantes :

## I. Comment les conditions hydrogéochimiques évoluent-elles dans les aquifères soumis à des

---

conditions dynamiques (par exemple, les fluctuations de la nappe phréatique) ?

- II. Quel est le rôle des zones de transition dynamiques dans les aquifères (par exemple, la frange capillaire et la zone hyporhéique) sur la biodégradation du DCM et des micropolluants ?
- III. Quelle est la relation entre la diversité et la composition des communautés bactériennes, la biodégradation du DCM et des micropolluants dans des conditions hydrogéochimiques dynamiques ?
- IV. Comment les taux et les voies de dissipation du DCM et des micropolluants varient-ils avec la dynamique hydrogéochimique et microbienne ?
- V. Quels sont les schémas réactionnels les plus pertinents (simples, fiables et mécanistes) pour évaluer le transport réactif et la dissipation (i) des contaminants chlorés historiques et (ii) des micropolluants dans les aquifères ?
- VI. La dissipation de ces polluants peut-elle être prédite de manière fiable par des MTRs pour in fine estimer le potentiel de remédiation d'un aquifère pollué ?

Afin de répondre à ces questions, ce projet de thèse repose sur le couplage de travaux expérimentaux et de modélisation pour améliorer la compréhension des processus d'atténuation naturels contrôlant la dégradation des polluants dans des aquifères de laboratoire en milieu quasi-naturel, et soumis à des conditions dynamiques.

Tout d'abord, l'effet des fluctuations de la nappe phréatique sur le DCM – un solvant industriel volatil et toxique fréquemment détecté dans les aquifères multi-contaminés – est présenté au **Chapitre 3**. Le DCM peut être dégradé de manière biotique ou abiotique, et dans des conditions oxiqes et anoxiques. L'étendue et les voies de dégradation du DCM dans les aquifères peuvent donc dépendre des fluctuations de la nappe phréatique et des réponses microbiennes aux variations hydrochimiques. Ceci est dû au fait que les fluctuations de la nappe phréatique peuvent avoir un impact sur le transfert de gaz (par exemple, O<sub>2</sub>), et l'évolution des conditions redox et des microorganismes de subsurface exposés à la redistribution des accepteurs d'électrons (par exemple, O<sub>2</sub>) et des donneurs (par exemple, la matière organique, y compris les contaminants). L'effet des fluctuations de la nappe phréatique sur la biodégradation du DCM a été examiné dans deux aquifères de laboratoire alimentés par de l'eau souterraine chargée en DCM, appauvrie en O<sub>2</sub> et provenant d'un ancien site industriel bien caractérisé. L'hydrochimie, les isotopes stables du DCM ( $\delta^{13}\text{C}$  et  $\delta^{37}\text{Cl}$ ), et la composition de la communauté bactérienne

---

ont été examinés pour déterminer l'élimination de la masse de DCM et les voies de dégradation dans des conditions stables (nappe phréatique statique) et transitoires (nappe phréatique fluctuante). Les résultats du Chapitre 3 ont démontrés une biodégradation accrue du DCM pendant les fluctuations de la nappe phréatique. L'élimination de la masse de DCM était plus prononcée dans des conditions transitoires (95 %) que dans des conditions stables (42 %). L'utilisation de la CSIA multi-éléments (c'est-à-dire  $^{13}\text{C}/^{12}\text{C}$  et  $^{37}\text{Cl}/^{35}\text{Cl}$ ) a permis de mettre en évidence une dégradation plus importante du DCM dans les conditions transitoires et d'identifier des voies de dégradation anaérobie du DCM différentes entre les conditions statique et dynamique. Cela correspond aux conditions réductrices dominantes et à l'identification de bactéries potentiellement anaérobies dégradant le DCM, telles que *Desulfosporosinus* (famille des *Peptococcaceae*), dont l'abondance est plus élevée dans les conditions transitoires au niveau de la zone capillaire. De plus, la co-occurrence fréquente de ces anaérobies dans les aquifères contaminés indique la possibilité de réseaux bactériens inter-espèces complexes et la dégradation concomitante du DCM sur les sites contaminés.

Pour approfondir l'étude de l'effet des fluctuations de la nappe phréatique sur la biodégradation du DCM, un modèle de transport réactif multiphase (MTR) est présenté au **Chapitre 4**. Ce modèle vise à améliorer la compréhension des principaux facteurs de biodégradation du DCM par les bactéries anaérobies pendant les fluctuations de la nappe phréatique, en particulier au niveau de la zone capillaire où l'oxygène reste disponible. Le modèle MTR multiphasique a été développé pour inclure la C-Cl CSIA (i.e.,  $\delta^{13}\text{C}$  et  $\delta^{37}\text{Cl}$ ) et les processus biologiques, tels que la croissance, la désintégration, l'attachement, le détachement ou la dormance et pour relier les changements des conditions redox avec les populations dégradant le DCM. Le modèle d'écoulement à deux phases (c'est-à-dire l'eau et le gaz) tient compte de la volatilisation et des processus de transport associés du DCM. Un formalisme mathématique est ainsi présenté sur la base de la dégradation concomitante du DCM selon quatre taux de réaction distincts. Quatre populations microbiennes distinctes sont potentiellement impliquées dans différentes voies de dégradation du DCM sont représentées en utilisant une cinétique de Michaelis-Menten et des taux de réaction spécifiques aux voies associées à un fractionnement isotopique distinct. Le carbone organique dissous (COD) a été considéré comme une source de carbone pour les organismes ne dégradant pas le DCM et servant de fournisseur de  $\text{CO}_2$  pour les voies de fermentation du DCM. Des simulations sur la dégradation concomitante du DCM par deux anaérobies connus du DCM ont montrées que les fluctuations de la nappe phréatique entraînent une biodégradation plus importante du DCM et sont corrélées aux flux de  $\text{CO}_2$  à travers la zone capillaire. Globale-

---

ment, les résultats du modèle ont montrés une augmentation de la dégradation du DCM dans des conditions fluctuantes, ce qui coïncide avec les résultats du Chapitre 3. Cela met en évidence les interactions dynamiques entre les populations bactériennes et les conditions hydrochimiques. Enfin, bien que le formalisme présenté soit dédié au DCM, une formulation générique peut être obtenue à partir de ce modèle, permettant son extension à d'autres composés chlorés (i.e., Cl-VOCs) dans le but de représenter la biodégradation concomitante des contaminants dans des conditions dynamiques dans les systèmes hydrogéologiques.

Alors qu'une preuve directe de la biodégradation du DCM dans des conditions transitoires a été fournie dans les chapitres 3 et 4, cette approche intégrative a été étendue à la biodégradation des micropolluants décrite dans le **Chapitre 5**. La dissipation d'un mélange de micropolluants (i.e., atrazine, terbutryn, S-métolachlore, métalaxyl, metformine et caféine) a été étudiée dans des aquifères de laboratoire dans des conditions mimant des interactions entre un cours d'eau et les eaux souterraines adjacentes, dans des conditions stables et des périodes d'exposition variables (à court et à long terme). Les changements dans la diversité bactérienne ont été évalués dans les deux systèmes aquifères pendant les phase de variation d'exposition et dans des conditions hydrologiques statiques. L'hypothèse est que ces variations d'exposition peuvent induire des changements bactériens et ainsi modifier les voies de transformation des micropolluants. Trois périodes d'injections de micropolluants pendant 140 jours ont donc été définies comme suit : (i) une première injection en pulse (environ 25  $\mu\text{M}$ ) pour identifier les processus de dissipation et l'adaptation bactérienne aux micropolluants, (ii) une injection constante (2 volumes de pores) à des concentrations 10 fois plus faibles (phase d'exposition chronique), et (iii) une seconde injection en pulse (25  $\mu\text{M}$ ) pour examiner si la transformation des micropolluants était accrue. L'atrazine, le terbutryn, le S-métolachlore et le métalaxyl ont persisté (dissipation <10%) dans les deux aquifères au cours de toutes les périodes, tandis que la dissipation du metformin (jusqu'à 14%) n'a été observée que de 90 à 140 jours, ce qui suggère une dégradation accrue au fil du temps. En revanche, la caféine a été dissipée (>90%) lors de toutes les périodes d'injection, ce qui concorde avec les taux de dégradation rapides ( $t_{1/2} < 3$  j) identifiés dans les expériences en microcosmes, réalisées en parallèle et la détection des produits de transformation (théobromine et xanthine). Un fractionnement significatif des isotopes stables du carbone ( $\Delta\delta^{13}\text{C} \geq 6,6$  ‰) a été observé pour la caféine dans les deux aquifères, alors qu'aucun enrichissement en  $^{15}\text{N}$  n'a eu lieu. Une dépendance à la concentration de la biotransformation de la caféine a en outre été suggérée par des simulations de modèles 1-D suivant la cinétique de Michaelis-Menten. La diversité bactérienne a augmentée avec le temps, ce qui

---

suggère une adaptation bactérienne à long terme aux expositions des micropolluants. Dans l'ensemble, ces résultats mettent en évidence la variabilité de la dégradation des micropolluants dans les aquifères soumis à un mélange de micropolluants, et soulignent l'intérêt d'une approche intégrée pour comprendre l'interaction entre l'hydrochimie de subsurface, les adaptations bactériennes et la biotransformation des micropolluants au cours des interactions entre les cours d'eau et les eaux souterraines.

En conclusion, le **chapitre 6** fournit une perspective générale sur les défis et les implications des approches intégratives pour évaluer l'atténuation naturelle des contaminants historiques (c'est-à-dire le DCM) et émergents (c'est-à-dire les micropolluants) dans les aquifères pollués. Ces approches comprennent (i) l'utilisation de ME-CSIA pour caractériser les différentes classes de polluants dans les aquifères, (ii) la mise en place d'approches biomoléculaires pour combler le fossé concernant la dynamique bactérienne dans les aquifères pollués, et (iii) des MTRs adaptés pour prédire le comportement des polluants dans les aquifères soumis à des conditions dynamiques. En outre, une discussion des principaux résultats concernant l'utilisation d'approches intégratives pour élucider le rôle des conditions biogéochimiques et hydrogéologiques dynamiques sur l'atténuation naturelle des polluants organiques dans les systèmes d'eaux souterraines est fournie. Enfin, les perspectives à court et à long terme de ce projet de thèse sont discutées.

## Contents

Abstract . . . . .	vii
List of Figures . . . . .	xxv
List of Tables . . . . .	xxviii
<b>1 General Introduction</b>	<b>1</b>
1.1 Human and ecological values of groundwater protection . . . . .	2
1.2 Origin and fate of legacy and emerging contaminants of groundwater . . . . .	3
1.2.1 Chlorinated volatile organic compounds (Cl-VOCs) . . . . .	4
1.2.2 Pesticides, pharmaceuticals and consumer products . . . . .	9
1.3 Dissipation processes driving reactive transport of contaminants in groundwater .	12
1.4 Dissipation processes in highly dynamic transition zones of aquifers . . . . .	14
1.4.1 The role of the capillary fringe in anoxic aquifers . . . . .	14
1.4.2 The role of the hyporheic zone in shallow aquifers . . . . .	15
1.5 Biodegradation: a key removal process of organic pollutants in contaminated aquifers . . . . .	16
1.5.1 Redox controlled biodegradation . . . . .	16
1.5.2 Bacterial dynamics during pollutants degradation . . . . .	18
1.5.3 Bacterial growth and related degradation kinetics . . . . .	19
1.5.4 Biomolecular markers for assessing pollutant biodegradation . . . . .	20
1.6 Assessment of organic pollutant degradation using compound-specific isotope analysis (CSIA) . . . . .	22
1.7 Reactive transport models to assist monitoring of in situ natural attenuation of organic pollutants . . . . .	28
1.8 Toward integrative approaches for comprehensive restoration of groundwater resources . . . . .	30
References . . . . .	32

<b>2</b>	<b>Aims and general approach</b>	<b>49</b>
2.1	Thesis aim and research questions . . . . .	50
2.2	General approach . . . . .	51
2.3	General methodology . . . . .	52
<b>3</b>	<b>Water table fluctuations affect dichloromethane biodegradation in laboratory aquifers contaminated with organohalides</b>	<b>57</b>
3.1	Introduction . . . . .	59
3.2	Materials and methods . . . . .	60
3.2.1	Chemicals . . . . .	60
3.2.2	Groundwater collection . . . . .	61
3.2.3	Laboratory aquifers operations . . . . .	61
3.2.4	Sampling . . . . .	63
3.2.5	Analytical methods . . . . .	63
3.2.5.1	Hydrochemistry . . . . .	63
3.2.5.2	VOCs concentrations and DCM C-Cl CSIA analysis . . . . .	64
3.2.5.3	DNA extraction from pore water and sand samples . . . . .	65
3.2.5.4	DNA sequencing . . . . .	65
3.2.6	Data analysis . . . . .	65
3.2.6.1	Evolution of isotopic data . . . . .	65
3.2.6.2	Bacterial community composition . . . . .	66
3.3	Results and discussion . . . . .	66
3.3.1	Water table fluctuations affect hydrochemical conditions . . . . .	66
3.3.2	Water table fluctuations affect DCM mass dissipation and C and Cl isotope fractionation . . . . .	67
3.3.3	DCM transformation pathways under transient and steady-state conditions	70
3.3.4	Water table fluctuations affect bacterial community composition and distribution of DCM-associated taxa . . . . .	72
3.4	Conclusions . . . . .	75
	References . . . . .	75
<b>4</b>	<b>Numerical simulations of dual carbon-chlorine isotope fractionation of pathway-specific dichloromethane biodegradation reactions</b>	<b>83</b>
4.1	Introduction . . . . .	85

4.2	Governing equations . . . . .	87
4.2.1	Assumptions . . . . .	87
4.2.2	Mass-momentum conservation equations for two-phase flow . . . . .	88
4.2.3	Mass balance equations for transport and mass exchange processes . . . . .	89
4.2.4	Mass transfer in porous media of soluble and gaseous species . . . . .	90
4.2.5	Pathway-specific reaction rates and isotope fractionation of DCM . . . . .	91
4.2.6	Stoichiometry of pathway-specific degradation reactions of DCM . . . . .	93
4.2.7	Modeling attachment processes in porous media . . . . .	96
4.2.8	Modeling microbial growth kinetics . . . . .	97
4.2.9	Coupled mass balance equations . . . . .	99
4.3	Modeling approach . . . . .	100
4.3.1	Previous implementations of the CubicM model . . . . .	100
4.3.2	CubicM model accounting for concomitant DCM biodegradation under dynamic conditions . . . . .	100
4.3.3	Evaluation strategy . . . . .	101
4.3.4	Simulations of incompressible two-phase transport (water/gas) and biodegradation of DCM in dynamic conditions . . . . .	102
4.4	Results and discussion . . . . .	105
4.4.1	Multi-phase flow across the capillary fringe . . . . .	105
4.4.2	Dynamics of individual bacterial populations under steady-state conditions	107
4.4.3	Concomitant DCM degradation under steady-state conditions . . . . .	110
4.4.4	Evidencing the role of water table fluctuations to enhance DCM degradation	113
4.5	Model limitations and future applications . . . . .	117
	References . . . . .	118
<b>5</b>	<b>Reactive transport of a micropollutant mixture in laboratory aquifers explored by CSIA, conceptual modeling and biomolecular markers</b>	<b>127</b>
5.1	Introduction . . . . .	129
5.2	Materials and methods . . . . .	131
5.2.1	Stream water collection . . . . .	131
5.2.2	Micropollutant mixture . . . . .	131
5.2.3	Degradation kinetics experiment . . . . .	132
5.2.4	Experimental setup and operation of laboratory aquifers . . . . .	133
5.2.5	Sampling procedure . . . . .	134



5.2.6	Analytical methods . . . . .	135
5.2.6.1	Hydrochemistry . . . . .	135
5.2.6.2	Micropollutants extraction and quantification . . . . .	135
5.2.6.3	Compound-specific isotope analysis . . . . .	135
5.2.6.4	DNA extraction and sequencing . . . . .	136
5.2.7	Conceptual modeling . . . . .	137
5.3	Results and discussion . . . . .	138
5.3.1	Kinetics of micropollutants biotransformation in stream water . . . . .	138
5.3.2	Micropollutants biotransformation in flow-through laboratory aquifers . .	140
5.3.3	C and N isotope fractionation of micropollutants . . . . .	143
5.3.4	Gradual bacterial adaptations during transient exposures of a micropollu- tant mixture . . . . .	145
5.4	Conclusions . . . . .	147
	References . . . . .	148
<b>6</b>	<b>General conclusions and perspectives</b>	<b>155</b>
6.1	Natural attenuation of DCM and micropollutants in laboratory aquifers under dynamic conditions . . . . .	157
6.1.1	Water table fluctuations affect DCM degradation . . . . .	158
6.1.2	Varying micropollutant exposures during stream-groundwater interactions	161
6.2	Integrative approaches to improve natural attenuation of organic contaminants in groundwater . . . . .	163
6.3	Toward improved reactive transport models to predict <i>in situ</i> natural attenuation at contaminated sites . . . . .	166
6.4	Implications and perspectives . . . . .	169
	References . . . . .	171
	<b>Appendices</b>	<b>177</b>
<b>A</b>	<b>Supporting information of Chapter 3</b>	<b>177</b>
A.1	Grounwater collection . . . . .	178
A.2	Quantification of VOCs . . . . .	178
A.3	Compound Specific Isotope Analysis (CSIA) of VOCs . . . . .	178
A.3.1	Cl-CSIA analysis of DCM . . . . .	178
A.3.2	C-CSIA analysis of DCM, cis-DCE and VC . . . . .	180

A.4	Oxygen evolution under transient and steady-state conditions . . . . .	182
A.5	Hydrochemical evolution . . . . .	184
A.6	Concentrations and carbon isotope composition of cis-DCE and VC . . . . .	187
A.7	Rayleigh plots of DCM degradation under transient and steady-state conditions .	188
A.8	State of the art of proposed DCM pathways and stoichiometry reactions based on stable isotope analysis . . . . .	189
A.9	Rarefaction curves for pore water and sand OTUs and bacterial diversity . . . . .	190
A.10	Relative abundance of bacterial communities in pore water samples . . . . .	191
A.11	Relative abundance of bacterial communities in sand samples . . . . .	193
<b>B</b>	<b>Supporting information of Chapter 4</b>	<b>197</b>
B.1	Mathematical model for two phase flow . . . . .	198
B.1.1	Mass-momentum conservation equations for the capillary fringe . . . . .	198
B.1.2	Fractional gas/water flow formulation . . . . .	198
B.2	Stoichiometry of pathway-specific degradation reactions of DCM . . . . .	200
B.3	Numerical resolution . . . . .	202
B.4	Parameters used for all test cases . . . . .	204
B.5	DCM gas phase concentrations . . . . .	208
B.6	Anaerobic DCM degradation by individual bacterial populations . . . . .	209
B.7	Concomitant DCM degradation under steady-state conditions . . . . .	211
B.8	Concomitant DCM degradation under transient conditions . . . . .	213
B.9	Simulated evolution (2D-domain) of concomitant DCM degradation by bacterial populations $X_3$ ( <i>D. formicoaceticum</i> ) and $X_4$ ( <i>Ca. D. elyunquensis</i> ) in the presence of a non-DCM degrader ( $X_5$ ) . . . . .	215
<b>C</b>	<b>Supporting information of Chapter 5</b>	<b>223</b>
C.1	Chemical reagents of the micropollutant mixture and transformation products . .	224
C.2	Saline conservative tracer . . . . .	225
C.3	Micropollutants extraction and quantification measurements . . . . .	226
C.4	Compound-specific isotope analysis (CSIA) of micropollutants . . . . .	228
C.5	DNA extraction and rarefaction curves . . . . .	229
C.6	Simple parsimonious reactive transport model . . . . .	232
C.7	Microcosms experiments . . . . .	233
C.8	Carbon and nitrogen isotope fractionation in microcosm experiments . . . . .	235

C.9 Hydrochemistry of laboratory aquifers . . . . .	236
C.10 BTCs and carbon and nitrogen isotopes of a micropollutant mixture in laboratory aquifers . . . . .	237
C.11 BTCs of transformation products in laboratory aquifers . . . . .	243
C.12 Changes in bacterial diversity . . . . .	244
C.13 Relative abundance of phyla in sand samples . . . . .	246
C.14 Relative abundance of genera in pore water samples . . . . .	247

## List of Figures

1.1	Sources of major groundwater contaminants from agricultural, urban and industrial areas. . . . .	3
1.2	Schematic overview of subsurface contamination by chlorinated solvents from spillages, and associated dissipation processes affecting their fate and transport in groundwater. . . . .	6
1.3	Conceptual illustration of a subsurface environment including the vadose (I), capillary fringe (II) and saturated zones (III). . . . .	15
1.4	Conceptual illustration of stream-groundwater interactions across the hyporheic zone during lateral stream water flow to adjacent groundwater (losing streams). .	16
1.5	Scheme of microbially-mediated redox reactions for organic-rich substrates such as natural organic matter (NOM), as well as organic contaminants. . . . .	17
1.6	A generalized vertical cross section illustrating processes influencing the transport and fate of an organic contaminant plume. . . . .	19
1.7	Overview on isotopes of chemical elements. . . . .	23
1.8	Evolution of stable carbon isotope ratios during degradation reactions. . . . .	25
2.1	Graphical outline of this thesis project. . . . .	52
2.2	General schematic overview of laboratory aquifers investigated in this thesis project.	53
3.1	Schematic overview and operations of laboratory aquifers fed with DCM-spiked groundwater under steady-state and transient conditions. . . . .	62
3.2	DCM concentrations, and carbon and chlorine isotope values over distance from inflow in laboratory aquifers under steady-state and transient conditions . . . . .	69
3.3	Dual plot of $\Delta\delta^{13}\text{C}$ versus $\Delta\delta^{37}\text{Cl}$ for the degradation of DCM under steady-state and transient conditions. . . . .	71
3.4	NMDS ordination plot of bacterial diversity profiles from pore water and sand samples. . . . .	72

3.5	Relative abundance of taxa associated with DCM degradation and OHR in laboratory aquifers under steady-state and transient conditions in the saturated zone ( $z=15$ cm) and capillary fringe ( $z=40$ cm), and over time (from 0 to 80 days). . . . .	73
4.1	Schematic overview of mass exchange processes across the porous media with regard to DCM degradation. . . . .	91
4.2	Model domain based on experimental setup of laboratory aquifers. . . . .	104
4.3	Oxygen profiles during abiotic and biotic transport under steady-state conditions and transient conditions. . . . .	106
4.4	DCM profiles in water during abiotic transport case under steady-state conditions, and abiotic transport case under transient conditions. . . . .	107
4.5	Experimental observations in laboratory aquifers and numerical simulations for anaerobic DCM degradation by known anaerobic bacterial populations. . . . .	109
4.6	Evolution of redox species during DCM degradation by bacterial population $X_3$ ( <i>D. formicoaceticum</i> ) in the presence of a non-DCM degrader ( $X_5$ ) under steady-state conditions. . . . .	110
4.7	Experimental observations in laboratory aquifers and numerical simulations for concomitant anaerobic DCM degradation under steady-state conditions. . . . .	112
4.8	Experimental observations in laboratory aquifers and numerical simulations for concomitant anaerobic DCM degradation under transient conditions. . . . .	114
4.9	Numerical results of dual plot of $\Delta^{13}\delta\text{C}$ versus $\Delta^{37}\delta\text{Cl}$ for anaerobic DCM degradation. . . . .	115
4.10	Simulated evolution (2D-domain) of distinct bacterial populations during concomitant DCM degradation under steady-state conditions. . . . .	116
4.11	Simulated evolution (2D-domain) of distinct bacterial populations during concomitant DCM degradation under transient conditions. . . . .	117
5.1	Laboratory aquifers receiving stream water and transient exposures of a micropollutant mixture. . . . .	134
5.2	Dissipation of micropollutants in biotic stream water microcosms over time. . . . .	139
5.3	Caffeine concentrations and carbon ( $\delta^{13}\text{C}$ ) and nitrogen ( $\delta^{15}\text{N}$ ) isotope signatures during the three periods of injections of a micropollutant mixture. . . . .	141
5.4	Simulated caffeine BTC and carbon isotope fractionation ( $\delta^{13}\text{C}$ ) during the second pulse injection (90–140 d). . . . .	144

5.5	Relative abundance of bacterial phyla during transient exposure to the micropollutant mixture in laboratory aquifers. . . . .	146
A.1	Results of the DCM $\delta^{37}\text{Cl}$ GCq-MS validation protocol. . . . .	180
A.2	Oxygen concentrations <i>versus</i> pressure head under transient and steady-state conditions at depth 25 cm from the bottom. . . . .	182
A.3	Oxygen concentrations <i>versus</i> pressure head under transient and steady-state conditions at depth 10 cm from the bottom. . . . .	183
A.4	Relative oxygen concentration <i>versus</i> depth under transient and steady-state conditions at x=65 cm from the inflow . . . . .	183
A.5	Evolution of $\text{Fe}^{2+}$ concentrations along the flow path in aquifers under steady-state and transient conditions. . . . .	184
A.6	Evolution of Eh values along the flow path in aquifers under steady-state and transient conditions. . . . .	184
A.7	Concentrations and carbon isotope composition of <i>cis</i> -DCE and VC under transient and steady-state conditions. . . . .	187
A.8	Rayleigh plots of carbon and chlorine isotope ratios vs. residual DCM fraction for DCM degradation in the saturated zone of laboratory aquifers under $\text{O}_2$ -depleted conditions from day 0 to 35. . . . .	188
A.9	Rarefaction curves based on OTUs, $S_{\text{chao1}}$ diversity and Shannon diversity from pore water and sand samples under transient and steady-state conditions. . . . .	190
A.10	Relative abundance of bacterial phyla in pore water samples over time in a DCM contaminated lab-scale aquifer under transient conditions. . . . .	191
A.11	Relative abundance of bacterial phyla in pore water samples over time in a DCM contaminated lab-scale aquifer under steady-state conditions. . . . .	192
A.12	Relative abundance of bacterial phyla in sand samples at day 88 (end of experiment), and at depths of 15, 40 and 65 cm. . . . .	193
B.1	Evolution of DCM gas-phase concentrations during one water table fluctuation cycle (0–13 days). . . . .	208
B.2	Evolution of redox species during DCM degradation by bacterial population $X_2$ ( <i>Dehalobacter</i> sp.) in the presence of a non-DCM degrader ( $X_5$ ) under steady-state conditions. . . . .	209

B.3	Evolution of redox species during DCM degradation by bacterial population $X_4$ ( <i>Ca. D. elyunquensis</i> ) in the presence of a non-DCM degrader ( $X_5$ ) under steady-state conditions. . . . .	210
B.4	Evolution of redox species during concomitant DCM degradation by bacterial populations $X_3$ ( <i>D. formicoaceticum</i> ) and $X_4$ ( <i>Ca. D. elyunquensis</i> ) in the presence of a non-DCM degrader ( $X_5$ ) under steady-state conditions. . . . .	211
B.5	Evolution of redox species during concomitant DCM degradation by bacterial populations $X_2$ ( <i>Dehalobacter</i> sp.), $X_3$ ( <i>D. formicoaceticum</i> ) and $X_4$ ( <i>Ca. D. elyunquensis</i> ) in the presence of a non-DCM degrader ( $X_5$ ) under steady-state conditions. .	212
B.6	Evolution of redox species during concomitant DCM degradation by bacterial populations $X_3$ ( <i>D. formicoaceticum</i> ) and $X_4$ ( <i>Ca. D. elyunquensis</i> ) in the presence of a non-DCM degrader ( $X_5$ ) under transient conditions. . . . .	213
B.7	Evolution of redox species during concomitant DCM degradation by bacterial populations $X_2$ ( <i>Dehalobacter</i> sp.), $X_3$ ( <i>D. formicoaceticum</i> ) and $X_4$ ( <i>Ca. D. elyunquensis</i> ) in the presence of a non-DCM degrader ( $X_5$ ) under transient conditions. . . .	214
B.8	Simulated evolution (2D-domain) of DCM in water, and carbon and chlorine isotope ratios over time during concomitant DCM degradation under steady-state conditions. . . . .	215
B.9	Simulated evolution (2D-domain) of DCM in water, and carbon and chlorine isotope ratios over time during concomitant DCM degradation under transient conditions. . . . .	216
B.10	Simulated evolution (2D-domain) of DOC, ferric iron and $\text{CO}_2$ over time during concomitant DCM degradation under steady-state conditions. . . . .	217
B.11	Simulated evolution (2D-domain) of DOC, ferric iron and $\text{CO}_2$ over time during concomitant DCM degradation under transient conditions. . . . .	218
B.12	Simulated evolution (2D-domain) of Cl, acetate and formate over time during concomitant DCM degradation under steady-state conditions. . . . .	219
B.13	Simulated evolution (2D-domain) of Cl, acetate and formate over time during concomitant DCM degradation under transient conditions. . . . .	220
C.1	Measured saline (NaCl) conservative tracer BTC in a laboratory aquifer. . . . .	225
C.2	Rarefaction curves based on observed OTUs (top), $S_{\text{chao1}}$ diversity (middle) and Shannon diversity (bottom) from integrative water samples collected at 45 cm, 105 cm and 160 cm (outflow) distance from inflow. . . . .	230

C.3	Rarefaction curves based on observed OTUs (top), $S_{\text{chao1}}$ diversity (middle) and Shannon diversity (bottom) from integrative sand samples collected at 45 cm and 105 cm distance from inflow, and at 15 cm and 45 cm depth (from bottom to top of the aquifers). . . . .	231
C.4	Relative concentrations ( $C/C_0$ ) of a micropollutant mixture consisting of caffeine, metalaxyl and metformin, and atrazine, <i>S</i> -metolachlor and terbutryn in abiotic microcosm experiments as a function of time. . . . .	234
C.5	Concentrations of micropollutants transformation products in biotic microcosm experiments as a function of time. . . . .	234
C.6	Rayleigh plots of carbon isotope ratios vs. residual caffeine fraction in biotic freshwater microcosm experiments under oxic conditions. . . . .	235
C.7	Metformin concentrations during transient injections of a micropollutant mixture over time. . . . .	238
C.8	Atrazine concentrations and stable isotopes during transient injections of a micropollutant mixture over time. . . . .	239
C.9	Metalaxyl concentrations and stable isotopes during transient injections of a micropollutant mixture over time. . . . .	240
C.10	Terbutryn concentrations and stable isotopes during transient injections of a micropollutant mixture over time. . . . .	241
C.11	<i>S</i> -metolachlor concentrations and stable isotopes during transient injections of a micropollutant mixture over time. . . . .	242
C.12	Observed transformation products of a micropollutant mixture in laboratory aquifers receiving stream water during the second injection period. . . . .	243
C.13	NMDS ordination plot of bacterial diversity profiles from pore water over time in duplicate aquifers. . . . .	244
C.14	Changes in bacterial diversity indices over time in laboratory aquifers exposed to a micropollutant mixture. . . . .	245
C.15	Relative abundance of bacterial phyla in sand samples at day 220 (end of experiment), with increasing distance from inflow and at depths of 15 cm and 45 cm. . . . .	246
C.16	Relative abundance of bacterial genera from pore water samples over time and with increasing distance from inflow. . . . .	247





## List of Tables

1.1	Physicochemical properties of chlorinated ethenes (CEs). . . . .	5
1.2	Physicochemical properties of chlorinated methanes (CMs). . . . .	8
1.3	Physicochemical properties of selected legacy and currently used pesticides, consumer products and pharmaceuticals. . . . .	11
1.4	State of the art of biomolecular markers for assessing natural attenuation of groundwater contaminants. . . . .	21
1.5	Bulk carbon and chlorine isotope enrichment factors ( $\varepsilon_{bulk}^C$ and $\varepsilon_{bulk}^{Cl}$ , respectively) and ME-CSIA slopes ( $\Lambda^{C/Cl}$ ) for biotic degradation of Cl-VOCs in laboratory microcosm studies. . . . .	27
1.6	State of the art and implications of assessing natural attenuation of Cl-VOCs and micropollutants in groundwater. . . . .	32
3.1	DCM biodegradation (B in %) in laboratory aquifers under transient and steady-state conditions. . . . .	70
4.1	Initial abundance of DCM carbon-chlorine isotopologues. . . . .	92
4.2	Pathway-specific reactions based on C-Cl CSIA considered in the model. . . . .	94
A.1	Setup of GC-qMS for chlorine isotope analysis. . . . .	179
A.2	Hydrochemistry of lab-scale aquifers fed with spiked-DCM groundwater under transient and steady-state conditions. . . . .	185
A.3	Total organic carbon (TOC), non-purgeable organic carbon (NPOC) and inorganic carbon (IC) in lab-scale aquifers fed with spiked-DCM groundwater under transient and steady-state conditions. . . . .	186
A.4	Proposed DCM degradation pathways and stoichiometry reactions based on stable isotopes. . . . .	189
B.1	Flow parameters according to Brooks-corey model. . . . .	199

B.2	Parameter set for all test cases (no calibration is done from experiment), index $j$ is referred to $j$ th-isotopologue of DCM. (Part 1)	204
B.3	Parameter set for all test cases (no calibration is done from experiment), index $j$ is referred to $j$ th-isotopologue of DCM. (Part 2)	205
B.4	Pathway-specific reaction rates of DCM carbon-chlorine isotopologues following Glutathione S-transferase pathway and mediated by <i>Hyphomicrobium</i> sp. strain MC8b.	206
B.5	Pathway-specific reaction rates of DCM carbon-chlorine isotopologues under anoxic iron-reducing condition ( $\kappa = 2$ ) and mediated by <i>Dehalobacter</i> sp.	206
B.6	Pathway-specific reaction rates of DCM carbon-chlorine isotopologues in anoxic condition ( $\kappa = 3$ ) and mediated by <i>Dehalobacterium formicoaceticum</i> .	206
B.7	Pathway-specific reaction rates of DCM carbon-chlorine isotopologues in anoxic condition ( $\kappa = 4$ ) and mediated by <i>Ca. Dichloromethanomonas elyunquensis</i> .	207
C.1	Mass spectrometry parameters for quantification of transformation products of the micropollutant mixture and parent compound metformin by LC–MS/MS.	227
C.2	Estimated parameters from fitted caffeine BTCs.	232
C.3	Hydrochemistry of stream water microcosm experiments under oxic conditions.	233
C.4	Carbon ( $\delta^{13}\text{C}$ ) and nitrogen isotope ( $\delta^{15}\text{N}$ ) fractionation in freshwater microcosm experiments under oxic conditions.	235
C.5	Hydrochemistry of outflow samples ( $x=160$ cm) in laboratory aquifers under oxic conditions. Sampling days correspond to first pulse injection (0–40 d), the constant injection (40–90 d) and second pulse injection (90–140 d).	236
C.6	Mass recovery of a micropollutant mixture from outflow samples ( $x=160$ cm) in laboratory aquifers under oxic conditions.	237

# **Chapter 1**

## **General Introduction**

## 1.1 Human and ecological values of groundwater protection

Aquifers represent an important part of the global water cycle hosting one of the most valuable freshwater resources: groundwater (Prommer et al., 2019). Although hidden in the subsurface, groundwater interacts with rivers, lakes and wetlands by exchanging water flow and feeding surface reservoirs, or by taking some of their flow when surface water is present in excess (Poeter et al., 2020). Such hydrogeological connections result in complex groundwater ecosystems driven by the interplay of flow and solute transport, environmental conditions, biogeochemical processes and microbial dynamics (Griebler and Lueders, 2009; Prommer et al., 2019). The continuous interactions of these physical and chemical processes, including transition zones with soils, sediments and surface water, as well as the role of microorganisms in the cycling of chemical substances (e.g., nutrients), ultimately define groundwater quality (Grant Ferris et al., 2021; Griebler and Lueders, 2009).

Groundwater is intrinsically linked to various aspects of human development serving as a precious drinking water resource, for food and energy production, health and recreation (Velis et al., 2017). However, aquifers around the world are vulnerable to the extensive applications of natural and synthetic chemicals which may be persistent and toxic to aquatic life and human health (Fenner et al., 2013; Schwarzenbach et al., 2010). The risks of groundwater contamination from waste emissions of anthropogenic activities may thus result in severe groundwater quality degradation (Burri et al., 2019). Major contaminants of groundwater include organic pollutants which are a diverse class of products with widespread use in agricultural, urban, and industrial environments (Figure 1.1 and Section 1.2). Two main classes of organic pollutants can be defined as:

- (i) the legacy industrial contaminants such as volatile organic compounds (VOCs) (Section 1.2.1), which can be partially or fully hydrophobic, therefore, they may occur dissolved in water or in a separate phase as non-aqueous phase liquids (NAPLs), further classified as light (L) and dense (D) according to their density relative to water (Fetter et al., 2018), and
- (ii) the emerging contaminants, such as pesticides and pharmaceuticals (Section 1.2.2), which are ubiquitously released from urban and agricultural areas. Emerging contaminants are characterized for their toxicity, persistence and potential mobilization depending on their physico-chemical characteristics and aquifer's matrix (e.g., organic content) (Burri et al., 2019).

In general, when an aquifer becomes contaminated with harmful chemicals it may become unusable for decades (Burri et al., 2019), thus suitable remediation strategies are required for their removal (US EPA, 1999b). In the European Union alone, it is estimated that 2.5 million sites are potentially contaminated, of which about 14% (340,000) are likely to need remediation measures with an average cost between 5,000 € to 500,000 € (Van Liedekerke et al., 2014). The U.S. Environmental Protection Agency estimates that as of 2020 roughly 61% (200 million people) of the U.S. population live within 3 miles (4.8 km) of a contaminated site (US EPA, 2015). Hence, the preservation of groundwater resources against contamination is of paramount importance to ensure adequate groundwater quality for ecosystem functions and human health.

**In this context, an interdisciplinary effort between hydrogeologists, biogeochemists and microbiologists is essential to understand the controlling processes affecting the fate and transport of contaminants in groundwater, and for ultimately designing the most effective remediation techniques.**

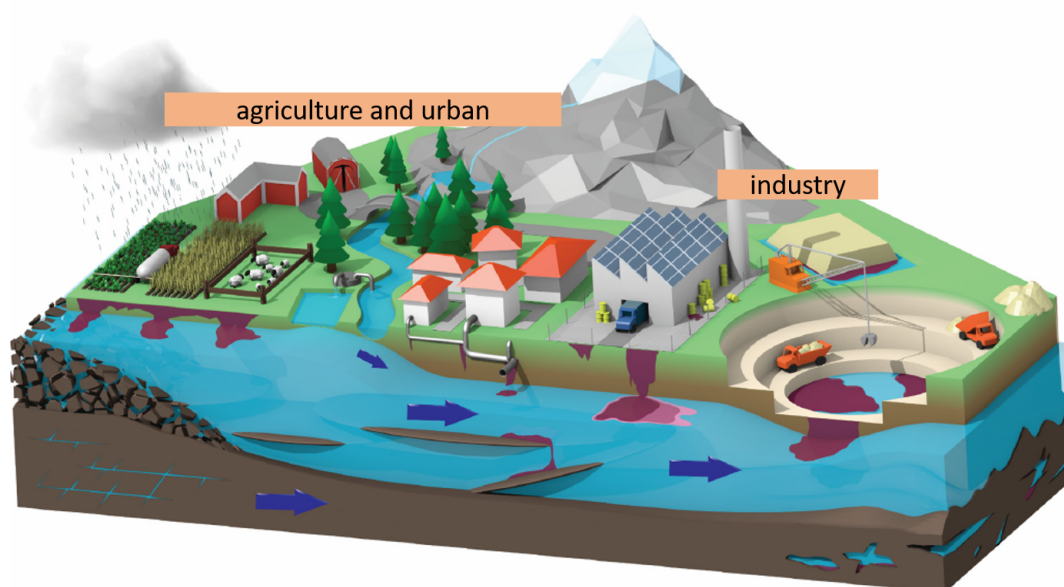


**Figure 1.1:** Sources of major groundwater contaminants from agricultural, urban and industrial areas. Adapted from Burri et al. (2019).

## 1.2 Origin and fate of legacy and emerging contaminants of groundwater

Understanding the intrinsic differences between the physico-chemical properties of each chemical pollutant and their major sources is essential to evaluate and predict their fate and transport in aquifers. In this section, the origin and characteristics of the two major classes of groundwater contaminants is presented. Section 1.2.1 describes the lessons learnt from legacy contaminants

focusing on chlorinated volatile organic compounds (Cl-VOCs) such as chlorinated ethenes (CEs) and **dichloromethane (DCM)**; the latter being among the most common Cl-VOCs at contaminated sites (Leeson et al., 2004; US EPA, 2020). Section 1.2.2 presents the case of emerging contaminants such as pesticides and pharmaceuticals which are part of the thousands of synthetic and natural trace contaminants that can be present in both surface and groundwater at the nanogram to microgram per liter level ( $\text{ng L}^{-1}$  to  $\mu\text{g L}^{-1}$ ) (Schwarzenbach et al., 2010). Among the numerous micropollutants, the presence of **atrazine**, **terbutryn**, **S-metolachlor**, **metalaxyl**, **caffeine** and **metformin** is discussed (i) due to their demonstrated co-occurrence in both surface water (Hildebrandt et al., 2008) and groundwater (Lesser et al., 2018; Loos et al., 2010), and (ii) the lack of comprehensive studies to elucidate the fate of such micropollutant mixtures in shallow aquifers.

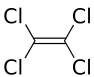
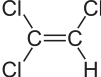
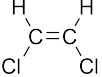
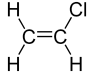
Further sections within Chapter 1 describe the physical and chemical processes involved during reactive transport of legacy and emerging contaminants in groundwater (Section 1.3), and in highly dynamic transition zones such as the capillary fringe and stream-groundwater transition zones (Section 1.4). Section 1.5 emphasizes biodegradation as a key process for sustainable depletion of pollutants in aquifers, and highlights the state of the art and implications for assessing natural attenuation of Cl-VOCs and micropollutants. Innovative tools to assess biodegradation of these pollutants are further discussed, including the use of biomolecular markers (Section 1.5.2), stable isotopes (Section 1.6) and reactive transport models (RTM; Section 1.7). Finally, Section 1.8 presents the advantages of integrative approaches for monitoring natural attenuation of organic pollutants in aquifers, providing a comprehensive framework to help unravel the often overlooked effect of dynamic hydrogeological and biogeochemical conditions on pollutant biodegradation.

### 1.2.1 Chlorinated volatile organic compounds (Cl-VOCs)

Legacy soil and groundwater contamination by chlorinated volatile organic compounds (Cl-VOCs) remains a global environmental concern. Cl-VOCs contain at least one chlorinated atom and are volatile and mostly recalcitrant to degradation (Huang et al., 2014; Zimmermann et al., 2020). Chlorinated solvents have been employed historically in the industry for cleaning and degreasing applications, including (poly)chlorinated methanes (CMs), (poly)chlorinated ethanes (CAs) and (poly)chlorinated ethenes (CEs) (Huang et al., 2014; Weatherill et al., 2018). Among these, the most common chlorinated solvents released to the environment include tetrachloroethene (PCE, or perchloroethene), trichloroethene (TCE), trichloroethane (TCA) and di-

chloromethane (DCM) (Leeson et al., 2004; US EPA, 2020) (Tables 1.1 and 1.2).

**Table 1.1:** Physicochemical properties of chlorinated ethenes (CEs). *Adapted from Huang et al. (2014) and Leeson et al. (2004).*

Properties	tetrachloroethylene	trichloroethylene	cis-1,2-dichloroethylene	vinyl chloride
<b>Physicochemical properties</b>				
Abbreviation	PCE	TCE	1,2-DCE	VC
Structure				
Formula	C <sub>2</sub> Cl <sub>4</sub>	C <sub>2</sub> HCl <sub>3</sub>	C <sub>2</sub> H <sub>2</sub> Cl <sub>2</sub>	C <sub>2</sub> H <sub>3</sub> Cl
Molar mass (g mol <sup>-1</sup> )	168.5	131.4	96.9	62.5
Density (g L <sup>-1</sup> )	1.63 (20 °C)	1.46 (20 °C)	1.28 (20 °C)	0.96 (-13 °C)
Melting (°C)	-19	-73	-81.47	-153.8
Boiling (°C)	121.1	87.2	60.2	-13.4
Solubility (g L <sup>-1</sup> )	0.15 (20 °C)	1.28 (20 °C)	1-5 (16 °C)	slightly soluble
n-Octanol-water (log Pow)	2.9	2.42	2.0	0.6
Vapor pressure (at 20 °C; in kPa)	1.9	7.8	26.66	516.95
Henry's constant (at 20 °C) (×10 <sup>-3</sup> atm m <sup>3</sup> mol <sup>-1</sup> )	26.3	11.7	7.4	79.2
K <sub>oc</sub> (mL g <sup>-1</sup> )	247	90	35.5	56
<b>Degradation capacity and known degradation pathways</b>				
Aerobic oxidation	no	no	possible	yes
Aerobic cometabolism	no	yes	yes	yes
Anaerobic reductive dechlorination	yes	yes	yes	yes
Anaerobic oxidation	no	no	possible	yes
Cometabolic anaerobic reduction	yes	yes	yes	yes
Abiotic transformation	yes	yes	yes	yes

Subsurface contamination with Cl-VOCs often results from *point sources* such as solid-waste disposal to landfill sites, and accidental release from pipelines, tanks and spillages at industrial sites (Rivett et al; 2011). They tend to migrate across soils and the vadose zone until reaching the water table forming plumes at high concentration ranges ( $\mu\text{g L}^{-1}$  to  $\text{mg L}^{-1}$ ), often in the form of dense non-aqueous phase liquids (DNAPLs) (Rivett et al., 2011) (Figure 1.2). As



the oxygen supply across the soil and saturated zone becomes limiting, anoxic conditions are predominantly observed at contaminated sites. Thus, anaerobic degradation is described as a key removal process for Cl-VOCs in subsurface environments (Bradley, 2000; Chapelle, 1996; Leeson et al., 2004).

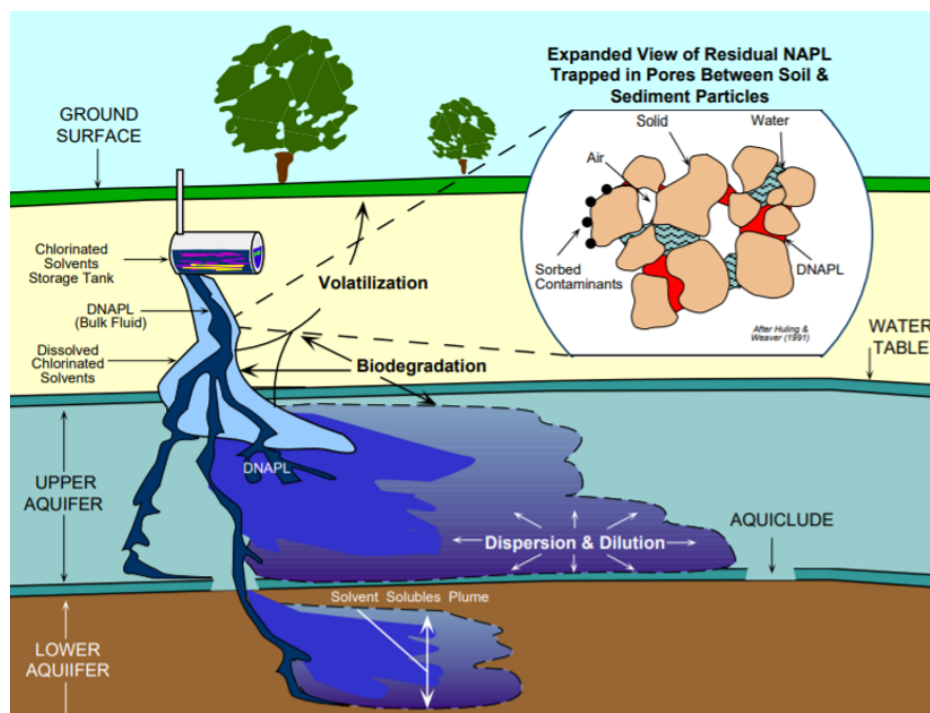


**Figure 1.2:** Schematic overview of subsurface contamination by chlorinated solvents from spillages, and associated dissipation processes affecting their fate and transport in groundwater. *Adapted from US EPA (1999a).*

In recent decades, a comprehensive understanding of the transport and fate of Cl-VOCs in the subsurface has been achieved through intensive research efforts, including field site characterisation, laboratory experiments and numerical modeling (Huang et al., 2014; Kuder et al., 2016; Leeson et al., 2004; Weatherill et al., 2018; Zimmermann et al., 2020). Investigations on the removal of chlorinated ethenes (CEs) have been among the most detailed and recognized in the literature (Chapelle, 1996; Hunkeler et al., 2011; Kuder et al., 2016; Leeson et al., 2004; Leitner et al., 2018; Rivett et al., 2011; Stroo et al., 2012; US EPA, 1999a; Van Breukelen et al., 2005). In particular, the reductive dechlorination sequence from PCE to TCE to *cis*-dichloroethene (cDCE) to vinyl chloride (VC) to ethene (i.e., from high to low degree of chlorination) has been extensively described (Abe et al., 2009; Bradley, 2000; DiStefano et al., 1991, 1992; Kuder et al., 2013; Schmidt et al., 2010) (Table 1.1). This has led to important knowledge regarding (i) redox conditions as the primary determinant of reductive dechlorination of CEs (Chapelle, 1996;

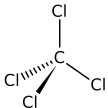
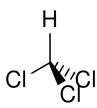
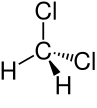
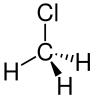
Chapelle et al., 1996), (ii) the possible co-metabolic oxidation of cDCE to VC to ethene (McCarty and Semprini, 2017), (iii) the microorganisms and enzymes involved in anaerobic CEs degradation pathways (Dolinová et al., 2017), and (iv) the development of reactive transport models to help predicting the natural attenuation of CEs at contaminated sites (Antelmi et al., 2021; Höhener, 2016; Höhener and Atteia, 2010; Hunkeler et al., 2009b; Thoeument and Van Breukelen, 2020; Van Breukelen et al., 2005).

The recognition of the intrinsic relationships between biogeochemical conditions and microbial dynamics for efficient removal of CEs made possible the development of advanced and integrative *in situ* bioremediation strategies, leading unprecedented lessons for the removal of other halogenated contaminants (Blázquez-Pallí et al., 2019; Hellal et al., 2021; Hermon et al., 2018). Along with CEs, chlorinated methanes such as dichloromethane are commonly found at contaminated sites thus forming complex contaminant mixtures (Blázquez-Pallí et al., 2019; Hellal et al., 2021; Hermon et al., 2018; Wright et al., 2017).

### **Groundwater contamination by dichloromethane (DCM)**

Dichloromethane or methylene chloride (DCM,  $\text{CH}_2\text{Cl}_2$ ) is a volatile halogenated hydrocarbon known for having toxic, mutagenic and potentially carcinogenic effects on living organisms (Shestakova and Sillanpää, 2013; US EPA, 2020) (Table 1.2). DCM has a wide-range of uses including solvent for plastics, insecticides, paints, degreasing and cleaning fluids, as well as for the extraction of essential oils, food processing, pharmaceutical and chemical intermediates applications (Shestakova and Sillanpää, 2013). As of 2016, the leading applications for DCM are as a solvent in the production of pharmaceuticals and polymers and paint removers (US EPA, 2020). DCM can also be present at contaminated sites as the degradation product of anaerobic chloroform ( $\text{CF}$ ,  $\text{CH}_1\text{Cl}_3$ ) degradation (Grostern et al., 2010). It has been reported that DCM is present in at least 389 contaminated sites in the U.S., representing 30% of the total number of Superfund sites (Koenig et al., 2015). To date, DCM is included in the list of priority pollutants of the U.S. Agency for Toxic Substances and Disease Registry (ATSDR, 2019), and of the European Commission (Commission, 2013).

**Table 1.2:** Physicochemical properties of chlorinated methanes (CMs). *Adapted from Huang et al. (2014) and Leeson et al. (2004).*

Properties	carbon tetrachloride	chloroform	dichloromethane	chloromethane
<b>Physicochemical properties</b>				
Abbreviation	CTC	CF	DCM	CM
Structure				
Formula	$\text{CCl}_4$	$\text{CHCl}_3$	$\text{CH}_2\text{Cl}_2$	$\text{CH}_3\text{Cl}$
Molar mass ( $\text{g mol}^{-1}$ )	153.8	119.4	84.9	50.5
Density ( $\text{g cm}^{-3}$ )	1.58 (20 °C)	1.48 (20 °C)	1.32 (20 °C)	2.30 (0 °C)
Melting point (°C)	-22.92	-63.5	-96.6	-97.4
Boiling point (°C)	76.72	61.2	39.6	-23.8
Solubility ( $\text{g L}^{-1}$ )	0.785 (25 °C)	8.0 (20 °C)	13.0 (20 °C)	5.32 (25 °C)
n-Octanol-water coef. (Log Pow)	2.64	1.97	1.25	0.91
Vapor pressure (at 20 °C; in kPa)	11.94	21.08	47	506.09
Henry's constant (at 20 °C) ( $\times 10^{-3}$ $\text{atm m}^3 \text{mol}^{-1}$ )	28.9	3.8	1.7	9.6
$K_{oc}$ ( $\text{mL g}^{-1}$ )	71	60	8	13
<b>Degradation capacity and known degradation pathways</b>				
Aerobic oxidation	no	no	yes	possible
Aerobic cometabolism	no	yes	yes	yes
Anaerobic reductive dechlorination	yes	yes	yes	yes
Anaerobic oxidation	no	no	yes	possible
Cometabolic anaerobic reduction	yes	yes	yes	possible
Abiotic transformation	yes	yes	yes	yes

In order to develop proper remediation strategies for the removal of DCM from contaminated aquifers, current research efforts focus on DCM degradation mechanisms and pathways, and the identification and follow-up of microorganisms involved during degradative reactions (Blázquez-Pallí et al., 2019; Hellal et al., 2021; Hermon et al., 2018; Wright et al., 2017). Indeed, numerous bacteria capable of degrading DCM under both oxic and anoxic conditions have

been identified (Chen et al., 2020; Hayoun et al., 2020; Mägli et al., 1998, 1996; Muller et al., 2011; Torgonskaya et al., 2019; Vuilleumier and Leisinger, 1996) (Table 1.2). To date, only few anaerobic DCM degradation mechanisms are known, challenging the design of remediation strategies in prevailing anoxic contaminated sites.

Furthermore, the natural dynamics of hydrogeological and biogeochemical conditions in aquifers, such as water table fluctuations, are often excluded from interpretations of fate and transport of DCM (Meckenstock et al., 2015). In fact, water table fluctuations can strongly impact (i) the transfer of gases due to volatilization of Cl-VOCs (Jeannotat and Hunkeler, 2013; McCarthy and Johnson, 1993; Werner and Höhener, 2002) or by bringing oxygen into anoxic areas (Haberer et al., 2012; Williams and Oostrom, 2000), (ii) the evolution of hydrochemical conditions (Haberer et al., 2012; Seybold et al., 2002), and (iii) the evolution/adaptation of bacterial/microbial populations that control biodegradation pathways of contaminants (Peralta et al., 2014; Rühle et al., 2015) (Section 1.4). In this context, **water table fluctuations** may exert control on the removal of DCM. Further investigations are thus needed to bridge the gap regarding the effect of dynamic hydrogeological and biogeochemical conditions **as a yet unrecognized major control of DCM removal at contaminated aquifers**.

### 1.2.2 Pesticides, pharmaceuticals and consumer products

Contaminants of emerging concern (CECs) are widely used in the domestic and agricultural sectors. Because CECs are typically detected in the  $\text{ng L}^{-1}$  to  $\mu\text{g L}^{-1}$  concentration range, they are often referred to as micropollutants (Schwarzenbach, 2006). The ubiquitous release of micropollutants results in the deterioration of water quality, aquatic life and human health, as many of these chemicals may exert toxic effects even at such low concentrations (Barbosa et al., 2016; Schwarzenbach et al., 2010). Micropollutants cover a wide variety of substances such as pesticides, pharmaceuticals and consumer products. Pesticides are extensively used in agriculture to prevent and control harmful pests and crop yield losses worldwide (Damalas and Koutroubas, 2016). On the other hand, pharmaceuticals and consumer products are ubiquitously released into aquatic ecosystems often from inefficient wastewater treatment facilities (WWTF) (Richardson and Kimura, 2016). Examples of consumer products may cover recreational compounds such as caffeine and nicotine, shampoos, insect repellents, sunscreens, and industrial compounds from plastic packaging (Lapworth et al., 2012). The frequent and continuous release of micropollutants from *diffusive (or non-point) sources*, and eventually their transformation products (TPs), have resulted in their simultaneous presence as complex mixtures

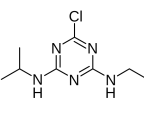
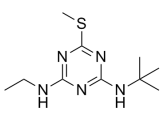
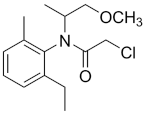
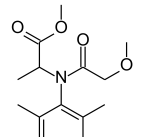
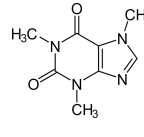
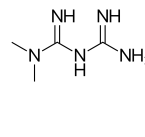
in both surface water (Bradley et al., 2016, 2021; Hildebrandt et al., 2008), and groundwater (aus der Beek et al., 2016; Baran et al., 2021; Loos et al., 2010; Masoner et al., 2019; Seiler et al., 1999).

Although the major inputs of micropollutants may occur in soils and surface water bodies, **surface-groundwater interactions** may result in the mobilization of these substances across subsurface interfaces, forming a **key diffuse pathway for discharge of micropollutants into groundwater** (Conant et al., 2019; Hintze et al., 2020; Lewandowski et al., 2011; Weatherill et al., 2018). Current knowledge on the fate and transport of micropollutants in groundwater is far less understood compared to legacy contaminants (Fenner et al., 2021; Lapworth et al., 2012) (Table 1.6). Current challenges to assess the removal of micropollutants in groundwater is their presence at low to very low concentrations ( $\text{ng L}^{-1}$  to  $\mu\text{g L}^{-1}$ ) and their high polarity (Elsner and Imfeld, 2016), generally requiring advanced methodological tools for their detection in large volume samples (Fenner et al., 2021). Moreover, the lack of evidence of micropollutants biodegradation mechanisms and pathways, as well as the identification of specific microbial degraders, hampers the predictability of their biodegradation and thus the design of suitable remediation strategies to follow-up and cleanup polluted aquifers (Meckenstock et al., 2015).

### **Assessing micropollutants as groundwater contaminant mixtures**

Micropollutants are often detected in complex mixtures which urges for more studies tackling the fate and transport of chemical mixtures rather than single compounds. Among the many micropollutants, *atrazine* belongs to the worldwide most prominent groundwater contaminants, and its persistence has been evidenced even after decades of its ban in 1992 in Germany (Vonberg et al., 2014). Atrazine was found to be even more persistent in groundwater than in soils. For instance, atrazine and its transformation product (TP) desethylatrazine (DEA), one of its main TPs, were still detected in German aquifers more than 10 years after its ban (Vonberg et al., 2014). Further studies later demonstrated that persistence of atrazine in groundwater at concentrations  $<1 \mu\text{g L}^{-1}$  was not only associated with the absence of suitable microorganisms, but that mass transfer across the cell membrane may become rate-limiting for degradation at such trace levels (Kundu et al., 2019; Sun et al., 2021a). Hence, the long-term atrazine groundwater contamination exemplifies the current challenge for the remediation of micropollutants in aquifers at low concentrations.

**Table 1.3:** Physicochemical properties of selected legacy and currently used pesticides, consumer products and pharmaceuticals.

	atrazine	terbutryn	S-metolachlor	metalaxyl	caffeine	metformin
Status (EU) <sup>a</sup>	banned (2004)	banned (2002)	approved (2021)	approved (2023)	approved	approved
Priority concern	yes	yes	yes	no	no	no
<b>Chemical structures and transformation products<sup>b,c</sup></b>						
Structure						
Formula	C <sub>8</sub> H <sub>14</sub> ClN <sub>5</sub>	C <sub>10</sub> H <sub>19</sub> N <sub>5</sub> S	C <sub>15</sub> H <sub>22</sub> ClNO <sub>2</sub>	C <sub>15</sub> H <sub>21</sub> NO <sub>4</sub>	C <sub>8</sub> H <sub>10</sub> N <sub>4</sub> O <sub>2</sub>	C <sub>14</sub> H <sub>11</sub> N <sub>5</sub>
Group	Triazine	Triazine	Chloroacetamide	Phenylamide	Methylxanthines	Biguanide
Molar mass (g mol <sup>-1</sup> )	215.68	241.36	283.79	279.33	194.19	129.16
Transformation products	desethylatrazine (DEA), deisopropylatrazine (DIA), hydroxyatrazine (HA)	terbutryn sulfoxide, 2-hydroxyatrazine, desethylterbutryn, desethyl-2-hydroxyterbutryn	S-met ethanesulfonic acid, S-met oxanilic acid	carboxylic acid metalaxyl (Metalaxyl-M-TP CGA108906), dimethylmetalaxyl (Metalaxyl Metabolite CGA 62826)	theobromine, xanthine, paraxanthine	guanyurea
<b>physicochemical properties<sup>d,e</sup></b>						
pKa	1.6	4.3	-	-	10.9	-
half-life (days) <sup>f</sup>	430-829*	266-400*	56-182†	9-127†	<4 d‡	28-98⊥
solubility (mg L <sup>-1</sup> )	35	25	480	8400	13000	300
oct./water coef. (Log P <sub>ow</sub> )	2.7	3.7	3	1.7	-	-
sorption (K <sub>oc</sub> ; mL g <sup>-1</sup> )	100	2432	185	163	-	-

a: [https://ec.europa.eu/food/plants/pesticides/eu-pesticides-database\\_en](https://ec.europa.eu/food/plants/pesticides/eu-pesticides-database_en)b: <https://pubchem.ncbi.nlm.nih.gov/>

c: Bollmann et al. (2017); Dash and Gummadi (2006); Krutz et al. (2006); Lin et al. (2008); Masbou et al. (2018); Trautwein and Kümmerer (2011)

d: <http://www.pesticideinfo.org/>e: <http://npic.orst.edu/ingred/ppdmmove.htm>

f: Droz (2020); Nödler et al. (2014); Straub et al. (2019); Talja et al. (2008); Torabi et al. (2020)

\*: groundwater; †: soil; ‡: river water; ⊥: activated sludge

The co-occurrence of atrazine with other urban and agricultural pesticides such as terbutryn, metalaxyl and S-metolachlor, the consumer product caffeine, and the anti-diabetic drug metformin has previously been reported in both surface (Hildebrandt et al., 2008) and ground water (Lesser et al., 2018; Loos et al., 2010). Overall, this underscores that **assessing the natural removal of such complex micropollutant mixtures is of utmost importance to ensure the preservation of groundwater quality**. Table 1.3 shows the physico-chemical properties of these micropollutants along with their described main removal pathways and transformation products (TPs).

### 1.3 Dissipation processes driving reactive transport of contaminants in groundwater

Point sources of legacy contaminants such as Cl-VOCs are often well defined which allows for easier conceptualization, monitoring and prediction compared to diffuse sources of micropollutants (Lapworth et al., 2012). In certain situations, however, key entry pathways of micropollutants into groundwater may be identified. For instance, during stream-groundwater exchange near agricultural areas and/or WWTF effluents (Hintze et al., 2020; Schaper et al., 2018), surface runoff (Hensen et al., 2018) and artificial recharge (Maeng et al., 2010). Once released into the subsurface, organic pollutants are often subjected to various physical and chemical processes, affected by temporal and spatial variations which contribute to their overall dissipation.

Advection-dispersion. Contaminant flux is primarily affected by advection-dispersion processes relative to the groundwater flow velocity. Here, the role of diffusion and hydrodynamic dispersion have important implications for the spreading of the contaminants, particularly in the vertical direction of the groundwater flow (Cirpka, 2015). At the plume's fringe, transverse dispersion is the main process bringing together contaminants and solutes from the ambient groundwater, such as oxygen and nutrients, creating an ideal mixing zone for the occurrence of reactive processes (Bauer et al., 2008; Chu et al., 2005; Cirpka, 2015; Rolle et al., 2013) (Section 1.5.1). Similarly, transverse hydrodynamic dispersion is essential for the mixing of solutes across transition zones such as the capillary fringe and the SWI (sediment-water interface). These transition zones have been demonstrated to be highly dynamic zones and potential hotspots for contaminant removal (e.g., Peter et al. (2019); Rühle et al. (2015)) (Section 1.4).

Distribution among phases. The distribution of contaminants across water, gas and solid phases in the subsurface also contribute to contaminant dissipation. In the case of Cl-VOCs, gas-water distribution and volatilization, given by their Henry's Law constants, are major routes for their

dissipation from NAPL sources, causing their further distribution across the capillary fringe and vadose zone by gas diffusion (Kim and Corapcioglu, 2003; McCarthy and Johnson, 1993; Werner and Höhener, 2002). On the other hand, sorption of contaminants onto the solid surface of the porous media mainly occurs in the presence of organic carbon (McCarty et al., 1981). This is described by the partitioning coefficient  $K_d$  or  $K_{oc}$  which predicts the distribution among water and solid phases, given by the fraction of organic carbon ( $f_{oc}$ ). Altogether, these physical processes may determine the spatial and temporal evolution of the dissolved contaminants. Hence, a thorough understanding of these processes are required for appropriate contaminant source characterization and remediation strategies.

Degradative processes. Degradation of organic pollutants in the subsurface results from several abiotic and/or biotic transformation processes, involving chemical reactions and/or microbial activity (Fenner et al., 2013), respectively. In this context, degradative processes rather reflect the true removal of the contaminants from the subsurface, and reliable methods such as compound-specific isotope analysis (Section 1.6) have proven useful to tease apart the contribution of physical (non-destructive) and degradative (destructive) processes on the overall contaminant dissipation. Nevertheless, *biodegradation* is one of the most favored and sustainable means to remove organic pollutants from contaminated aquifers (Fenner et al., 2013; Meckenstock et al., 2015; Thullner et al., 2007). Indeed, microorganisms exert a major control on the redox chemistry of their surroundings (Section 1.5.1) by relying on the transfer of electrons during breakdown of contaminants to obtain energy for their growth and maintenance (Meckenstock et al., 2015; Thullner et al., 2007).

The combination of physical processes with microbially-mediated redox reactions thus creates ideal zones for unique biogeochemical conditions to favor biodegradation of organic contaminants in aquifers (Rolle et al., 2008) (Section 1.5.2). Hence, the highly complex interplay of flow and transport processes, biogeochemical reactions and microbial dynamics ultimately determine the fate and transport of contaminants in groundwater.



## 1.4 Dissipation processes in highly dynamic transition zones of aquifers

### 1.4.1 The role of the capillary fringe in anoxic aquifers

Dissipation of organic pollutants occurs across subsurface environments including transition zones such as the capillary fringe. The capillary fringe exists at the interface of the saturated and vadose zones and is highly dependent upon fluctuations of the local water table (Smith et al., 2018). This fluctuating interface has been demonstrated as a highly active zone regarding physico-chemical processes and microbial activity subjected to dynamic conditions over time (Griebler and Lueders, 2009; Smith et al., 2018). For instance, previous studies have evidenced a distinct bacterial community composition and activity at the capillary fringe compared to the saturated zone due to changes in nutrients and redox conditions upon water table fluctuations (Jost et al., 2015; Peralta et al., 2014; Rühle et al., 2015).

Oxygen transfer across the capillary fringe was also evidenced, which may alter sequential anoxic/oxic conditions and favor complete microbial degradation of various organic pollutants in aquifers under anoxic conditions (Haberer et al., 2012; Pronk et al., 2020; Seybold et al., 2002). In fact, it has been considered that transient environmental conditions results in some obligate anaerobes (e.g., the strictly anaerobic sulfate-reducing bacterium *Desulfovibrio vulgaris*) to adapt to extreme fluctuations in oxygenation (Holman et al., 2009). Hence, the temporal water table fluctuations in contaminated aquifers may represent a yet unrecognized controlling factor of biodegradation by repeatedly changing the environmental conditions (Meckenstock et al., 2015). This is particularly relevant for Cl-VOCs, such as dichloromethane (DCM), as water table fluctuations are known to also affect their mass transfer from groundwater to the unsaturated zone (Jeannotat and Hunkeler, 2013; McCarthy and Johnson, 1993). Hence, understanding dissipation processes across the capillary fringe upon water table fluctuations in anoxic aquifers contaminated with Cl-VOCs is essential for improved predictions of their degradation extent and pathways in dynamic subsurface environments.

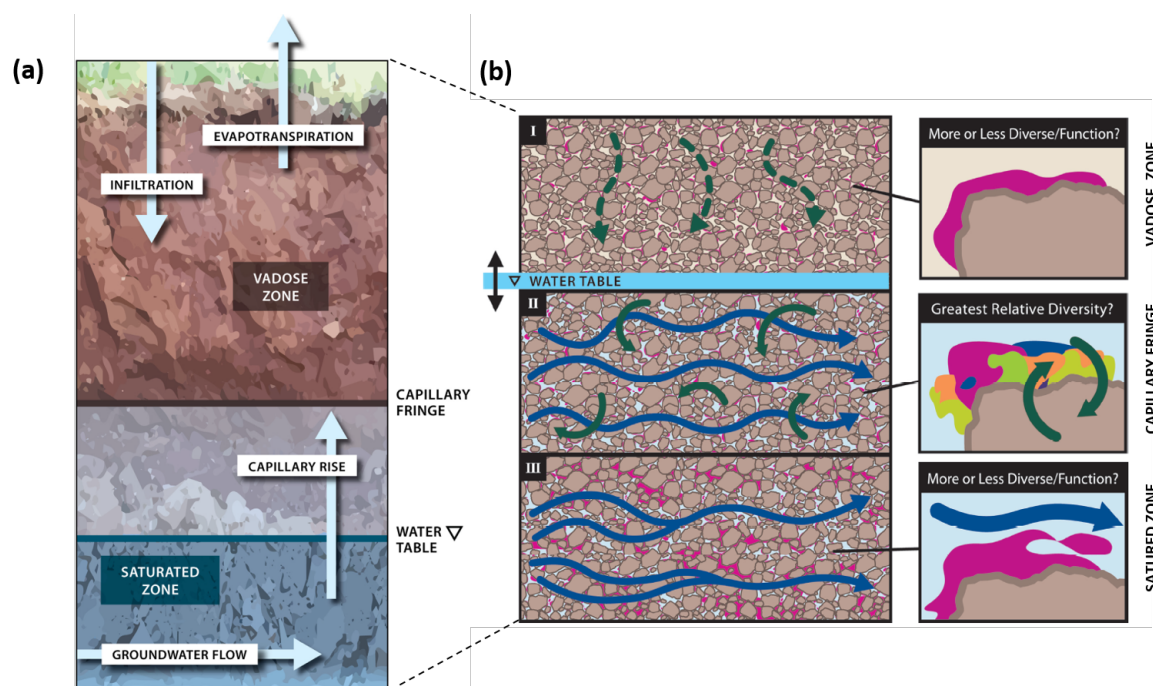


**Figure 1.3:** (a) Conceptual illustration of a subsurface environment including the vadose (I), capillary fringe (II) and saturated zones (III). Arrows depict the movement of water. (b) Description of subsurface flow and mixing zones upon water table fluctuations and potential effects on biogeochemical and microbial dynamics. *Adapted from Smith et al. (2018).*

#### 1.4.2 The role of the hyporheic zone in shallow aquifers

Groundwater continuously interacts with surface waters, including rivers, lakes and wetlands (Poeter et al., 2020). In near-surface aquifers, the hyporheic zone (HZ), i.e., the transition zone between surface water and groundwater, is located beneath the stream bed and the two sides of the riparian zone (Zhang et al., 2017) (Figure 1.4). The HZ may thus represent a natural biogeochemical barrier against groundwater contamination (Boulton et al., 2010; Lewandowski et al., 2011). Due to the increasing inputs of micropollutants (e.g., pesticides and pharmaceuticals) in surface waters, attention has been put on the biotransformation potential of micropollutants across the HZ (Boulton et al., 2010; Droz et al., 2021; Jaeger et al., 2021; Lewandowski et al., 2011; Posselt et al., 2020; Rutere et al., 2020).

Indeed, HZs can sustain micropollutants biotransformation particularly at the sediment-water interface (SWI) described beneath the stream bed (Droz et al., 2021; Mechelke et al., 2020; Peter et al., 2019; Schaper et al., 2018). This zone is driven primarily by hydraulic residence times, surface-groundwater exchange, mass transfer rates, nutrient turnover and microbial diversity (Conant et al., 2019; Drouin et al., 2021; Peter et al., 2019; Posselt et al., 2020).

As anoxic conditions are usually established at the bottom of the SWI, this may result in possibly lower micropollutants degradation rates (Droz et al., 2021), and thus their potential mobilization and accumulation in shallow groundwater (Hintze et al., 2020; Iker et al., 2010; Jakobsen et al., 2019; Lesser et al., 2018; Loos et al., 2010). In conditions where stream level is higher than adjacent groundwater, e.g., due to seasonal hydrological changes (Winter et al., 1998), the losing streams may also laterally flow into groundwater (Ghysels et al., 2021; Winter et al., 1998), further mobilizing micropollutants into oxygen rich zones in shallow aquifers (Hancock, 2002) (Figure 1.4). This lateral transition zone represents a yet poorly understood highly dynamic mixing area of stream-groundwater hydrochemistry and microbial dynamics subjected to seasonal variations in micropollutants inputs and environmental conditions (e.g., precipitation). Thus, ideal conditions for aerobic degradation of micropollutants may be here established (Figure 1.4).

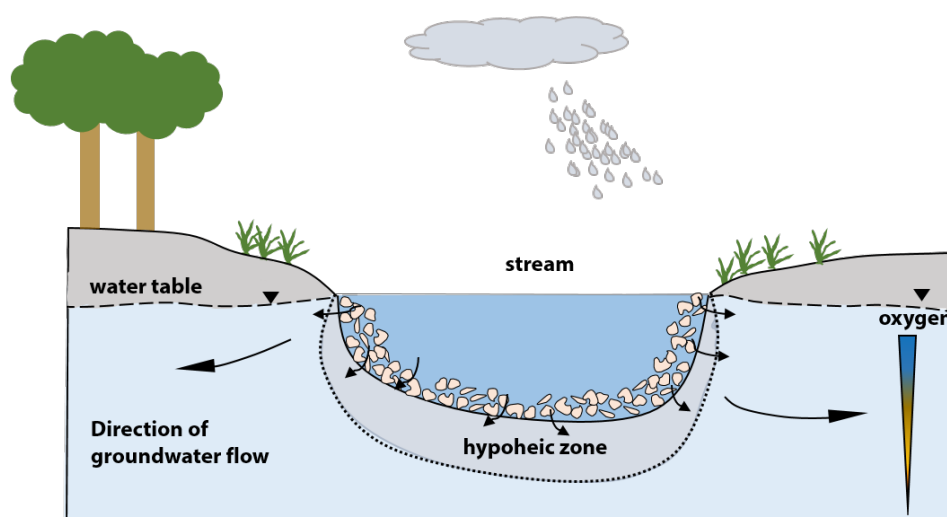


**Figure 1.4:** Conceptual illustration of stream-groundwater interactions across the hyporheic zone during lateral stream water flow to adjacent groundwater (losing streams). *Adapted from Winter et al. (1998).*

## 1.5 Biodegradation: a key removal process of organic pollutants in contaminated aquifers

### 1.5.1 Redox controlled biodegradation

Microbially-mediated redox reactions are the most important biogeochemical processes controlling the fate and transport of organic-rich substances such as natural organic matter (NOM) and organic pollutants in groundwater. Microorganisms can utilize these substances via different types of terminal electron acceptors (TEAs) during transfer of electrons from electron

donor substrates (e.g., a contaminant or organic-rich substance) to terminal electron acceptors (TEA) to obtain energy required for their growth and maintenance (Meckenstock et al., 2015; Thullner et al., 2008) (Figure 1.5). The concept of redox zonation suggests that microorganisms use the available dissolved electron acceptors that are successively depleted in the order of their thermodynamic energy yield; from oxygen to nitrate, Mn(IV), Fe(III) and sulphate, before methanogenesis takes place (Christensen et al., 2001) (Figure 1.5). Similarly, some organic contaminants such as CEs (chlorinated ethenes) can be used as electron acceptors during reductive dechlorination in the presence of donors such as hydrogen and/or low-molecular-weight organic compounds (e.g., lactate or acetate) (He et al., 2002). Under certain conditions, a single terminal electron accepting process (TEAP) may dominate in groundwater since the supply of oxygen is often limited, leading to predominantly anoxic conditions. Due to the often overlapping redox zones driven by the natural heterogeneity of the systems, the occurrence of simultaneous redox processes creates a complex yet rich chemical framework for the natural attenuation of contaminants in groundwater (Christensen et al., 2001).

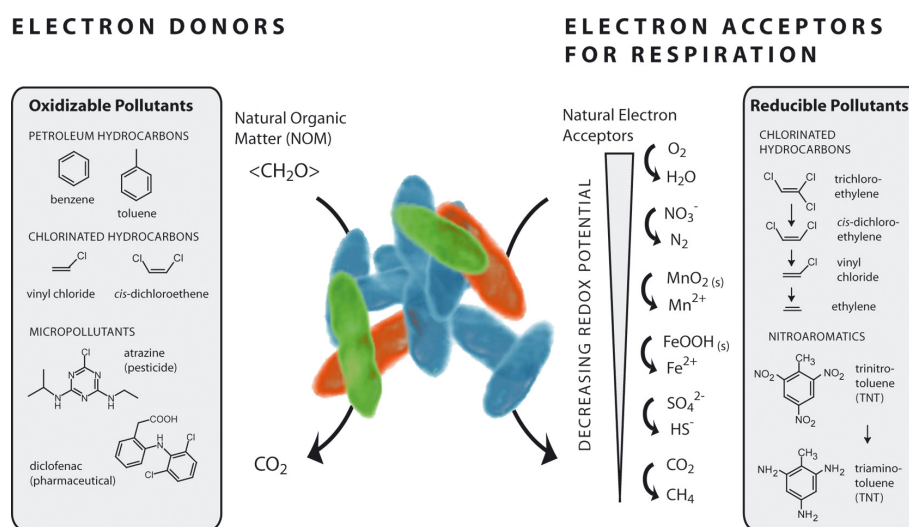


**Figure 1.5:** Scheme of microbially-mediated redox reactions for organic-rich substrates such as natural organic matter (NOM), as well as organic contaminants. *Adapted from Meckenstock et al. (2015).*

The description of mixing-controlled processes occurring at the plume fringe brought forward a better understanding of the interplay of dynamic hydrogeological conditions on natural attenuation processes (Christensen et al., 2001; Meckenstock et al., 2015). Indeed, redox reactions within a contaminant plume are primarily limited by the diffusive flux driven by transverse dispersion (Section 1.3), where soluble electron acceptors such as O<sub>2</sub>, NO<sub>3</sub><sup>-</sup> and SO<sub>4</sub><sup>2-</sup> diffuse inwards from the surrounding groundwater and are made available for microorganisms to support degradation processes (Rolle et al., 2008) (Figure 1.6). Thus, the plume fringe (i.e., the

transition zone between the contaminant plume and the ambient groundwater) is recognized as a potential hotspot for microbial activity due to continuous replenishment of available electron acceptors (e.g.,  $O_2$ ,  $NO_3^-$ ) (Meckenstock et al., 2015).

The establishment of steep hydrogeochemical gradients at the contaminant plume fringe and mixing (transition) zones (Section 1.4) was also correlated with an increase in biomass and biodegradation rates using mathematical models (Eckert et al., 2015; Rolle et al., 2008), laboratory experiments (Bauer et al., 2008; Thullner et al., 2007), and field studies (Anneser et al., 2008; Christensen et al., 2001; Grossman et al., 2002; van Breukelen and Griffioen, 2004). Hence, the spatial distribution of biodegradation reactions will be driven not only by mixing-controlling processes, but also by the availability of electron acceptors, organic substrates and nutrients, the toxicity of the target contaminant, and microbial growth and kinetics of the degradation reactions (Meckenstock et al., 2015; Rolle et al., 2008). Thus, integrating high-resolution hydrochemical monitoring across contaminant plumes can help to interpret the redox controlled biodegradation reactions affecting overall transformation rates and mechanisms of organic pollutants in groundwater.

### 1.5.2 Bacterial dynamics during pollutants degradation

The establishment of redox conditions in aquifers provides a major control on the types of reactions and microorganisms that can reside in that particular environment (Meile and Scheibe, 2019). In subsurface environments, including the saturated zone, capillary fringe and vadose zone, microbial communities mainly consist of *bacteria* which can be present in two distinct phases: as free-living (planktonic) and associated with a surface (i.e., biofilm; Figure 1.6) (Griebler and Lueders, 2009; Smith et al., 2018). Significant differences in bacterial community composition, structure and activity between free-living and attached bacteria are commonly accepted (Lehman et al., 2001; Smith et al., 2018). However, most environmental studies examining biodegradation processes mainly focus on the activity of planktonic groundwater bacterial communities.

Bacterial survival is essential to cope with the presence of toxic compounds under highly dynamic hydrogeological conditions. Bacteria can develop efficient adaptation mechanisms to ensure their necessary physiological functions and thus preservation of groundwater ecosystems (Murínová and Dercová, 2014). The surface bacterial structures, cell walls and cytoplasmic membranes surrounding each bacterial cell creates a first selective barrier between the cell interior and the surrounding environment (Murínová and Dercová, 2014). Thus, the most adaptive

bacterial mechanisms concerns the maintenance of their outer cell membrane fluidity to regulate or impede the mass transfer of toxic contaminants across the cell (Ehrl et al., 2018; Murínová and Dercová, 2014). Globally, the term adaptation mainly refers to phenomena that may take place both in individual cells and at the community level undergoing a series of enzyme induction processes, resulting in possibly biochemical changes to initiate biodegradation of a specific substrate (Poursat et al., 2019b).

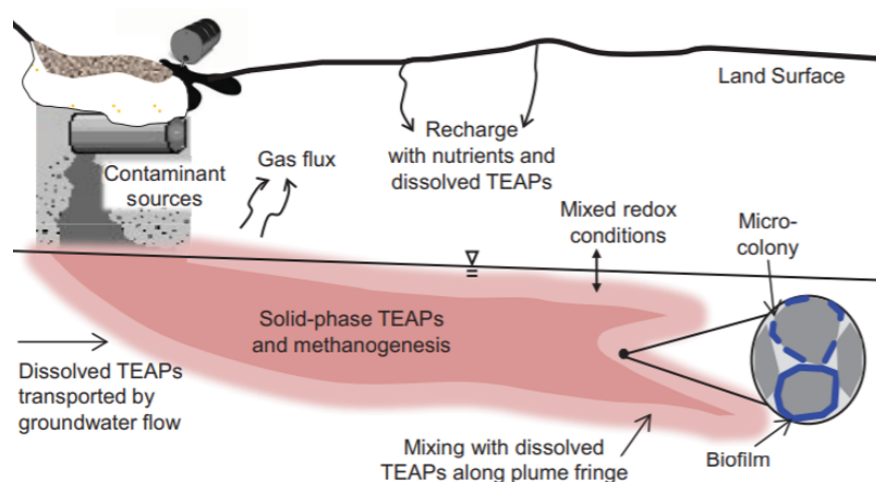


**Figure 1.6:** A generalized vertical cross section illustrating processes influencing the transport and fate of an organic contaminant plume. Adapted from Essaid et al. (2015).

### 1.5.3 Bacterial growth and related degradation kinetics

The link between bacterial growth and biodegradation kinetics has been the subject of numerous studies to unravel the main factors controlling pollutant biodegradation (Fenner et al., 2021; Grösbacher et al., 2018; Meckenstock et al., 2015). Growth-linked biodegradation kinetics are given by the substrate availability either in the bulk liquid or surrounding the biofilms (Kovárová-Kovar and Egli, 1998). Here, the type of contamination, i.e., point-source *versus* diffuse contamination, will result in distinct impacts on the bacterial growth and evolution and, in turn, on biodegradation kinetics (Griebler and Lueders, 2009). For instance, legacy contaminants such as Cl-VOCs are typically present in high concentrations at contaminant plumes (i.e., high substrate availability), where they can be metabolically degraded (i.e., used as sources of carbon or other nutrients) and, according to the established redox conditions, selection for microorganisms and evolution of degradation pathways may occur (Fenner et al., 2021) (Table 1.6). With the implementation of biomolecular tools (Section 1.5.4 and Table 1.4), the identification of specific degraders, metabolic pathways, and enzyme purification and characterization through

laboratory assays has brought forward important knowledge on the complex interactions during bacterial growth-linked degradation reactions.

To date, biodegradation of micropollutants in groundwater is far less understood, with only few specific degraders and functional genes so far identified (Table 1.4). Because micropollutants are present in the  $\text{ng L}^{-1}$  to  $\mu\text{g L}^{-1}$  range, this results in low concentrations in the bulk liquid next to the bacterial cell, resulting in possibly insufficient substrate uptake (bioavailability) (Fenner et al., 2021; Thullner et al., 2008). This raises concerns about the persistence of micropollutants at trace levels (Ehrl et al., 2018, 2019; Sun et al., 2021a), and calls for advanced studies to elucidate the underlying mechanisms for micropollutants biotransformation. Currently, research efforts are devoted to understand the selective pressure of micropollutants on the response of the bacterial community dynamics. Indeed, micropollutants are suggested to be co-metabolically transformed, i.e., active enzymes may no longer be harbored by a single microorganism only, but may be distributed over the bacterial community (Fenner et al., 2021; Imfeld and Vuilleumier, 2012). Hence, understanding the interplay of environmental conditions (e.g., the presence of a co-substrate such as natural organic matter, variable micropollutants loadings, water table fluctuations, etc.) on the overall bacterial community is essential toward a more comprehensive understanding of the biodegradation of micropollutants in dynamic hydrogeological systems.

### 1.5.4 Biomolecular markers for assessing pollutant biodegradation

Advances in biomolecular techniques such as high throughput DNA sequencing (Illumina, Nanopore, etc.) are becoming essential tools for assessing biodegradation potential of organic pollutants in contaminated aquifers (Hellal et al., 2021; Hermon et al., 2018; Imfeld et al., 2018; Wright et al., 2017). Sequencing of DNA or mRNA pools of a bacterial community, namely metagenomic or metatranscriptomic sequencing, respectively, allows to examine the metabolic and biochemical capacities of individual populations or bacterial communities, and elucidate active biotransformation functions (Fenner et al., 2021). In addition, (meta)proteomics can help to define whether a present degradation pathway is active through active enzymes counting and the expression of individual genes (Kleiner, 2019). In addition, the incorporation of isotopically labeled substrates in laboratory assays or *in situ* experiments may help determining carbon sources of individual microorganisms in bacterial communities, as well as carbon assimilation pathways used by autotrophic microorganisms (Fischer et al., 2016; Kleiner, 2019).

**Table 1.4:** State of the art of biomolecular markers for assessing natural attenuation of groundwater contaminants. *Adapted from Elsner and Imfeld (2016) and Imfeld and Vuilleumier (2012).*

	Legacy contaminants (Cl-VOCs)	Micropollutants/ Emerging contaminants
Current situation	* Bioindicators of aquifer conditions based on bacterial communities * Key dehalogenases and dehalogenation-associated taxa: indicators of biodegradation	* Reference degrading strains: not available * Functional genes for degradation: not known
Main blindspots of microbial markers	* Adaptation to toxicity and activity regulation: overlooked properties of degrading strains * Imperfect correlation: Key dehalogenases/dehalogenation-associated taxa/degradation	* Most genes in metagenomes: not annotated * Many genes encode functions not reflected by their annotation
Opportunities	* New functional gene biomarkers to come – particularly for anaerobic environments * Potential effect and importance of other taxa for organohalide respiration activity?	* Bioindicators of toxicity based on bacterial community dynamics * Coupling kingdoms (fungi, protists) * Analytical and isotopic analyses indicate biological degradation

The isolation, identification and follow-up of degrading strains and biomolecular markers (i.e., taxa associated with pollutant degradation and genes involved in degradation) have led to unprecedented knowledge on pollutant biodegradation pathways and mechanisms (Table 1.4). For instance, biodegradation of DCM has been evidenced under oxic conditions by methylophilic bacteria belonging to the *Hyphomicrobium* genus, notably *Hyphomicrobium* sp. strain GJ21 (Bringel et al., 2017; Nikolausz et al., 2006), and under anoxic conditions by *Dehalobacterium formicoaceticum* (Mägli et al., 1998, 1996), mixed consortiums containing *Dehalobacter* (Lee et al., 2012) and *Dehalobacterium* spp. (Blázquez-Pallí et al., 2019), and the yet to be isolated *Candidatus* Dichloromethanomonas elyunquensis (Kleindienst et al., 2019, 2017) and *Candidatus* Formimonas warabiya (Holland et al., 2021).

In contrast, few microorganisms have been identified for micropollutants biotransformation. For instance, atrazine biodegradation has been shown by *Arthrobacter aurescens* TC1 which can grow on atrazine both as C and N source, and has been suggested to degrade other s-triazine herbicides detected in the environment (Kundu et al., 2019). To date, knowledge gaps remain for a wide range of yet unidentified taxa associated with micropollutants biodegradation capacity. Hence, understanding adaptive mechanisms at the bacterial community level in response to dis-



turbances by the presence of micropollutants is of relevance for adequate remediation strategies of aquifers impacted by the presence of micropollutants (Imfeld and Vuilleumier, 2012). Recently, high throughput sequencing (e.g., 16S rRNA gene sequencing) has been used to examine the response of soil and groundwater bacterial communities exposed to micropollutants, including *S-metolachlor* (Imfeld et al., 2018; Torabi et al., 2020), metformin (Poursat et al., 2019a), and metalaxyl (Wang et al., 2019). More recently, the effect of micropollutants as chemical mixtures has been examined in stream water and the hyporheic zone, providing insights into more realistic scenarios on their environmental fate (Jaeger et al., 2019; Posselt et al., 2020; Rutere et al., 2020; Tamminen et al., 2022).

In this context, the implementation of biomolecular markers (e.g., 16S rRNA gene sequencing) to assess pollutant biodegradation has further proven advantageous in combination with stable isotope analysis (Section 1.6), providing a more robust evidence of the extent and pathway of pollutant biodegradation at contaminated sites, notably for legacy groundwater contaminants (Table 1.4).

### **1.6 Assessment of organic pollutant degradation using compound-specific isotope analysis (CSIA)**

Contaminants in groundwater are subjected to the simultaneous occurrence of non-destructive (e.g., dispersion, volatilization, sorption) and destructive processes (e.g., abiotic reactions, biodegradation), both affecting overall contaminant dissipation (Section 1.3). Appropriate monitoring tools are required to evaluate the contribution of degradation to overall dissipation, and to distinguish degradation from non-destructive processes (Kuntze et al., 2019). In addition to conventional methods such as quantification of contaminant concentrations and transformation products, compound-specific isotope analysis (CSIA) has proven to be an effective tool to (i) evaluate the extent of *in situ* degradation processes, (ii) identify contaminant sources, (iii) evidence the occurrence of degradation independently from non-destructive processes, and (iv) tease apart underlying abiotic and biotic degradation pathways and mechanisms (Hunkeler et al., 2009a; Kuntze et al., 2019; Meckenstock et al., 2004; Thullner et al., 2012).

#### **Principles of CSIA**

Isotopes of the same element have the same number of protons but vary in the number of neutrons and therefore they have different masses (Figure 1.7). In the context of assessment of natural attenuation of organic pollutants, the focus is given to naturally stable isotopes, such as

carbon and hydrogen, and additional elements including chlorine, bromine, nitrogen, oxygen or sulfur present in the target contaminant molecule (Kuntze et al., 2019). All these elements exhibit at least two stable isotopes (Figure 1.7). Contaminant molecules containing different numbers of heavy and light isotopes inside their structure are denoted as isotopologues (Elsner and Hunkeler, 2008).

The isotopic composition of an organic compound (e.g.,  $^{13}\text{C}/^{12}\text{C}$ ,  $^{15}\text{N}/^{14}\text{N}$  or  $^{37}\text{Cl}/^{35}\text{Cl}$ ) is expressed as delta notation ( $\delta$ ) relative to an international standard according to Eq. 1.1 (Coplen, 2011). For example, the international standard for carbon is V-PDB (Vienna-Pee Dee Belemnite;  $^{13}\text{C}/^{12}\text{C}$ ), atmospheric air for nitrogen ( $^{15}\text{N}/^{14}\text{N}$ ), and the Standard Mean Ocean Chloride (SMOC) for chlorine ( $^{37}\text{Cl}/^{35}\text{Cl}$ ) (Coplen, 2011; Kaufmann et al., 1984). Because variations in natural isotope abundance are typically small, the  $\delta$  values are mostly reported in per mil (‰) or milli-Urey (mUr) (Coplen, 2011).

$$\delta^h E = \left( \frac{R_{\text{sample}}}{R_{\text{standard}}} - 1 \right) \cdot 1000 \quad (1.1)$$

where  $R$  denotes the ratio of heavy to light isotopes of element  $E$  ( $R_{\text{sample}} = {}^h E / {}^l E$ ) of a sample (i.e., organic contaminant) or in a standard material ( $R_{\text{standard}}$ ). The normalization of measurements to a reference material allows for inter-comparison of results obtained in different laboratories (Elsner, 2010).

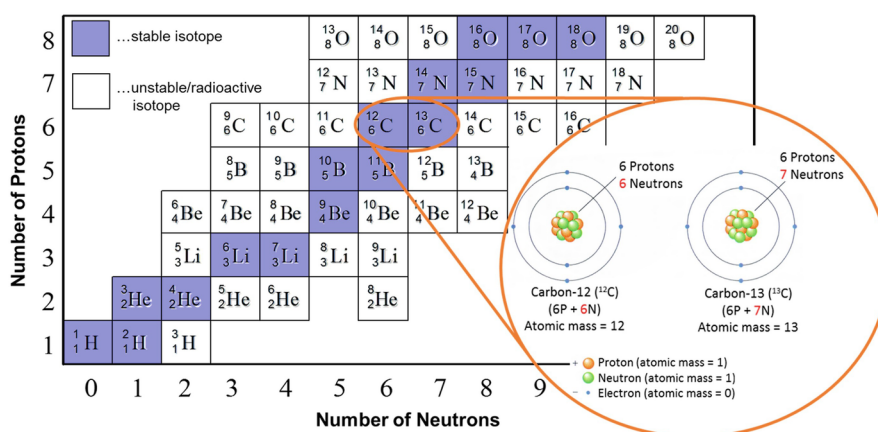


**Figure 1.7:** Overview on isotopes of chemical elements (H, He, Li, Be, B, C, N and O). Zoomed in: A simple atomic model of the two stable carbon isotopes based on their atomic masses. P, protons; N, neutrons. Adapted from Kuntze et al. (2019).

Gas chromatography-isotope ratio mass spectrometry (GC-IRMS) is mainly used to measure stable isotopes of individual organic pollutants by three main steps: (i) separation of individual carbon-bearing compounds (in the case of C-CSIA) on a gas chromatograph, (ii) quantitative

conversion of each compound to CO<sub>2</sub> in a high temperature combustion oven, and (iii) introduction and detection of the CO<sub>2</sub> derived from each compound into the mass spectrometer for isotopic analysis (Hunkeler et al., 2009a; Meckenstock et al., 2004). This principle is similarly followed for nitrogen-bearing compounds converted to N<sub>2</sub> (Berg et al., 2007), or chlorinated analytes converted into compounds containing only one chlorine atom (e.g., CsCl, CH<sub>3</sub>Cl) (Elsner and Hunkeler, 2008; Horst et al., 2017; Jin et al., 2011). In the case of chlorinated compounds, however, successful applications via conventional methods such as GC coupled with a quadrupole mass spectrometer (GC-qMS) have been demonstrated based on ion-current ratios of molecular/fragment ions (Elsner and Hunkeler, 2008; Jin et al., 2011; Ponsin et al., 2019; Renpenning et al., 2014).

The complete conversion of the target contaminant during combustion has important implications for CSIA applications. First, the molecules are combusted (e.g., CO<sub>2</sub> or NO<sub>2</sub>) to obtain an average isotopic signature meaning that with increasing molecule size (e.g., molecules with >12 C atoms), dilution of the isotopic effect may hamper adequate evaluation of biodegradation (Elsner, 2010). Second, various reactive positions may exist in a single molecule in which the position-specific information gets lost in the compound average isotopic signature (Elsner, 2010). However, the latter can be overcome by correcting bulk enrichment factors ( $\epsilon_{bulk}^E$ ) by approximating the atoms located at the reactive site relative to the total number of atoms of the element considered (Elsner et al., 2005). Finally, to ensure successful CSIA applications an optimal range of concentrations should be established by sufficient collection of sampling volumes, pre-concentration steps, and cleanup techniques to remove or reduce matrix effects (Kuntze et al., 2019). This is particularly challenging for micropollutants present at very low concentrations (Elsner and Imfeld, 2016).

### Isotope fractionation and interpretation of CSIA data

(Bio)degradation reactions involving bond cleavage generally lead to a fractionation of stable isotopes, i.e., a change in isotope ratios or  $\delta$  values. This isotope fractionation is caused by a kinetic isotope effect (KIE) (Elsner, 2010). KIEs depend on rate differences for the cleavage of chemical bonds containing light isotopes compared to those containing heavy isotopes. Due to the preferential transformation of the lighter isotope species (e.g., <sup>12</sup>C, <sup>14</sup>N or <sup>35</sup>Cl), compounds bearing a heavy isotope (e.g., <sup>13</sup>C, <sup>15</sup>N or <sup>37</sup>Cl) will accumulate in the residual fraction of the contaminant (normal isotope effect). This KIE results in an enrichment of heavy isotopes in the non-degraded residual fraction of the pollutant, leading to changes in the isotope ratio toward

more positive  $\delta$  values (Fischer et al., 2016; Kuntze et al., 2019) (Figure 1.8)). In few cases, degradation of pollutants leads to an enrichment of light isotopes (e.g.,  $^{14}\text{N}$ ) in the non-degraded residual fraction (inverse isotope effect), which has been observed in few studies such as for nitrogen isotope fractionation of atrazine by *Polaromonas* sp. Nea-C in chemostat experiments (Ehrl et al., 2018).

To assess pollutant degradation at contaminated field sites and/or laboratory experiments, isotope fractionation associated with processes other than (bio)degradation should be well understood. However, it has been suggested that isotope fractionation due to (bio)degradation is typically larger than for physical processes such as sorption (Höhener and Yu, 2012; Imfeld et al., 2014; Kopinke et al., 2005; Wanner et al., 2017), water-air partitioning (Horst and Lacrampe-Couloume, 2020; Jeannotat and Hunkeler, 2012, 2013; Kuder et al., 2009), and diffusion in both water and gas phases (Bouchard et al., 2008; Horst and Lacrampe-Couloume, 2020; Jeannotat and Hunkeler, 2012, 2013; Kopinke et al., 2017; Kuder et al., 2009; Rolle et al., 2013; Sun et al., 2021b; Wanner and Hunkeler, 2019).

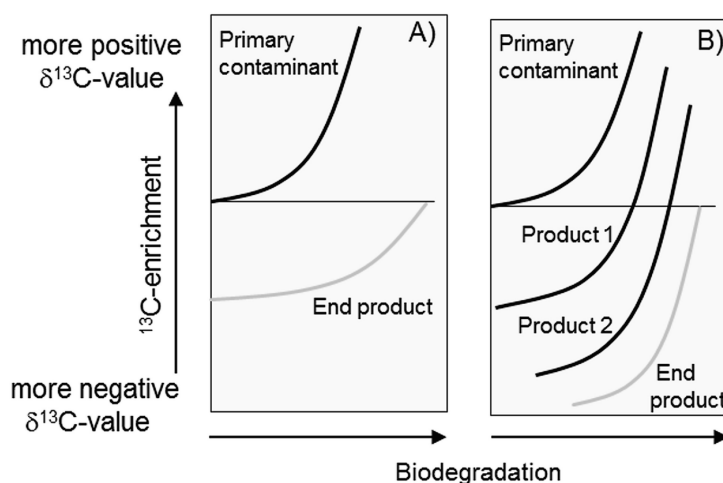


**Figure 1.8:** Evolution of stable carbon isotope ratios during (a) degradation with negligible accumulation of transformation products, and (b) transformation chain: degradation with significant accumulation of transformation products (e.g., reductive dechlorination of TCE to ethene). Adapted from Fischer et al. (2016).

Determining stable isotope fractionation can thus be used for quantitative estimations of contaminant transformation following the Rayleigh equation (Elsner, 2010):

$$\ln \left( \frac{R_{t,E}}{R_{0,E}} \right) = \ln \left( \frac{C_t}{C_0} \right) \cdot \frac{\varepsilon_{bulk}^E}{1000} \quad (1.2)$$

where  $R_{t,E}/R_{0,E}$  is the isotope ratio of element  $E$  (i.e.,  $^{13}\text{C}/^{12}\text{C}$  or  $^{37}\text{Cl}/^{35}\text{Cl}$ ) and  $C_t/C_0$  are the

concentrations of an organic contaminant at a given time (t) and at the initial time (0). Isotope enrichment factors ( $\varepsilon_{bulk}^E$ , in ‰) may thus be obtained in laboratory experiment and used for quantitative estimations of contaminant transformation *in situ* (Fischer et al., 2016).

The extent of (bio)degradation (in %) can be estimated between contaminant source zones ( $\delta^h E_0$ ) and downstream the contaminated aquifer ( $\delta^h E_t$ ) (i.e., 2 sampling points along the groundwater flow path) according to Eq. 1.3 (Hunkeler et al., 2005). For the selection of appropriate  $\varepsilon_{bulk}^E$  values, prior investigations on the hydrochemical conditions of the aquifer system, quantification of transformation products and identification of microorganisms associated with a specific degradation pathway have been recommended (Thullner et al., 2012).

$$B_E[\%] = 1 - f \cdot 100 = \left[ 1 - \left( \frac{\delta^h E_t + 1000}{\delta^h E_0 + 1000} \right)^{\frac{1000}{\varepsilon_{bulk}^E}} \right] \cdot 100 \quad (1.3)$$

Multi-element CSIA (ME-CSIA) involving the follow-up of changes in isotope ratios of two elements or more (e.g.,  $^{13}\text{C}/^{12}\text{C}$  vs  $^{37}\text{Cl}/^{35}\text{Cl}$  or  $^{15}\text{N}/^{14}\text{N}$ ), results more advantageous over a single isotope element approach to evaluate transformation pathways of organic contaminants (Höhener and Imfeld, 2021; Ojeda et al., 2020). When the stable isotope ratios of two elements (dual-CSIA) are compared in a dual plot, the slope ( $\Lambda$ ) provides a quantitative parameter of the corresponding transformation pathway (Elsner, 2010; Ojeda et al., 2020), and allows to tease apart degradation pathways and mechanisms (e.g., anaerobic *versus* aerobic degradation pathways, biotic *versus* abiotic reactions).

$$\Lambda^{C/Cl} = \frac{\ln[(\delta^{13}\text{C}_t/1000 + 1)/(\delta^{13}\text{C}_0/1000 + 1)]}{\ln[(\delta^{37}\text{Cl}_t/1000 + 1)/(\delta^{37}\text{Cl}_0/1000 + 1)]} = \frac{\varepsilon_{bulk}^C}{\varepsilon_{bulk}^{Cl}} \quad (1.4)$$

In recent years, ME-CSIA has received attention to derive abiotic and biotic reaction pathways and mechanisms, especially for halogenated hydrocarbons (Audí-Miró et al., 2013; Chen et al., 2018; Franke et al., 2020; Palau et al., 2017; Wiegert et al., 2012, 2013). Table 1.5 shows the state of the art of recent applications of ME-CSIA, in combination with biomolecular markers (Section 1.5.4), to infer degradation pathways and mechanisms of Cl-VOCs in contaminated aquifers. Furthermore, the implementation of ME-CSIA in field studies has proven useful to identify undergoing Cl-VOCs degradation pathways (Blázquez-Pallí et al., 2019; Hunkeler et al., 2011; Palau et al., 2016; Wiegert et al., 2012, 2013), and underscores CSIA as a powerful line of evidence on the occurrence and monitoring of biodegradation of legacy Cl-VOCs in contaminated aquifers. Finally, the integration of stable isotopes and biomolecular markers in reactive transport models (RTM) has proven valuable for better predicting pollutant biodegradation at contaminated sites (Section 1.7).

**Table 1.5:** Bulk carbon and chlorine isotope enrichment factors ( $\varepsilon_{bulk}^C$  and  $\varepsilon_{bulk}^{Cl}$ , respectively) and ME-CSIA slopes ( $\Lambda^{C/Cl}$ ) for biotic degradation of Cl-VOCs in laboratory microcosm studies.

	Culture (enzyme)	degradation mechanism/pathway	$\varepsilon_{bulk}^C$	$\varepsilon_{bulk}^{Cl}$	$\Lambda^{C/Cl}$	Reference
DCM	<i>Hyphomicrobium</i> sp. strain MC8b	Glutathione S-transferase	-42.4	-3.8	11.2	Hayoun et al. (2020); Heraty et al. (1999)
DCM	<i>Methylobacterium extorquens</i> DM4	Glutathione S-transferase	-71±2.0	-7.0±0.4	9.5±0.54	Torgonskaya et al. (2019)
DCM	<i>Hyphomicrobium</i> sp.	Glutathione S-transferase	-22 to -46	-	-	Hermon et al. (2018)
DCM	<i>Dehalobacterium formicoaceticum</i>	Fermentation harboring WLP	-42.4±0.7	-5.3±0.1	7.8±0.1	Chen et al., 2018, 2020
DCM	Mixed culture containing <i>Dehalobacterium</i> sp.	Fermentation	-31±3	-5.2±0.6	5.9±0.3	Blázquez-Pallí et al. (2019)
DCM	Consortium RM harboring <i>Ca. Dichloromethanomonas elyunquensis</i>	Mineralization (acetogenesis required)	-18.3±0.2	-5.2±0.1	3.4±0.03	Chen et al. (2018)
DCM	Mixed culture containing <i>Dehalobacter</i> sp. (DCMD)	Fermentation	-16±2	-	-	Lee et al. (2015)
PCE	<i>Clostridium</i> sp., <i>Desulfotobacterium aromaticivorans</i>	reductive dechlorination	-5.6±0.7	-2.0±0.5	2.9±0.9	Wiegert et al. (2013)
PCE	<i>Desulfotobacterium</i> sp.	reductive dechlorination	-19.0±0.9	-5.0±0.1	3.8±0.2	Cretnik et al. (2014)
TCE	<i>Dehalococcoides</i>	reductive dechlorination	-15.3 to -16.4±0.4	-3.6±0.3	4.8±0.2	Kuder et al. (2013)
TCE	<i>Geobacter lovleyi</i>	reductive dechlorination	-12.2±1.0	-3.6±0.1	3.4±0.2	Cretnik et al. (2014)
TCE	<i>Clostridium</i> sp., <i>Desulfotobacterium aromaticivorans</i>	reductive dechlorination	-8.8±0.2	-3.5±0.5	2.7±0.8	Wiegert et al. (2013)
cDCE	<i>Dehalococcoides</i>	reductive dechlorination	-18.5±1.8	-1.6±0.1	11.4±0.6	Abe et al. (2009)
cDCE	$\beta$ -Proteobacterium strain JS666	aerobic oxidation	-8.5±0.1	-0.3±0.07	32.3±6.4	Abe et al. (2009)
VC	<i>Dehalococcoides</i>	reductive dechlorination	-18.5±1.8	-1.6±0.1	11.4±0.6	Abe et al. (2009)
VC	$\beta$ -Proteobacterium strain JS666	aerobic oxidation	-25.0±0.7	-1.7±0.1	13.7±0.3	Abe et al. (2009)

For micropollutants biodegradation, however, only few studies have implemented ME-CSIA to characterize their relevant degradation mechanisms and pathways (Elsner and Imfeld, 2016). For instance, enrichment factors associated with biotic degradation of terbutryn, metformin and caffeine have not yet been reported. Despite the evident knowledge gap regarding micropollutants degradation and associated isotope fractionation, the lessons learnt from assessing natural attenuation of Cl-VOCs open the way for future research fields to exploit CSIA (including ME-CSIA) as a line of evidence for micropollutants transformation in groundwater, particularly considering the predominance of anaerobic transformation reactions in subsurface environments.

## **1.7 Reactive transport models to assist monitoring of in situ natural attenuation of organic pollutants**

Natural attenuation of organic pollutants relies primarily on biodegradation as the most important process for their sustainable removal at polluted sites (Section 1.5). Reactive transport models (RTMs) have been implemented to expand our understanding of the underlying physical and chemical processes that govern the transport and fate of organic pollutants in the subsurface. RTMs can translate the complex interplay of the physical and chemical processes occurring across multiple space and time scales through mathematical concepts (Kuder et al., 2016; Maher and Mayer, 2019). Generally, the reaction network can be built by considering (i) the presence of reactants (e.g., organic pollutants or redox species) and products (Section 1.5.1), (ii) stoichiometry of the chemical and microbial reactions (Section 1.5.2), (iii) growth-linked degradation kinetics (Section 1.5.3), and (iv) the thermodynamics of the redox zonation across the contaminant plume (Maher and Mayer, 2019). Thus, RTMs may define a good basis for predicting natural attenuation in contaminated aquifers by considering the interplay of hydrogeochemical, biological and hydrogeological conditions.

Together with the implementation of integrative concepts, including the definition of microbially-mediated reactions (Section 1.5) along with isotope fractionation resulting from contaminant (bio)degradation (Section 1.6), RTMs can help to bridge the gap on the controlling factors affecting the fate and transport of contaminants in groundwater (Kuder et al., 2016). Moreover, such integrative RTMs may improve site characterization by evidencing the existence of active biodegradation processes (or hotspots), and thus define the feasibility of current and future bioremediation strategies (Antelmi et al., 2021).

In the last two decades, a broad range of RTMs relying on analytical and/or numerical solutions have been applied to validate the concept of CSIA as a novel tool to assess natural attenuation of organic pollutants in aquifers, particularly for Cl-VOCs (e.g., reductive dechlorination of CEs) (Antelmi et al., 2021; Breukelen and Prommer, 2008; Höhener, 2016; Höhener and Atteia, 2010; Hunkeler et al., 2009b; Kuder et al., 2016; Van Breukelen et al., 2017). RTMs may also be based on a conceptual framework examining physical processes and their associated isotopic fractionation, such as sorption (Breukelen and Prommer, 2008; Eckert et al., 2013; Schürner et al., 2016; Wanner et al., 2017), transverse hydrodynamic dispersion (Breukelen and Prommer, 2008; Rolle et al., 2010; Van Breukelen and Rolle, 2012); diffusion in the aqueous (Jeannotat and Hunkeler, 2012, 2013; Wanner and Hunkeler, 2015) and gas phases (Bouchard et al., 2008; Jeannotat and Hunkeler, 2012, 2013), and water-air partitioning (Horst and Lacrampe-

Couloume, 2020; Jeannotat and Hunkeler, 2012, 2013; Kuder et al., 2009). Nevertheless, these physical processes are often associated with low to negligible isotopic fractionation compared to degradation reactions in the saturated zone (Section 1.6). Finally, the concept of CSIA was further validated through RTMs applications at the field scale (Antelmi et al., 2021; D’Affonseca et al., 2011; Wanner et al., 2018a,b) proving that CSIA can help to evidence biodegradation extent and pathways within complex hydrogeological systems. Nevertheless, most of the existing RTMs including isotope fractionation are devoted to CEs given the advanced knowledge on degradation mechanisms and pathways (Table 1.5). To date, biodegradation of DCM in anoxic contaminated aquifers have not yet been explored through integrative RTMS including available CSIA data.

It is also evident that microorganisms need to be represented in such RTMs, however, the manner and level of detail in which microbial activities are described may vary significantly (Meile and Scheibe, 2019). Globally, microbial activity is linked with substrate concentration, and can be expressed in the form of first-order or Michaelis-Menten kinetics. Nevertheless, such expressions do not explicitly represent the microorganisms behind the degradation reactions and assume that the entire microbial community is able to adapt to changing environmental conditions (Meile and Scheibe, 2019). For growth-linked biodegradation, Monod kinetics rather describe the link between growth and substrate utilization which may explicitly consider biomass growth of the microorganism (Kovárová-Kovar and Egli, 1998). Note that both terms, Monod and Michaelis-Menten, are often used interchangeably, although the latter describes degradation processes catalyzed by a single enzyme (Kovárová-Kovar and Egli, 1998).

As such, limitations of microbial growth related to substrate concentrations and the dependence of electron acceptors or donors are often introduced with a dual-Monod term (Rolle et al., 2008). This type of formulation allows building the sequential network between electron acceptors and donors in redox zonations (e.g., by including inhibition terms) (Section 1.5.1). Furthermore, by explicitly expressing the microbial populations other biological processes such as decay, attachment, detachment or dormancy may be considered which could affect biodegradation under dynamic biogeochemical conditions (Eckert et al., 2013; Hron et al., 2015). Similarly, the introduction of maintenance factors can be considered given that substrates may be utilized for other functions than new cell material (van Bodegom, 2007), particularly during initial adaptation phases (Kundu et al., 2019). In the case of micropollutants, only few integrative RTMs have been employed to examine reactive transport of micropollutants in aquifers (Schürner et al., 2016; Sun et al., 2021a). Here, the implementation of RTMs has underscore mass-transfer



limitations across the cells due to low bioavailability of micropollutants (Sun et al., 2021a).

Although the understanding of individual physical and chemical processes is advanced, their interactions are not yet fully understood, which challenge efficient reactive transport models (RTM) for predictive applications. In this context, the combination of biomolecular approaches with isotope measurements (CSIA) and numerical modeling may prove a powerful approach to improve predictions of natural attenuation of organic contaminants in dynamic hydrogeological systems. The type of contaminant and source zone will ultimately determine the necessary complexity of the RTMs to address the interplay of environmental conditions as a controlling factor on the removal of contaminants from groundwater systems.

### **1.8 Toward integrative approaches for comprehensive restauration of groundwater resources**

The almost ubiquitous presence of organic pollutants in groundwater has urged to improve cost-effective remediation strategies for the detoxification of contaminated aquifers through natural attenuation processes. The term natural attenuation thus covers all naturally occurring physical (advection-dispersion, volatilization, sorption), chemical (abiotic reaction with solids) and biological processes (microbial transformation) in aquifers that lead to the removal of contaminants (US EPA, 1999b; Wiedemeier et al., 1999) (Section 1.3). The design of reliable and cost-effective bioremediation techniques requires a thorough understanding of the controls and limitations of the biodegradation potential of bacterial communities in aquifers (Meckenstock et al., 2015). To derive the actual biodegradation potential under *in situ* conditions, integrative approaches are needed to decipher the interplay between contaminant transport, redox-controlled reactions, microbial growth and biodegradation of contaminants (Grösbacher et al., 2018).

Bioremediation of contaminated aquifers relies on the exploitation of microorganisms to break down the organic pollutants. Monitored natural attenuation (MNA) is a promising, cost-effective and minimal invasive *in-situ* bioremediation technique (US EPA, 1999b; Wiedemeier et al., 1999). However, due to quick response to protect sensible targets (e.g., protection of water supply wells) MNA is generally coupled with other active remediation processes (e.g., pump and treat procedures, permeable reactive barriers, etc.) and is often implemented for residual contaminations or low concentration plumes (Antelmi et al., 2021). MNA relies on an integrative approach, which includes (i) monitoring contaminant concentrations in the field and evolution of hydrochemical conditions, (ii) laboratory assays with microorganisms from the field, and (iii) evidence of *in situ* biodegradation potential (e.g., using stable isotope analysis

and/or biomolecular markers) (Hunkeler et al., 2009a; NRC, 2000). Alternatively, enhanced natural attenuation (ENA) is based on the alteration of environmental conditions of contaminated aquifers to increase microbial activity (Scow and Hicks, 2005). These technologies may involve the addition of electron acceptors and donors, as well as nutrients to stimulate naturally occurring microbial populations (biostimulation) or by introducing specific microorganisms to enhance the biodegradation of a target compound (bioaugmentation) (Scow and Hicks, 2005).

Despite our growing knowledge of individual processes involved in natural attenuation of contaminants in groundwater, we still lack a comprehensive framework to integrate the effect of hydrogeochemical variations associated with water table fluctuations and the dynamics of bacterial communities with regard to pollutant degradation extent and pathways (Section 1.4). In particular, the intrinsic heterogeneity and dynamics of groundwater ecosystems are often overlooked which hampers the predictability of biodegradation (Meckenstock et al., 2015). Few studies have focused on these spatial and temporal variations affecting pollutant biodegradation; however, these developments are often carried out in parallel and rarely in synergy. The combination of biomolecular markers, stable isotopes and modeling approaches may prove powerful tools for assessing the processes modulating the transformation of pollutants within dynamic hydrogeological systems. Due to the complexity of field conditions, laboratory aquifers have been of interest due to their feasibility to mimic *in situ* degradation of organic pollutants in groundwater (Bauer et al., 2008; Qiu et al., 2013; Rolle et al., 2010; Schürner et al., 2016; Sun et al., 2021a), and for facilitating mass balance calculations in reasonably controlled systems.

The recent progress on using integrative approaches in laboratory aquifers shed light on plume-fringe controlled processes (Bauer et al., 2008; Rolle et al., 2010), the effect of concentration dependent degradation kinetics (Qiu et al., 2013; Schürner et al., 2016), and the effect of bioavailability of micropollutants at low concentration levels (in the  $\mu\text{g L}^{-1}$  range) (Sun et al., 2021a). However, most of this recent work is often carried out on the basis of a single microbial population and/or distilled or synthetic water. Hence, the use of laboratory aquifers including the dynamics of *endogenous* bacterial populations from natural groundwater may bring novel insights into the underlying processes affecting overall bacterial communities during biodegradation processes in dynamic hydrogeological systems. Particularly for micropollutants biotransformation in near-surface aquifers, the evolution of bacterial populations in relation to contaminant exposure is poorly understood. Despite the knowledge gap on specific microorganisms capable of degrading micropollutants (Table 1.6), studies tackling the relationships between varying micropollutant exposures and their effect on the overall bacterial

communities may pave the way towards comprehensive concepts for the removal of emerging contaminants from groundwater. Finally, RTMs based on integrative experimental data may help to explore and infer biodegradation pathways and mechanisms affected during dynamic hydrogeological conditions.

**Table 1.6:** State of the art and implications of assessing natural attenuation of Cl-VOCs and micropollutants in groundwater. *Adapted from Elsner and Imfeld (2016).*

	Legacy contaminants (Cl-VOCs)	Micropollutants/ Emerging contaminants	Implications for assessing their natural attenuation
<b>Occurrence in the environment</b>			
Contaminant Source	Typically point- source (spillages, improper storage)	Typically diffuse (pesticides applications, WWTF effluents)	* Point-sources easier to conceptualise, monitor and predict. * Diffuse sources challenged by multiple pathways to groundwater.
Typical concentrations			
	mg L <sup>-1</sup>	<μg L <sup>-1</sup>	
Present in mixtures	Yes	Yes	
<b>Chemical Properties</b>			
Polarity			* Contaminant distribution among phases.
Volatility			* Validation of appropriate analytical methods (concentrations/CSIA).
Molecular size			
<b>Characteristics of biodegradation</b>			
Current knowledge	Often well-established	Often unknown	*Use of available biomarkers advantageous to infer degradation pathways.
Microorganisms involved	Often known	Often unknown	* ME-CSIA to evidence extent and degradation pathways.
Microbial metabolism	Metabolic: selective substrate use, induction of specific catabolic pathway	Potentially co-metabolic: non-selective transformation of substrates below induction threshold of catabolic pathways.	
Favorable conditions	often anoxic	often oxic	

## References of Chapter 1

- Abe, Y., Aravena, R., Zopfi, J., Shouakar-Stash, O., Cox, E., Roberts, J. D., and Hunkeler, D. (2009). Carbon and chlorine isotope fractionation during aerobic oxidation and reductive dechlorination of vinyl chloride and *cis*-1,2-dichloroethene. *Environmental Science & Technology*, 43(1):101–107.
- Anneser, B., Einsiedl, F., Meckenstock, R. U., Richters, L., Wisotzky, F., and Griebler, C. (2008). High-resolution monitoring of biogeochemical gradients in a tar oil-contaminated aquifer. *Applied Geochemistry*, 23(6):1715–1730.
- Antelmi, M., Mazzon, P., Höhener, P., Marchesi, M., and Alberti, L. (2021). Evaluation of MNA in a chlorinated solvents-contaminated aquifer using reactive transport modeling coupled with isotopic fractionation analysis. *Water*, 13(21):2945.
- ATSDR (2019). Substance priority list. Accessed: 2022-01-20.
- Audí-Miró, C., Cretnik, S., Otero, N., Palau, J., Shouakar-Stash, O., Soler, A., and Elsner, M. (2013). Cl and C isotope analysis to assess the effectiveness of chlorinated ethene degradation by zero-valent iron: Evidence from dual element and product isotope values. *Applied Geochemistry*, 32:175–183.
- aus der Beek, T., Weber, F.-A., Bergmann, A., Hickmann, S., Ebert, I., Hein, A., and Küster, A. (2016). Pharmaceuticals in the environment – Global occurrences and perspectives. *Environmental Toxicology and Chemistry*, 35(4):823–835.
- Baran, N., Surdyk, N., and Auterives, C. (2021). Pesticides in groundwater at a national scale (France): Impact of regulations, molecular properties, uses, hydrogeology and climatic conditions. *Science of The Total Environment*, 791:148137.
- Barbosa, M. O., Moreira, N. F. F., Ribeiro, A. R., Pereira, M. F. R., and Silva, A. M. T. (2016). Occurrence and removal of organic micropollutants: An overview of the watch list of EU decision 2015/495. *Water Research*, 94:257–279.
- Bauer, R. D., Maloszewski, P., Zhang, Y., Meckenstock, R. U., and Griebler, C. (2008). Mixing-controlled biodegradation in a toluene plume – Results from two-dimensional laboratory experiments. *Journal of Contaminant Hydrology*, 96(1):150–168.
- Berg, M., Bolotin, J., and Hofstetter, T. B. (2007). Compound-specific nitrogen and carbon isotope analysis of nitroaromatic compounds in aqueous samples using solid-phase microextraction coupled to GC/IRMS. *Analytical Chemistry*, 79(6):2386–2393.
- Blázquez-Pallí, N., Shouakar-Stash, O., Palau, J., Trueba-Santiso, A., Varias, J., Bosch, M., Soler, A., Vicent, T., Marco-Urrea, E., and Rosell, M. (2019). Use of dual element isotope analysis and microcosm studies to determine the origin and potential anaerobic biodegradation of dichloromethane in two multi-contaminated aquifers. *Science of The Total Environment*, 696:134066.

- Bollmann, U. E., Fernández-Calvino, D., Brandt, K. K., Storgaard, M. S., Sanderson, H., and Bester, K. (2017). Biocide runoff from building facades: Degradation kinetics in soil. *Environmental Science & Technology*, 51(7):3694–3702.
- Bouchard, D., Höhener, P., and Hunkeler, D. (2008). Carbon isotope fractionation during volatilization of petroleum hydrocarbons and diffusion across a porous medium: A column experiment. *Environmental Science & Technology*, 42(21):7801–7806.
- Boulton, A. J., Datry, T., Kasahara, T., Mutz, M., and Stanford, J. A. (2010). Ecology and management of the hyporheic zone: Stream-groundwater interactions of running waters and their floodplains. *Journal of the North American Benthological Society*, 29(1):26–40.
- Bradley, P. M. (2000). Microbial degradation of chloroethenes in groundwater systems. *Hydrogeology Journal*, 8(1):104–111.
- Bradley, P. M., Journey, C. A., Button, D. T., Carlisle, D. M., Clark, J. M., Mahler, B. J., Nakagaki, N., Qi, S. L., Waite, I. R., and VanMetre, P. C. (2016). Metformin and other pharmaceuticals widespread in wadeable streams of the Southeastern United States. *Environmental Science & Technology Letters*, 3(6):243–249.
- Bradley, P. M., Journey, C. A., Romanok, K. M., Breitmeyer, S. E., Button, D. T., Carlisle, D. M., Huffman, B. J., Mahler, B. J., Nowell, L. H., Qi, S. L., et al. (2021). Multi-region assessment of chemical mixture exposures and predicted cumulative effects in USA wadeable urban/agriculture-gradient streams. *Science of the Total Environment*, 773:145062.
- Breukelen, B. M. V. and Prommer, H. (2008). Beyond the Rayleigh equation: Reactive transport modeling of isotope fractionation effects to improve quantification of biodegradation. *Environmental Science & Technology*, 42(7):2457–2463.
- Bringel, F., Postema, C. P., Mangenot, S., Bibi-Triki, S., Chaignaud, P., Farhan Ul Haque, M., Gruffaz, C., Hermon, L., Louhichi, Y., Maucourt, B., Muller, E. E. L., Nadalig, T., Lajus, A., Rouy, Z., Médigue, C., Barbe, V., Janssen, D. B., and Vuilleumier, S. (2017). Genome sequence of the dichloromethane-degrading bacterium *Hyphomicrobium* sp. strain GJ21. *Genome Announcements*, 5(30):e00622–17.
- Burri, N. M., Weatherl, R., Moeck, C., and Schirmer, M. (2019). A review of threats to groundwater quality in the anthropocene. *Science of the Total Environment*, 684:136–154.
- Chapelle, F. H. (1996). Identifying redox conditions that favor the natural attenuation of chlorinated ethenes in contaminated ground-water systems. *Symposium on Natural Attenuation of Chlorinated Organics in Groundwater: EPA/540/R-96/509. US EPA, Washington, DC*, pages 17–22.
- Chapelle, F. H., Bradley, P. M., Lovley, D. R., and Vroblesky, D. (1996). Measuring rates of biodegradation in a contaminated aquifer using field and laboratory methods. *Ground Water*, 34(4):691–698.
- Chen, G., Fisch, A. R., Gibson, C. M., Erin Mack, E., Seger, E. S., Campagna, S. R., and Löffler, F. E. (2020). Mineralization versus fermentation: Evidence for two distinct anaerobic bacterial degradation pathways for dichloromethane. *The ISME Journal*, 14(4):959–970.
- Chen, G., Shouakar-Stash, O., Phillips, E., Justicia-Leon, S. D., Gilevska, T., Sherwood Lollar, B., Mack, E. E., Seger, E. S., and Löffler, F. E. (2018). Dual carbon-chlorine isotope analysis indicates distinct anaerobic dichloromethane degradation pathways in two members of *Peptococcaceae*. *Environmental Science & Technology*, 52(15):8607–8616.

- Christensen, T. H., Kjeldsen, P., Bjerg, P. L., Jensen, D. L., Christensen, J. B., Baun, A., Albrechtsen, H.-J., and Heron, G. (2001). Biogeochemistry of landfill leachate plumes. *Applied geochemistry*, 16(7-8):659–718.
- Chu, M., Kitanidis, P. K., and McCarty, P. L. (2005). Modeling microbial reactions at the plume fringe subject to transverse mixing in porous media: When can the rates of microbial reaction be assumed to be instantaneous?: Microbial reaction subject to transverse mixing. *Water resources research*, 41(6).
- Cirpka, O. A. (2015). Transverse mixing in heterogeneous aquifers. *Procedia Environmental Sciences*, 25:66–73.
- Commission, E. (2013). Priority substances and certain other pollutants according to Annex II of Directive 2008/105/EC - Environment – European Commission.
- Conant, B., Robinson, C. E., Hinton, M. J., and Russell, H. A. J. (2019). A framework for conceptualizing groundwater-surface water interactions and identifying potential impacts on water quality, water quantity, and ecosystems. *Journal of Hydrology*, 574:609–627.
- Coplen, T. B. (2011). Guidelines and recommended terms for expression of stable-isotope-ratio and gas-ratio measurement results. *Rapid Communications in Mass Spectrometry*, 25(17):2538–2560.
- Cretnik, S., Bernstein, A., Shouakar-Stash, O., Löffler, F., and Elsner, M. (2014). Chlorine isotope effects from isotope ratio mass spectrometry suggest intramolecular c-cl bond competition in trichloroethene (TCE) reductive dehalogenation. *Molecules*, 19(5):6450–6473.
- D’Affonseca, F., Prommer, H., Finkel, M., Blum, P., and Grathwohl, P. (2011). Modeling the long-term and transient evolution of biogeochemical and isotopic signatures in coal tar-contaminated aquifers. *Water Resources Research*, 47(5).
- Damalas, C. A. and Koutroubas, S. D. (2016). Farmers’ exposure to pesticides: Toxicity types and ways of prevention. *Toxics*, 4(1):1.
- Dash, S. S. and Gummadi, S. N. (2006). Catabolic pathways and biotechnological applications of microbial caffeine degradation. *Biotechnology Letters*, 28(24):1993–2002.
- DiStefano, T. D., Gossett, J. M., and Zinder, S. H. (1991). Reductive dechlorination of high concentrations of tetrachloroethene to ethene by an anaerobic enrichment culture in the absence of methanogenesis. *Applied and Environmental Microbiology*, 57(8):2287–2292.
- DiStefano, T. D., Gossett, J. M., and Zinder, S. H. (1992). Hydrogen as an electron donor for dechlorination of tetrachloroethene by an anaerobic mixed culture. *Applied and Environmental Microbiology*, 58(11):3622–3629.
- Dolinová, I., Štrojsová, M., Černík, M., Němeček, J., Macháčková, J., and Ševcu, A. (2017). Microbial degradation of chloroethenes: a review. *Environmental Science and Pollution Research*, 24(15):13262–13283.
- Drouin, G., Fahs, M., Droz, B., Younes, A., Imfeld, G., and Payraudeau, S. (2021). Pollutant dissipation at the sediment-water interface: A robust discrete continuum numerical model and recirculating laboratory experiments. *Water Resources Research*, 57(3):e2020WR028932.
- Droz, B. (2020). *Pesticides dissipation at the sediment-water interface: insight from compound-specific isotope analysis (CSIA)*. Doctoral thesis, University of Strasbourg.
- Droz, B., Drouin, G., Maurer, L., Villette, C., Payraudeau, S., and Imfeld, G. (2021). Phase transfer and biodegradation of pesticides in water-sediment systems explored by compound-specific isotope analysis and conceptual modeling. *Environmental Science & Technology*, 55(8):4720–4728.

- Eckert, D., Kürzinger, P., Bauer, R., Griebler, C., and Cirpka, O. A. (2015). Fringe-controlled biodegradation under dynamic conditions: Quasi 2-D flow-through experiments and reactive-transport modeling. *Journal of Contaminant Hydrology*, 172:100–111.
- Eckert, D., Qiu, S., Elsner, M., and Cirpka, O. A. (2013). Model complexity needed for quantitative analysis of high resolution isotope and concentration data from a toluene-pulse experiment. *Environmental Science & Technology*, 47(13):6900–6907.
- Ehrl, B. N., Gharasoo, M., and Elsner, M. (2018). Isotope fractionation pinpoints membrane permeability as a barrier to atrazine biodegradation in gram-negative *Polaromonas* sp. Nea-C. *Environmental Science & Technology*, 52(7):4137–4144.
- Ehrl, B. N., Kundu, K., Gharasoo, M., Marozava, S., and Elsner, M. (2019). Rate-limiting mass transfer in micropollutant degradation revealed by isotope fractionation in chemostat. *Environmental Science & Technology*, 53(3):1197–1205.
- Elsner, M. (2010). Stable isotope fractionation to investigate natural transformation mechanisms of organic contaminants: Principles, prospects and limitations. *Journal of Environmental Monitoring*, 12(11):2005–2031.
- Elsner, M. and Hunkeler, D. (2008). Evaluating chlorine isotope effects from isotope ratios and mass spectra of polychlorinated molecules. *Analytical Chemistry*, 80(12):4731–4740.
- Elsner, M. and Imfeld, G. (2016). Compound-specific isotope analysis (CSIA) of micropollutants in the environment – Current developments and future challenges. *Current Opinion in Biotechnology*, 41:60–72.
- Elsner, M., Zwank, L., Hunkeler, D., and Schwarzenbach, R. P. (2005). A new concept linking observable stable isotope fractionation to transformation pathways of organic pollutants. *Environmental Science & Technology*, 39(18):6896–6916.
- Essaid, H. I., Bekins, B. A., and Cozzarelli, I. M. (2015). Organic contaminant transport and fate in the subsurface: Evolution of knowledge and understanding. *Water Resources Research*, 51(7):4861–4902.
- Fenner, K., Canonica, S., Wackett, L. P., and Elsner, M. (2013). Evaluating pesticide degradation in the environment: Blind spots and emerging opportunities. *Science*, 341(6147):752–758.
- Fenner, K., Elsner, M., Lueders, T., McLachlan, M. S., Wackett, L. P., Zimmermann, M., and Drewes, J. E. (2021). Methodological advances to study contaminant biotransformation: New prospects for understanding and reducing environmental persistence? *ACS ES&T Water*, 1(7):1541–1554.
- Fetter, C. W., Boving, T., and Kremer, D. (2018). *Contaminant Hydrogeology (Third edition)*. Waveland Press, Long Grove, Illinois.
- Fischer, A., Manefield, M., and Bombach, P. (2016). Application of stable isotope tools for evaluating natural and stimulated biodegradation of organic pollutants in field studies. *Current Opinion in Biotechnology*, 41:99–107.
- Franke, S., Seidel, K., Adrian, L., and Nijenhuis, I. (2020). Dual element (c/cl) isotope analysis indicates distinct mechanisms of reductive dehalogenation of chlorinated ethenes and dichloroethane in *Dehalococcoides mccartyi* strain BTF08 with defined reductive dehalogenase inventories. *Frontiers in Microbiology*, 11:1507.
- Ghysels, G., Anibas, C., Awol, H., Tolche, A., Schneidewind, U., and Huysmans, M. (2021). The significance of vertical and lateral groundwater–surface water exchange fluxes in riverbeds and riverbanks: Comparing 1D analytical flux estimates with 3D groundwater modelling. *Water*, 13(3):306.

- Grant Ferris, F., Szponar, N., and Edwards, B. A. (2021). *Groundwater Microbiology*. The Groundwater Project.
- Griebler, C. and Lueders, T. (2009). Microbial biodiversity in groundwater ecosystems. *Freshwater Biology*, 54(4):649–677.
- Grösbacher, M., Eckert, D., Cirpka, O. A., and Griebler, C. (2018). Contaminant concentration versus flow velocity: Drivers of biodegradation and microbial growth in groundwater model systems. *Biodegradation*, 29(3):211–232.
- Grossman, E. L., Cifuentes, L. A., and Cozzarelli, I. M. (2002). Anaerobic methane oxidation in a landfill-leachate plume. *Environmental Science & Technology*, 36(11):2436–2442.
- Groster, A., Duhamel, M., Dworatzek, S., and Edwards, E. A. (2010). Chloroform respiration to dichloromethane by a dehalobacter population: Growth-linked reductive dechlorination of chloroform. *Environmental Microbiology*, 12(4):1053–1060.
- Haberer, C. M., Rolle, M., Cirpka, O. A., and Grathwohl, P. (2012). Oxygen transfer in a fluctuating capillary fringe. *Vadose Zone Journal*, 11(3):vzj2011.0056.
- Hancock, P. J. (2002). Human impacts on the stream–groundwater exchange zone. *Environmental Management*, 29(6):763–781.
- Hayoun, K., Geersens, E., Laczny, C. C., Halder, R., Lázaro Sánchez, C., Manna, A., Bringel, F., Ryckelynck, M., Wilmes, P., Muller, E. E. L., Alpha-Bazin, B., Armengaud, J., and Vuilleumier, S. (2020). Dichloromethane degradation pathway from unsequenced *Hyphomicrobium* sp. MC8b rapidly explored by pan-proteomics. *Microorganisms*, 8(12):1876.
- He, J., Sung, Y., Dollhopf, M. E., Fathepure, B. Z., Tiedje, J. M., and Löffler, F. E. (2002). Acetate versus hydrogen as direct electron donors to stimulate the microbial reductive dechlorination process at chloroethene-contaminated sites. *Environmental Science & Technology*, 36(18):3945–3952.
- Hellal, J., Joulain, C., Urien, C., Ferreira, S., Denonfoux, J., Hermon, L., Vuilleumier, S., and Imfeld, G. (2021). Chlorinated ethene biodegradation and associated bacterial taxa in multi-polluted groundwater: Insights from biomolecular markers and stable isotope analysis. *Science of The Total Environment*, 763:142950.
- Hensen, B., Lange, J., Jackisch, N., Zieger, F., Olsson, O., and Kümmerer, K. (2018). Entry of biocides and their transformation products into groundwater via urban stormwater infiltration systems. *Water Research*, 144:413–423.
- Heraty, L., Fuller, M., Huang, L., Abrajano, T., and Sturchio, N. (1999). Isotopic fractionation of carbon and chlorine by microbial degradation of dichloromethane. *Organic Geochemistry*, 30(8):793–799.
- Hermon, L., Denonfoux, J., Hellal, J., Joulain, C., Ferreira, S., Vuilleumier, S., and Imfeld, G. (2018). Dichloromethane biodegradation in multi-contaminated groundwater: Insights from biomolecular and compound-specific isotope analyses. *Water Research*, 142:217–226.
- Hildebrandt, A., Guillaumon, M., Lacorte, S., Tauler, R., and Barceló, D. (2008). Impact of pesticides used in agriculture and vineyards to surface and groundwater quality (north Spain). *Water Research*, 42(13):3315–3326.
- Hintze, S., Glauser, G., and Hunkeler, D. (2020). Influence of surface water - groundwater interactions on the spatial distribution of pesticide metabolites in groundwater. *Science of The Total Environment*, 733:139109.
- Höhener, P. (2016). Simulating stable carbon and chlorine isotope ratios in dissolved chlorinated groundwater pollutants with BIOCHLOR-ISO. *Journal of Contaminant Hydrology*, 195:52–61.



- Höhener, P. and Atteia, O. (2010). Multidimensional analytical models for isotope ratios in groundwater pollutant plumes of organic contaminants undergoing different biodegradation kinetics. *Advances in Water Resources*, 33(7):740–751.
- Höhener, P. and Imfeld, G. (2021). Quantification of lambda in multi-elemental compound-specific isotope analysis. *Chemosphere*, 267:129232.
- Höhener, P. and Yu, X. (2012). Stable carbon and hydrogen isotope fractionation of dissolved organic groundwater pollutants by equilibrium sorption. *Journal of Contaminant Hydrology*, 129-130:54–61.
- Holland, S. I., Ertan, H., Montgomery, K., Manefield, M. J., and Lee, M. (2021). Novel dichloromethane-fermenting bacteria in the *Peptococcaceae* family. *The ISME Journal*, 15:1709–1721.
- Holman, H.-Y. N., Wozei, E., Lin, Z., Comolli, L. R., Ball, D. A., Borglin, S., Fields, M. W., Hazen, T. C., and Downing, K. H. (2009). Real-time molecular monitoring of chemical environment in obligate anaerobes during oxygen adaptive response. *Proceedings of the National Academy of Sciences*, 106(31):12599–12604.
- Horst, A. and Lacrampe-Couloume, G. (2020). Isotope fractionation ( $^2\text{H}/^1\text{H}$ ,  $^{13}\text{C}/^{12}\text{C}$ ,  $^{37}\text{Cl}/^{35}\text{Cl}$ ) in trichloromethane and trichloroethene caused by partitioning between gas phase and water. *Environmental Science: Processes and Impacts*, 22(3):617–626.
- Horst, A., Renpenning, J., Richnow, H.-H., and Gehre, M. (2017). Compound specific stable chlorine isotopic analysis of volatile aliphatic compounds using gas chromatography hyphenated with multiple collector inductively coupled plasma mass spectrometry. *Analytical Chemistry*, 89(17):9131–9138.
- Hron, P., Jost, D., Bastian, P., Gallert, C., Winter, J., and Ippisch, O. (2015). Application of reactive transport modeling to growth and transport of microorganisms in the capillary fringe. *Vadose Zone Journal*, 14(5).
- Huang, B., Lei, C., Wei, C., and Zeng, G. (2014). Chlorinated volatile organic compounds (Cl-VOCs) in environment – Sources, potential human health impacts, and current remediation technologies. *Environment International*, 71:118–138.
- Hunkeler, D., Aravena, R., Berry-Spark, K., and Cox, E. (2005). Assessment of degradation pathways in an aquifer with mixed chlorinated hydrocarbon contamination using stable isotope analysis. *Environmental Science & Technology*, 39(16):5975–5981.
- Hunkeler, D., Aravena, R., Shouakar-Stash, O., Weisbrod, N., Nasser, A., Netzer, L., and Ronen, D. (2011). Carbon and chlorine isotope ratios of chlorinated ethenes migrating through a thick unsaturated zone of a sandy aquifer. *Environmental Science & Technology*, 45(19):8247–8253.
- Hunkeler, D., Meckenstock, R., and Sherwood Lollar, B. (2009a). A guide for assessing biodegradation and source identification of organic ground water contaminants using compound specific isotope analysis (CSIA). U.S. Environmental Protection Agency, Washington, D.C., EPA/600/R-08/148, pages 1–82.
- Hunkeler, D., Van Breukelen, B. M., and Elsner, M. (2009b). Modeling chlorine isotope trends during sequential transformation of chlorinated ethenes. *Environmental Science & Technology*, 43(17):6750–6756.
- Iker, B. C., Kambesis, P., Oehrle, S. A., Groves, C., and Barton, H. A. (2010). Microbial atrazine breakdown in a karst groundwater system and its effect on ecosystem energetics. *Journal of Environmental Quality*, 39(2):509–518.
- Imfeld, G., Besaury, L., Maucourt, B., Donadello, S., Baran, N., and Vuilleumier, S. (2018). Toward integrative bacterial monitoring of metolachlor toxicity in groundwater. *Frontiers in Microbiology*, 9.

- Imfeld, G., Kopinke, F.-D., Fischer, A., and Richnow, H.-H. (2014). Carbon and hydrogen isotope fractionation of benzene and toluene during hydrophobic sorption in multistep batch experiments. *Chemosphere*, 107:454–461.
- Imfeld, G. and Vuilleumier, S. (2012). Measuring the effects of pesticides on bacterial communities in soil: A critical review. *European Journal of Soil Biology*, 49:22–30.
- Jaeger, A., Coll, C., Posselt, M., Mechelke, J., Rutere, C., Betterle, A., Raza, M., Mehrstens, A., Meinikmann, K., Portmann, A., Singh, T., Blaen, P. J., Krause, S., Horn, M. A., Hollender, J., Benskin, J. P., Sobek, A., and Lewandowski, J. (2019). Using recirculating flumes and a response surface model to investigate the role of hyporheic exchange and bacterial diversity on micropollutant half-lives. *Environmental Science: Processes and Impacts*, 21(12):2093–2108.
- Jaeger, A., Posselt, M., Schaper, J. L., Betterle, A., Rutere, C., Coll, C., Mechelke, J., Raza, M., Meinikmann, K., Portmann, A., Blaen, P. J., Horn, M. A., Krause, S., and Lewandowski, J. (2021). Transformation of organic micropollutants along hyporheic flow in bedforms of river-simulating flumes. *Scientific Reports*, 11(1):13034.
- Jakobsen, R., Hinsby, K., Aamand, J., van der Keur, P., Kidmose, J., Purtschert, R., Jurgens, B., Sültenfuss, J., and Albers, C. N. (2019). History and sources of co-occurring pesticides in an abstraction well unraveled by age distributions of depth-specific groundwater samples. *Environmental Science & Technology*, 54(1):158–165.
- Jeannotat, S. and Hunkeler, D. (2012). Chlorine and carbon isotopes fractionation during volatilization and diffusive transport of trichloroethene in the unsaturated zone. *Environmental Science & Technology*, 46(6):3169–3176.
- Jeannotat, S. and Hunkeler, D. (2013). Can soil gas VOCs be related to groundwater plumes based on their isotope signature? *Environmental Science & Technology*, 47(21):12115–12122.
- Jin, B., Laskov, C., Rolle, M., and Haderlein, S. B. (2011). Chlorine isotope analysis of organic contaminants using GC-qMS: Method optimization and comparison of different evaluation schemes. *Environmental Science & Technology*, 45(12):5279–5286.
- Jost, D., Haberer, C. M., Grathwohl, P., Winter, J., and Gallert, C. (2015). Oxygen transfer in a fluctuating capillary fringe: Impact of microbial respiratory activity. *Vadose Zone Journal*, 14(5):vzj2014.04.0039.
- Kaufmann, R., Long, A., Bentley, H., and Davis, S. (1984). Natural chlorine isotope variations. *Nature*, 309(5966):338–340.
- Kim, J. and Corapcioglu, M. (2003). Modeling dissolution and volatilization of LNAPL sources migrating on the groundwater table. *Journal of Contaminant Hydrology*, 65(1-2):137–158.
- Kleindienst, S., Chourey, K., Chen, G., Murdoch, R. W., Higgins, S. A., Iyer, R., Campagna, S. R., Mack, E. E., Seger, E. S., Hettich, R. L., and Löffler, F. E. (2019). Proteogenomics reveals novel reductive dehalogenases and methyltransferases expressed during anaerobic dichloromethane metabolism. *Applied Environmental Microbiology*, 85(6):e02768–18.
- Kleindienst, S., Higgins, S. A., Tsementzi, D., Chen, G., Konstantinidis, K. T., Mack, E. E., and Löffler, F. E. (2017). ‘*Candidatus* dichloromethanomonas elyunquensis’ gen. nov., sp. nov., a dichloromethane-degrading anaerobe of the *Peptococcaceae* family. *Systematic and Applied Microbiology*, 40(3):150–159.
- Kleiner, M. (2019). Metaproteomics: Much more than measuring gene expression in microbial communities. *mSystems*, 4(3):e00115–19.
- Koenig, J., Lee, M., and Manefield, M. (2015). Aliphatic organochlorine degradation in subsurface environments. *Reviews in Environmental Science and Bio/Technology*, 14(1):49–71.

- Kopinke, F.-D., Georgi, A., Imfeld, G., and Richnow, H.-H. (2017). Isotope fractionation of benzene during partitioning – Revisited. *Chemosphere*, 168:508–513.
- Kopinke, F.-D., Georgi, A., Voskamp, M., and Richnow, H. H. (2005). Carbon isotope fractionation of organic contaminants due to retardation on humic substances: Implications for natural attenuation studies in aquifers. *Environmental Science & Technology*, 39(16):6052–6062.
- Kovárová-Kovar, K. and Egli, T. (1998). Growth kinetics of suspended microbial cells: From single-substrate-controlled growth to mixed-substrate kinetics. *Microbiology and molecular biology reviews*, 62(3):646–666.
- Krutz, L. J., Gentry, T. J., Senseman, S. A., Pepper, I. L., and Tierney, D. P. (2006). Mineralisation of atrazine, metolachlor and their respective metabolites in vegetated filter strip and cultivated soil. *Pest Management Science*, 62(6):505–514.
- Kuder, T., Philp, P., and Allen, J. (2009). Effects of volatilization on carbon and hydrogen isotope ratios of MTBE. *Environmental Science & Technology*, 43(6):1763–1768.
- Kuder, T., Philp, R., Van Breukelen, B. M., Thoeument, H., and Vanderford, M. (2016). Integrated stable isotope – Reactive transport model approach for assessment of chlorinated solvent degradation. Technical report, University of Oklahoma Norman United States.
- Kuder, T., van Breukelen, B. M., Vanderford, M., and Philp, P. (2013). 3D-CSIA: Carbon, chlorine, and hydrogen isotope fractionation in transformation of TCE to ethene by a *Dehalococcoides* culture. *Environmental Science & Technology*, 47(17):9668–9677.
- Kundu, K., Marozava, S., Ehrl, B., Merl-Pham, J., Griebler, C., and Elsner, M. (2019). Defining lower limits of biodegradation: atrazine degradation regulated by mass transfer and maintenance demand in *Arthrobacter aurescens* TC1. *The ISME Journal*, 13(9):2236–2251.
- Kuntze, K., Eisenmann, H., Richnow, H.-H., and Fischer, A. (2019). Compound-specific stable isotope analysis (CSIA) for evaluating degradation of organic pollutants: An overview of field case studies. *Anaerobic Utilization of Hydrocarbons, Oils, and Lipids*, pages 323–360.
- Lapworth, D. J., Baran, N., Stuart, M. E., and Ward, R. S. (2012). Emerging organic contaminants in groundwater: A review of sources, fate and occurrence. *Environmental Pollution*, 163:287–303.
- Lee, M., Low, A., Zemb, O., Koenig, J., Michaelsen, A., and Manefield, M. (2012). Complete chloroform dechlorination by organochlorine respiration and fermentation: Microbial chloroform metabolism. *Environmental Microbiology*, 14(4):883–894.
- Lee, M., Wells, E., Wong, Y. K., Koenig, J., Adrian, L., Richnow, H. H., and Manefield, M. (2015). Relative contributions of dehalobacter and zerovalent iron in the degradation of chlorinated methanes. *Environmental Science & Technology*, 49(7):4481–4489.
- Leeson, A., Beevar, E., Henry, B., Fortenberry, J., and Coyle, C. (2004). Principles and practices of enhanced anaerobic bioremediation of chlorinated solvents. Technical report, Naval Facilities Engineering Service Center Port Hueneme CA.
- Lehman, R. M., Roberto, F. F., Earley, D., Bruhn, D. F., Brink, S. E., O’Connell, S. P., Delwiche, M. E., and Colwell, F. S. (2001). Attached and unattached bacterial communities in a 120-Meter corehole in an acidic, crystalline rock aquifer. *Applied and Environmental Microbiology*, 67(5):2095–2106.

- Leitner, S., Reichenauer, T. G., and Watzinger, A. (2018). Impact of sorption processes on PCE concentrations in organohalide-respiring aquifer sediment samples. *Science of The Total Environment*, 615:1061–1069.
- Lesser, L. E., Mora, A., Moreau, C., Mahlnecht, J., Hernández-Antonio, A., Ramírez, A. I., and Barrios-Piña, H. (2018). Survey of 218 organic contaminants in groundwater derived from the world's largest untreated wastewater irrigation system: Mezquital Valley, Mexico. *Chemosphere*, 198:510–521.
- Lewandowski, J., Putschew, A., Schwesig, D., Neumann, C., and Radke, M. (2011). Fate of organic micropollutants in the hyporheic zone of a eutrophic lowland stream: Results of a preliminary field study. *Science of The Total Environment*, 409(10):1824–1835.
- Lin, C., Lerch, R., Garrett, H., and George, M. (2008). Bioremediation of atrazine-contaminated soil by forage grasses: Transformation, uptake, and detoxification. *Journal of Environmental Quality*, 37(1):196–206.
- Loos, R., Locoro, G., Comero, S., Contini, S., Schwesig, D., Werres, F., Balsaa, P., Gans, O., Weiss, S., Blaha, L., Bolchi, M., and Gawlik, B. M. (2010). Pan-european survey on the occurrence of selected polar organic persistent pollutants in ground water. *Water Research*, 44(14):4115–4126.
- Maeng, S. K., Ameda, E., Sharma, S. K., Grützmacher, G., and Amy, G. L. (2010). Organic micropollutant removal from wastewater effluent-impacted drinking water sources during bank filtration and artificial recharge. *Water Research*, 44(14):4003–4014.
- Mägli, A., Messmer, M., and Leisinger, T. (1998). Metabolism of dichloromethane by the strict anaerobe *Dehalobacterium formicoaceticum*. *Applied and Environmental Microbiology*, 64(2):646–650.
- Mägli, A., Wendt, M., and Leisinger, T. (1996). Isolation and characterization of *Dehalobacterium formicoaceticum* gen. nov. sp. nov., a strictly anaerobic bacterium utilizing dichloromethane as source of carbon and energy. *Archives of Microbiology*, 166(2):101–108.
- Maher, K. and Mayer, K. U. (2019). Tracking diverse minerals, hungry organisms, and dangerous contaminants using reactive transport models. *Elements*, 15(2):81–86.
- Masbou, J., Meite, F., Guyot, B., and Imfeld, G. (2018). Enantiomer-specific stable carbon isotope analysis (ESIA) to evaluate degradation of the chiral fungicide metalaxyl in soils. *Journal of Hazardous Materials*, 353:99–107.
- Masoner, J. R., Kolpin, D. W., Cozzarelli, I. M., Barber, L. B., Burden, D. S., Foreman, W. T., Forshay, K. J., Furlong, E. T., Groves, J. F., Hladik, M. L., Hopton, M. E., Jaeschke, J. B., Keefe, S. H., Krabbenhoft, D. P., Lowrance, R., Romanok, K. M., Rus, D. L., Selbig, W. R., Williams, B. H., and Bradley, P. M. (2019). Urban stormwater: An overlooked pathway of extensive mixed contaminants to surface and groundwaters in the United States. *Environmental Science & Technology*, 53(17):10070–10081.
- McCarthy, K. A. and Johnson, R. L. (1993). Transport of volatile organic compounds across the capillary fringe. *Resources Research*, 29(6):1675–1683.
- McCarty, P. L., Reinhard, M., and Rittmann, B. E. (1981). Trace organics in groundwater. *Environmental Science & Technology*, 15(1):40–51.
- McCarty, P. L. and Semprini, L. (2017). Ground-water treatment for chlorinated solvents. In *Handbook of bioremediation*, pages 87–116. CRC Press.
- Mechelke, J., Rust, D., Jaeger, A., and Hollender, J. (2020). Enantiomeric fractionation during biotransformation of chiral pharmaceuticals in recirculating water-sediment test flumes. *Environmental Science & Technology*, 54(12):7291–7301.

- Meckenstock, R. U., Elsner, M., Griebler, C., Lueders, T., Stumpp, C., Aamand, J., Agathos, S. N., Albrechtsen, H.-J., Bastiaens, L., Bjerg, P. L., Boon, N., Dejonghe, W., Huang, W. E., Schmidt, S. I., Smolders, E., Sorensen, S. R., Springael, D., and van Breukelen, B. M. (2015). Biodegradation: Updating the concepts of control for microbial cleanup in contaminated aquifers. *Environmental Science & Technology*, 49(12):7073–7081.
- Meckenstock, R. U., Morasch, B., Griebler, C., and Richnow, H. H. (2004). Stable isotope fractionation analysis as a tool to monitor biodegradation in contaminated acquifers. *Journal of Contaminant Hydrology*, 75(3):215–255.
- Meile, C. and Scheibe, T. D. (2019). Reactive transport modeling of microbial dynamics. *Elements*, 15(2):111–116.
- Muller, E. E., Bringel, F., and Vuilleumier, S. (2011). Dichloromethane-degrading bacteria in the genomic age. *Research in Microbiology*, 162(9):869–876.
- Murínová, S. and Dercová, K. (2014). Response mechanisms of bacterial degraders to environmental contaminants on the level of cell walls and cytoplasmic membrane. *International Journal of Microbiology*, 2014:1–16.
- Nikolausz, M., Nijenhuis, I., Ziller, K., Richnow, H.-H., and Kästner, M. (2006). Stable carbon isotope fractionation during degradation of dichloromethane by methylotrophic bacteria. *Environmental Microbiology*, 8(1):156–164.
- Nödler, K., Tsakiri, M., and Licha, T. (2014). The impact of different proportions of a treated effluent on the biotransformation of selected micro-contaminants in river water microcosms. *IJERPH*, 11(10):10390–10405.
- NRC (2000). *Natural Attenuation for Groundwater Remediation*. National Research Council. National Academies Press.
- Ojeda, A. S., Phillips, E., and Sherwood Lollar, B. (2020). Multi-element (C, H, Cl, Br) stable isotope fractionation as a tool to investigate transformation processes for halogenated hydrocarbons. *Environmental Science: Processes and Impacts*, 22(3):567–582.
- Palau, J., Jamin, P., Badin, A., Vanhecke, N., Haerens, B., Brouyere, S., and Hunkeler, D. (2016). Use of dual carbon-chlorine isotope analysis to assess the degradation pathways of 1,1,1-trichloroethane in groundwater. *Water Research*, 92:235–243.
- Palau, J., Yu, R., Hatijah Mortan, S., Shouakar-Stash, O., Rosell, M., Freedman, D. L., Sbarbati, C., Fiorenza, S., Aravena, R., Marco-Urrea, E., Elsner, M., Soler, A., and Hunkeler, D. (2017). Distinct dual C-Cl isotope fractionation patterns during anaerobic biodegradation of 1,2-dichloroethane: Potential to characterize microbial degradation in the field. *Environmental Science & Technology*, 51(5):2685–2694.
- Peralta, A. L., Ludmer, S., Matthews, J. W., and Kent, A. D. (2014). Bacterial community response to changes in soil redox potential along a moisture gradient in restored wetlands. *Ecological Engineering*, 73:246–253.
- Peter, K. T., Herzog, S., Tian, Z., Wu, C., McCray, J. E., Lynch, K., and Kolodziej, E. P. (2019). Evaluating emerging organic contaminant removal in an engineered hyporheic zone using high resolution mass spectrometry. *Water Research*, 150:140–152.
- Poeter, E., Fan, Y., Cherry, J., Wood, W., and Mackay, D. (2020). *Groundwater in Our Water Cycle: Getting to Know Earth's Most Important Fresh Water Source*. The Groundwater Project.
- Ponsin, V., Torrentó, C., Lihl, C., Elsner, M., and Hunkeler, D. (2019). Compound-specific chlorine isotope analysis of the herbicides atrazine, acetochlor, and metolachlor. *Analytical Chemistry*, 91(22):14290–14298.
- Posselt, M., Mechelke, J., Rutere, C., Coll, C., Jaeger, A., Raza, M., Meinikmann, K., Krause, S., Sobek, A., Lewandowski, J., Horn, M. A., Hollender, J., and Benskin, J. P. (2020). Bacterial diversity controls trans-

- formation of wastewater-derived organic contaminants in river-simulating flumes. *Environmental Science & Technology*, 54(9):5467–5479.
- Poursat, B. A. J., van Spanning, R. J. M., Braster, M., Helmus, R., de Voogt, P., and Parsons, J. R. (2019a). Biodegradation of metformin and its transformation product, guanyurea, by natural and exposed microbial communities. *Ecotoxicology and Environmental Safety*, 182:109414.
- Poursat, B. A. J., van Spanning, R. J. M., de Voogt, P., and Parsons, J. R. (2019b). Implications of microbial adaptation for the assessment of environmental persistence of chemicals. *Critical Reviews in Environmental Science & Technology*, 49(23):2220–2255.
- Prommer, H., Sun, J., and Kocar, B. D. (2019). Using reactive transport models to quantify and predict groundwater quality. *Elements*, 15(2):87–92.
- Pronk, G. J., Mellage, A., Milojevic, T., Smeaton, C. M., Engel, K., Neufeld, J. D., Rezanezhad, F., and Cappellen, P. V. (2020). Carbon turnover and microbial activity in an artificial soil under imposed cyclic drainage and imbibition. *Vadose Zone Journal*, 19(1):e20021.
- Qiu, S., Eckert, D., Cirpka, O. A., Huenniger, M., Knappett, P., Maloszewski, P., Meckenstock, R. U., Griebler, C., and Elsner, M. (2013). Direct experimental evidence of non-first order degradation kinetics and sorption-induced isotopic fractionation in a mesoscale aquifer:  $^{13}\text{C}/^{12}\text{C}$  analysis of a transient toluene pulse. *Environmental Science & Technology*, 47(13):6892–6899.
- Renpenning, J., Keller, S., Cretnik, S., Shouakar-Stash, O., Elsner, M., Schubert, T., and Nijenhuis, I. (2014). Combined C and Cl isotope effects indicate differences between corrinoids and enzyme (*Sulfurospirillum multivorans* PceA) in reductive dehalogenation of tetrachloroethene, but not trichloroethene. *Environmental Science & Technology*, 48(20):11837–11845.
- Richardson, S. D. and Kimura, S. Y. (2016). Water analysis: Emerging contaminants and current issues. *Analytical Chemistry*, 88(1):546–582.
- Rivett, M. O., Wealthall, G. P., Dearden, R. A., and McAlary, T. A. (2011). Review of unsaturated-zone transport and attenuation of volatile organic compound (VOC) plumes leached from shallow source zones. *Journal of Contaminant Hydrology*, 123(3):130–156.
- Rolle, M., Chiogna, G., Bauer, R., Griebler, C., and Grathwohl, P. (2010). Isotopic fractionation by transverse dispersion: Flow-through microcosms and reactive transport modeling study. *Environmental Science & Technology*, 44(16):6167–6173.
- Rolle, M., Chiogna, G., Hochstetler, D. L., and Kitanidis, P. K. (2013). On the importance of diffusion and compound-specific mixing for groundwater transport: An investigation from pore to field scale. *Journal of Contaminant Hydrology*, 153:51–68.
- Rolle, M., Clement, T. P., Sethi, R., and Di Molfetta, A. (2008). A kinetic approach for simulating redox-controlled fringe and core biodegradation processes in groundwater: Model development and application to a landfill site in Piedmont, Italy. *Hydrological Processes: An International Journal*, 22(25):4905–4921.
- Rühle, F. A., von Netzer, F., Lueders, T., and Stumpp, C. (2015). Response of transport parameters and sediment microbiota to water table fluctuations in laboratory columns. *Vadose Zone Journal*, 14(5):vzj2014.09.0116.
- Rutere, C., Posselt, M., and Horn, M. A. (2020). Fate of trace organic compounds in hyporheic zone sediments of contrasting organic carbon content and impact on the microbiome. *Water*, 12(12):3518.

- Schaper, J. L., Posselt, M., McCallum, J. L., Banks, E. W., Hoehne, A., Meinikmann, K., Shanafield, M. A., Batelaan, O., and Lewandowski, J. (2018). Hyporheic exchange controls fate of trace organic compounds in an urban stream. *Environmental Science & Technology*, 52(21):12285–12294.
- Schmidt, K. R., Augenstein, T., Heidinger, M., Ertl, S., and Tiehm, A. (2010). Aerobic biodegradation of cis-1,2-dichloroethene as sole carbon source: Stable carbon isotope fractionation and growth characteristics. *Chemosphere*, 78(5):527–532.
- Schürner, H. K. V., Maier, M. P., Eckert, D., Brejcha, R., Neumann, C.-C., Stumpp, C., Cirpka, O. A., and Elsner, M. (2016). Compound-specific stable isotope fractionation of pesticides and pharmaceuticals in a mesoscale aquifer model. *Environmental Science & Technology*, 50(11):5729–5739.
- Schwarzenbach, R. P. (2006). The challenge of micropollutants in aquatic systems. *Science*, 313(5790):1072–1077.
- Schwarzenbach, R. P., Egli, T., Hofstetter, T. B., von Gunten, U., and Wehrli, B. (2010). Global water pollution and human health. *Annual review of environment and resources*, 35(1):109–136.
- Scow, K. M. and Hicks, K. A. (2005). Natural attenuation and enhanced bioremediation of organic contaminants in groundwater. *Current Opinion in Biotechnology*, 16(3):246–253.
- Seiler, R. L., Zaugg, S. D., Thomas, J. M., and Howcroft, D. L. (1999). Caffeine and pharmaceuticals as indicators of waste water contamination in wells. *Groundwater*, 37(3):405–410.
- Seybold, C. A., Mersie, W., Huang, J., and McNamee, C. (2002). Soil redox, pH, temperature, and water-table patterns of a freshwater tidal wetland. *Wetlands*, 22(1):149–158.
- Shestakova, M. and Sillanpää, M. (2013). Removal of dichloromethane from ground and wastewater: A review. *Chemosphere*, 93(7):1258–1267.
- Smith, H. J., Zelaya, A. J., De León, K. B., Chakraborty, R., Elias, D. A., Hazen, T. C., Arkin, A. P., Cunningham, A. B., and Fields, M. W. (2018). Impact of hydrologic boundaries on microbial planktonic and biofilm communities in shallow terrestrial subsurface environments. *FEMS Microbiology Ecology*, 94(12):fyi191.
- Straub, J. O., Caldwell, D. J., Davidson, T., D'Aco, V., Kappler, K., Robinson, P. F., Simon-Hettich, B., and Tell, J. (2019). Environmental risk assessment of metformin and its transformation product guanyurea. I. Environmental fate. *Chemosphere*, 216:844–854.
- Stroo, H. F., Leeson, A., Marqusee, J. A., Johnson, P. C., Ward, C. H., Kavanaugh, M. C., Sale, T. C., Newell, C. J., Pennell, K. D., Lebrón, C. A., and Unger, M. (2012). Chlorinated ethene source remediation: Lessons learned. *Environmental Science & Technology*, 46(12):6438–6447.
- Sun, F., Mellage, A., Gharasoo, M., Melsbach, A., Cao, X., Zimmermann, R., Griebler, C., Thullner, M., Cirpka, O. A., and Elsner, M. (2021a). Mass-transfer-limited biodegradation at low concentrations – Evidence from reactive transport modeling of isotope profiles in a bench-scale aquifer. *Environmental Science & Technology*, 55(11):7386–7397.
- Sun, F., Peters, J., Thullner, M., Cirpka, O. A., and Elsner, M. (2021b). Magnitude of diffusion- and transverse dispersion-induced isotope fractionation of organic compounds in aqueous systems. *Environmental Science & Technology*, 55(8):4772–4782.
- Talja, K. M., Kaukonen, S., Kilpi-Koski, J., Malin, I., Kairesalo, T., Romantschuk, M., Tuominen, J., and Kontro, M. H. (2008). Atrazine and terbutryn degradation in deposits from groundwater environment within the boreal region in lahti, finland. *Journal of Agricultural and Food Chemistry*, 56(24):11962–11968.

- Tamminen, M., Spaak, J., Tlili, A., Eggen, R., Stamm, C., and Räsänen, K. (2022). Wastewater constituents impact biofilm microbial community in receiving streams. *Science of The Total Environment*, 807:151080.
- Thoeument, H. and Van Breukelen, B. M. (2020). Virtual experiments to assess opportunities and pitfalls of CSIA in physical-chemical heterogeneous aquifers. *Journal of contaminant hydrology*, 231:103638.
- Thullner, M., Centler, F., Richnow, H.-H., and Fischer, A. (2012). Quantification of organic pollutant degradation in contaminated aquifers using compound specific stable isotope analysis – Review of recent developments. *Organic Geochemistry*, 42(12):1440–1460.
- Thullner, M., Kampara, M., Richnow, H. H., Harms, H., and Wick, L. Y. (2008). Impact of bioavailability restrictions on microbially induced stable isotope fractionation. 1. Theoretical calculation. *Environmental Science & Technology*, 42(17):6544–6551.
- Thullner, M., Regnier, P., and Van Cappellen, P. (2007). Modeling microbially induced carbon degradation in redox-stratified subsurface environments: Concepts and open questions. *Geomicrobiology Journal*, 24(3):139–155.
- Torabi, E., Wiegert, C., Guyot, B., Vuilleumier, S., and Imfeld, G. (2020). Dissipation of s-metolachlor and butachlor in agricultural soils and responses of bacterial communities: Insights from compound-specific isotope and biomolecular analyses. *Journal of Environmental Sciences*, 92:163–175.
- Torgonskaya, M. L., Zyakun, A. M., Trotsenko, Y. A., Laurinavichius, K. S., Kümmel, S., Vuilleumier, S., and Richnow, H. H. (2019). Individual stages of bacterial dichloromethane degradation mapped by carbon and chlorine stable isotope analysis. *Journal of Environmental Sciences*, 78:147–160.
- Trautwein, C. and Kümmerer, K. (2011). Incomplete aerobic degradation of the antidiabetic drug metformin and identification of the bacterial dead-end transformation product guany lurea. *Chemosphere*, 85(5):765–773.
- US EPA (1999a). Monitored Natural Attenuation of Chlorinated Solvents. Technical Report EPA/600/F-98/022, Office of Research and Development, U.S. Environmental Protection Agency, Washington, D.C. EPA/600/F-98/022.
- US EPA (1999b). Use of monitored natural attenuation at superfund, RCRA corrective action, and underground storage tank sites. Technical report, Office of Solid Waste and Emergency Response. U.S. Environmental Protection Agency, Washington D.C.
- US EPA (2015). OLEM programs address contamination at superfund, Brownfields and RCRA sites near 61 percent of the U.S. population. Overviews and Factsheets, Office of Research and Development, U.S. Environmental Protection Agency, Washington, DC 20460.
- US EPA (2020). Risk evaluation for methylene chloride (dichloromethane, DCM). Technical report, Office of Chemical Safety and Pollution Prevention. U.S. Environmental Protection Agency, Washington, D.C., EPA-740-R1-8010.
- van Bodegom, P. (2007). Microbial maintenance: A critical review on its quantification. *Microbiology Ecology*, 53(4):513–523.
- van Breukelen, B. M. and Griffioen, J. (2004). Biogeochemical processes at the fringe of a landfill leachate pollution plume: potential for dissolved organic carbon, Fe(II), Mn(II), NH<sub>4</sub>, and CH<sub>4</sub> oxidation. *Journal of Contaminant Hydrology*, 73(1):181–205.
- Van Breukelen, B. M., Hunkeler, D., and Volkerling, F. (2005). Quantification of sequential chlorinated ethene degradation by use of a reactive transport model incorporating isotope fractionation. *Environmental Science & Technology*, 39(11):4189–4197.



- Van Breukelen, B. M. and Rolle, M. (2012). Transverse hydrodynamic dispersion effects on isotope signals in ground-water chlorinated solvents' plumes. *Environmental Science & Technology*, 46(14):7700–7708.
- Van Breukelen, B. M., Thouement, H. A. A., Stack, P. E., Vanderford, M., Philp, P., and Kuder, T. (2017). Modeling 3D-CSIA data: Carbon, chlorine, and hydrogen isotope fractionation during reductive dechlorination of TCE to ethene. *Journal of Contaminant Hydrology*, 204:79–89.
- Van Liedekerke, M., Prokop, G., Rabl\_Berger, S., Kibblewhite, M., and Louwagie, G. (2014). Progress in the management of contaminated sites in Europe. Technical report, EUR 26376. Luxembourg (Luxembourg): Publications Office of the European Union; 2013. JRC85913.
- Velis, M., Conti, K. I., and Biermann, F. (2017). Groundwater and human development: synergies and trade-offs within the context of the sustainable development goals. *Sustainability Science*, 12(6):1007–1017.
- Vonberg, D., Vanderborght, J., Cremer, N., Pütz, T., Herbst, M., and Vereecken, H. (2014). 20 years of long-term atrazine monitoring in a shallow aquifer in western germany. *Water Research*, 50:294–306.
- Vuilleumier, S. and Leisinger, T. (1996). Protein engineering studies of dichloromethane dehalogenase/glutathione s-transferase from *Methylophilus* sp. strain DM11. Ser12 but not Tyr6 is required for enzyme activity. *European journal of biochemistry*, 239(2):410–417.
- Wang, F., Zhou, T., Zhu, L., Wang, X., Wang, J., Wang, J., Du, Z., and Li, B. (2019). Effects of successive metalaxyl application on soil microorganisms and the residue dynamics. *Ecological Indicators*, 103:194–201.
- Wanner, P. and Hunkeler, D. (2015). Carbon and chlorine isotopologue fractionation of chlorinated hydrocarbons during diffusion in water and low permeability sediments. *Geochimica et Cosmochimica Acta*, 157:198–212.
- Wanner, P. and Hunkeler, D. (2019). Isotope fractionation due to aqueous phase diffusion – What do diffusion models and experiments tell? – A review. *Chemosphere*, 219:1032–1043.
- Wanner, P., Parker, B. L., Chapman, S. W., Aravena, R., and Hunkeler, D. (2017). Does sorption influence isotope ratios of chlorinated hydrocarbons under field conditions? *Applied Geochemistry*, 84:348–359.
- Wanner, P., Parker, B. L., Chapman, S. W., Lima, G., Gilmore, A., Mack, E. E., and Aravena, R. (2018a). Identification of degradation pathways of chlorohydrocarbons in saturated low-permeability sediments using compound-specific isotope analysis. *Environmental Science & Technology*, 52(13):7296–7306.
- Wanner, P., Parker, B. L., and Hunkeler, D. (2018b). Assessing the effect of chlorinated hydrocarbon degradation in aquitards on plume persistence due to back-diffusion. *Science of The Total Environment*, 633:1602–1612.
- Weatherill, J. J., Atashgahi, S., Schneidewind, U., Krause, S., Ullah, S., Cassidy, N., and Rivett, M. O. (2018). Natural attenuation of chlorinated ethenes in hyporheic zones: A review of key biogeochemical processes and in-situ transformation potential. *Water Research*, 128:362–382.
- Werner, D. and Höhener (2002). The influence of water table fluctuations on the volatilization of contaminants from groundwater. In: S. Thorton qnd S. Oswald (eds) *Groundwater quality: Natural and enhanced restoration of groundwater pollution (Proceedings of the groundwater quality 2001 conference held at Sheffield, UK, June 2001. IAHS PUBLICATION no. 275, pages 213–218.*
- Wiedemeier, T. H., Rifai, H. S., Newell, C. J., and Wilson, J. T. (1999). *Natural attenuation of fuels and chlorinated solvents in the subsurface*. John Wiley & Sons.

- Wiegert, C., Aeppli, C., Knowles, T., Holmstrand, H., Evershed, R., Pancost, R. D., Macháčková, J., and Gustafsson, O. (2012). Dual carbon-chlorine stable isotope investigation of sources and fate of chlorinated ethenes in contaminated groundwater. *Environmental Science & Technology*, 46(20):10918–10925.
- Wiegert, C., Mandalakis, M., Knowles, T., Polymenakou, P. N., Aeppli, C., Macháčková, J., Holmstrand, H., Evershed, R. P., Pancost, R. D., and Gustafsson, O. (2013). Carbon and chlorine isotope fractionation during microbial degradation of tetra- and trichloroethene. *Environmental Science & Technology*, 47(12):6449–6456.
- Williams, M. and Oostrom, M. (2000). Oxygenation of anoxic water in a fluctuating water table system: an experimental and numerical study. *Journal of Hydrology*, 230(1):70–85.
- Winter, T., Harvey, J. W., Franke, O., and Alley, W. (1998). Ground water and surface water a single resource. Circular, U.S. Geological Survey.
- Wright, J., Kirchner, V., Bernard, W., Ulrich, N., McLimans, C., Campa, M. F., Hazen, T., Macbeth, T., Marabello, D., McDermott, J., Mackelprang, R., Roth, K., and Lamendella, R. (2017). Bacterial community dynamics in dichloromethane-contaminated groundwater undergoing natural attenuation. *Frontiers in Microbiology*, 8:2300.
- Zhang, Y., Wang, J., Yang, P., and Xie, S. (2017). Movement of lateral hyporheic flow between stream and groundwater. *Science China Earth Sciences*, 60(11):2033–2040.
- Zimmermann, J., Halloran, L. J. S., and Hunkeler, D. (2020). Tracking chlorinated contaminants in the subsurface using compound-specific chlorine isotope analysis: A review of principles, current challenges and applications. *Chemosphere*, 244:125476.



# Chapter 2

## Aims and general approach

## 2.1 Thesis aim and research questions

This thesis aims to improve the understanding of how dynamic biogeochemical and hydrogeological conditions affect the natural attenuation of organic pollutants in contaminated aquifers. An integrative approach including concentration measurements, hydrochemical analysis, biomolecular markers, compound-specific isotope analysis (CSIA), and reactive transport modeling was used to examine and compare the reactive transport of two classes of organic pollutants in laboratory aquifers: i) dichloromethane (DCM) representing point-source contamination of legacy chlorinated industrial contaminants (Section 1.2.1), and ii) a micropollutant mixture representing diffuse contamination from seasonal pesticide applications and inefficient waste release from WWTF (Section 1.2.2). The results and perspectives of this thesis project respond to the following research questions:

- I. How are hydrogeochemical conditions evolving in aquifers subjected to dynamic conditions (e.g., water table fluctuations)?
- II. What is the role of dynamic transition zones in aquifers (e.g., the capillary fringe and the hyporheic zone) on DCM and micropollutant biodegradation?
- III. What is the relationship between the diversity and composition of bacterial communities and biodegradation of DCM and micropollutants under dynamic hydrogeochemical conditions?
- IV. How do rates and dissipation pathways of DCM and micropollutants vary along with hydrogeochemical and bacterial dynamics?
- V. What are the most relevant (simple, reliable and mechanistic) reaction schemes to evaluate reactive transport and dissipation of (i) Cl-VOCs and (ii) micropollutants in aquifers?
- VI. Can the dissipation of these pollutants be reliably predicted to estimate reactive transport and ultimately the potential for remediation of a polluted aquifer?

## 2.2 General approach

In order to answer these questions, the general approach of this thesis project relies on the coupling of experimental and modeling work to improve the understanding of natural attenuation processes controlling DCM and micropollutants degradation in laboratory aquifers under near-natural settings (i.e., fed with natural groundwater or stream water), and subjected to dynamic conditions (i.e., water table fluctuations or varying micropollutant exposures) (see Figure 2.1).

In **Chapter 3**, dichloromethane biodegradation was examined in laboratory aquifers fed with anoxic contaminated groundwater from a former industrial site (Thermeroil, France). Here, one aquifer remained under steady-state conditions, while the second aquifer underwent two water table fluctuation events. Evolution of DCM concentrations and stable isotopes (i.e., C and Cl), hydrochemical conditions and bacterial dynamics were examined across the sand compartment and over time to investigate the effect of water table fluctuations on DCM degradation extent and pathways.

**Chapter 4** describes the development of a multi-phase reactive transport model for the prediction of natural attenuation of DCM in aquifers subjected to variations in the water table. The experimental domain presented in Chapter 3 is used to model DCM biodegradation under static and fluctuating conditions. A mathematical formalism specific to DCM biodegradation, in line with experimental observations described in Chapter 3, was developed by (i) integrating the state of the art of current knowledge on anaerobic DCM biodegradation in groundwater, (ii) coupling the information obtained by ME-CSIA to infer degradation pathways, and (iii) derive pathway-specific reaction rates to identifying the response of potential pollutant degraders during water table fluctuations.

**Chapter 5** describes the biodegradation potential of a micropollutant mixture examined in laboratory aquifers (duplicates) fed with stream water from an agricultural catchment (Souffel, Bas Rhin, France), mimicking lateral stream-to-groundwater flow interactions into oxygen rich areas of adjacent groundwater (Section 1.4). Varying micropollutants exposure periods (i.e., pulse-like and constant injection periods) were performed, representing the seasonal variations of micropollutants inputs in streams. The micropollutant mixture includes legacy and currently used pesticides such as atrazine, terbutryn, metalaxyl and *S*-metolachlor, the pharmaceutical metformin and the largely consumer product caffeine. Observed isotope fractionation was further examined by integrating a conceptual model.

Finally, a general perspective on the implications of natural attenuation of legacy and emerging contaminants is given in **Chapter 6**, and synthesizes the main findings towards the use of

integrative approaches to elucidate the role of dynamic biogeochemical and hydrogeological conditions on the natural attenuation of organic pollutants in hydrogeological systems.

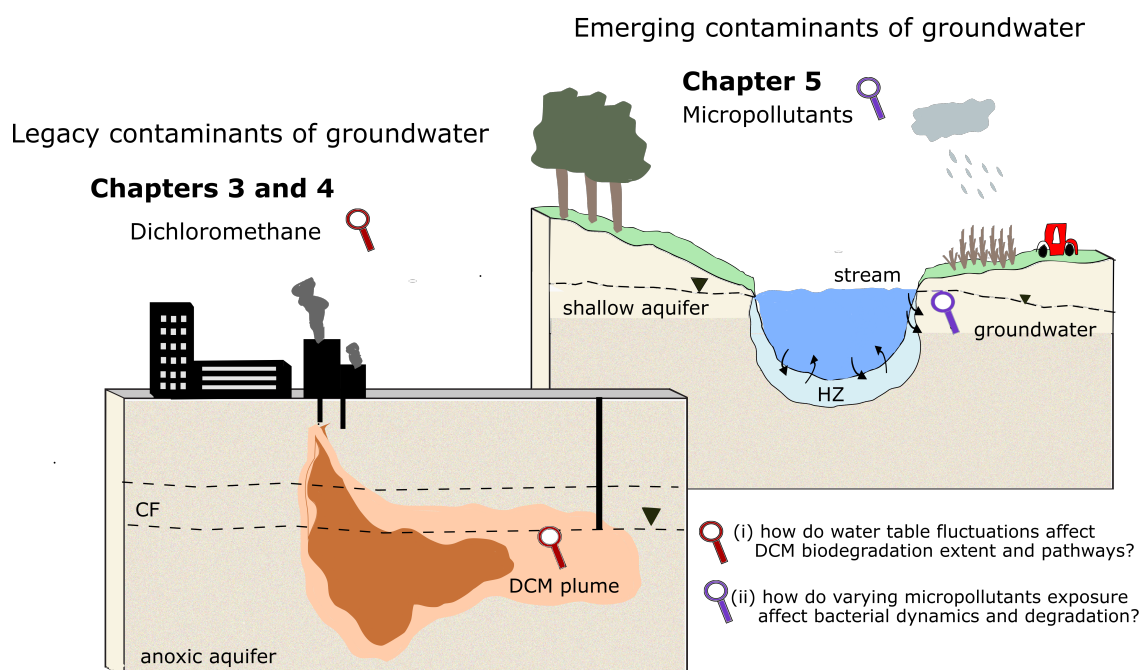


**Figure 2.1:** Graphical outline of this thesis project aiming at deciphering the effect of dynamic environmental conditions on pollutant degradation extent and pathways.

### 2.3 General methodology

This thesis project was carried out on the basis of a general methodology following the above mentioned research questions for the reactive transport of dichloromethane (Chapters 3 and 4) and a micropollutant mixture (Chapter 5). The following sections describe the set up of two laboratory aquifers under near-natural settings, relying on the monitoring of (i) hydrochemical conditions, (ii) contaminant concentrations and stable isotopes, and (iii) bacterial community dynamics. A general description of the implementation of two reactive transport models is provided. Further chapters in this thesis will provide a detailed methodological description.

#### Description of laboratory aquifers

To characterize, conceptualize and model the reactive transport of dichloromethane (DCM) and a mixture of micropollutants in groundwater, the experiments were conducted in two lab-scale aquifers with dimensions of 160 cm × 80 cm × 7 cm (length × height × width), and filled with

sterilized quartz sand (grain size: 0.4–0.6 mm; depth: 70 cm) (Figure 2.2). The experiments were carried out in a temperature-controlled room at  $18 \pm 1$  °C. Both lab-scale aquifers were established under-near natural conditions by continuously receiving field groundwater or stream water. The operation of the aquifers is detailed in corresponding Chapters 3 and 5.

Globally, during the filling procedure, the water table was slowly raised and maintained above the top of the porous medium to limit the volume of entrapped air. The water table was slowly lowered to its final position (see corresponding Chapters 3 and 5 ). Groundwater was supplied from sterile 10 L reservoirs connected to each aquifer. The water table was monitored by tensiometers (ceramic cup and pressure sensors Keller AG, Switzerland) located at 10, 35 and 60 cm depth from the bottom, and at 35, 65, 95, and 125 cm from the inflow. The inlet and outlet ports were vertically spaced by 5 cm and accounted for 8 ports on each lateral border. Filters (2 mm diameter, porosity 1, DURAN®) were located at each port to avoid sand clogging. Sampling ports were placed horizontally at 35, 65, 95 and 125 cm from the inflow, and vertically at 15, 40 and 65 cm from the bottom. Samples were taken via stainless steel needles connected to Luer-lock™ stopcocks. A headspace zone of 10 cm above the sand compartment was established and covered by a top glass mounted with 3 sampling ports equipped with activated carbon cartridges and opened to the atmosphere.

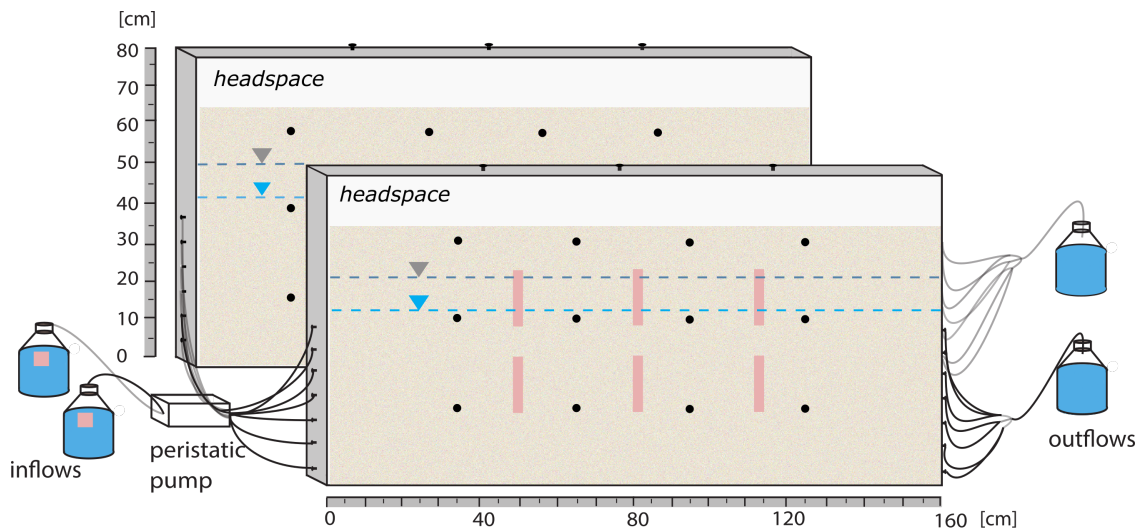


**Figure 2.2:** General schematic overview of laboratory aquifers used in this thesis project. In each experiment, laboratory aquifers were operated in parallel under specific conditions (e.g., type of inflow water, position of water table, sampling resolution) detailed in Chapters 3–5.



### Hydrochemical conditions

For hydrochemical investigations, dissolved oxygen ( $O_2$ ) was monitored *in situ* by oxygen sensitive optode foils (PreSens GmbH, Regensburg, Germany) glued onto the inner side of the front glass pane of the laboratory aquifers.  $O_2$  measurements were performed using a non-invasive oxygen method which consists on an optical fiber oxygen sensor (VisiSens, PreSens, GmbH, Regensburg, Germany) placed outside the front glass pane and moved along the optode foils to record oxygen levels by means of a luminophore. Redox potential (Eh), pH and electrical conductivity were monitored prior sampling events using laboratory probes (SCHOTT® Instruments). Major ions were also measured by ion chromatography (Dionex ICS-1100, Thermo Scientific, USA). Total organic carbon (TOC) (NF EN 1484), dissolved organic carbon (DOC) and dissolved inorganic carbon (DIC) were also quantified.

### Bacterial dynamics

Bacterial dynamics was examined from both pore water and sand samples collected according to aquifer's depth and distance from inflow. DNA was extracted using the DNeasy Power Water kit according to the manufacturer's protocol (Qiagen, Hilden, Germany). Extracted DNA was quantified using Qubit fluorometric quantification with the Qubit dsDNA HS Assay kit (ThermoFischer Scientific, MA, USA). The V4-V5 hypervariable region of the 16S rRNA gene was PCR amplified by an optimized and standardized amplicon library preparation protocol (Metabio®<sup>®</sup>, GenoScreen, Lille, France). Multivariate statistical analysis of relative observed taxonomic units (OTU) abundance was performed. Non-metric multidimensional scaling (NMDS) based on Bray-Curtis dissimilarities of log-transformed data was performed to visualize dissimilarities between bacterial taxa associated with contaminant degradation.

### Compound-specific isotope analysis (CSIA)

ME-CSIA was used for identification and quantification of the extent of degradation of the selected contaminants. Briefly, carbon and nitrogen isotope composition was determined by gas chromatography-combustion-isotope ratio mass spectrometry (GC-C-IRMS), with a gas chromatograph (Trace 1310) coupled via a GC/Conflow IV interface to an isotope ratio mass spectrometer (Delta V plus, Thermo Fisher Scientific). An in-house method was developed for chlorine isotope analysis using a gas chromatograph (GC, Trace 1300, Thermo Fisher Scientific) coupled with a mass spectrometer (MS, ISQ®<sup>®</sup>, Thermo Fisher Scientific). In-house standards of the target contaminants were prepared daily and analyzed prior to sample measurements. Re-

producibility of triplicate measurements was evaluated according to established linearity ranges. Carbon, nitrogen and chlorine isotope ratios were reported in  $\delta$  notation as parts per thousand (‰) relative to the international reference material Vienna Pee Dee-Belemnite (V-PDB), atmospheric air and the reference Standard Mean Ocean Chloride (SMOC), respectively.

### **Implementation of reactive transport models**

The interplay of groundwater flow, solute transport and reactive processes were investigated using two adapted RTMs. Experimental results presented in Chapter 3 (for DCM) and Chapter 5 (micropollutants) were considered to determine the best suited formalisms and to assist in the interpretation of observed reactive transport processes. The main objectives of the developed numerical model frameworks were to implement (i) biotic and abiotic processes, (ii) a dual isotope approach (when suitable) along with description of isotopologues of the target contaminant, (iii) and changes in diversity of the bacterial communities associated with contaminant degradation. To this end, a multi-phase flow (2-D) model was implemented with regard to Chapter 3, accounting for DCM mass exchange of 6 isotopologues across the capillary fringe, pathway-specific degradation rates of 4 distinct bacterial populations (biomass) and dual-Monod kinetics. A detail description of the model is presented in Chapter 4. A simplistic reactive transport framework was implemented for the case of micropollutants (Chapter 5), where a 1-D model was used to elucidate caffeine biodegradation accounting for sorption, Michaelis-Menten kinetics and evolution of the two main isotopologues.



# Chapter 3

## **Water table fluctuations affect dichloromethane biodegradation in laboratory aquifers contaminated with organohalides**

This is an edited version of the peer reviewed article: Prieto-Espinoza, M., Weill, S., Belfort, B., Muller, E. E. L., Masbou, J., Lehmann, F., Vuilleumier, S., & Imfeld, G. (2021). Water table fluctuations affect dichloromethane biodegradation in lab-scale aquifers contaminated with organohalides. *Water Research*, 203, 117530.

<https://doi.org/10.1016/j.watres.2021.117530>

## Water table fluctuations affect dichloromethane biodegradation in laboratory aquifers contaminated with organohalides

### Abstract

Dichloromethane (DCM) is a toxic industrial solvent frequently detected in multi-contaminated aquifers. It can be degraded biotically or abiotically, and under oxic and anoxic conditions. The extent and pathways of DCM degradation in aquifers may thus depend on water table fluctuations and microbial responses to hydrochemical variations. Here, we examined the effect of water table fluctuations on DCM biodegradation in two laboratory aquifers fed with O<sub>2</sub>-depleted DCM-spiked groundwater from a well-characterized former industrial site. Hydrochemistry, stable isotopes of DCM ( $\delta^{13}\text{C}$  and  $\delta^{37}\text{Cl}$ ), and bacterial community composition were examined to determine DCM mass removal and degradation pathways under steady-state (static water table) and transient (fluctuating water table) conditions. DCM mass removal was more pronounced under transient (95%) than under steady-state conditions (42%). C and Cl isotopic fractionation values were larger under steady-state ( $\varepsilon_{bulk}^C = -23.6 \pm 3.2 \text{ ‰}$ , and  $\varepsilon_{bulk}^{Cl} = -8.7 \pm 1.6 \text{ ‰}$ ) than under transient conditions ( $\varepsilon_{bulk}^C = -11.8 \pm 2.0 \text{ ‰}$ , and  $\varepsilon_{bulk}^{Cl} = -3.1 \pm 0.6 \text{ ‰}$ ). Dual C-Cl isotope analysis suggested the prevalence of distinct anaerobic DCM degradation pathways, with  $\Lambda^{C/Cl}$  values of  $1.92 \pm 0.30$  and  $3.58 \pm 0.42$  under steady-state and transient conditions, respectively. Water table fluctuations caused changes in redox conditions and oxygen levels, resulting in a higher relative abundance of *Desulfosporosinus* (*Peptococcaceae* family). Taken together, our results show that water table fluctuations enhanced DCM biodegradation, and correlated with bacterial taxa associated with anaerobic DCM degradation. Our integrative approach allows to evaluate anaerobic DCM degradation under dynamic hydrogeological conditions, and may help improving bioremediation strategies at DCM contaminated sites.

### 3.1 Introduction

Dichloromethane (DCM,  $\text{CH}_2\text{Cl}_2$ ) is a toxic, persistent and halogenated volatile organic compound (VOC) widely used in industrial settings (Schlosser et al., 2015). Due to accidental spills and improper storage at industrial sites, DCM is commonly detected in contaminated aquifers along with other VOCs (Hermon et al., 2018; Shestakova and Sillanpää, 2013; US EPA, 2020). DCM is included in the list of priority pollutants of the U.S. Agency for Toxic Substances and Disease Registry (ATSDR, 2019), and of the European Commission (European Commission, 2013).

Monitored natural attenuation (MNA) has become a promising remediation strategy to detoxify contaminated aquifers (Pope et al., 2004; Smets and Pritchard, 2003). MNA relies on an integrative approach, which includes (i) monitoring contaminant concentrations in the field, (ii) laboratory assays with microorganisms from the field, and (iii) evidence of *in situ* biodegradation potential using stable isotope analysis and/or biomolecular methods (NRC, 1993). Monitoring contaminant concentrations is not sufficient to identify contaminant transformation, as concentrations alone reflect both non-destructive (e.g., dilution, sorption) and destructive dissipation processes (e.g., biodegradation). Compound-specific isotope analysis (CSIA) is increasingly used to measure the extent of contaminant transformation *in situ* (Hunkeler et al., 2009). CSIA relies on changes in stable isotope ratios (e.g.,  $^{13}\text{C}/^{12}\text{C}$ ) of an organic contaminant undergoing a (bio)degradation reaction. Typically, molecules containing light isotopes (e.g.,  $^{12}\text{C}$ ) are degraded preferentially compared to those containing heavy isotopes (e.g.,  $^{13}\text{C}$ ). This generally results in a change of stable isotope ratios in the remaining contaminant mass, which may be specific of the transformation pathway (Elsner and Imfeld, 2016). The stable isotope fractionation can be used for quantitative estimations of contaminant transformation *in situ* by using isotope fractionation values (e.g.,  $\epsilon_{\text{C}}$ ) derived from reference laboratory experiments (Fischer et al., 2016).

Dual-isotope analysis, involving the follow-up of changes in isotope ratios of two elements (e.g.,  $^{13}\text{C}/^{12}\text{C}$  and  $^{37}\text{Cl}/^{35}\text{Cl}$ ), is more informative and robust over a single isotope element approach to evaluate transformation pathways of organic contaminants (Ojeda et al., 2020). When the stable isotope ratios of two elements are compared in a dual plot, the slope ( $\Delta$ ) provides a quantitative parameter of the corresponding transformation pathway (Elsner, 2010; Ojeda et al., 2020). For DCM, the transformation pathway of methylotrophic bacteria, featuring a glutathione-dependent DCM dehalogenase, was the first to be examined by dual C-Cl CSIA (i.e.,  $^{13}\text{C}/^{12}\text{C}$  and  $^{37}\text{Cl}/^{35}\text{Cl}$ ) under oxic conditions (Heraty et al., 1999; Torgonskaya et al., 2019). Recently, dual C-Cl CSIA provided evidence of distinct anaerobic DCM pathways for

*Dehalobacterium formicoaceticum*, and for mixed cultures containing DCM-degrading organisms such as *Candidatus Dichloromethanomonas elyunquensis* (Chen et al., 2018; Kleindienst et al., 2019), and for a bacterial consortium featuring a *Dehalobacterium* strain (Blázquez-Pallí et al., 2019; Trueba-Santiso et al., 2017).

So far, DCM transformation pathways have been examined in groundwater microcosms under static conditions. However, the interplay of hydrochemical and hydrogeological dynamics on DCM biodegradation in contaminated aquifers has not yet been addressed. Water table fluctuations are known to affect (i) mass transfer of VOCs (e.g., DCM) from groundwater to the unsaturated zone (Jeannotat and Hunkeler, 2013; McCarthy and Johnson, 1993), (ii) redox conditions due to redistribution of terminal electron acceptors (e.g., O<sub>2</sub>) (Haberer et al., 2012; Seybold et al., 2002), and (iii) bacterial community composition due to changes in nutrients, redox conditions and exposure to pollutants (Peralta et al., 2014; Rühle et al., 2015). The effect of water table fluctuations on DCM biodegradation is difficult to probe *in situ* as it requires a high spatial and temporal monitoring resolution (Zhang and Furman, 2021). In this context, laboratory aquifers under near-natural settings may prove useful, as flow fields can be controlled and mass fluxes can be established (Schürner et al., 2016).

The purpose of the present study was to examine the effect of water table fluctuations on the hydrochemistry, bacterial community composition, and DCM degradation extent and pathways under controlled conditions. Two laboratory aquifers, fed with contaminated groundwater from a well-characterized former industrial site (Hellal et al., 2020; Hermon et al., 2018), were set up to examine the reactive transport of DCM under transient (i.e., induced water table fluctuations) and steady-state (i.e., static water table) conditions. Concentrations of chloroethenes *cis*-DCE and VC in the contaminated groundwater were also monitored. The objectives of the present study were (i) to examine DCM dissipation processes in groundwater under steady-state and transient conditions, (ii) to infer DCM degradation pathways using dual C-Cl CSIA, and (iii) to analyse bacterial community composition associated with DCM biodegradation by sequencing the 16S rRNA gene.

## 3.2 Materials and methods

### 3.2.1 Chemicals

DCM, *cis*-DCE and VC standards were purchased from Sigma-Aldrich (St: Louis, MO, USA; analytical grade purity: >99%). A second DCM standard was purchased from VWR (Radnor, Pennsylvania, USA; analytical grade purity: >99%). Stock solutions of standards were prepared

in methanol at  $1 \text{ g L}^{-1}$  and diluted in water. Aliquots were stored at  $4 \text{ }^{\circ}\text{C}$ . DCM standards from Sigma-Aldrich and VWR are referenced here as DCM<sub>1</sub> and DCM<sub>2</sub>, respectively.

### 3.2.2 Groundwater collection

Groundwater was collected from the source zone of a well-characterized contaminated aquifer (well Pz-28) (Hellal et al., 2020; Hermon et al., 2018), and used as inflow water in both laboratory aquifers. Isotope and biomolecular analyses evidenced *in situ* anaerobic DCM and *cis*-DCE biodegradation in the source zone of the contaminated aquifer, as well as bacterial genera associated with organohalide respiration (OHR) such as *Geobacter* and *Dehalococcoides* (Hellal et al., 2020; Hermon et al., 2018). Field groundwater sampling and hydrochemical characteristics are provided as Supporting Information (SI, Sections A.1 and A.5).

### 3.2.3 Laboratory aquifers operations

A detail description of the laboratory aquifers is provided in Section 2.3. Experiments were conducted in a temperature-controlled room at  $18 \pm 1 \text{ }^{\circ}\text{C}$ . Both aquifers were continuously fed with  $\text{O}_2$ -depleted contaminated groundwater ( $\text{O}_2 < 1 \text{ mg L}^{-1}$ ) at a rate of  $430 \text{ mL d}^{-1}$ , corresponding to an average water velocity of  $0.02 \text{ m d}^{-1}$ . Groundwater was supplied from two sterile and gas-tight 10 L glass reservoirs connected to each aquifer (Figure 3.1). Each reservoir was kept under constant  $\text{N}_2$ -flux and consisted of a mixture of groundwater and sterilized  $\text{O}_2$ -depleted distilled water at a ratio of 1:3. This allowed to avoid clogging of the pipes feeding the aquifers due to mineral precipitation. Pure DCM was directly spiked and mixed into the reservoirs to reach aqueous concentrations of  $0.47 \text{ mM}$ , equivalent to typical concentrations at contaminated sites (Hermon et al., 2018; Wright et al., 2017).

Both aquifers were operated simultaneously. Prior to the experiments, an incubation period of 70 days was established by operating both aquifers with a continuous flow of DCM-spiked groundwater to reach initial steady-state conditions and allow bacterial adaptation. Monitoring of DCM concentrations and carbon stable isotope ratios during the incubation period (70 days) evidenced DCM biodegradation capacity in both aquifers (data not shown). The water table was positioned at a depth of 33 cm and a capillary fringe of approximately 12 cm was determined visually. During the experimental phase (day 0 to 88), one aquifer remained under steady-state conditions while the second aquifer underwent two water table fluctuation events (Figure 3.1). Under steady-state conditions, a constant horizontal water flow was established using a peristaltic pump (IPC 8, ISMATEC, Glattbrugg, Switzerland). Transient conditions were established



by (i) lowering the water table by 16 cm for 24 h (day 3), (ii) continuous horizontal flow at a low water level for 6 d (up to day 10), and (iii) raising the water table to its initial position for 24 h (day 11). A second identical water table fluctuation event was performed from day 21 to 32 (Figure 3.1).

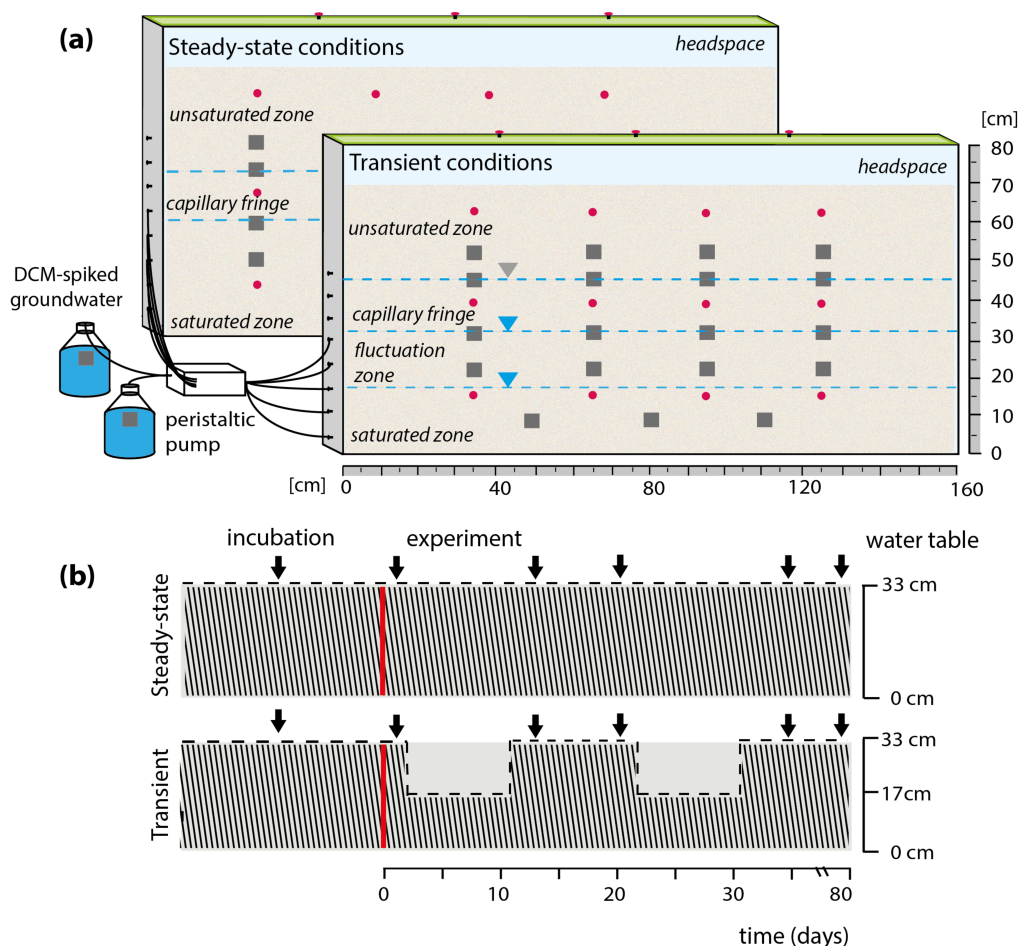


**Figure 3.1:** Lab-scale aquifers fed with DCM-spiked groundwater under steady-state and transient conditions. (a) Schematic overview of the aquifers (flow path from left to right) indicating the saturated zone (SZ), unsaturated zone (UZ), headspace, position of sampling ports (red dots), oxygen foils (grey squares) and top glass (green) covering the aquifers along with three sampling ports opened to the atmosphere. (b) Operations to establish steady-state and transient conditions in the laboratory aquifers and sampling. Water table level is indicated in dotted lines. The end of the incubation period (total 70 days) is marked with a red line. Black arrows show sampling events of water and gas samples. Sampling within the incubation period took place 35 days prior to the experiment.

### 3.2.4 Sampling

Sampling was carried out in both aquifers before and after each water table fluctuation event on days 0 and 13 (first water table fluctuation), and at days 20 and 35 (second water table fluctuation). Pore water samples were collected for hydrochemical analysis, VOCs concentration measurements, carbon and chlorine isotope analysis, and bacterial diversity and community composition. Pore water samples were collected using gas-tight syringes (Hamilton Bonaduz AG, Bonaduz, Switzerland) from inlet and outlet reservoirs, and sampling ports located at depths of 15 and 40 cm from the bottom, and at 35, 65, 95 and 125 cm from the inflow (Figure 3.1). For quantification and CSIA, 20 mL glass vials (Interchim, Montluçon, France) were filled with 1 mL of pore water sample and 1 mL of saturated salt solution (triplicate measurements). Vials were immediately crimped with a Teflon septum with a magnetic crimp (Interchim, Montluçon, France), and stored upside down at 4 °C until further analysis. Gas-phase samples (volume: 2 cm<sup>3</sup>) were collected from the unsaturated zone (z=65 cm) and headspace (z=80 cm), and stored similarly as liquid samples.

Water samples for DNA analysis were collected from inlet and outlet reservoirs (8 mL) and from sampling ports located at depths of 15 and 40 cm (pooling 2 mL in total per single height). Additionally, pore water samples were collected during the incubation period (35 days prior to the experiments, see Figure 3.1), and prior to the core sampling (day 80) for DNA and hydrochemical analysis. Both aquifers were fully drained and sand samples from four cores (length: 70 cm, and inner diameter: 5 cm) were collected for DNA analysis into sterile polyethylene tubes, and stored at -20 °C until further analysis. Core sand samples covering the full depth of the aquifers were retrieved at 40, 70, 100, and 130 cm from the inflow. Three core subsamples representing the saturated zone (SZ), capillary fringe (CF) and unsaturated zones (UZ) were obtained by cutting under sterile conditions each frozen sand core at depths of 25 and 50 cm, respectively.

### 3.2.5 Analytical methods

#### 3.2.5.1 Hydrochemistry

Oxygen (O<sub>2</sub>) concentrations were monitored *in situ* by O<sub>2</sub> sensitive optode foils (PreSens GmbH, Regensburg, Germany) located at the inlet reservoirs and across the sand compartments (Figure 3.1). Under transient conditions, O<sub>2</sub> concentrations were monitored hourly during water table fluctuation events. Redox potential (Eh), pH and electrical conductivity were monitored prior to sampling events using laboratory probes (SCHOTT® Instruments). Major ions were measured

by ion chromatography (Dionex ICS-5000, Thermo Scientific, USA).  $\text{Fe}^{2+}$  was also measured by the BAP method (Tamura et al., 1974). Total organic carbon (TOC), dissolved organic carbon (DOC) and dissolved inorganic carbon (DIC) were analyzed by a TOC analyzer (TOC-V-CPH Shimadzu, NF EN 1484).

### 3.2.5.2 VOCs concentrations and DCM C-Cl CSIA analysis

A detailed description of analytical methods is given in the SI (Section A.2). Briefly, DCM, *cis*-DCE and VC were quantified by analyzing 200  $\mu\text{L}$  of headspace sample using a gas chromatograph (GC, Trace 1300, Thermo Fisher Scientific) coupled with a mass spectrometer (MS, ISQ<sup>®</sup>, Thermo Fisher Scientific), as described elsewhere (Hermon et al., 2018).

Stable carbon isotope composition of DCM, *cis*-DCE and VC was determined by gas chromatography-combustion-isotope ratio mass spectrometry (GC-C-IRMS), with a gas chromatograph (Trace 1310) coupled via a GC/Conflow IV interface to an isotope ratio mass spectrometer (Delta V plus, Thermo Fisher Scientific) (Hermon et al., 2018) (see SI, Section A.3). In-house standards of DCM, *cis*-DCE and VC were prepared daily and analyzed prior to sample measurements. Reproducibility of triplicate measurements was  $\leq 0.2$  ‰ ( $1\sigma$ ) within the linearity range (0.5–50  $\text{mg L}^{-1}$ ). Carbon isotope ratios were reported in  $\delta$  notation as parts per thousand (‰) relative to the international reference material Vienna Pee Dee-Belemnite (V-PDB) (Coplen et al., 2006).

Chlorine isotope composition of DCM was determined by GC-qMS based on the two most abundant fragment ion peaks  $[\text{}^{35}\text{Cl}^{12}\text{C}_1\text{H}_2]^+$  ( $m/z$  49) and  $[\text{}^{37}\text{Cl}^{12}\text{C}_1\text{H}_2]^+$  ( $m/z$  51), as suggested elsewhere (Heckel et al., 2017; Jin et al., 2011). The detailed GC-qMS setup is provided as SI (Section A.3). Chlorine isotope ratios were reported in  $\delta$  notation in parts per thousand [‰] relative to the Standard Mean Ocean (SMOC) (Kaufmann et al., 1984). Chlorine isotope ratios were corrected by an external two-point calibration with pure DCM in-house standards ( $\delta^{37}\text{Cl}_{\text{DCM}_1} = 3.68 \pm 0.10$ ‰ and  $\delta^{37}\text{Cl}_{\text{DCM}_2} = -3.35 \pm 0.12$ ‰) characterized at Isotope Tracer Technologies Inc., Waterloo, Canada by IRMS after conversion to  $\text{CH}_3\text{Cl}$  (Holt et al., 1997), and at the Departament de Mineralogia, Petrologia i Geologia Aplicada, University of Barcelona using GC-qMS. Reported uncertainties include both accuracy and reproducibility based on long-term measurements and standard deviations. Typical reproducibility was  $\leq 0.5$ ‰ ( $1\sigma$ ) within the tested linearity range (0.5–20  $\text{mg L}^{-1}$ ). Chlorine isotope compositions of native *cis*-DCE and VC were not analyzed.

### 3.2.5.3 DNA extraction from pore water and sand samples

Pore water samples were filtered through sterile 0.22  $\mu\text{m}$  membrane filters (Swinnex holder, 13 mm, Millipore, Bedford, USA) and stored at  $-20^\circ\text{C}$  until DNA extraction, as described previously (Hermon et al., 2018). Sand core subsamples were retrieved from both aquifers at the end of the experiments (day 88). Under sterile conditions, the bottom and top first 1 cm of the core samples were removed. Each core subsample was thoroughly mixed and a subsample of 1 g of sand was used for DNA extraction. For both pore water and core samples, DNA was extracted using the DNeasy Power Water kit according to the manufacturer's protocol (Qiagen, Hilden, Germany). Extracted DNA was quantified using Qubit fluorometric quantification with the Qubit dsDNA HS Assay kit (ThermoFischer Scientific, MA, USA).

### 3.2.5.4 DNA sequencing

The V4-V5 hypervariable region of the 16S rRNA gene was PCR amplified by an optimized and standardized amplicon library preparation protocol (Metabiote<sup>®</sup>, GenoScreen, Lille, France), including a positive (mock community) and negative (blank) control (Hermon et al., 2018). Libraries were sequenced by paired-end Illumina MiSeq 2x250 bases. Demultiplexing and trimming was followed by paired read assembly (minimum overlap 30 nt, minimum identity of 97%), resulting in a total of 3,614,309 sequences. Denoising, chimera checking, generation of operational taxonomic units (OTUs), taxonomic classification using Greengenes (v13.8 as reference), and alpha-diversity metrics were performed using a custom-scripted bioinformatics pipeline of GenoScreen (Hermon et al., 2018). The percentage of 16S rRNA gene sequences of taxa featuring known DCM-degrading strains (identity  $>97\%$ ) was determined.

## 3.2.6 Data analysis

### 3.2.6.1 Evolution of isotopic data

The average isotope value of the residual non-degraded fraction of DCM was derived according to the Rayleigh equation (Elsner, 2010):

$$\ln \left( \frac{R_{t,E}}{R_{0,E}} \right) = \ln \left( \frac{C_t}{C_0} \right) \cdot \frac{\varepsilon_{bulk}^E}{1000} \quad (3.1)$$

where  $R_{t,E}/R_{0,E}$  is the isotope ratio of element  $E$  (i.e.  $^{13}\text{C}/^{12}\text{C}$  and  $^{37}\text{Cl}/^{35}\text{Cl}$ ) and  $C_t/C_0$  are the concentrations of a compound (i.e., DCM) at a given time ( $t$ ) and at the initial time ( $0$ ). Carbon and chlorine isotopic composition are reported in delta notation ( $\delta^h E$ ) following  $\delta^h E =$

$[(R_{\text{sample}}/R_{\text{standard}})-1] \times 1000$  (Elsner, 2010). Bulk isotope fractionation values ( $\varepsilon_{\text{bulk}}^E$ , in ‰) are obtained by least squares linear regression without forcing the slope through the origin. The uncertainty corresponds to the 95% confidence interval (CI) and the error was determined using ordinary linear regression (Elsner et al., 2007).

Changes of carbon *versus* chlorine isotope signatures were plotted to derive the  $\Lambda^{\text{C/Cl}}$  value from the slope of the linear regression using the least-squares algorithm of the York method (York et al., 2004) and the IsoplotR package in R (Vermeesch, 2018). The York method takes into account the error in both  $x$ - and  $y$ -variables assuming they are independent from each other, giving more accurate calculations of  $\Lambda$  and a better estimate of the uncertainty (Ojeda et al., 2019).

$$\Lambda^{\text{C/Cl}} = \frac{\ln[(\delta^{13}\text{C}_t/1000 + 1)/(\delta^{13}\text{C}_0/1000 + 1)]}{\ln[(\delta^{37}\text{Cl}_t/1000 + 1)/(\delta^{37}\text{Cl}_0/1000 + 1)]} \approx \frac{\varepsilon_{\text{bulk}}^{\text{C}}}{\varepsilon_{\text{bulk}}^{\text{Cl}}} \quad (3.2)$$

DCM biodegradation was estimated based on changes in carbon and chlorine isotope ratios over time and across the flow path (i.e., at different observation points). The extent of DCM biodegradation ( $B_E$ , in %) was estimated using the Rayleigh model (Elsner, 2010; Hunkeler et al., 2005; Thullner et al., 2012). A range of  $B$  was obtained from reported  $\varepsilon_{\text{C}}$  and  $\varepsilon_{\text{Cl}}$  values for both aerobic and anaerobic bacterial DCM degradation (Chen et al., 2018; Lee et al., 2015; Torgonskaya et al., 2019).

$$B_E[\%] = 1 - f \cdot 100 = \left[ 1 - \left( \frac{\delta^h E_t + 1000}{\delta^h E_0 + 1000} \right)^{\frac{1000}{\varepsilon_{\text{bulk}}^E}} \right] \cdot 100 \quad (3.3)$$

### 3.2.6.2 Bacterial community composition

Sequencing data from pore water and sand samples were deposited to the ENA archive, BioProject accession number PRJEB43379. Multivariate statistical analysis of relative OTU abundance was performed with R (core Team, 2019). Non-metric multidimensional scaling (NMDS) based on Bray-Curtis dissimilarities of log-transformed data was performed to visualize dissimilarities between bacterial taxa associated with DCM degradation (Hellal et al., 2020).

## 3.3 Results and discussion

### 3.3.1 Water table fluctuations affect hydrochemical conditions

Hydrochemical variations are summarized in the SI (Sections A.4 and A.5). Overall, saturated  $\text{O}_2$  concentrations ( $8.4 \text{ mg L}^{-1}$ ) were observed in the unsaturated zone (UZ) in both aquifers

( $z=60$  cm), while  $O_2$ -depleted levels were established in the saturated zone (SZ;  $z=0-33$  cm;  $O_2 < 1.0$  mg L<sup>-1</sup>). The increase of redox potential over time (Eh ranged from  $-100$  to  $+0$  mV at days 0 and 35, respectively) was consistent with  $O_2$  dynamics in the fluctuation zone ( $z=17-33$  cm; SI Section A.5) (Pronk et al., 2020). Concentrations of  $O_2$  rapidly increased up to  $1.5$  mg L<sup>-1</sup> during drainage periods ( $z=25$  cm; SI, Section A.5). During the first imbibition period, water moved in an upward direction,  $O_2$  concentrations decreased slightly but did not return to initial concentrations ( $1.3$  mg L<sup>-1</sup>). From the second imbibition period until the end of the experiment,  $O_2$  levels slowly decreased indicating that the system progressively returned to initial conditions ( $O_2 < 1$  mg L<sup>-1</sup>) (Haberer et al., 2012).

Re-oxygenation of groundwater below the water table was likely associated with entrapped air serving as a source of  $O_2$  to the underlying  $O_2$ -depleted water (Williams and Oostrom, 2000). Redox potential and  $O_2$  varied upon water table fluctuation. Nevertheless, the high concentration of  $Fe^{2+}$  in both aquifers (up to  $2.8$  mg L<sup>-1</sup>) suggested prevailing reducing conditions, in line with reducing conditions observed *in situ* for the groundwater used in this study (Hellal et al., 2020; Hermon et al., 2018) (SI, Section A.5). No other reduced species were detected in both aquifers ( $< D.L.$ ). *Cis*-DCE and VC, the two main chloroethenes in the groundwater source of this study (Hellal et al., 2020; Hermon et al., 2018), were also followed to further examine the established hydrochemical conditions in the laboratory aquifers. Only *cis*-DCE was detected at the inflow of both aquifers with average concentrations of  $15$  mg L<sup>-1</sup> and  $\delta^{13}C_{DCE}$  values of  $-23.5 \pm 0.4\text{‰}$  (SI, Section A.6). Up to 90% of *cis*-DCE dissipated at the outflows after 35 days. Values of  $\delta^{13}C$  for *cis*-DCE were smaller ( $\Delta\delta^{13}C_{DCE} < 2\text{‰}$ ) at the outflows than  $\delta^{13}C$  values observed within the first 65 cm from inflow ( $\Delta\delta^{13}C_{DCE} > 10\text{‰}$ ). Similarly, VC concentrations of up to  $6$  and  $12$  mg L<sup>-1</sup> were detected within the first 65 cm from inflow under steady-state and transient conditions, respectively, and average  $\delta^{13}C_{VC}$  values of  $-39.2 \pm 0.8\text{‰}$  ( $n=20$ ) were formed along the flow path ( $\delta^{13}C_{VC,standard} = -29.5 \pm 0.2\text{‰}$ ) (SI, Section A.6). Together with the detection of OHRB (see below), this suggests that reductive dechlorination occurred in both aquifers, in agreement with observations at the groundwater source (Hellal et al., 2020; Hermon et al., 2018).

### 3.3.2 Water table fluctuations affect DCM mass dissipation and C and Cl isotope fractionation

The absence of gas-phase DCM (gas-phase Q.L. =  $0.13$   $\mu$ g L<sup>-1</sup>, sampling volume:  $2$  cm<sup>3</sup>) in the UZ ( $z=65$  cm) and headspace ( $z=80$  cm) of both aquifers throughout the experiment, and

inlet-outlet DCM mass balance indicated that volatilization did not contribute significantly (<10 %) to the overall DCM dissipation in both aquifers. Steep concentration gradients are generally formed across the capillary fringe due to slow diffusion in water and small vertical dispersivity (Jeannotat and Hunkeler, 2013). Previous studies showed that mass transport of PCE and TCE from the SZ to the UZ (i.e., within the 15 cm above the water table) led to 90% smaller gas-phase concentrations with respect to the aqueous-phase concentrations at the water table under steady-state (Jeannotat and Hunkeler, 2013; McCarthy and Johnson, 1993). While variations of VOCs concentrations in the gas-phase increase in the UZ when the water table drops as a result of residual water being in contact with the gas, concentrations decrease again when the water table is raised, returning to concentration equilibrium (Jeannotat and Hunkeler, 2013; McCarthy and Johnson, 1993). Hence, undetected gas-phase DCM concentrations in the UZ ( $z=65$  cm) and headspace ( $z=80$  cm) is likely due to the low non-dimensional Henry's coefficient of DCM of 0.0549 at 18 °C (Gossett (1987); PCE and TCE of 0.495 and 0.265, respectively), the continuous replenishment of the aqueous phase by low horizontal groundwater flow, and measurements carried out before and after each water table fluctuation event.

In the SZ, DCM concentrations decreased along the flow path in both aquifers. After 35 days, a more pronounced DCM mass dissipation in the aquifer outlets was observed under transient (95%) than under steady-state (42%) conditions (Figure 3.2).  $\delta^{13}\text{C}$  and  $\delta^{37}\text{Cl}$  values of DCM in the inflow water remained constant throughout the experiments ( $-46.3 \pm 0.5\text{‰}$  and  $-3.5 \pm 0.12\text{‰}$ , respectively). Under both transient and steady-state conditions, DCM became significantly enriched in both  $^{13}\text{C}$  and  $^{37}\text{Cl}$  (Figure 3.2). C and Cl isotope data for DCM degradation showed a good fit to the Rayleigh model (Eq. 3.1) under both hydraulic regimes ( $R^2 > 0.92$ ) (SI, Section A.7). The apparent C and Cl isotope fractionation values ( $\epsilon_{\text{bulk}}^{\text{C}}$  and  $\epsilon_{\text{bulk}}^{\text{Cl}}$ ) of  $-23.6 \pm 3.2\text{‰}$  and  $-8.7 \pm 1.6\text{‰}$ , respectively, were larger under steady-state than under transient conditions ( $\epsilon_{\text{bulk}}^{\text{C}}$  and  $\epsilon_{\text{bulk}}^{\text{Cl}}$  values of  $-11.8 \pm 2.0\text{‰}$  and  $-3.1 \pm 0.6\text{‰}$ , respectively; SI, Section A.7). In previous reports, DCM volatilization was associated with low C and Cl fractionation ( $\epsilon^{\text{C}} = +0.65\text{‰}$  and  $\epsilon^{\text{Cl}} = -0.48\text{‰}$ ) compared to DCM biodegradation (Huang et al., 1999). Thus, the magnitude of  $\epsilon_{\text{bulk}}^{\text{C}}$  and  $\epsilon_{\text{bulk}}^{\text{Cl}}$  values under both hydraulic regimes suggest that DCM biodegradation prevailed in the aquifers.

The extent of DCM biodegradation (B) along the flow path was calculated based on reported  $\epsilon^{\text{C}}$  values ranging from  $-71\text{‰}$  to  $-15.5\text{‰}$  and  $\epsilon^{\text{Cl}}$  values from  $-7\text{‰}$  to  $-5.2\text{‰}$  (Chen et al., 2018; Lee et al., 2015; Torgonskaya et al., 2019). The range of  $\epsilon^{\text{C}}$  and  $\epsilon^{\text{Cl}}$  values was defined based on the assumption that both aerobic and anaerobic DCM degradation pathways may co-occur

in both aquifers, which is supported by hydrochemical variations and micro-oxic environments in the groundwater source (Hermon et al., 2018). Values of  $B$  under steady-state and transient conditions ranged from 22% to 55%, and from 22% to 90%, respectively (Table 3.1), corresponding to the DCM mass dissipation observed under both hydraulic regimes. Time-dependent first-order biodegradation rate constants ( $\lambda_t$ ) were calculated according to the Rayleigh model, as described in the SI of Hermon et al. (2018), with values of  $3.4 \times 10^{-3} \text{ d}^{-1}$  and  $5.7 \times 10^{-3} \text{ d}^{-1}$  under steady-state and transient conditions, respectively. Worthy of note, similar *in situ*  $\lambda_t$  were estimated at the groundwater source of this study (Hermon et al., 2018), thus demonstrating the established near-natural settings within the laboratory aquifers.

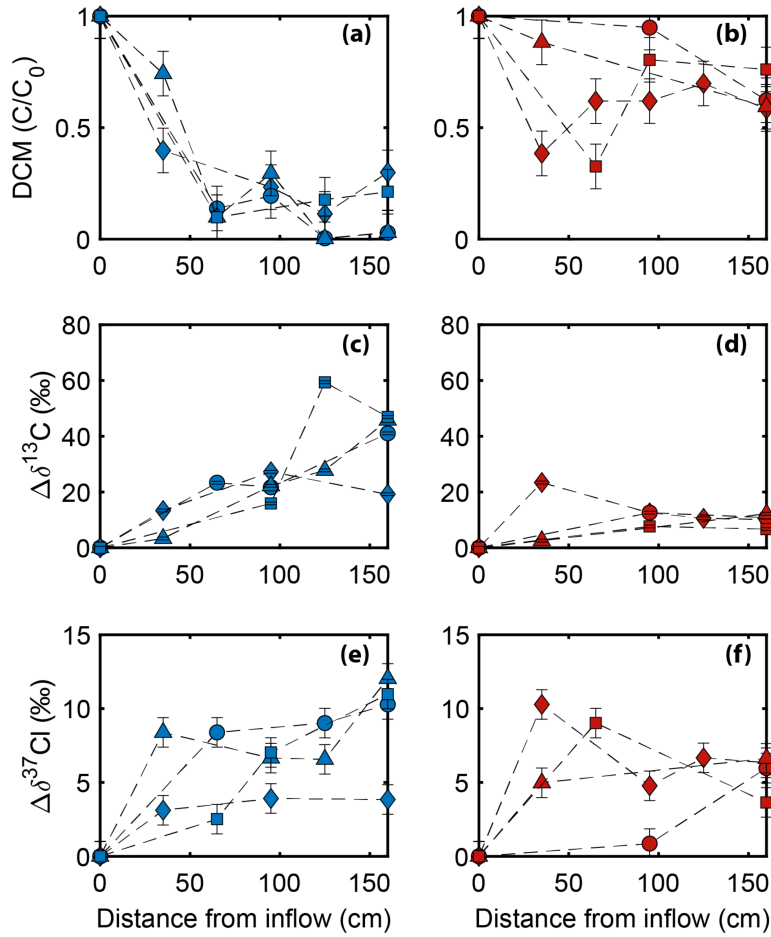


**Figure 3.2:** DCM concentrations under steady-state (red) and transient (blue) conditions (a, b), carbon isotope values (c, d) and chlorine isotope values (e, f) over distance from inflow. Symbols represent observations at depth  $z=15$  cm and at different times: day 0 (diamonds), day 13 (circles), day 20 (triangles) and day 35 (squares). Error bars associated with DCM concentrations and stable isotope values represent standard errors ( $3 \leq n$ ).



**Table 3.1:** DCM biodegradation (B [%]) under transient and steady-state conditions from days 0 to 35. A range of B [%] was estimated using the full range of  $\varepsilon^C$  and  $\varepsilon^{Cl}$  values reported so far for both aerobic and anaerobic bacterial degradation of DCM. Reported  $\varepsilon^{Cl}$  values range from  $-71\text{‰}$  ( $^C B_{\min}$ ) to  $-15.5\text{‰}$  ( $^C B_{\max}$ ), and  $\varepsilon^C$  value of  $-7\text{‰}$  ( $^{Cl} B_{\min}$ ) to  $-5.2\text{‰}$  ( $^{Cl} B_{\max}$ ) (Chen et al., 2018; Lee et al., 2015; Torgonskaya et al., 2019).

Condition	Days	$\Delta\delta^{13}C$	$\Delta\delta^{37}Cl$	$^C B_{\min}$	$^C B_{\max}$	$^{Cl} B_{\min}$	$^{Cl} B_{\max}$
	[%]	[‰]	[‰]	[%]	[%]	[%]	[%]
Transient	0	17.6	4.8	22	66	48	58
	13	31.8	9.2	36	85	73	83
	20	40.3	10.3	33	86	80	85
	35	49.2	7.0	48	91	66	75
Steady-state	0	17.6	5.6	22	66	55	66
	13	11.7	5.9	16	54	34	43
	20	12.1	5.8	14	48	56	67
	35	11.6	6.3	15	51	57	66

### 3.3.3 DCM transformation pathways under transient and steady-state conditions

Estimated  $\Lambda^{C/Cl}$  values were lower under steady-state ( $1.92 \pm 0.30$ ;  $p < 0.03$ ) than under transient conditions ( $3.58 \pm 0.42$ ;  $p < 0.01$ ) (Figure 3.3). This suggests distinct DCM C-Cl bond cleavage mechanisms under dynamic hydrogeological conditions. The calculated  $\Lambda^{C/Cl}$  values under transient conditions fall within the range of reported  $\Lambda^{C/Cl}$  values during anaerobic DCM degradation (3.40–7.89) and are similar to  $\Lambda^{C/Cl}$  values reported for *Ca. Dichloromethanomonas elyunquensis* ( $3.40 \pm 0.03$ ) (Chen et al., 2018), which suggests the prevalence of anaerobic DCM pathways. Most strikingly, the lower  $\Lambda^{C/Cl}$  value determined under steady-state conditions ( $1.92 \pm 0.30$ ) has not been reported previously. Still, this value likely also reflects anaerobic DCM degradation, given that so far higher  $\Lambda^{C/Cl}$  values (8.1 to 11.2) are rather associated with aerobic DCM degradation pathways (Heraty et al., 1999; Torgonskaya et al., 2019) (SI, Section A.8).

To date, anaerobic DCM degradation by bacteria affiliated with the *Peptococcaceae* family has been examined using C-Cl CSIA. Two distinct anaerobic degradation pathways were reported for DCM fermentation by *Dehalobacterium formicoaceticum* ( $\Lambda^{C/Cl} = 7.89 \pm 0.12$ ) and DCM mineralization by *Ca. Dichloromethanomonas elyunquensis* ( $\Lambda^{C/Cl} = 3.40 \pm 0.03$ ), and proposed to be associated with the Wood-Ljungdahl pathway (WLP) (Blázquez-Pallí et al., 2019; Chen et al., 2020, 2018; Kleindienst et al., 2019).

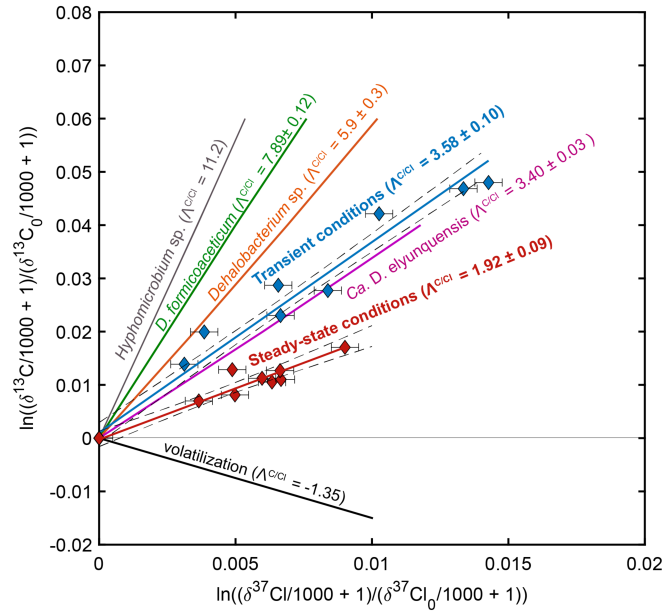


**Figure 3.3:** Dual plot of  $\Delta\delta^{13}\text{C}$  versus  $\Delta\delta^{37}\text{Cl}$  for the degradation of DCM under steady-state (red diamonds) and transient (blue diamonds) conditions. The continuous lines represent the linear regression to derive the  $\Lambda^{\text{C/Cl}}$  values and dashed lines represent the 95% confidence interval (C.I.), according to the York method. Reported values for DCM degradation by *Hyphomicrobium* strain MC8b (Heraty et al., 1999), *Dehalobacterium formicoaceticum* and *Ca. D. elyunquensis* (Chen et al., 2018), and *Dehalobacterium* sp. (Blázquez-Pallí et al., 2019) were added for comparison. Black line represents 99% of DCM volatilization (Huang et al., 1999).

In addition, Blázquez-Pallí et al. (2019) reported a distinct  $\Lambda^{\text{C/Cl}}$  value ( $5.9 \pm 0.3$ ) for anaerobic DCM degradation by a *Dehalobacterium*-containing culture, differing from that associated with *Dehalobacterium formicoaceticum* ( $\Lambda^{\text{C/Cl}}$  value =  $7.89 \pm 0.12$ ), although the two strains belong to the same genus. Different characteristics of the bacterial cell envelope or enzyme locations may result in distinct C and Cl isotope fractionation (Trueba-Santiso et al., 2017). The differences in  $\Lambda^{\text{C/Cl}}$  values under steady-state and transient conditions may thus reflect distinct C-Cl bond cleavage reactions and distinct anaerobic DCM degradation pathways. Further, our findings suggest that the prevalence of a given pathway depend on hydrochemical and hydrogeological dynamics in aquifers. Nevertheless, both laboratory aquifers likely feature a variety of DCM-degrading microorganisms, with the possibility of simultaneous operations of several different aerobic and anaerobic degradation pathways (Van Breukelen, 2007). In particular, the slight increase in  $\text{O}_2$  levels in the fluctuation zone under transient conditions may be indicative of micro-oxic environments (SI, Sections A.4 and A.5). However, the  $\Lambda^{\text{C/Cl}}$  values obtained in our aquifers rather suggest the dominance of different anaerobic DCM degradation pathways,

which is further supported by the presence of taxa associated with anoxic conditions (see below).

### 3.3.4 Water table fluctuations affect bacterial community composition and distribution of DCM-associated taxa

In total, 3,649,087 high-quality sequences were obtained, from which 69% and 31% corresponded to pore water ( $n=56$ ) and sand samples ( $n=24$ ), respectively. Rarefaction curves of diversity indices reached asymptotes with increasing sequencing depth, indicating sufficient sequencing efforts to capture the biodiversity extent of bacterial communities in both pore water and sand samples (SI, Section A.9).

Changes in bacterial diversity were analyzed using NMDS ordination of relative OTU abundance. Diversity in sand samples (day 88) varied mainly as a function of  $O_2$  gradients in the SZ and UZ (Figure 3.4). In contrast, differences in bacterial diversity in pore water samples (day 0–80) between inlet and outlet reservoirs suggested bacterial adaptation to DCM contamination along the flow path (Figure 3.4). Nevertheless, similar bacterial diversity under transient and steady-state conditions for both pore water and sand samples suggested that water table fluctuations did not play a major role in shaping the overall composition of bacterial communities (SI, Sections A.10 and A.11).

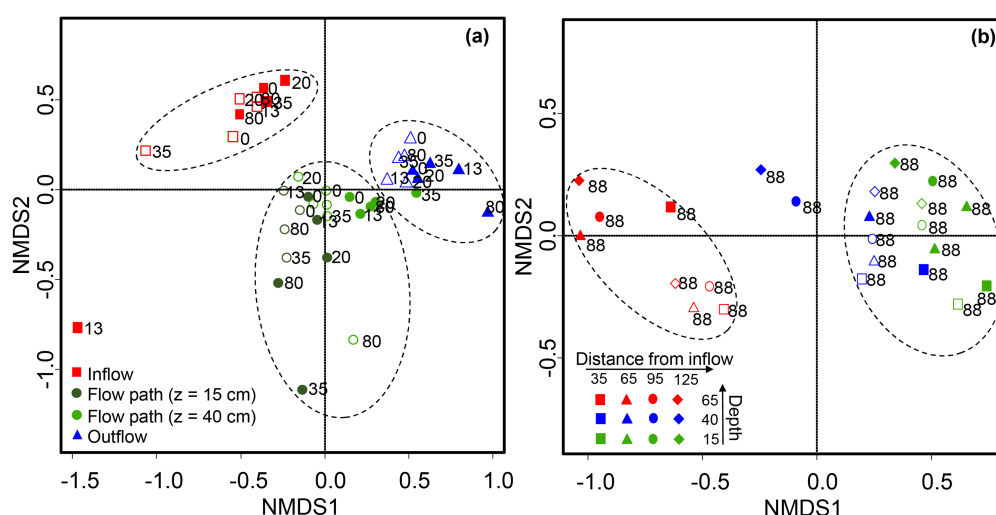


**Figure 3.4:** NMDS ordination plot of bacterial diversity profiles from (a) pore water and (b) sand samples. Full symbols: transient conditions, empty symbols: steady-state conditions. Numbers next to symbols represent sampling day at 0, 13, 20, 35 and 80 for pore water samples and at day 88 for sand samples. Plot stress: (a) 0.11% and (b) 0.06%.

Dominant taxa in aquifers may be associated with pollutants degradation pathways. In both aquifers, *Firmicutes* was the most abundant phylum in sand samples with up to 60% of retrieved sequences at lower depths ( $z=15\text{cm}$ ; SI, Section A.11). Previous studies have shown the presence of this phylum in highly contaminated aquifers with VOCs (Hellal et al., 2020; Wright et al., 2017). Moreover, *Firmicutes* bacteria are known to utilize DCM as a sole carbon source under anoxic conditions (Kleindienst et al., 2017). Hence, the occurrence of *Firmicutes* supports the prevalence of anaerobic DCM biodegradation in both aquifers.

In pore water samples, the dominant OTU was associated with *Desulfosporosinus* under both steady-state and transient conditions (Figure 3.5). Under steady-state conditions, *Desulfosporosinus* and *Geobacter* represented on average 25% and 12% of obtained sequences in the SZ, respectively, while *Dehalobacterium* and *Dehalococcoides* represented each approximately 10% (Figure 3.5). Under transient conditions, in contrast, *Desulfosporosinus* increased from 25% to 58% relative abundance between days 0 and 13 in the SZ ( $z=15\text{ cm}$ ), corresponding to the first water table fluctuation event (Figure 3.5). *Geobacter* was the second most abundant genus in the SZ representing up to 15% followed by *Dehalobacterium* (4%).

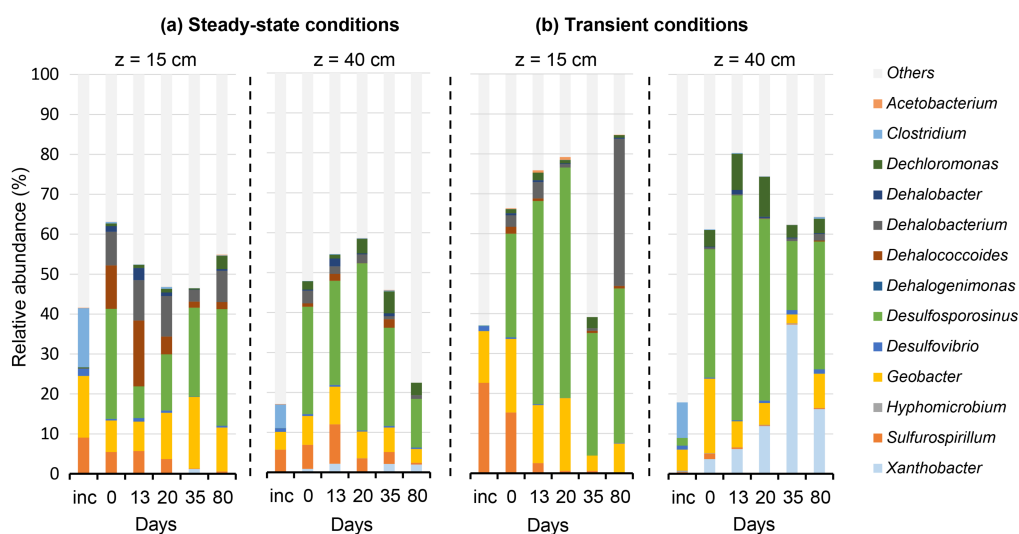


**Figure 3.5:** Relative abundance of taxa associated with DCM degradation and OHR in lab-scale aquifers under (a) steady-state and (b) transient conditions in the saturated zone ( $z=15\text{ cm}$ ) and capillary fringe ( $z=40\text{ cm}$ ), and over time (from 0 to 80 days). Data includes the initial incubation period of 70 days ("inc" represents sampling 35 days prior to the experiments). Relative abundance (%) of OTUs was normalized to the total sequence abundance for all defined OTUs.

Co-occurrence of *Desulfosporosinus*, *Geobacter*, *Sulfurospirillum* and *Dehalococcoides* was reported previously in contaminated aquifers with halogenated contaminants (Hellal et al., 2020; Wright et al., 2017). This parallel enrichment of different OTUs without demonstrated association with DCM degradation suggest interspecies interactions in our laboratory aquifers. Such interactions could be indicative of concomitant degradation of DCM and other halogenated contaminants, as shown recently in investigations of other contaminated sites (Blázquez-Pallí et al., 2019; Hellal et al., 2020; Hermon et al., 2018; Trueba-Santiso et al., 2020; Wright et al., 2017). Detection of bacterial genera associated with OHR such as *Dehalococcoides* further supports the concomitant degradation of DCM and *cis*-DCE in our laboratory aquifers. Furthermore, reductive dechlorination of chlorinated ethenes such as *cis*-DCE relies on H<sub>2</sub> as electron donor (DiStefano et al., 1992). Recently, it was proposed that DCM mineralization by *Ca. D. elyunquensis* produces H<sub>2</sub> and CO<sub>2</sub> (Chen et al., 2020), which may sustain reductive dechlorination in mixed contaminant plumes. Notably, for growth with DCM, *Ca. D. elyunquensis* requires the presence of H<sub>2</sub>-consuming partner populations performing H<sub>2</sub>/CO<sub>2</sub> reductive acetogenesis, while *Dehalobacterium formicoaceticum* showed a strong dependence on CO<sub>2</sub> (Chen et al., 2020). Concomitant degradation of DCM and chlorinated ethenes in contaminated aquifers may thus result from interspecies metabolic networks associated with dehalogenative metabolism.

More generally, dynamic environmental conditions such as water table fluctuations can increase microbial metabolic activity (Pronk et al., 2020). Thus, we hypothesized that in the present study, water table fluctuations promoted a larger enrichment of *Desulfosporosinus* compared to steady-state conditions (Figure 3.5). Kleindienst et al. (2019) reported that *Ca. D. elyunquensis* expressed similar WLP-associated enzymes as those of *Dehalobacter* and *Desulfosporosinus* spp. Hence, the similar C and Cl isotope fractionation determined here for DCM biodegradation under transient conditions ( $\Delta^{C/Cl} = 3.58 \pm 0.42$ ) and by *Ca. D. elyunquensis* ( $\Delta^{C/Cl} = 3.40 \pm 0.03$ ) (Chen et al., 2018) suggest *Desulfosporosinus* as a potential DCM-degrading bacterium, in line with a previous report (Wright et al., 2017). In contrast, the higher abundance of *Dehalobacterium* under steady-state conditions, and similar C fractionation values to those of a *Dehalobacterium*-containing culture (Blázquez-Pallí et al., 2019), suggest the occurrence of a fermentative DCM metabolism by as yet unknown *Dehalobacterium* strains ( $\Delta^{C/Cl} = 1.92 \pm 0.30$ ). Worthy of note, a recent study proposed *Ca. Formimonas warabiya* strain DCMF as a novel DCM-fermenting bacterium of the *Peptococcaceae* family, capable to metabolize DCM to acetate via the WLP (Holland et al., 2021) (SI, Section A.8). Clearly, bacteria associated with the *Peptococcaceae* family may play an important role in DCM biodegradation at contaminated

sites.

### 3.4 Conclusions

Our study examined the effect of dynamic environmental conditions such as water table fluctuations on (i) hydrochemical conditions, (ii) bacterial responses, and (iii) DCM degradation pathways in multi-contaminated aquifers. Our integrative approach combining C-Cl CSIA and biomolecular analyses suggested the prevalence of two distinct, possibly co-occurring, anaerobic DCM degradation pathways under steady-state and transient conditions. Bacterial diversity and distribution of DCM-associated taxa was similar under both conditions. However, responses to water table fluctuations resulted in different bacterial community composition dominated by bacteria from the *Peptococcaceae* family, in particular *Desulfosporosinus* sp. We showed that environmental dynamics, which are often excluded from laboratory degradation experiments, can affect *in situ* DCM transformation. While current knowledge of anaerobic transformation pathways of DCM limits interpretation of DCM *in situ* biodegradation, fundamental research considering dynamics of environmental conditions are needed to improve bioremediation approaches at DCM contaminated sites in the future.

### Acknowledgments

The author acknowledges Dr. Jennifer Hellal for providing access to the Themeroil site, Dr. Charline Wiegert for help in mounting the laboratory aquifers and preliminary surveys, and Dr. Jordi Palau for measurements of chlorine standards. The author is grateful to Benoît Guyot, and Colin Fourtet, for technical assistance in the laboratory, Carmen Lázaro Sánchez for DNA extractions, and Dr. Tetyana Gylevska for fruitful discussions.

## References of Chapter 3

- ATSDR (2019). Substance priority list. Accessed: 2022-01-20.
- Blázquez-Pallí, N., Shouakar-Stash, O., Palau, J., Trueba-Santiso, A., Varias, J., Bosch, M., Soler, A., Vicent, T., Marco-Urrea, E., and Rosell, M. (2019). Use of dual element isotope analysis and microcosm studies to determine the origin and potential anaerobic biodegradation of dichloromethane in two multi-contaminated aquifers. *Science of The Total Environment*, 696:134066.
- Chen, G., Fisch, A. R., Gibson, C. M., Erin Mack, E., Seger, E. S., Campagna, S. R., and Löffler, F. E. (2020). Mineralization versus fermentation: Evidence for two distinct anaerobic bacterial degradation pathways for dichloromethane. *The ISME Journal*, 14(4):959–970.
- Chen, G., Shouakar-Stash, O., Phillips, E., Justicia-Leon, S. D., Gilevska, T., Sherwood Lollar, B., Mack, E. E., Seger, E. S., and Löffler, F. E. (2018). Dual carbon-chlorine isotope analysis indicates distinct anaerobic dichloromethane degradation pathways in two members of *Peptococcaceae*. *Environmental Science & Technology*, 52(15):8607–8616.
- Coplen, T. B., Brand, W. A., Gehre, M., Gröning, M., Meijer, H. A. J., Toman, B., and Verkouteren, R. M. (2006). New guidelines for  $\delta^{13}\text{C}$  measurements. *Analytical Chemistry*, 78(7):2439–2441.
- core Team, R. (2019). R: A language and environment for statistical computing, version 3.5.3. Place: Vienna, Austria.
- DiStefano, T. D., Gossett, J. M., and Zinder, S. H. (1992). Hydrogen as an electron donor for dechlorination of tetrachloroethene by an anaerobic mixed culture. *Applied and Environmental Microbiology*, 58(11):3622–3629.
- Elsner, M. (2010). Stable isotope fractionation to investigate natural transformation mechanisms of organic contaminants: Principles, prospects and limitations. *Journal of Environmental Monitoring*, 12(11):2005–2031.
- Elsner, M. and Imfeld, G. (2016). Compound-specific isotope analysis (CSIA) of micropollutants in the environment – Current developments and future challenges. *Current Opinion in Biotechnology*, 41:60–72.
- Elsner, M., McKelvie, J., Lacrampe Couloume, G., and Sherwood Lollar, B. (2007). Insight into methyl *tert* -butyl ether (MTBE) stable isotope fractionation from abiotic reference experiments. *Environmental Science & Technology*, 41(16):5693–5700.
- European Commission (2013). Priority substances and certain other pollutants according to annex II of directive 2008/105/EC - Environment - European Commission.
- Fischer, A., Manefield, M., and Bombach, P. (2016). Application of stable isotope tools for evaluating natural and stimulated biodegradation of organic pollutants in field studies. *Current Opinion in Biotechnology*, 41:99–107.
- Gossett, J. M. (1987). Measurement of Henry's law constants for C1 and C2 chlorinated hydrocarbons. *Environmental Science & Technology*, 21(2):202–208.

- Haberer, C. M., Rolle, M., Cirpka, O. A., and Grathwohl, P. (2012). Oxygen transfer in a fluctuating capillary fringe. *Vadose Zone Journal*, 11(3):vzj2011.0056.
- Heckel, B., Rodríguez-Fernández, D., Torrentó, C., Meyer, A., Palau, J., Domenech, C., Rosell, M., Soler, A., Hunkeler, D., and Elsner, M. (2017). Compound-specific chlorine isotope analysis of tetrachloromethane and trichloromethane by gas chromatography-isotope ratio mass spectrometry vs gas chromatography-quadrupole mass spectrometry: Method development and evaluation of precision and trueness. *Analytical Chemistry*, 89(6):3411–3420.
- Hellal, J., Joulain, C., Urien, C., Ferreira, S., Denonfoux, J., Hermon, L., Vuilleumier, S., and Imfeld, G. (2020). Chlorinated ethene biodegradation and associated bacterial taxa in multi-polluted groundwater: Insights from biomolecular markers and stable isotope analysis. *Science of The Total Environment*, page 142950.
- Heraty, L., Fuller, M., Huang, L., Abrajano, T., and Sturchio, N. (1999). Isotopic fractionation of carbon and chlorine by microbial degradation of dichloromethane. *Organic Geochemistry*, 30(8):793–799.
- Hermon, L., Denonfoux, J., Hellal, J., Joulain, C., Ferreira, S., Vuilleumier, S., and Imfeld, G. (2018). Dichloromethane biodegradation in multi-contaminated groundwater: Insights from biomolecular and compound-specific isotope analyses. *Water Research*, 142:217–226.
- Holland, S. I., Ertan, H., Manefield, M. J., and Lee, M. (2021). A novel, dichloromethane-fermenting bacterium in the *Peptococcaceae* family, *Candidatus formamonas warabiya*, gen. nov. sp. nov. *The ISME Journal*, 5(6):1709–1721.
- Holt, B. D., Sturchio, N. C., Abrajano, T. A., and Heraty, L. J. (1997). Conversion of chlorinated volatile organic compounds to carbon dioxide and methyl chloride for isotopic analysis of carbon and chlorine. *Analytical Chemistry*, 69(14):2727–2733.
- Huang, L., Sturchio, N., Abrajano, T., Heraty, L., and Holt, B. (1999). Carbon and chlorine isotope fractionation of chlorinated aliphatic hydrocarbons by evaporation. *Organic Geochemistry*, 30(8):777–785.
- Hunkeler, D., Aravena, R., Berry-Spark, K., and Cox, E. (2005). Assessment of degradation pathways in an aquifer with mixed chlorinated hydrocarbon contamination using stable isotope analysis. *Environmental Science & Technology*, 39(16):5975–5981.
- Hunkeler, D., Meckenstock, R., and Sherwood Lollar, B. (2009). A guide for assessing biodegradation and source identification of organic ground water contaminants using compound specific isotope analysis (CSIA). U.S. Environmental Protection Agency, Washington, D.C., EPA/600/R-08/148, pages 1–82.
- Jeannotat, S. and Hunkeler, D. (2013). Can soil gas VOCs be related to groundwater plumes based on their isotope signature? *Environmental Science & Technology*, 47(21):12115–12122.
- Jin, B., Laskov, C., Rolle, M., and Haderlein, S. B. (2011). Chlorine isotope analysis of organic contaminants using GC-qMS: Method optimization and comparison of different evaluation schemes. *Environmental Science & Technology*, 45(12):5279–5286.
- Kaufmann, R., Long, A., Bentley, H., and Davis, S. (1984). Natural chlorine isotope variations. *Nature*, 309(5966):338–340.
- Kleindienst, S., Chourey, K., Chen, G., Murdoch, R. W., Higgins, S. A., Iyer, R., Campagna, S. R., Mack, E. E., Seger, E. S., Hettich, R. L., and Löffler, F. E. (2019). Proteogenomics reveals novel reductive dehalogenases and methyltransferases expressed during anaerobic dichloromethane metabolism. *Applied and Environmental Microbiology*, 85(6).



- Kleindienst, S., Higgins, S. A., Tsementzi, D., Chen, G., Konstantinidis, K. T., Mack, E. E., and Löffler, F. E. (2017). 'Candidatus Dichloromethanomonas elyunquensis' gen. nov., sp. nov., a dichloromethane-degrading anaerobe of the *Peptococcaceae* family. *Systematic and Applied Microbiology*, 40(3):150–159.
- Lee, M., Wells, E., Wong, Y. K., Koenig, J., Adrian, L., Richnow, H. H., and Manefield, M. (2015). Relative contributions of *Dehalobacter* and zerovalent iron in the degradation of chlorinated methanes. *Environmental Science & Technology*, 49(7):4481–4489.
- McCarthy, K. A. and Johnson, R. L. (1993). Transport of volatile organic compounds across the capillary fringe. *Resources Research*, 29(6):1675–1683.
- NRC (1993). *In Situ Bioremediation: When Does it Work?* National Academies Press.
- Ojeda, A. S., Phillips, E., Mancini, S. A., and Lollar, B. S. (2019). Sources of uncertainty in biotransformation mechanistic interpretations and remediation studies using CSIA. *Analytical Chemistry*, 91(14):9147–9153.
- Ojeda, A. S., Phillips, E., and Sherwood Lollar, B. (2020). Multi-element (C, H, Cl, Br) stable isotope fractionation as a tool to investigate transformation processes for halogenated hydrocarbons. *Environmental Science: Processes & Impacts*, 22(3):567–582.
- Peralta, A. L., Ludmer, S., Matthews, J. W., and Kent, A. D. (2014). Bacterial community response to changes in soil redox potential along a moisture gradient in restored wetlands. *Ecological Engineering*, 73:246–253.
- Pope, D., Hurt, K., Wilson, B., Acree, S., Levine, H., and Mangion, S. (2004). Performance monitoring of MNA remedies for VOCs in ground water. Technical report, U.S. Environmental Protection Agency, Washington, D.C., EPA/600/R-04/027.
- Pronk, G. J., Mellage, A., Milojevic, T., Smeaton, C. M., Engel, K., Neufeld, J. D., Rezanezhad, F., and Cappellen, P. V. (2020). Carbon turnover and microbial activity in an artificial soil under imposed cyclic drainage and imbibition. *Vadose Zone Journal*, 19(1):e20021.
- Rühle, F. A., von Netzer, F., Lueders, T., and Stumpp, C. (2015). Response of transport parameters and sediment microbiota to water table fluctuations in laboratory columns. *Vadose Zone Journal*, 14(5):vzj2014.09.0116.
- Schlosser, P. M., Bale, A. S., Gibbons, C. F., Wilkins, A., and Cooper, G. S. (2015). Human health effects of dichloromethane: Key findings and scientific issues. *Environ Health Perspect*, 123(2):114–119.
- Schürner, H. K. V., Maier, M. P., Eckert, D., Brejcha, R., Neumann, C.-C., Stumpp, C., Cirpka, O. A., and Elsner, M. (2016). Compound-specific stable isotope fractionation of pesticides and pharmaceuticals in a mesoscale aquifer model. *Environmental Science & Technology*, 50(11):5729–5739.
- Seybold, C. A., Mersie, W., Huang, J., and McNamee, C. (2002). Soil redox, pH, temperature, and water-table patterns of a freshwater tidal wetland. *Wetlands*, 22(1):149–158.
- Shestakova, M. and Sillanpää, M. (2013). Removal of dichloromethane from ground and wastewater: A review. *Chemosphere*, 93(7):1258–1267.
- Smets, B. F. and Pritchard, P. (2003). Elucidating the microbial component of natural attenuation. *Current Opinion in Biotechnology*, 14(3):283–288.
- Tamura, H., Goto, K., Yotsuyanagi, T., and Nagayama, M. (1974). Spectrophotometric determination of iron(II) with 1,10-phenanthroline in the presence of large amounts of iron(III). *Talanta*, 21(4):314 – 318.

- Thullner, M., Centler, F., Richnow, H.-H., and Fischer, A. (2012). Quantification of organic pollutant degradation in contaminated aquifers using compound specific stable isotope analysis – Review of recent developments. *Organic Geochemistry*, 42(12):1440–1460.
- Torgonskaya, M. L., Zyakun, A. M., Trotsenko, Y. A., Laurinavichius, K. S., Kümmel, S., Vuilleumier, S., and Richnow, H. H. (2019). Individual stages of bacterial dichloromethane degradation mapped by carbon and chlorine stable isotope analysis. *Journal of Environmental Sciences*, 78:147–160.
- Trueba-Santiso, A., Fernández-Verdejo, D., Marco-Rius, I., Soder-Walz, J. M., Casabella, O., Vicent, T., and Marco-Urrea, E. (2020). Interspecies interaction and effect of co-contaminants in an anaerobic dichloromethane-degrading culture. *Chemosphere*, 240:124877.
- Trueba-Santiso, A., Parladé, E., Rosell, M., Lliros, M., Mortan, S. H., Martínez-Alonso, M., Gaju, N., Martín-González, L., Vicent, T., and Marco-Urrea, E. (2017). Molecular and carbon isotopic characterization of an anaerobic stable enrichment culture containing *Dehalobacterium* sp. during dichloromethane fermentation. *Science of The Total Environment*, 581-582:640–648.
- US EPA (2020). Risk evaluation for methylene chloride (dichloromethane, DCM). Technical report, U.S. Environmental Protection Agency, Washington, D.C., EPA-740-R1-8010.
- Van Breukelen, B. M. (2007). Extending the rayleigh equation to allow competing isotope fractionating pathways to improve quantification of biodegradation. *Environmental Science & Technology*, 41(11):4004–4010.
- Vermeesch, P. (2018). IsoplotR: A free and open toolbox for geochronology. *Geoscience Frontiers*, 9.
- Williams, M. and Oostrom, M. (2000). Oxygenation of anoxic water in a fluctuating water table system: an experimental and numerical study. *Journal of Hydrology*, 230(1):70–85.
- Wright, J., Kirchner, V., Bernard, W., Ulrich, N., McLimans, C., Campa, M. F., Hazen, T., Macbeth, T., Marabello, D., McDermott, J., Mackelprang, R., Roth, K., and Lamendella, R. (2017). Bacterial community dynamics in dichloromethane-contaminated groundwater undergoing natural attenuation. *Frontiers in Microbiology*, 8:2300.
- York, D., Evensen, N. M., Martínez, M. L., and De Basabe Delgado, J. (2004). Unified equations for the slope, intercept, and standard errors of the best straight line. *American Journal of Physics*, 72(3):367–375.
- Zhang, Z. and Furman, A. (2021). Soil redox dynamics under dynamic hydrologic regimes – A review. *Science of The Total Environment*, 763:143026.



## Preface to Chapter 4

Results from Chapter 3 demonstrated enhanced DCM biodegradation during water table fluctuations in laboratory aquifers fed with anoxic DCM contaminated groundwater. The use of ME-CSIA (i.e.,  $^{13}\text{C}/^{12}\text{C}$  and  $^{37}\text{Cl}/^{35}\text{Cl}$ ) further evidenced larger DCM degradation under transient conditions compared to steady-state, and revealed distinct DCM anaerobic degradation pathways associated with steady-state and transient conditions. This was in line with the prevailing reducing conditions and identification of potentially anaerobic DCM-degrading bacteria, which resulted in higher abundance during transient conditions and their location across the transition zone and the CF. The often co-occurrence of these anaerobes in contaminated aquifers points the possibly complex interspecies bacterial networks and concomitant DCM degradation at contaminated sites.

A multi-phase reactive transport model is presented in **Chapter 4** to improve the understanding of the main drivers of DCM biodegradation by anaerobic bacteria during water table fluctuations, particularly near the water table and at the CF where oxygen remains available. A mathematical formalism is presented on the basis of concomitant DCM degradation according to four distinct pathway-specific reaction rates based on available C- and/or Cl-CSIA. Although the presented formalism is dedicated to DCM, a generic formulation can be obtained from this model providing its extension to other chlorinated compounds (i.e., Cl-VOCs) aiming at developing a comprehensive understanding of concomitant pollutant biodegradation in dynamic hydrogeological systems.



# Chapter 4

## **Numerical simulations of dual carbon-chlorine isotope fractionation of pathway-specific dichloromethane biodegradation reactions**

In preparation for *Water Resources Research*: Prieto-Espinoza, M., Di Chiara, R., Weill, S. & Imfeld, G. Numerical simulations of dual carbon-chlorine isotope fractionation of pathway-specific dichloro- methane biodegradation reactions.

## **Numerical simulations of dual carbon-chlorine isotope fractionation of dichloromethane biodegradation reactions**

### **Abstract**

Reactive transport in porous media involves a complex interplay of multiple processes relative to transport of elements and pollutants, chemical reactions and microbial activities. At surface-groundwater interfaces, the role of the capillary fringe is of particular interest as water table variations influence the transfer of gases (e.g., O<sub>2</sub>), the evolution of redox conditions and the adaptation of bacterial populations and communities controlling biodegradation pathways of halogenated contaminants, such as dichloromethane (DCM). DCM is a toxic and volatile halogenated compound frequently detected in multi-contaminated aquifers. Recently, it was suggested that water table fluctuations enhanced DCM degradation in anoxic laboratory aquifers. The integration of hydrochemical, bacterial and stable isotopic composition further suggested distinct DCM degradation pathways under steady-state and transient conditions, highlighting the impact of water table fluctuations on DCM biodegradation. In this study, a multi-phase flow reactive transport model was further developed to describe multi-component reactive transport processes in laboratory aquifers under steady-state and transient conditions. The multi-phase flow model includes dual-element CSIA (i.e.,  $\delta^{13}\text{C}$  and  $\delta^{37}\text{Cl}$ ), biological processes, and relate changes in redox conditions with DCM-degrading populations. Four distinct bacterial populations potentially involved in distinct DCM degradation pathways were implemented according to pathway-specific reaction rates and isotope fractionation. DOC was also considered as a carbon source for non-DCM degraders, thus representing a broad bacterial community composition. Numerical simulations suggested that the contribution of non-DCM degraders on the overall DCM biodegradation was essential, and correlated with an increase in DOC turnover during water table fluctuations and CO<sub>2</sub> production. The production of CO<sub>2</sub> was further associated with an increase in metabolic activity of DCM degraders associated with anaerobic metabolism. Simulations on concomitant DCM degradation proved better at correlating with experimental observations, particularly for transient conditions. This highlighted the importance of the whole bacterial dynamics with regard to natural attenuation of pollutants in groundwater, rather than the enzymatic activity of a single bacterial population, and may be considered for future *in situ* assessments of the natural attenuation of DCM in dynamic hydrogeological systems.

## 4.1 Introduction

Reactive transport in porous media involves a complex interplay of multiple processes relative to flow of water and gases, transport of elements and pollutants, chemical reactions and microbial activities (Meile and Scheibe, 2019). The role of the capillary fringe (CF) – the transition zone between the saturated and vadose zone – is of particular interest as water table variations may influence the transfer of gases (e.g.,  $O_2$  and volatile compounds) (Haberer et al., 2012; McCarthy and Johnson, 1993; Werner and Höhener, 2002; Williams and Oostrom, 2000), the evolution of redox conditions (Seybold et al., 2002), and the adaptation of bacterial populations and communities (Jost et al., 2015a; Pronk et al., 2020; Rühle et al., 2015), possibly controlling biodegradation extent and pathways of halogenated contaminants, such as dichloromethane (DCM,  $CH_2Cl_2$ ).

Biodegradation – the capacity of microorganisms to breakdown an organic contaminant – is largely considered as the most important natural removal process in aquifers. Indeed, physical processes such as dilution and volatilization do not reflect contaminant transformation (Meckenstock et al., 2015). Hence, appropriate monitoring tools are required to evidence, quantify and distinguish the contribution of contaminant biodegradation to overall dissipation processes. To this end, multiple lines of evidence have proven successful including i) a detailed site characterization and monitoring contaminant concentrations, (ii) identification of *endogenous* microorganisms and their potential degradation capacity, and (iii) *in situ* evidence of degradation potential using stable isotopes and biomolecular markers (Hellal et al., 2021; Hunkeler et al., 2009a). In the last few decades, compound-specific isotope analysis (CSIA) has been recognized as a powerful tool for direct identification and quantification of *in situ* transformation processes, based on changes in stable isotope ratios during a degradation reaction (Elsner, 2010; Hunkeler et al., 2009a). With multi-element CSIA (ME-CSIA), the changes of stable isotope ratios of two elements or more (e.g.,  $^{13}C/^{12}C$  and  $^{37}Cl/^{35}Cl$ ) provide a quantitative parameter of the corresponding *in situ* degradation pathway (Ojeda et al., 2020).

Implementations of reactive transport models (RTM) are useful to evaluate and predict the natural attenuation of contaminants in hydrogeological systems, accounting for the interplay of physical and chemical processes (Hunkeler et al., 2009b; Kuder et al., 2016). Numerous RTMs relying on CSIA data have been successfully applied to quantitatively evidence contaminant degradation in aquifers, particularly for chlorinated ethenes (CEs), further demonstrating the promising insights of CSIA in reactive transport modeling (Antelmi et al., 2021; Badin et al., 2018; D’Affonseca et al., 2011; Eckert et al., 2013; Höhener, 2016; Höyng et al., 2015; Hunkeler



et al., 2009b; Kuder et al., 2016; Prommer et al., 2009; Van Breukelen et al., 2005). However, these RTMs are often applied in simple configurations (e.g., only one bacteria, steady state, batch case, etc.), and thus often exclude the intrinsic relationships between hydrogeochemical variations caused by water table fluctuations, and their potential effects on the diversity and distribution of bacterial communities and degradation pathways in aquifers. To date, few applications of RTMs have been performed to study biodegradation under more complex and dynamic hydrogeological systems, which hampers a proper evaluation of their ability to describe and predict biodegradation processes in real configurations. Predicting degradation of halogenated solvents, such as DCM, during water table fluctuations calls for new implementations accounting for multi-phase flow and transport processes including multi-component reactive processes along with stable isotope fractionation and bacterial dynamics.

Recently, enhanced DCM biodegradation during water table fluctuations was suggested in laboratory aquifers fed with anoxic DCM contaminated groundwater (see Chapter 3). ME-CSIA (i.e.,  $^{13}\text{C}/^{12}\text{C}$  and  $^{37}\text{Cl}/^{35}\text{Cl}$ ) evidenced larger DCM degradation under transient conditions compared to steady-state, and revealed distinct anaerobic DCM degradation pathways associated with steady-state and transient conditions. This was in line with the prevailing reducing conditions and identification of potentially anaerobic DCM-degrading bacteria belonging to the *Peptococaceae* family such as *Desulfosporosinus*, *Dehalobacterium* and *Dehalobacter* spp., which resulted in higher abundance during transient conditions and their location across the fluctuation zone and CF (see Chapter 3). However, the effect of water table fluctuations on DCM biodegradation by these anaerobic bacteria has not been fully clarified, particularly at the fluctuation zone and CF where oxygen remains available. Similarly, the often co-occurrence of these anaerobes in contaminated aquifers emphasizes the role of interspecies bacterial networks and possible concomitant DCM degradation at contaminated sites (Blázquez-Pallí et al., 2019; Hermon et al., 2018; Wright et al., 2017). Previous studies addressing bacterial dynamics across the CF, notably for the case of aerobes (Bauer et al., 2008; Eckert et al., 2015) and facultative anaerobes (Hron et al., 2015; Jost et al., 2015a), suggested that biomass mainly concentrates at the plume fringe and/or CF. In this context, the application of RTMs, together with experiments, can shed light on the relevance of transient environmental conditions on contaminant removal. This may also provide an opportunity to highlight the underlying processes affecting bacterial dynamics, giving access to the spatio-temporal evolution of substrates and bacterial populations in subsurface environments through applications of RTMs.

In this study, we thus propose a multi-phase reactive transport model including volatiliza-

tion and the associated transport processes of DCM isotopologues, pathway-specific reaction rates based on available C- and/or Cl-CSIA data (i.e.,  $^{13}\text{C}/^{12}\text{C}$  and  $^{37}\text{Cl}/^{35}\text{Cl}$ ) for four distinct bacterial populations associated with aerobic and anaerobic DCM degradation, as well as biological processes such as growth, decay, attachment, detachment or dormancy. Notably, the model focuses on anaerobic DCM degradation by the bacterial isolate *Dehalobacterium formicoaceticum* (Chen et al., 2020, 2018; Mägli et al., 1998), and mixed enriched cultures containing DCM-degrading organisms such as *Candidatus Dichloromethanomonas elyunquensis* (Chen et al., 2020, 2018; Kleindienst et al., 2019) and *Dehalobacter* sp. (Holland et al., 2019; Lee et al., 2015), recently proposed to share a unique gene cassette implicated in anaerobic DCM degradation (Murdoch et al., 2022). In addition, a bacterial population (i.e., non-DCM degrader) associated with dissolved organic carbon (DOC) assimilation was included and related to  $\text{CO}_2$  production, representing a broad bacterial community composition. Indeed, the presence of dissolved  $\text{CO}_2$  has been suggested essential during anaerobic DCM metabolisms (Chen et al., 2020).

The objectives of this study are (i) to develop a mathematical formalism describing multi-component reactive transport processes including evolution of stable isotopes (i.e.,  $^{13}\text{C}/^{12}\text{C}$  and  $^{37}\text{Cl}/^{35}\text{Cl}$ ) and five distinct bacterial populations in saturated and unsaturated porous media, including the CF and multi-phase flow, (ii) to identify and quantify bacterial processes associated with DCM degradation, and (iii) to examine the effect of water table fluctuations on DCM degradation pathways. It is worth mentioning that due to the high computational demand, the current stage of the model does not aim at fitting the experimental results presented in Chapter 3. Hence, no automated calibration was here attempted for the reactive transport simulations.

## 4.2 Governing equations

### 4.2.1 Assumptions

Mass exchange of DCM isotopologues was implemented assuming that volatilization was carried out with the same rate. Further discussions within this chapter do not consider isotope fractionation associated with diffusion, as the unsaturated zone was not monitored in high-resolution during the experiments presented in Chapter 3. First-order kinetic exchange between the gas and water phases for  $\text{O}_2$  and  $\text{CO}_2$  were also assumed. Sorption is not included in the model.

The mathematical formalism here proposed includes the possibility of both aerobic and anaerobic DCM degradation in porous media by four distinct bacterial populations (i.e., in the form of biomass)  $X_k$  utilizing DCM as the sole carbon source. A description of the considered

DCM degradation pathways is detailed in Section 4.2.6. The model formalism is restricted to only DCM-degrading bacteria whose pathways have been evidenced by C and/or Cl isotope data, providing a possibility for quantitative assessment of DCM degradation.

To describe a complete bacterial network with the presence of microorganisms without a direct association with DCM degradation, a bacterial population ( $X_5$ ) was implemented and linked to DOC assimilation (i.e., DOC as the only carbon source). This non-DCM degrader produces dissolved  $\text{CO}_2$ , essential for DCM fermentation and anaerobic DCM mineralization (Chen et al., 2020).

All modeled bacterial populations rely on the availability of  $\text{O}_2$ ,  $\text{Fe}^{3+}$  and/or  $\text{CO}_2$  species. However, inhibition terms were here not accounted for due to evidence of a high abundance of anaerobic bacterial populations in the fluctuation zone and CF of the laboratory aquifers (see Chapter 3, Figure 3.5). Consumption of these species are supposed to occur in the water phase only. Interactions of these species with the solid phase are neglected (no sorption). Only the biomass  $X_s$  can be fixed on the solid matrix (Figure 4.1). Biomass is thus considered immobile and fixed on the solid phase and its volume is assumed negligible (i.e., no effect on permeability/porosity, clogging effect negligible). Biodegradation products such as  $\text{CO}_2$ ,  $\text{Cl}^-$ , acetate ( $\text{CH}_3\text{COO}^-$ ) and formate ( $\text{HCOO}^-$ ) are considered for mass balance conservation, according to pathway-specific reactions (Section 4.2.5). Altogether, this model formalism proposes a flexible reactive scheme to shed light on the bacterial interactions involved during DCM degradation, accounting for the effect of water table fluctuations and possibly concomitant degradation.

## 4.2.2 Mass-momentum conservation equations for two-phase flow

Considering an incompressible multi-phase flow in porous media, the macroscale mass balance equation for each  $\alpha$  phase reads:

$$\phi \frac{\partial s_\alpha}{\partial t} + \nabla \cdot \mathbf{q}_\alpha = Q_\alpha, \quad (4.1)$$

where  $s_\alpha$  is the saturation of  $\alpha$  phase,  $\phi$  is the porosity,  $\mathbf{q}_\alpha$  is the superficial velocity and  $Q_\alpha$  is a source term used for injection/extraction wells.

At the scale of a Representative Elementary Volume (REV) of porous media, the vector of specific discharge  $\mathbf{q}_\alpha$ , i.e., the superficial or Darcy's velocity, of each  $\alpha$  phase at a reference pressure for a saturation distribution is given by Muskat law:

$$\mathbf{q}_\alpha = \epsilon_\alpha \mathbf{v}_\alpha = -\frac{kr_\alpha(s_\alpha)}{\mu_\alpha} \mathbf{K}_s \cdot (\nabla p_\alpha - \rho_\alpha \mathbf{g}), \quad (4.2)$$

where  $\mathbf{K}_s$  is the absolute permeability tensor,  $kr_\alpha$  is the relative permeability,  $\mathbf{g}$  the gravitational acceleration vector, and  $\mu_\alpha$  and  $p_\alpha$  are the dynamic viscosity and intrinsic pressure of  $\alpha$  phase, respectively. The volume fraction is defined as  $\epsilon_\alpha = \phi s_\alpha$ .

Due to capillary effects, averaged pressure fields of each phase are not equal, therefore, a macroscale capillary pressure  $p_c$  depending on the water saturation  $s_w$  is defined:

$$p_c = p_n - p_w \quad (4.3)$$

where  $p_n$  is the pressure of the non-wetting phase and  $p_w$  the pressure of the wetting phase in [Pa]. The  $p_c$  values were obtained from the Brooks-Corey model (Brooks, 1965). A description of mass-momentum conservation equations for the capillary fringe is provided in the Supporting Information (Section B.1).

### 4.2.3 Mass balance equations for transport and mass exchange processes

The model consists of three  $\alpha$  phases: solid phase  $s$ , gaseous phase  $g$  and one liquid phase  $w$ , for water. In order to simplify physics of the problem, the three phases are considered incompressible. Each of these phases is composed of species  $i$  and have their own volumetric mass density  $\rho_\alpha$  and saturation  $s_\alpha$ . The saturations must satisfy the closure relation  $\sum_\alpha s_\alpha = 1$ . For each species  $i$  present in  $\alpha$  phase, the advection-dispersion (macroscopic mass conservation) equations describing reactive transport and mass transfer exchange of liquid and gas phase species  $i$  are written as:

$$\partial_t(\epsilon_\alpha c_{\alpha,i}) + \nabla \cdot (\epsilon_\alpha c_{\alpha,i} \mathbf{v}_\alpha + \epsilon_\alpha \mathbf{j}_{\alpha,i}) = \epsilon_\alpha r_{\alpha,i} + \sum_{\beta \neq \alpha} e_{\alpha,i}^{\alpha\beta}, \quad (4.4)$$

where  $c_{\alpha,i}$  is the mass concentration of species  $i$  in  $\alpha$  phase,  $\mathbf{v}_\alpha$  is the mean pore velocity of  $\alpha$  phase,  $\mathbf{j}_{\alpha,i}$  is the intrinsic mass dispersion vector,  $r_{\alpha,i}$  is the biodegradation rate and  $e_{\alpha,i}^{\alpha\beta}$  the rate of mass transfer of species  $i$  into the  $\alpha$  phase at the  $\alpha\beta$  interface (dissolution) in  $\text{kg}/(\text{m}^3 \text{s})$  (Figure 4.1).

The Fick's law is used to describe the diffusive fluxes  $\mathbf{j}_{\alpha,i}$  together with the second model of Millington and Quirk for the dependence of the effective diffusion coefficient on phase saturation, as proposed elsewhere (Hron et al., 2015):

$$\mathbf{j}_{\alpha,i} = -s_\alpha^2 \phi^{\frac{3}{4}} D_{\alpha,i}^{mol} \nabla c_{\alpha,i} \quad (4.5)$$

For mechanical interactions of the fluid with the porous media causing mixing of solutes across  $\alpha$  phase, a diffusion/dispersion tensor is used to estimate the corresponding fluxes:

$$\mathbf{j}_{\alpha,i} = - \left( s_{\alpha}^2 \phi^{\frac{3}{4}} D_{\alpha,i}^{mol} \mathbf{I} + \alpha_t |\mathbf{q}_{\alpha}| \mathbf{I} + (\alpha_l - \alpha_t) \frac{\mathbf{q}_{\alpha} \mathbf{q}_{\alpha}}{|\mathbf{q}_{\alpha}|} \right) \nabla c_{\alpha,i} \quad (4.6)$$

with Darcy's velocity as  $\mathbf{q}_{\alpha} = \epsilon_{\alpha} \mathbf{v}_{\alpha}$ ,  $\alpha_l$  and  $\alpha_t$  are the longitudinal and transverse dispersivities, respectively, and  $D_{\alpha,i}^{mol}$  is the molecular diffusion of species  $i$  in  $\alpha$  phase.

#### 4.2.4 Mass transfer in porous media of soluble and gaseous species

The porous media is considered partially saturated with water and gas phases with a mixture of several constituents (e.g.,  $O_2$ , DCM and  $CO_2$ ) (see Figure 4.1). In the case of local non-equilibrium, volatilization of component  $i$  from the aqueous ( $w$ ) to the gaseous ( $g$ ) phase (and conversely the leaching of component  $i$  present in the gas phase by re-solubilization) corresponding to the adimensional Henry's constant, is given by (Geistlinger et al., 2005; Holocher et al., 2003; Hron et al., 2015):

$$e_{g,i}^{wg} = \epsilon_g \Gamma_{volat,i} \left( p_i^{vap} \frac{M_{mol,i}}{C_i^{eq} RT} \rho_w \omega_{w,i} - \rho_g \omega_{g,i} \right) = -e_{w,i}^{wg} \quad (4.7)$$

where  $\Gamma_{volat,i}$  is the mass transfer coefficient by volatilization [1/s], and  $C_i^{eq}$  is the water solubility,  $M_{mol,i}$  is the molar mass and  $p_i^{vap}$  is the vapour pressure of species  $i$  (pure form) [kg/(m s<sup>2</sup>)]. Phase composition (i.e., mass concentration) is relative to the mass fraction of species  $i$  in  $\alpha$  phase (i.e.,  $\omega_{\alpha,i}$ ) and the mass phase density (i.e.,  $\rho_w$  and  $\rho_g$ ).

The volatilization rate can thus be approached following Hron et al. (2015), with  $\Gamma_{volat,i} = \beta A_{gw}$ , where  $A_{gw}$  is the total effective interstitial surface area, while  $\beta$  is the mass exchange coefficient for a spherical structure (i.e., spherical gas bubble):

$$\beta = D_{w,i}^{mol} \left( \frac{2}{d_p} + \frac{1}{\delta} \right) \text{ and } A_{gw} = \kappa_a s_g \frac{6\phi}{d_p} \quad (4.8)$$

with  $d_p$  the harmonic mean particle diameter,  $\kappa_a$  is the fraction of air bubble surface area exposed to mobile water (constant),  $D_{w,j}^{mol}$  is the molecular diffusion coefficient for species  $i$  in water and  $\delta$  is the thickness of the film layer:

$$\delta = \sqrt{\frac{\pi d_p D_{w,j}}{||\mathbf{v}_w||}} \quad (4.9)$$

For  $O_2$ , at 21°C, the Henry's constant is set as  $k_H^{cc,O_2} = \frac{1}{H_k^{cc}} = 3.28 \times 10^{-2}$  (see Speight et al. (2005)). The equilibrium concentration in water, corresponding to a relative gas concentration in air equal to 20.95%, is 9.1 mg/L. Considering solubility of  $O_2$   $C_{O_2}^{eq} = 8.26 \times 10^{-3}$  g/L, a

plausible vapor pressure of  $O_2$  is estimated as  $p_{O_2}^{vap} = 19184$  Pa. Using a similar approach, vapor pressure of  $CO_2$  is estimated as  $p_{CO_2}^{vap} = 78123$  Pa, with a Henry's constant  $k_H^{cc,CO_2} = 0.8317$ , and an equilibrium concentration in water equal to  $6.06 \times 10^{-4}$  g/L.

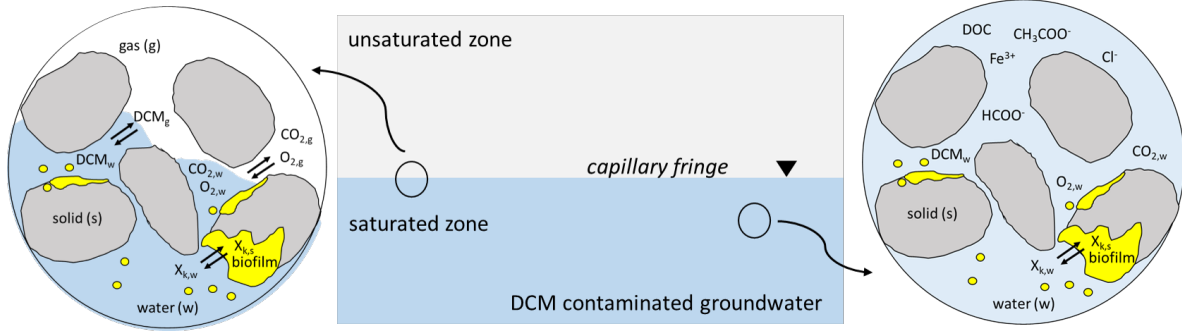


**Figure 4.1:** Schematic overview of mass exchange processes across the porous media with regard to DCM degradation.

#### 4.2.5 Pathway-specific reaction rates and isotope fractionation of DCM

Evolution of carbon and chlorine isotopes of DCM via different bacterial mediated degradation reactions was simulated accounting for dual-element isotopologues (Hunkeler et al., 2009b; Jin et al., 2018). The relative abundance of DCM isotopologues, considering the occurrence of both stable C and Cl isotopes and position-specific isotopologues, can be computed with a binomial distribution (Jin et al., 2018):

$$A_j = \binom{1}{a} X^a (1-X)^{1-a} \cdot \binom{2}{b} Y^b (1-Y)^{2-b} \quad (4.10)$$

where  $A_j$  is the relative abundance of the  $j$ th DCM position-specific isotopologue containing  $a$   $^{13}C$  out of a total of one carbon atom and  $b$   $^{37}Cl$  out of a total of two chlorine atoms.  $X$  and  $Y$  are the abundances of heavy C and Cl isotopes, respectively.

The initial C-Cl DCM isotopologues abundance was computed according to initial isotopic signatures of DCM of  $\delta^{13}C_0 = -46.38 \pm 0.37\text{‰}$  and  $\delta^{37}Cl_0 = 3.68 \pm 0.10\text{‰}$ , and the international standards of C (VPDB,  $R_{PDB}^0 = 0.0112372$ ) and Cl (SMOC,  $R_{SMOC}^0 = 0.319766$ ) isotope ratios (Coplen et al., 2006; Kaufmann et al., 1984):

$$R_{^{13}C}^0 = \left( \frac{\delta^{13}C_0}{1000} + 1 \right) R_{PDB}^0 \quad \text{and} \quad X = A_{^{13}C} = \frac{R_{^{13}C}^0}{1 + R_{^{13}C}^0}, \quad A_{^{12}C} = 1 - A_{^{13}C} \quad (4.11)$$

$$R_{^{37}Cl}^0 = \left( \frac{\delta^{37}Cl_0}{1000} + 1 \right) R_{SMOC}^0 \quad \text{and} \quad Y = A_{^{37}Cl} = \frac{R_{^{37}Cl}^0}{1 + R_{^{37}Cl}^0}, \quad A_{^{35}Cl} = 1 - A_{^{37}Cl} \quad (4.12)$$

where  $R_{13C}^0$  and  $R_{37Cl}^0$  represent the initial C and Cl DCM isotope ratios, respectively. Table 4.1 shows the considered C-Cl DCM isotopologues, the number of present  $^{12}C$ ,  $^{13}C$ ,  $^{37}Cl$  and  $^{35}Cl$  atoms, and the relative abundance of each isotopologue.

**Table 4.1:** Initial abundance of DCM carbon-chlorine isotopologues.

DCM $j$ th isotopologue	Carbon		Chlorine		Abundance $A_j$ [%]
	$^{12}C$	$^{13}C$ (=a)	$^{35}Cl$	$^{37}Cl$ (=b)	
1 : $CCl_2$	1	0	2	0	56.7744
2 : $^{13}CCl_2$	0	1	2	0	0.6379
3 : $CCl - ^{37}Cl$	1	0	1	1	36.3090
4 : $^{13}CCl - ^{37}Cl$	0	1	1	1	0.4080
5 : $C^{37}Cl_2$	1	0	0	2	5.8052
6 : $^{13}C^{37}Cl_2$	0	1	0	2	0.6052

During a given reaction of a contaminant, the isotopes present in the bond cleavage are primarily affected (position-specific isotopes); therefore, bulk enrichment factors (e.g.,  $\varepsilon_C$ ) obtained from laboratory experiments are usually corrected to account for position-specific isotope effects (apparent kinetic isotope effect, AKIE) (Elsner, 2010). Position-specific fractionation factors for the  $j$ th DCM isotopologue can thus be computed as:

$$\alpha_C = \frac{1}{AKIE_C} \approx 1 + \frac{n_C}{z_C} \varepsilon_C \quad (4.13)$$

$$\alpha_{Cl} = \frac{1}{AKIE_{Cl}} \approx 1 + \frac{n_{Cl}}{z_{Cl}} \varepsilon_{Cl} \quad (4.14)$$

where  $\alpha_C$  and  $\alpha_{Cl}$  are the C and Cl fractionation factors at the reactive position, respectively.  $\varepsilon$  is here referred to as the *bulk* enrichment factor,  $n$  is the number of atoms of the considered element (i.e., C or Cl) and  $z$  is the number of atoms at the reactive position.

Four distinct DCM degradation pathways are here considered based on experimental results presented in Chapter 3. A description of their degradation pathways is provided in Section 4.2.6. The C- and Cl- enrichment factors for each bacterial population are assigned to pathway-specific degradation reactions. Let's  $\kappa$  be the  $\kappa$ -bacterial population involved in the  $\kappa$ -pathway-specific degradation reaction of DCM (Table 4.2). In the case of DCM, chemically composed by 1 C atom and 2 Cl atoms, we consider that  $n_C = a = 1$  and  $n_{Cl} = b = 2$  (e.g., Eq. 4.13). Reactive positions will thus be simply affected with  $z_C = 1$  and  $z_{Cl} = 2$ . We can postulate the  $\kappa$ -pathway-specific reaction rates of the  $j$ th position-specific isotopologue as:

$$\alpha_{j,C_1Cl_2}^\kappa = \alpha_C^{\kappa,a_j} \alpha_{Cl}^{\kappa,b_j} \quad (4.15)$$

$$\text{with } \alpha_C^{\kappa, a_j} = (\alpha_C^{\kappa})^{a_j} = \left(1 + \frac{1}{z_C} \varepsilon_C^{\kappa}\right)^{a_j} \text{ and } \alpha_{Cl}^{\kappa, b_j} = (\alpha_{Cl}^{\kappa})^{b_j} = \left(1 + \frac{2}{z_{Cl}} \varepsilon_{Cl}^{\kappa}\right)^{b_j} \quad (4.16)$$

#### 4.2.6 Stoichiometry of pathway-specific degradation reactions of DCM

Four distinct DCM degradation pathways are considered representing the co-occurrence of potential DCM-degraders in polluted aquifers, as evidenced previously (Blázquez-Pallí et al., 2019; Hermon et al., 2018; Lee et al., 2015; Wright et al., 2017). Concomitant anaerobic DCM degradation is also considered for *Dehalobacter*, *Dehalobacterium* and *Desulfosporosinus* taxa, as evidenced in Chapter 3.

Stoichiometry reactions were used to approximate biomass growth and evolution of redox species, according to proposed DCM degradation pathways further described by C and/or Cl isotope data (Chen et al., 2018; Heraty et al., 1999; Lee et al., 2015) (Table 4.2). When bacterial activity is simulated in the form of biomass growth, the overall stoichiometry of the reaction is altered (Barry et al., 2002). This is due to a fraction of the substrate can be utilized to synthesize new biomass, while the rest is oxidized to gain energy (Rittmann, 2006).

The presented stoichiometry equations are thus estimated assuming an electron-transfer fraction of 0.5 from DCM (or DOC in the case of  $X_5$ ) to the synthesis of new biomass of all bacterial populations. Biomass is represented as the chemical species  $C_5H_7O_2N$  (Eckert et al., 2012). This allows to obtain approximations of the stoichiometry of simulated species. Here, DCM is considered as the sole carbon source for bacterial populations  $X_1$  to  $X_4$ . A detailed description of all stoichiometry reactions is provided in the SI (Section B.2).

#### DCM degradation by *Hyphomicrobium* sp. strain MC8b – Bacterial population $X_1$

DCM degradation under oxic conditions is considered by the facultative methylotrophic bacteria *Hyphomicrobium* sp. strain MC8b catalyzed by the glutathione S-transferase *DcmA*, and leads to oxidation of DCM to carbon dioxide ( $CO_2$ ) and inorganic chloride ( $Cl^-$ ) (Hayoun et al., 2020; Heraty et al., 1999):

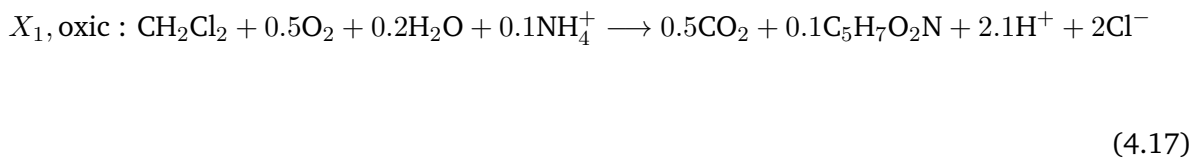




**Table 4.2:** Pathway-specific reactions considered in the model based on current knowledge on C-Cl CSIA of specific DCM degraders.

Cultures	$\varepsilon_C$	$\varepsilon_{Cl}$	$\Lambda^{C/Cl a}$	Degradation pathway	Source
<b>Aerobic cultures</b>					
$X_1$ <i>Hyphomicrobium</i> sp. strain MC8b	-42.4 <sup>b</sup>	-3.8 <sup>b</sup>	11.2 <sup>c</sup>	Glutathione S-transferase	(Heraty et al., 1999) (Hayoun et al., 2020)
<b>Anaerobic cultures</b>					
$X_2$ Consortium DCMD harboring <i>Dehalobacter</i> sp.	-15.5	-5.2 <sup>d</sup>	2.98 <sup>d</sup>	iron-reducing	(Lee et al., 2015)
$X_3$ <i>Dehalobacterium formicoaceticum</i>	-42.4±0.7	-5.3±0.1	7.89±0.12	Fermentation harboring WLP	(Chen et al., 2020, 2018)
$X_4$ Consortium RM harboring <i>Ca. Dichloromethanomonas elyunquensis</i>	-18.3±0.2	-5.2±0.1	3.40±0.03	Mineralization (acetogenesis required)	(Chen et al., 2020, 2018)

<sup>a</sup> Uncertainties of  $\varepsilon$  and  $\Lambda$  values correspond to the 95% confidence interval (CI).

<sup>b</sup> Uncertainties were not provided by the author.

<sup>c</sup>  $\Lambda^{C/Cl}$  values were calculated based on reported  $\varepsilon_C$  and  $\varepsilon_{Cl}$  data by the referenced authors.

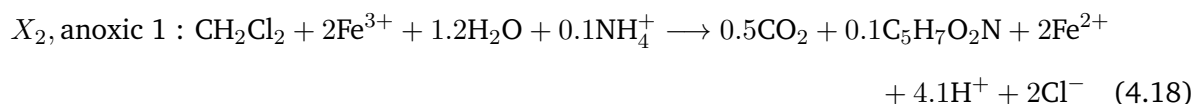
<sup>d</sup>  $\varepsilon_{Cl}$  value was assumed similar to those proposed by *Ca. D. elyunquensis*. Authors did not report  $\varepsilon_{Cl}$ .

### DCM degradation by *Dehalobacter* sp. – Bacterial population $X_2$

DCM fermentation by *Dehalobacter* sp. culture DCMD was initially proposed by Lee et al. (2012). Further enrichment of the inoculum led to a shift from *Dehalobacter* sp. to a DCM-fermenting bacterium 'DCMF' (Holland et al., 2019), recently proposed as *Candidatus Formimonas warabiya* – a novel genus within the *Peptococcaceae* family (Holland et al., 2021). Similarly, another *Dehalobacter* genus was initially implicated in anaerobic DCM degradation from pristine river sediments, although a novel genus was later proposed (Justicia-Leon et al., 2012; Kleindienst et al., 2019, 2017). This suggests that closely-related *Dehalobacter* microorganisms may be directly implicated in anaerobic DCM degradation.

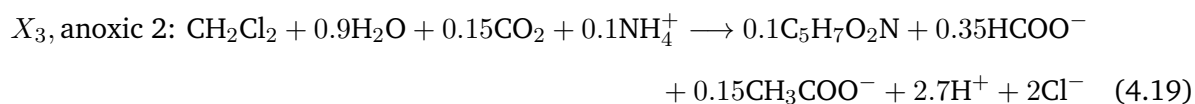
To date, only few anaerobic DCM degradation pathways have been described using CSIA. This includes anaerobic DCM degradation correlated to *Dehalobacter* sp. culture DCMD in microcosm experiments in the presence of zero valent iron (ZVI) (Lee et al., 2015). Similarly, anaerobic DCM degradation has been suggested in contaminated aquifers under prevailing iron-reducing conditions, where the presence of *Dehalobacter* sp. was associated with highly contaminated areas at the plume source (Hermon et al., 2018). This is in line with previous studies that have further suggested ferric iron ( $Fe^{3+}$ ) as a likely predominant electron acceptor for anaerobic DCM degradation (Wright et al., 2017; Yu et al., 2014). In this context, it is here proposed a potential DCM degradation pathway under iron-reducing conditions, possibly mediated by closely

related *Dehalobacter* spp. (Lee et al., 2015). However, since the authors did not report  $\varepsilon_{\text{Cl}}$  for *Dehalobacter* sp., it was assumed a similar  $\varepsilon_{\text{Cl}}$  value to those proposed by other anaerobic DCM degraders (see Table 4.2). Finally, the proposed pathway remains tentative for future evidence of anaerobic DCM degradation under iron-reducing conditions.



#### DCM degradation by *Dehalobacterium formicoaceticum* – Bacterial population $X_3$

DCM degradation under strictly anoxic conditions have remained elusive. To date, the only anaerobic DCM isolate is *Dehalobacterium formicoaceticum* affiliated with the *Peptococcaceae* family. *Dehalobacterium formicoaceticum* utilizes DCM as growth substrate during fermentation, and requires the presence of  $\text{CO}_2$  in the medium (i.e., limiting factor). *D. formicoaceticum* generates acetate ( $\text{CH}_3\text{COO}^-$ ), formate ( $\text{HCOO}^-$ ) and inorganic chloride ( $\text{Cl}^-$ ) as *final* products, following the Wood-Ljungdahl pathway (WLP) (Chen et al., 2020; Kleindienst et al., 2019):

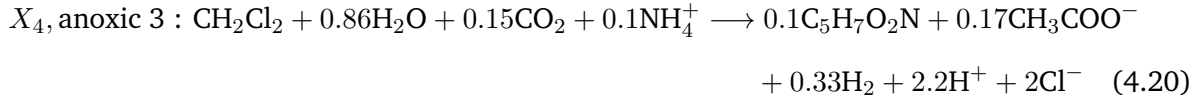


#### DCM degradation by *Candidatus Dichloromethanomonas elyunquensis* – Bacterial population $X_4$

It has been recently proposed that DCM mineralization by *Candidatus Dichloromethanomonas elyunquensis*, affiliated with the *Peptococcaceae* family and closely related to *Desulfosporosinus* and *Dehalobacter* genera (Justicia-Leon et al., 2012; Kleindienst et al., 2019, 2017), leads to the production of both  $\text{H}_2$  and  $\text{CO}_2$  (Chen et al., 2020). Notably, for growth with DCM, *Ca. D. elyunquensis* requires the presence of  $\text{H}_2$ -consuming partner populations performing  $\text{H}_2/\text{CO}_2$  reductive acetogenesis (Chen et al., 2020). DCM metabolism by *Ca. D. elyunquensis* also follows the Wood-Ljungdahl pathway and is dependent on  $\text{CO}_2$  (Chen et al., 2020).

For the purpose of this model,  $\text{H}_2$ -consuming partner populations are not considered. Anaerobic DCM degradation is restricted to a global stoichiometry reaction proposed previously (Chen et al., 2018), in which anaerobic DCM degradation by *Ca. D. elyunquensis* leads to the production of acetate ( $\text{CH}_3\text{COO}^-$ ),  $\text{CO}_2$  and inorganic chloride ( $\text{Cl}^-$ ), following the WLP (Chen et al.,

2020; Kleindienst et al., 2019). Bacterial effects regarding  $H_2$  production are not considered in the model.

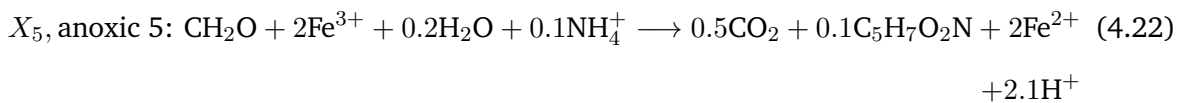


#### DOC assimilation by a non-DCM degrader population – Bacterial population $X_5$

Groundwater bacterial communities in contaminated aquifers are composed by a wide range of different microorganisms. Mutualistic interactions between DCM degraders and other members of the bacterial community (e.g.,  $H_2$ -consuming partner populations) have pointed to the importance of the dynamics of the whole bacterial community on DCM degradation (Chen et al., 2017; Trueba-Santiso et al., 2020). Anaerobic DCM degradation requires the presence of  $CO_2$ , notably during fermentative pathways by *Dehalobacterium formicoaceticum* and mineralization by *Ca. D. elyunquensis* (including acetogenesis) (Chen et al., 2020). Consider mineralization of dissolved organic carbon (DOC,  $CH_2O$ ) mediated by a non-DCM degrader, bacterial population  $X_5$  (facultative anaerobe), under both aerobic and anaerobic metabolisms, and expected to produce  $CO_2$ :



The anaerobic pathway mediated by the same bacterial population  $X_5$  is considered for iron-reducing conditions:



#### 4.2.7 Modeling attachment processes in porous media

In order to evaluate  $\kappa$ -specific bacterial transport and attachment in saturated and unsaturated porous media, cells adhesion to sand grains with a reversible formulation involving an adhesion term  $a_{w, X_\kappa}$  from liquid phase is expressed as (Hron et al., 2015):

$$a_{w, X_\kappa} = -\epsilon_w k_\kappa^{att} \psi_\kappa c_{w, X_\kappa} + \epsilon_s k_\kappa^{det} c_{s, X_\kappa} \quad (4.23)$$

where  $c_{w, X_\kappa}$  is the bacterial concentration of  $\kappa$ -population in the water phase,  $c_{s, X_\kappa}$  is the bacterial concentration of  $\kappa$ -population in the solid phase,  $k_\kappa^{att}$  is the first order deposition

coefficient for  $\kappa$ -population,  $k_{\kappa}^{det}$  is the first order detachment coefficient for  $\kappa$ -population and  $\psi_{\kappa}$  is a dimensionless deposition function (Eq. 4.25). The solid phase mass balance equation for  $\kappa$ -microbial solid concentration  $c_{s,X_{\kappa}}$  is given by:

$$\frac{\partial \epsilon_s c_{s,X_{\kappa}}}{\partial t} = -a_{w,X_{\kappa}} \quad (4.24)$$

To take into account variations of the solid surface adhesion along time evolution, the variation of deposition behavior is indexed with water saturation in the general form for  $\psi_{\kappa}$ :

$$\psi_{\kappa} = 1 - \frac{c_{s,X_{\kappa}}}{s_w c_{s,X_{\kappa}}^{\max}} \quad (4.25)$$

where  $c_{s,X_{\kappa}}^{\max}$  is the  $\kappa$ -specific maximum attainable bacterial concentration on the solid phase. As  $c_{s,X_{\kappa}}$  rises, solid surface become less attractive for new cell's adhesion and, therefore,  $\psi_{\kappa}$  function tends to zero (Hron et al., 2015).

#### 4.2.8 Modeling microbial growth kinetics

Kinetics of anaerobic and aerobic growth of  $k$ -bacterial populations are limited by the availability of dissolved oxygen  $c_{w,O_2}$ , ferric iron  $c_{w,Fe}$ , carbon dioxide  $c_{w,CO_2}$  and bioconvertible dissolved  $j$ th isotopologues of DCM, denoted  $c_{w,j}$ . We can defined a *total bacterial concentration* as:  $c_{X_{\kappa}} = c_{w,X_{\kappa}} + c_{s,X_{\kappa}} \frac{\epsilon_s}{\epsilon_w}$ . Both phases (i.e., planktonic and attached) are assumed to be able to consume nutrients and starve. New cells are considered immediately mobile in the water phase and are able to attach to solid grains (Eq. 4.23).

The aerobic and anaerobic specific growth rates are based on the Contois model (Contois, 1959). The Contois modification is able to describe variations of half-saturation constant in Monod models during a single growth cycle (i.e., the dependence of  $\mu_{max}$  on the biomass density) (Kovárová-Kovar and Egli, 1998). Pathway-specific reaction rates based on C and Cl isotopes (Eq. 4.15) are introduced for bacterial populations  $X_1$  to  $X_4$ , described as DCM-degrading populations (Section 4.2.6).

$$r_j^1 = r_j^{ox} = \mu_{\max}^{ox,1} \frac{\alpha_C^{1,a_j} \alpha_{Cl}^{1,b_j} c_{w,j}}{c_{X_1} B_{DCM}^{ox} + c_{w,DCM}} \frac{c_{w,O_2}}{c_{X_1} B_{O_2} + c_{w,O_2}}, \text{oxic, } X_1 \text{ DCM-degrader} \quad (4.26)$$

$$r_j^2 = r_j^{an,1} = \mu_{\max}^{an,2} \frac{\alpha_C^{2,a_j} \alpha_{Cl}^{2,b_j} c_{w,j}}{c_{X_2} B_{DCM}^{an,1} + c_{w,DCM}} \frac{c_{w,Fe}}{c_{X_2} B_{Fe} + c_{w,Fe}}, \text{anoxic, } X_2 \text{ DCM-degrader} \quad (4.27)$$

$$r_j^3 = r_j^{an,2} = \mu_{\max}^{an,3} \frac{\alpha_C^{3,a_j} \alpha_{Cl}^{3,b_j} c_{w,j}}{c_{X_3} B_{DCM}^{an,2} + c_{w,DCM}} \frac{c_{w,CO_2}}{c_{X_3} B_{CO_2} + c_{w,CO_2}}, \text{anoxic, } X_3 \text{ DCM-degrader} \quad (4.28)$$

$$r_j^4 = r_j^{an,3} = \mu_{\max}^{an,4} \frac{\alpha_C^{4,a_j} \alpha_{Cl}^{4,b_j} c_{w,j}}{c_{X_4} B_{DCM}^{an,3} + c_{w,DCM}} \frac{c_{w,CO_2}}{c_{X_4} B_{CO_2} + c_{w,CO_2}}, \text{anoxic, } X_4 \text{ DCM-degrader} \quad (4.29)$$

where  $\mu_{\max}^{ox,1}$ ,  $\mu_{\max}^{an,2}$ ,  $\mu_{\max}^{an,3}$  and  $\mu_{\max}^{an,4}$  are the specific growth rates for aerobic, iron-reducing, fermentation, and anaerobic mineralization, respectively.  $j = 1, \mathcal{N}$  with  $\mathcal{N} = 6$  is the number of DCM isotopologues.  $c_{w,DCM}$  is the total DCM concentration of  $40 \text{ mg L}^{-1}$ , such as  $c_{w,DCM} = \sum_j^{\mathcal{N}} c_{w,j}$ . The constant  $B$  multiplied by  $c_X$  corresponds to the half-saturation constants in Monod kinetics.

$X_5$  bacterial population is capable of assimilating DOC as carbon source under both oxic and anoxic conditions. It is assumed that  $X_5$  new cells are growing anaerobically when dissolved  $O_2$  concentrations are low. However, with increasing  $O_2$  levels, they are able to grow in both modes but not faster than aerobic mode (Hron et al., 2015). Finally, no isotope fractionation is considered for non-DCM degrader  $X_5$  bacterial population.

$$r_{w,DOC}^{ox} = \mu_{\max}^{ox,5} \frac{c_{w,DOC}}{c_{X_5} B_{DOC} + c_{w,DOC}} \frac{c_{w,O_2}}{c_{X_5} B_{O_2} + c_{w,O_2}} \text{oxic, } X_5 \text{ DOC mineralization} \quad (4.30)$$

$$r_{w,DOC}^{an} = \mu_{\max}^{an,5} \frac{c_{w,DOC}}{c_{X_5} B_{DOC} + c_{w,DOC}} \frac{c_{w,Fe}}{c_{X_5} B_{Fe} + c_{w,Fe}} \text{anoxic, } X_5 \text{ DOC mineralization} \quad (4.31)$$

The reaction terms of the  $\kappa$ -specific bacterial populations denoting growth and decay ( $k_k^{dec}$ ; constant rate) of cells in both water and solid phases are given by:

$$r_{w,X_\kappa} = \epsilon_w \sum_j^{\mathcal{N}} r_j^\kappa c_{X_\kappa} - \epsilon_w k_\kappa^{dec} c_{w,X_\kappa} \quad (4.32)$$

$$r_{s,X_\kappa} = -\epsilon_s k_\kappa^{dec} c_{s,X_\kappa} \quad (4.33)$$

Finally, the balance equations for the  $j$ th isotopologues of DCM, and dissolved species  $O_2$ ,  $CO_2$  and ferric iron, have the form:

$$r_{w,j} = -\epsilon_w \sum_{\kappa=1}^4 \frac{r_j^\kappa}{Y_{X_\kappa/j}} c_{X_\kappa} \quad (4.34)$$

$$r_{w,O_2} = -\epsilon_w \left( E_{O_2/j} \frac{\sum_j r_j^1}{Y_{X_1/j}} + m_{O_2} c_{w,O_2} \right) c_{X_1} \quad (4.35)$$

$$r_{w,Fe} = -\epsilon_w \left( E_{Fe/j} \frac{\sum_j r_j^2}{Y_{X_2/j}} + m_{Fe} c_{w,Fe} \right) c_{X_2} \quad (4.36)$$

$$r_{w,CO_2}^3 = -\epsilon_w \left( E_{CO_2/j}^3 \frac{\sum_j r_j^3}{Y_{X_3/j}} + m_{CO_2}^3 c_{w,CO_2} \right) c_{X_3} \quad (4.37)$$

$$r_{w,CO_2}^4 = -\epsilon_w \left( E_{CO_2/j}^4 \frac{\sum_j r_j^4}{Y_{X_4/j}} + m_{CO_2}^4 c_{w,CO_2} \right) c_{X_4} \quad (4.38)$$

where yield factor coefficients  $Y_{X_\kappa/j}$  [biomass  $X_\kappa$  produced in g per mass of substrate  $j$  biodegraded in g],  $E_{EA/j}$  in [g of electron acceptor ( $EA$ ) consumed per mass of substrate  $j$  biodegraded in g] are associated with aerobic and/or anaerobic DCM degraders. Parameters  $m_{O_2}$ ,  $m_{Fe}$ ,  $m_{CO_2}$  are the non-growth-associated maintenance factors for dissolved  $O_2$ , ferric iron and  $CO_2$ , respectively. The maintenance factor is also dependent on electron acceptors (i.e.,  $O_2$ , ferric iron and  $CO_2$ ) availability. However, results presented in this chapter set the maintenance factors to 0 for all bacterial populations (SI, Section B.4). Production of formate and acetate (for DCM fermentation and mineralization by  $X_3$  and  $X_4$ , respectively), dissolved  $CO_2$  and  $Cl^-$  are also computed along time. The full balance equations considering multi-phase reactive transport modeling of DCM biodegradation by 4 distinct DCM-degrading populations, in the presence of a DOC-assimilating bacterial population are presented below.

#### 4.2.9 Coupled mass balance equations

The flow is considered incompressible, all transport equations are therefore solved in mass concentration. Considering the constant densities, for  $\alpha = w, g$ ,  $j = 1, \mathcal{N}$  with  $\mathcal{N} = 6$  (number of isotopologues) and  $\kappa \in [1, 5]$  affiliated with the five different bacterial populations, the balance equations can be written for each of the primary variables ( $i$ ):  $j$ th DCM isotopologues ( $CCl_2$ ,  $^{13}CCl_2$ ,  $C^{37}Cl - Cl$ ,  $^{13}C^{37}Cl - Cl$ ,  $C^{37}Cl_2$ ,  $^{13}C^{37}Cl_2$ ), and species  $O_2$ ,  $CO_2$ ,  $Fe^{3+}$ ,  $Cl^-$ , acetate, formate,  $C_{w,X_k}$ , and  $C_{s,X_k}$ . Iron (iron-reducing condition  $an, 1$ ), chlorine, formate and acetate produced by fermentation ( $an, 2$ ) and mineralization ( $an, 3$ ) are only present in dissolved form (Eq. 4.26 to 4.29).

$$\frac{\partial}{\partial t}(\epsilon_\alpha c_{\alpha,j}) + \nabla \cdot (\epsilon_\alpha c_{\alpha,j} \mathbf{v}_\alpha + \epsilon_\alpha \mathbf{j}_{\alpha,j}) = -\delta_{\alpha w} r_{w,j} + e_{\alpha,j}^{wg}, \text{ for } j \in \{1, \dots, 6\} \quad (4.39)$$

$$\begin{aligned} \frac{\partial}{\partial t}(\epsilon_\alpha c_{\alpha,O_2}) + \nabla \cdot (\epsilon_\alpha c_{\alpha,O_2} \mathbf{v}_\alpha + \epsilon_\alpha \mathbf{j}_{\alpha,O_2}) &= -\delta_{\alpha w} r_{w,O_2} + e_{\alpha,O_2}^{wg} \\ &\quad - \delta_{\alpha w} \epsilon_w E_{O_2/DOC} \frac{r_{w,DOC}^{ox}}{Y_{X_5/DOC}^{ox}} c_{X_5} \end{aligned} \quad (4.40)$$

$$\begin{aligned} \frac{\partial}{\partial t}(\epsilon_\alpha c_{\alpha,CO_2}) + \nabla \cdot (\epsilon_\alpha c_{\alpha,CO_2} \mathbf{v}_\alpha + \epsilon_\alpha \mathbf{j}_{\alpha,CO_2}) &= -\delta_{\alpha w} (r_{w,CO_2}^3 + r_{w,CO_2}^4) + e_{\alpha,CO_2}^{wg} \\ &\quad + \delta_{\alpha w} \epsilon_w \left( \Upsilon_{CO_2/DOC}^{ox} \frac{r_{w,DOC}^{ox}}{Y_{X_5/DOC}^{ox}} + \Upsilon_{CO_2/DOC}^{an} \frac{r_{w,DOC}^{an}}{Y_{X_5/DOC}^{an}} \right) c_{X_5} \\ &\quad + \delta_{\alpha w} \epsilon_w \sum_j \sum_\kappa \Upsilon_{CO_2/j}^\kappa \frac{r_j^\kappa}{Y_{X_\kappa/j}} c_{X_\kappa}, \kappa = \{1, 2, 3, 4\} \end{aligned} \quad (4.41)$$

$$\frac{\partial}{\partial t}(\epsilon_w c_{w,Fe}) + \nabla \cdot (\epsilon_w c_{w,Fe} \mathbf{v}_w + \epsilon_w \mathbf{j}_{w,Fe}) = -r_{w,Fe} - \delta_{\alpha w} \epsilon_w E_{Fe/DOC} \frac{r_{w,DOC}^{an}}{Y_{X_5/DOC}^{an}} c_{X_5} \quad (4.42)$$

$$\frac{\partial}{\partial t}(\epsilon_w c_{w,Cl}) + \nabla \cdot (\epsilon_w c_{w,Cl} \mathbf{v}_w + \epsilon_w \mathbf{j}_{w,Cl}) = \epsilon_w \sum_j \sum_{\kappa} \Upsilon_{Cl/j}^{\kappa} r_j^{\kappa} \frac{c_{X_{\kappa}}}{Y_{X_{\kappa}/j}}, \kappa = \{1, 2, 3, 4\} \quad (4.43)$$

$$\frac{\partial}{\partial t}(\epsilon_w c_{w,DOC}) + \nabla \cdot (\epsilon_w c_{w,DOC} \mathbf{v}_w + \epsilon_w \mathbf{j}_{w,DOC}) = -\epsilon_w \left( \frac{r_{w,DOC}^{ox}}{Y_{X_5/DOC}^{ox}} + \frac{r_{w,DOC}^{an}}{Y_{X_5/DOC}^{an}} \right) c_{X_5} \quad (4.44)$$

$$\frac{\partial}{\partial t}(\epsilon_w c_{w,HCO_2^-}) + \nabla \cdot (\epsilon_w c_{w,HCO_2^-} \mathbf{v}_w + \epsilon_w \mathbf{j}_{w,HCO_2^-}) = \epsilon_w \sum_j \Upsilon_{HCO_2^-/j}^3 \frac{r_j^3 c_{X_3}}{Y_{X_3/j}} \quad (4.45)$$

$$\begin{aligned} \frac{\partial}{\partial t}(\epsilon_w c_{w,C_2H_3O_2^-}) + \nabla \cdot (\epsilon_w c_{w,C_2H_3O_2^-} \mathbf{v}_w + \epsilon_w \mathbf{j}_{w,C_2H_3O_2^-}) = \\ \epsilon_w \sum_j \left( \Upsilon_{C_2H_3O_2^-/j}^3 \frac{r_j^3 c_{X_3}}{Y_{X_3/j}} + \Upsilon_{C_2H_3O_2^-/j}^4 \frac{r_j^4 c_{X_4}}{Y_{X_4/j}} \right) \end{aligned} \quad (4.46)$$

$$\frac{\partial}{\partial t}(\epsilon_w c_{w,X_{\kappa}}) + \nabla \cdot (\epsilon_w c_{w,X_{\kappa}} \mathbf{v}_w + \epsilon_w \mathbf{j}_{w,X_{\kappa}}) = r_{w,X_{\kappa}} + a_{w,X_{\kappa}}, \text{ for } \kappa \in \{1, \dots, 5\} \quad (4.47)$$

$$\frac{\partial}{\partial t}(\epsilon_s c_{s,X_{\kappa}}) = -a_{w,X_{\kappa}} - \epsilon_s k_{\kappa}^{dec} c_{s,X_{\kappa}}, \text{ for } \kappa \in \{1, \dots, 5\} \quad (4.48)$$

### 4.3 Modeling approach

#### 4.3.1 Previous implementations of the CubicM model

A detailed description of the numerical resolution is given in the SI (Section B.3). The mathematical formalism with regard to multi-phase flow and transport processes was previously developed at the Institut Terre et Environnement de Strasbourg, France (CubicM model; Dr. Raphaël Di Chiara) (Chastanet et al., 2014; Di Chiara Roupert, 2009; Di Chiara Roupert et al., 2017). This model initially included (i) a tri-phasic (gas-water-NAPL) flow, accounting for the migration of a mobile organic phase (NAPL of chlorinated ethenes) in aquifers, (ii) transport of several constituents in the water phase (saturated zone) and volatilization in the gas phase (vadose zone), (iii) sorption (equilibrium and kinetic), and (iv) degradation of dissolved constituents of the chlorinated ethene family, including a sequential degradation module (first order).

#### 4.3.2 CubicM model accounting for concomitant DCM biodegradation under dynamic conditions

A dual-isotope approach was here implemented regarding DCM biodegradation, where pathway-specific reactions rates were derived according to 4 distinct DCM degradation pathways, and one non-DCM degrader (Section 4.2.9). In total, the model includes 36 non-linear coupled equations

with over 40 parameters, accounting for the evolution of 8 species in both water and gas phases (i.e., the 6 DCM isotopologues,  $O_2$  and  $CO_2$ ) and 10 species in the water phase only (i.e.,  $Fe^{3+}$ , DOC, Cl, acetate, formate, and 5 planktonic bacterial populations). All bacterial populations can be further split considering active biomass in the dissolved and/or solid phase.

The coupling of all system of equations illustrates the highly complexity of the model and represents, by itself, a numerical challenge. The calibration of this model, based on experimental results presented in Chapter 3, requires a long-term investment owing the large number of parameters, the sensitivity of the model outputs – enhanced by the strong interactions between all the simulated variables – and the constraints on CPU time. Inverse modelling based on a Monte-Carlo approach would certainly be very useful to better understand how the overall model works, but will be considered in future developments. Therefore, and worthy of note, the calibration of the presented model is out of the scope of this thesis.

#### 4.3.3 Evaluation strategy

The overall objectives of this thesis chapter is to assess the ability of the proposed formalism (Section 4.2) to describe the key processes observed in the laboratory aquifers with regard to DCM degradation under both steady-state and transient conditions (see Chapter 3). As several bacterial populations/degradation pathways were included, with their effect on stable isotope fractionation, the strategy adopted is a classical step-by-step evaluation.

First, the multiphase flow and transport model – without reaction – is tested alone under steady-state and transient conditions to check its ability to describe the spatial and temporal evolution of the DCM plume and other redox species. Particular attention is paid to oxygen as it is an important player in the capillary fringe, and as experimental measurements are available. These first simulations allow to also examine how volatilization impacts the transport of DCM in the unsaturated zone under both steady-state and transient conditions.

For the reactive part, the model was restricted to test anaerobic DCM degradation (including all isotopologues and stable isotope fractionation due to biodegradation) by bacterial populations  $X_2$  (*Dehalobacter* culture),  $X_3$  (*Dhb. formicoaceticum*) and  $X_4$  (*Ca. D. elyunquensis*), all in the presence of  $X_5$  (non-DCM degrader) for the assimilation of DOC and production of  $CO_2$  required for anaerobic DCM metabolism (Chen et al., 2020). Worthy of note, aerobic DCM biodegradation was not simulated given that *Hyphomicrobium* taxa was not observed in the laboratory aquifers under both steady-state and transient conditions (see Chapter 3, Section 3.3.4), and in line with the prevailing reducing conditions in both laboratory aquifers (see Chapter 3,



Section 3.3.1).

Biomass was set active as planktonic and attached phase. DCM is considered as the only carbon source for anaerobic bacterial populations  $X_2$ ,  $X_3$  and  $X_4$ , and a possible competition effect with other dissolved carbon compounds (i.e., DOC, acetate, formate) is neglected. Finally, the following test cases were here examined:

**Test case 1: Bacterial dynamics of individual populations under steady-state conditions.**

Anaerobic DCM degradation by bacterial populations  $X_2$ ,  $X_3$  and  $X_4$  were tested individually, each in the presence of bacteria  $X_5$  (non-DCM degrader) under steady-state conditions.

**Test case 2: Concomitant DCM degradation under steady-state conditions.** Two concomitant DCM degradation test cases were examined as: (1) concomitant DCM degradation in the presence of bacterial populations  $X_3$  and  $X_4$ , and (2) concomitant DCM degradation in the presence of bacterial populations  $X_2$ ,  $X_3$  and  $X_4$ . In both cases, bacteria  $X_5$  was present (non-DCM degrader) under steady-state conditions.

**Test case 3: Concomitant DCM degradation under transient conditions.** Here, the two concomitant DCM degradation test cases (from test case 2) were examined under transient conditions, considering two water table fluctuation events, as described in Chapter 3, Figure 3.1.

Finally, the numerical simulations did not aim at fitting the observations presented in Chapter 3. Rather, the various variables presented in this model framework (Section 4.2), following the different test cases, are examined in accordance with the trends observed in both laboratory experiments. This may provide insights of the various processes possibly affecting DCM biodegradation under both steady-state and transient conditions.

#### **4.3.4 Simulations of incompressible two-phase transport (water/gas) and biodegradation of DCM in dynamic conditions**

##### **Boundary conditions**

All simulations were carried out on a numerical model representing the experimental laboratory aquifers (simplified 2D geometry) presented in Chapter 3 (Figure 4.2). The experiments and model simulations were carried out on a tank of length  $L_z = 1.6$  m and a height  $H_z = 0.8$  m with a Fontainebleau sand whose hydrodynamic parameters (porosity, capillary parameters,  $K_{sat}$ ) were determined using  $kr - pc$  curves in the laboratory (data not shown). The modeled

tank has 1808 elements of size 5 cm on 5 cm. Coordinates along x—axis of the headspace ports are 0.20 m, 0.80 m and 0.14 m, with 0.05 m width. The top layer is imposed with atmospheric pressure and gas concentrations of O<sub>2</sub> and CO<sub>2</sub> (see Section 4.2.4).

A hydrostatic water pressure corresponding to 33 cm is imposed on the upstream section and 32 cm at the downstream limit, with a hydraulic gradient of 0.625 %. The medium is initially saturated with water  $s_w = s_w^{\max}$ . The sections inlet, outlet and bottom are maintained at constant water saturation equal to  $s_w^{\max}$ . The water table fluctuation is set in the geometry with boundaries positioned at 17 cm from the bottom, corresponding to the lower water level kept in the experiments (see Chapter 3). All domain boundaries, excluding inlet and outlet sides, are impermeable for the liquid phase (zero Neumann boundary condition). For the gas phase, all but the two top sides are impermeable. The air pressure at the top of the domain is fixed to the atmospheric pressure, consistent to free boundary.

### Initial conditions

At the initial time, the tank is fully saturated. The medium is free of DCM (isotopologues) and O<sub>2</sub>. However, dissolved biomass  $X_k$ , ferric iron and DOC are initially present. A first drainage was performed to position the water table at 33 cm and allowed to reach a quasi-steady state for dissolved O<sub>2</sub> and CO<sub>2</sub> concentrations. We assume that the system tends towards equilibrium after sufficient time, that is to say that the concentration in water is such that  $c_{g,O_2}^{eq} = H_k^{cc,O_2} c_{w,O_2}$ . The forced drainage of the tank initially filled with water causes an air entry by the three free surfaces at the top of the domain. The water table stabilizes after approximately 0.5 days with drainage of the unsaturated zone which continues for 1.5 days. The saturation at the top of the domain is maintained at the residual saturation  $s_{wr}$  equals to 8.7%. An initial distribution in dissolved biomass  $X_w$  is also provided, while the fixed biomass  $X_s$  is initially zero. Initial conditions can read as:

$$\begin{aligned} \text{at } t = 0 : c_{w,X} &= 1 \times 10^{-5} \text{ g/L}, c_{s,X} = 0 \text{ g/L}, c_{w,j} = 0 \text{ g/L}, c_{w,j} = 0 \text{ g/L}, s_w = s_w^{\max} \\ c_{w,O_2} &= 0 \text{ g/L}, c_{w,CO_2} = 0 \text{ g/L}, c_{w,Cl} = 0 \text{ g/L}, c_{w,Ac} = 0 \text{ g/L}, \\ c_{w,Fe} &= 0.003 \text{ g/L}, c_{w,DOC} = 0.1 \text{ g/L} \end{aligned} \quad (4.49)$$

$$\begin{aligned} \text{at inlet/outlet} : p_g &= p_w = p_{atm} + \rho_w g z, s_w = 0.999, \\ \text{at top} : p_g &= p_{atm}, s_w = s_{wr} \end{aligned} \quad (4.50)$$

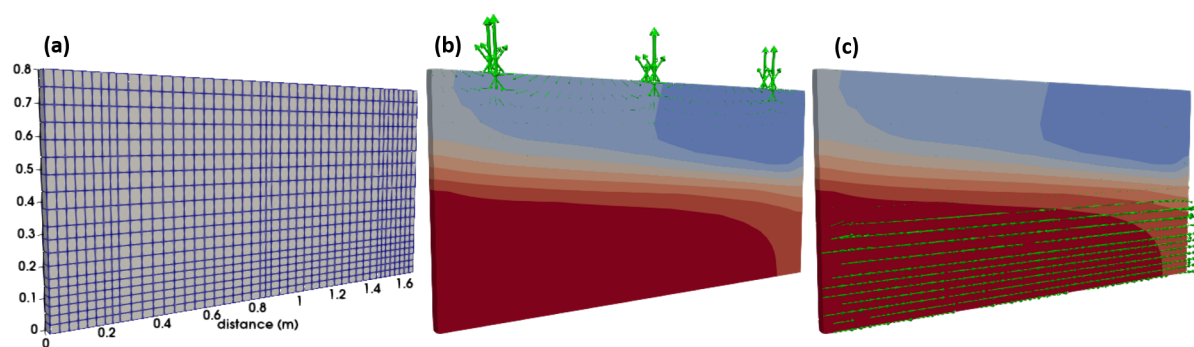


**Figure 4.2:** Model domain based on experimental setup of laboratory aquifers (inner dimensions: 1.6 m  $\times$  0.8 m  $\times$  0.05 m). (a) Example of delineated computational mesh with refinement in the saturated zone. (b) Overview of boundary conditions for gas flow at the three upper ports located at the top of the aquifers. (c) Overview of boundary conditions for water flow accounting for drainage and imbibition steps.

### Simulated periods

All parameters used are presented in the SI (Section B.4). All simulations and inflow concentrations mirror the experimental setup presented in Chapter 3. For all simulations, a first drainage period was carried out in order to reach a quasi-steady state regime after 1 day, i.e., 86 400 s, following initial conditions above described.

An **incubation period** was included. *Injection of DCM* (40 mg L<sup>-1</sup>) and dissolved species such as DOC (100 mg L<sup>-1</sup>), ferric iron (3 mg L<sup>-1</sup>) and biomass (0.01 mg L<sup>-1</sup>), was followed until 60 days under *steady-state conditions*. Note that the incubation period was reduced compared to experiments due to CPU time constraints.

**Steady-state conditions:** After the incubation period (i.e., 60 d), dichloromethane is then injected at a concentration of 40 mg L<sup>-1</sup> until the end of the simulation (100 days), along with dissolved species such as O<sub>2</sub>, Fe<sup>3+</sup>, and dissolved biomass. For the description of the results, the experimental time is described from day 0 (i.e., end of the incubation period) until 40 days (i.e., end of simulated periods).

**Transient conditions:** For *transient conditions*, the incubation time is kept (60 days of steady-state simulations). During the experimental time, the first lowering of the water table took place at day 0, following by injection of DCM for 6 days and dissolved species at a now low water table fluctuation ( $z=17$  cm). The water table was then increased to its original position ( $z=33$  cm) for 1 day and injection of dissolved species was kept until day 20. A similar second water table fluctuation took place from day 23 until the end of the experiment.

## 4.4 Results and discussion

### 4.4.1 Multi-phase flow across the capillary fringe

Mass exchange across the capillary fringe was examined for  $O_2$  and DCM for the (abiotic) transport case under both steady-state and transient conditions. All oxygen vertical profiles (over depth) were retrieved at  $x=0.65$  m. Overall, the model was able to capture the mass exchange of oxygen across the capillary fringe and the unsaturated zone (Figure 4.3), in agreement with observations from laboratory aquifers (Haberer et al., 2012). Under transient conditions, re-oxygenation of the underlying groundwater occurred after drainage events. However, model results featured much larger oxygenation of the underlying groundwater during continuing groundwater flow at a low water table, contrasting with experimental observations (see SI of Chapter 3, Section A.4). This may be the result of faster movement of the water table in the model simulations, possibly resulting in more oxygen penetration (Haberer et al., 2012). Nevertheless, oxygen levels tend to return to equilibrium once the position table returns to its original position, allowing the reestablishment of anoxic conditions in the saturated zone (Figure 4.3). In addition, the abiotic transport simulation here performed cannot be directly compared to experimental observations, particularly during water table fluctuations, owing to the likely presence of aerobic bacteria in the laboratory aquifers possibly utilizing DOC as carbon source (see below). Therefore, utilization of oxygen is likely to occur and limit oxygen diffusion during water table fluctuations events (Jost et al., 2015b; Rezanezhad et al., 2014). Future model calibration approaches may enable to better capture oxygen mass exchange, in agreement with experimental observations.

The model offers an opportunity to further examine DCM volatilization in an abiotic transport case. In Chapter 3, it was demonstrated that DCM concentrations in the gas-phase could not be detected due to limited DCM volatilization across the capillary fringe, and possibly DCM degradation across the unsaturated zone. Numerical simulations proved that steep DCM concentrations gradients were established across the capillary fringe due to slow diffusion in water and smaller vertical transverse dispersion (Figure 4.4). This is in agreement with previous studies on CEs volatilization and diffusion in the unsaturated zone (Jeannotat and Hunkeler, 2013; McCarthy and Johnson, 1993; Werner and Höhener, 2002). Globally, transport of DCM from the saturated zone to the unsaturated zone led to up to 99% smaller concentrations in the gas-phase (i.e., at 10–15 cm above the water table) with respect to the aqueous-phase concentrations at the water table under steady-state, remaining constant throughout the experimental period (Mc-

Carthy and Johnson, 1993) (SI, Section B.5). However, the model predicts a slight accumulation of DCM gas-phase concentrations at the top, possibly due to bad evacuation of DCM through the upper sampling points.

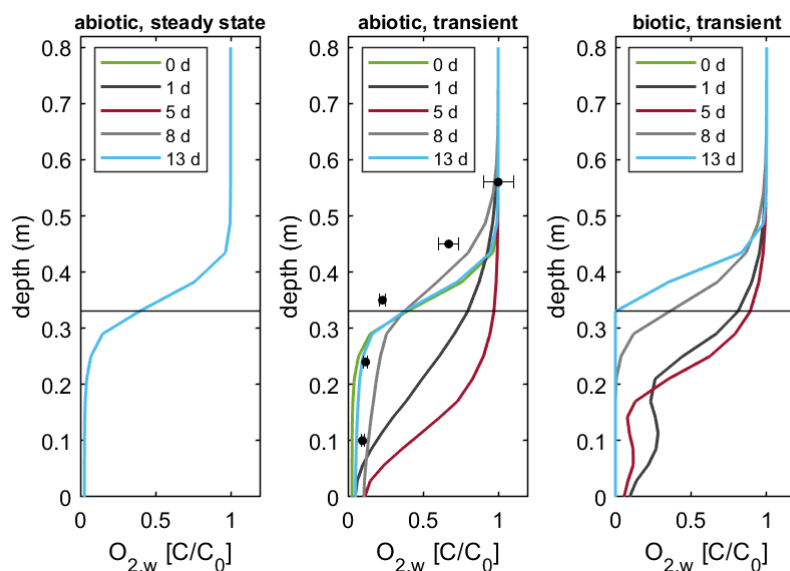


**Figure 4.3:** Oxygen evolution during one water table fluctuation cycle (0–13 days) in abiotic transport case under steady-state conditions (left), abiotic transport case under transient conditions (middle), and biotic case (test case 3) under transient conditions (right). The black dots in the middle plot represent experimental observations in laboratory aquifers under transient conditions after one imbibition event. Continuous horizontal line shows the initial position of the water table.

During transient conditions, DCM volatilization was enhanced in the fluctuation zone as a result of residual water being in contact with the gas (Figure 4.4), but rapidly diffused across the unsaturated zone. This is in agreement with McCarthy and Johnson (1993) who observed a temporary increase of gas-phase TCE concentrations in the unsaturated zone, particularly near the capillary fringe. However, concentrations rapidly decreased again when the water table was raised returning to concentration equilibrium (McCarthy and Johnson, 1993). Altogether, these results support the idea that volatilization is not a significant mechanism associated with DCM removal in the saturated during water table fluctuations, although diffusive fluxes are of relevance across the fluctuation zone.

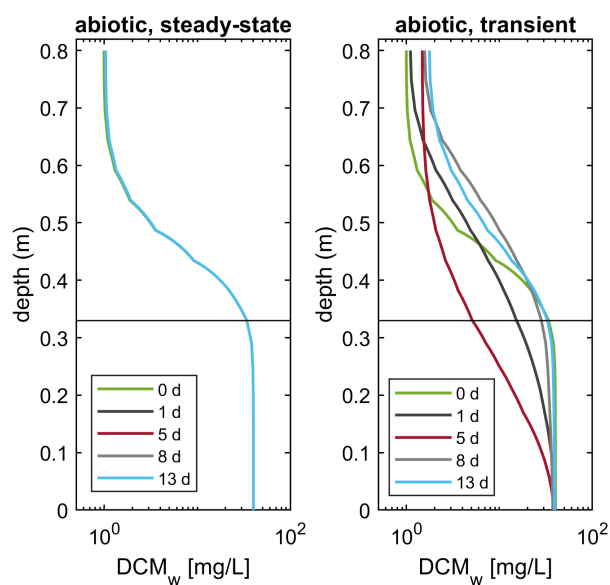


**Figure 4.4:** DCM evolution in water during abiotic transport case under steady-state conditions (left), and abiotic transport case under transient conditions (right). Continuous horizontal line shows the initial position of the water table.

#### 4.4.2 Dynamics of individual bacterial populations under steady-state conditions

An incubation period of 60 days was simulated for all biotic cases for individual bacterial populations  $X_2$ ,  $X_3$  and  $X_4$  (i.e., test case 2, under steady-state conditions). DCM degradation was evidenced for each of the individual populations accounting for up to 12% mass removal for bacterial population  $X_2$ , and 17% for bacterial populations  $X_3$  and  $X_4$  (Figure 4.5, at day 0). Globally, numerical results support that long incubation periods should be considered in experimental designs such as laboratory aquifers, to allow the development of sufficient cell density enough to substantially affect DCM degradation (Sun et al., 2021).

Although a higher DCM mass removal was observed in the laboratory aquifer under steady-state conditions (up to 42%), the model could capture the main trends of anaerobic DCM degradation under flow-through conditions. This similar trend supports the dominance of anaerobic DCM degradation in both laboratory aquifers (see Chapter 3). During the experimental phase (i.e., after the incubation period), a gradual increase of DCM degradation of up to 30% until day 35 was observed at probes located in  $z=0.15$  m for individual anaerobic DCM populations  $X_3$  and  $X_4$ , while DCM degradation by biomass  $X_2$  remained lower (up to 12%) (Figure 4.5). This was further evidenced with a change in carbon and chlorine isotope ratios over time, and according to distance from inflow (Figure 4.5). This was in accordance with the initial isotope

fractionation values obtained from reported anaerobic DCM degraders (see Table 4.2), suggesting a correct model description of pathway-specific reaction rates (see Figure 4.9 for dual-plots).

A global bacterial population  $X_5$ , representing those microorganisms without a direct association with DCM degradation, was considered for all test cases of individual bacterial populations under steady-state conditions. Here, bacterial population  $X_5$  is capable of utilizing both oxygen and ferric iron during assimilation of labile DOC. This leads to the formation of dissolved  $\text{CO}_2$ , which can be further utilized during anaerobic DCM degradation, notably for bacterial populations  $X_3$  and  $X_4$  associated with *D. formicoaceticum* and *Ca. D. elyunquensis*, respectively (Chen et al., 2020). In all test cases, biomass  $X_5$  was higher near the water table and across the capillary fringe (i.e., 12 cm above the water table). This is in agreement with previous studies showing that labile DOC is an important carbon source for numerous microbial mediated processes in the subsurface, and relevant at the capillary fringe (Chimner and Cooper, 2003; Jost et al., 2015a,b; Rezanezhad et al., 2014) (Figure 4.6, *and continues in SI, Section B.6*). For instance, the growth of *E. coli* – a facultative aerobic bacterium – utilizing DOC as carbon source in flow-through experiments predominated in the capillary fringe due to the presence and constant supply of both oxygen and nutrients in this zone (Jost et al., 2015a). This was further confirmed by a multi-phase flow model showing the relevance of the capillary fringe for carbon turnover (Hron et al., 2015).

The presence of ferric iron and  $\text{CO}_2$ , the latter mainly as the end product of DOC assimilation by bacteria  $X_5$ , promoted the growth of DCM anaerobes in the saturated zone. Similar to biomass  $X_5$ , growth of bacterial populations  $X_3$  and  $X_4$  was higher near the water table and the capillary fringe compared to deeper layers (Figure 4.6, *and continues in SI, Section B.6*). Contrastingly, evolution of biomass  $X_2$  over time was mainly observed in the saturated zone (SI, Figure B.2). This is due to limiting ferric iron over time (inflow concentrations:  $3 \text{ mg L}^{-1}$ ), already utilized during the incubation period, and competition with bacterial population  $X_5$  (SI, Figure B.2). Accordingly, anoxic conditions were established near the water table, where DOC assimilation occurred by the constant supply of oxygen and ferric iron (i.e., metabolic activity of biomass  $X_5$ ). Thus, dissolved  $\text{CO}_2$  was made available for anaerobic DCM degraders such as  $X_3$  and  $X_4$ . The presence of facultative anaerobes such as biomass  $X_5$  determined carbon turnover and oxygen depletion near the water table, thus maintaining anoxic conditions throughout the saturated zone. This suggests significant mutualistic relationships with microorganisms without direct effect on DCM degradation. For instance, such mutualistic interactions have been evidenced for acetogens controlling  $\text{H}_2$  and  $\text{CO}_2$  fluxes during anaerobic DCM degradation (Chen et al., 2020;

Trueba-Santiso et al., 2020).

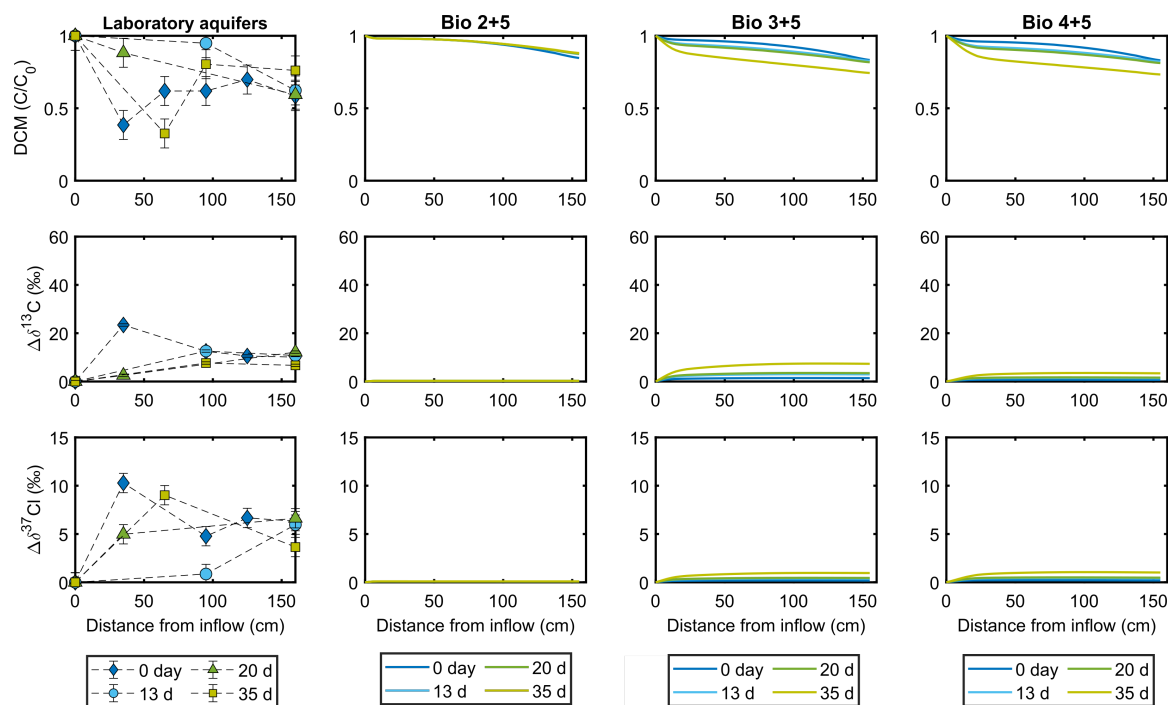


**Figure 4.5:** Experimental observations in laboratory aquifers and numerical simulations for anaerobic DCM degradation by individual populations  $X_2$  (*Dehalobacter* sp.),  $X_3$  (*D. formicoaceticum*) and  $X_4$  (*Ca. D. elyunquensis*) in the presence of a non-DCM degrader ( $X_5$ ) under steady-state conditions. Experimental observations and numerical simulations correspond to data at depth  $z=15$  cm and at different times: day 0 (diamonds, blue), day 13 (circles, light blue), day 20 (triangles, green) and day 35 (squares, light green). Error bars associated with DCM concentrations and stable isotope values represent standard errors ( $3 \leq n$ ).

The increase of biomass  $X_3$  and  $X_4$ , associated with anaerobic DCM degraders, across the capillary fringe was established despite the oxygenation occurring in this transition zone, coinciding with high  $\text{CO}_2$  production by non-DCM degraders (Figure 4.6 and SI, Figure B.3). The occurrence of anaerobic bacteria across the capillary fringe correlates with the fact that no inhibition terms associated with  $\text{O}_2$  were accounted for in the model, which argues for future considerations. Accordingly, potential anaerobic DCM degraders, such as *Dehalobacterium*, *Dehalobacter* and *Desulfosporosinus* spp., were present at the capillary fringe in the laboratory aquifers under steady-state conditions (see Chapter 3, Figure 3.5, at  $z=40\text{cm}$ ), contradicting evidence of their strictly anaerobic metabolisms, particularly for *Dehalobacterium* and *Dehalobacter* spp. (Holliger et al., 1998; Mägli et al., 1996). However, oxygen tolerance for some *Desulfosporosinus* strains have been previously reported (Agostino et al., 2020; Mardanov et al., 2016), arguing that oxygen tolerance may be developed due to frequent exposure to dissolved oxygen near the water ta-



ble, and thus such taxa may possess oxygen detoxification systems (Mardanov et al., 2016). This has also been suggested for anaerobic taxa *Desulfovibrio* spp. – regarded as sulphate-reducing microorganisms – showing oxygen tolerance to live close to oxygenated niches by entering in active dormancy state under oxidative conditions, while rapidly resume growing when conditions are switched to anoxic (Ramel et al., 2015). Thus, the establishment of anaerobic degrader niches across oxic/anoxic redox gradients near the water table and capillary fringe awaits for fundamental investigations (Lueders, 2017).

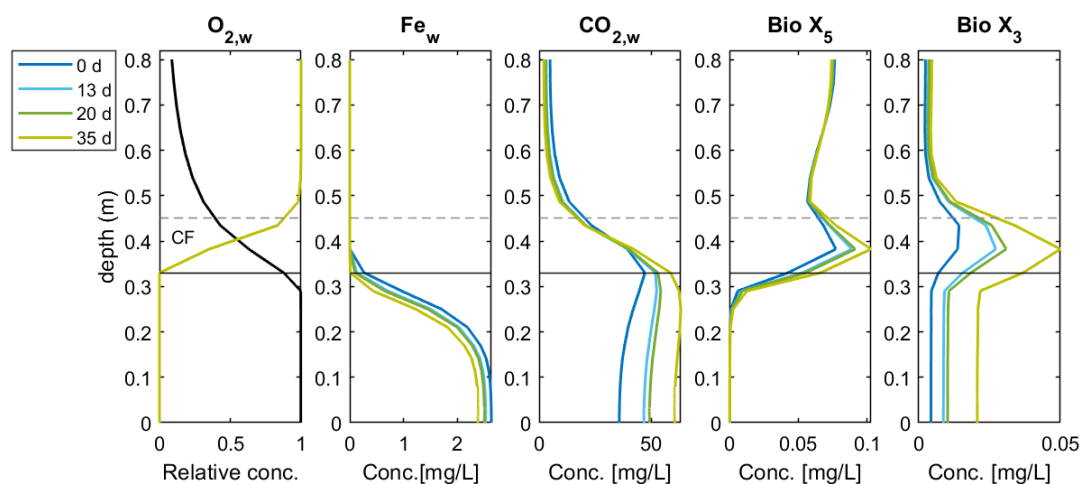


**Figure 4.6:** DCM degradation by bacterial population  $X_3$  (*D. formicoaceticum*) in the presence of a non-DCM degrader ( $X_5$ ) under steady-state conditions. Evolution of  $O_2$ , ferric Fe and  $CO_2$ , and bacterial populations  $X_5$  and  $X_3$ . In addition to oxygen vertical profile (left), the gravimetric saturation (in black) is given. Horizontal line is the position of the water table. Dashed line is the upper boundary of the capillary fringe.

Reactive transport modeling including microbial processes such as biomass growth, microbial maintenance and dormancy have further proven relevant to evaluate biodegradation across the capillary fringe (Hron et al., 2015) and in transient plumes (Eckert et al., 2015). The mathematical description of these processes are accounted for in this model (Section 4.2), providing an opportunity for its application to unravel key factors affecting biodegradation processes under dynamic conditions.

#### 4.4.3 Concomitant DCM degradation under steady-state conditions

Concomitant DCM degradation was tested accounting for active metabolism of bacterial populations  $X_3$  (fermentative pathway, Chen et al. (2020); Mägli et al. (1996)) and  $X_4$  (mineralization + acetogenesis, Chen et al. (2020); Kleindienst et al. (2019)), with and without the presence of biomass  $X_2$  (iron-reducing). Similar as for individual bacterial populations, numerical sim-

ulations of concomitant DCM degradation were carried out in the presence of biomass  $X_5$  and considering an incubation period of 60 days (test case 2, Section 4.3.3). As already discussed, numerical simulations for test case 1 show the relevance of the capillary fringe for promoting DCM degradation by bacterial population  $X_5$  through  $\text{CO}_2$  production during DOC mineralization. Concomitant DCM degradation under steady-state conditions (i.e., test case 2) proved a larger DCM mass removal over time (40%) (Figure 4.7) compared to test case 1 (Figure 4.5). Comparison between simulations in the presence or absence of biomass  $X_2$  suggests insignificant DCM degradation under iron-reducing conditions compared to other anaerobic DCM degradation pathways (Figure 4.7), as shown previously (see Figure 4.5). This is due to competition with bacterial population  $X_5$  for ferric iron, which it is more rapidly depleted due to lower inflow concentrations ( $3 \text{ mg L}^{-1}$ ) compared to DOC ( $100 \text{ mg L}^{-1}$ ) (SI, Section B.7).

Changes in concentrations and carbon isotope ratios were similar to that observed in the laboratory aquifers (Figure 4.7). However, changes in Cl isotope ratios were lower compared to experimental observations, due to low  $\varepsilon_{\text{Cl}}$  values considered in the model. Overall, DCM mass removal of up to 40% was observed under for both test cases, in line with observations presented in Chapter 3. This was accompanied with a change in C and Cl isotope ratios over time and distance from inflow, with  $\Delta^{13}\delta\text{C}$  of 12‰ and  $\Delta^{37}\delta\text{Cl}$  of <3‰ for both cases (Figure 4.7). However,  $\Lambda^{\text{C/Cl}}$  values associated with concomitant anaerobic DCM degradation resulted much higher than observed experimentally (see below).

Indeed, the often presence of potentially associated anaerobic DCM degraders at contaminated sites (Blázquez-Pallí et al., 2019; Hermon et al., 2018; Wright et al., 2017), and in both laboratory aquifers (see Chapter 3), further argues for fundamental investigations on the parallel enrichment of several anaerobic taxa. For instance, direct competition experiments between known anaerobic DCM degraders such as *D. formicoaceticum* and *Ca. D. elyunquensis* have not yet been performed, and await for elucidation of the possible co-existence of these DCM degradation pathways, further validating (or not) the proposed model formalism. Moreover, it has been recently proposed that known anaerobic DCM degraders from the *Peptococcaceae* family – here corresponding to bacterial populations  $X_2$ ,  $X_3$  and  $X_4$  – share a unique anaerobic gene cassette, containing proteins *mecE* and *mecF* (for methylene chloride catabolism). It is suggested that *mecE* and *mecF* encode a putative dehalogenating methyltransferase, possibly implicated in C-Cl bond cleavage and release of the chlorine substituents (Murdoch et al., 2022). In the future, the *mec* gene cassette may be utilized as a valuable remediation biomarker, providing another line of evidence for anaerobic DCM degradation at contaminated sites (Murdoch et al.,

2022).

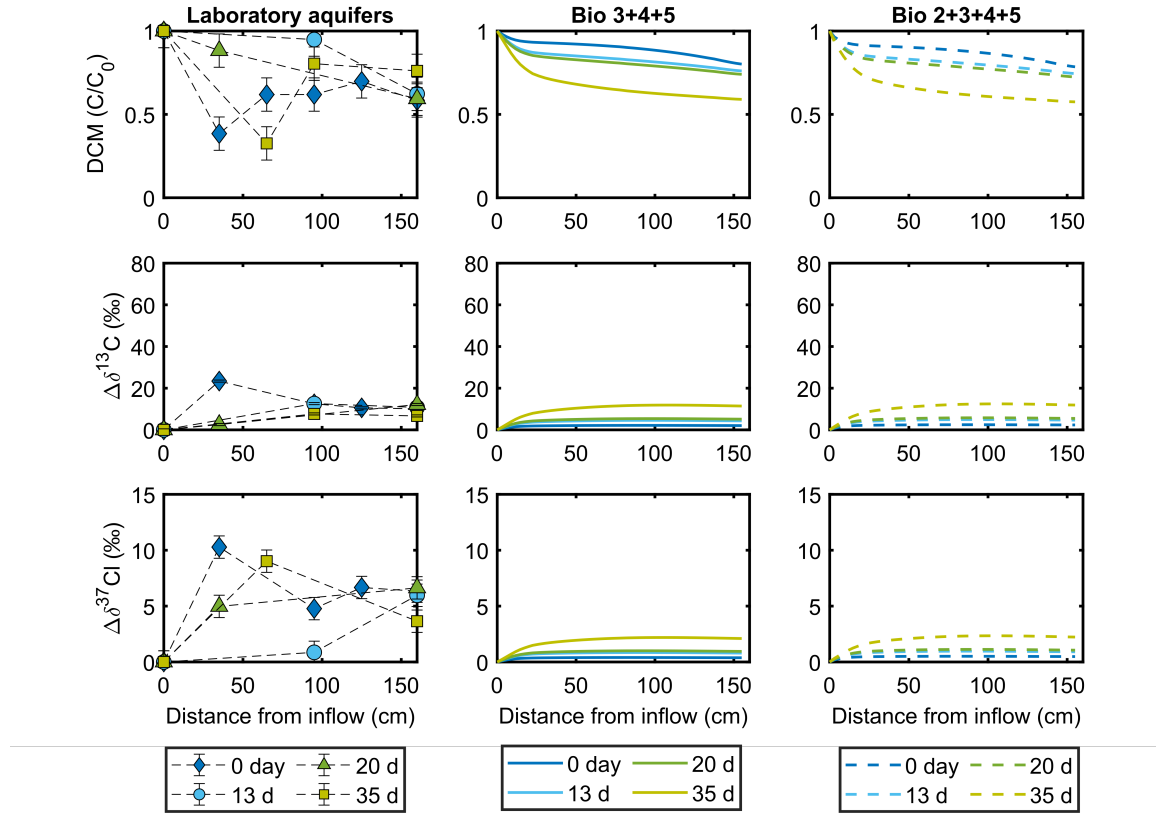


**Figure 4.7:** Experimental observations in laboratory aquifers (left panel) and numerical simulations for concomitant anaerobic DCM degradation by bacterial populations  $X_3$  (*D. formicoaceticum*) and  $X_4$  (*Ca. D. elyunquensis*) (middle panel; continuous lines), and in the presence of  $X_2$  (*Dehalobacter* sp.) (right panel; dashed lines). All simulations were carried out in the presence of a non-DCM degrader ( $X_5$ ) under steady-state conditions. Experimental observations and numerical simulations correspond to data at depth  $z=15$  cm and at different times: day 0 (diamonds, blue), day 13 (circles, light blue), day 20 (triangles, green) and day 35 (squares, light green).

Dual plots of concomitant DCM degradation proved distinct  $\Lambda^{C/Cl}$  values as of those from degradation by individual bacterial populations (Figure 4.9), reflecting the contribution of multiple DCM degradation pathways on the overall isotope signatures (Van Breukelen, 2007). Because the model accounts for isotope fractionation values of known DCM degraders (Table 4.2), the obtained  $\Lambda^{C/Cl}$  values during concomitant DCM degradation would result different from those observed experimentally, ultimately ignoring the presence of not yet recognized DCM degraders in the laboratory aquifers, as suggested previously (Chapter 3). For instance, the low  $\Lambda^{C/Cl}$  of  $1.92 \pm 0.30$  observed experimentally under steady-state conditions suggests that this value may well be associated with not yet reported anaerobic transformation pathways, possibly associated with undescribed microorganisms. Nevertheless, even closely related microorganisms

such as *Dehalobacterium* sp. may show distinct C and Cl isotope fractionation due to different characteristics of the bacterial cell envelope or enzyme locations (Trueba-Santiso et al., 2017).

For concomitant DCM degradation by bacterial populations  $X_2$  (*Dehalobacter* sp.),  $X_3$  (*D. formicoaceticum*) and  $X_4$  (*Ca. D. elyunquensis*), a  $\Lambda^{C/Cl}$  value of  $5.62 \pm 0.01$  was obtained (Figure 4.9). Similarly, concomitant DCM degradation without the presence of bacterial population  $X_2$  resulted in a  $\Lambda^{C/Cl}$  value of  $5.65 \pm 0.01$ . This further supports the dominance of anaerobic DCM degradation by both bacterial populations  $X_3$  and  $X_4$ , over metabolic activity of bacterial population  $X_2$  (see Section 4.4.2). Furthermore, the obtained  $\Lambda^{C/Cl}$  values from numerical simulations suggests that bacterial populations  $X_3$  and  $X_4$  contributed almost equally to DCM biodegradation, due to similar stoichiometry and growth rates for *D. formicoaceticum* and *Ca. D. elyunquensis*, as suggested previously (Chen et al., 2020). Because isotope fractionation is not affected by degradation rates, the large differences in simulated  $\Lambda^{C/Cl}$  values and that obtained experimentally during DCM degradation under steady-state conditions further supports that (i) DCM degradation was likely degraded via anaerobic metabolisms in the laboratory aquifers by not yet reported taxa associated with low C- and Cl- isotope fractionation, and (ii) the large isotope fractionation associated with concomitant DCM degradation may argue for the dominance of a single microorganism during DCM degradation under steady-state conditions, associated with low C- and Cl- isotope fractionation (see Figure 4.5). For instance, although low mass removal and C- and Cl- isotope fractionation was observed for the *Dehalobacter*-containing culture (see Bio 2+5 in Figure 4.5), calibration of bacterial growth kinetics parameters may result in a better fitting with experimental observations.

#### 4.4.4 Evidencing the role of water table fluctuations to enhance DCM degradation

Following the incubation period (i.e., after 60 days), transient conditions were also simulated based on the experimental design and assuming concomitant DCM degradation (test case 3). In this case, two water table fluctuations events were simulated as described in Section 4.3.3. Evolution of DCM concentration and stable isotopes were also followed in the saturated zone at probes located at  $z=0.15$  m, corresponding to sampling ports of the laboratory aquifers.

Accordingly, higher DCM mass removal (up to 97%) was observed under transient conditions for both test cases compared to steady-state (40%), in line with observations presented in Chapter 3. This was accompanied with a change in C and Cl isotope ratios over time and distance from inflow, with  $\Delta^{13}\delta C$  of 40‰ and  $\Delta^{37}\delta Cl$  of 8‰ for both cases (Figure 4.8). Overall, carbon isotope fractionation was comparable between experimental results and model simula-

tions, while chlorine isotope fractionation was slightly lower than that observed experimentally (Figure 4.8). It is also evident that although trends are very similar between model simulations and experimental observations, the model was not able to capture possibly hotspots across the porous media, likely resulting from heterogeneity within the systems. This may also explain the discrepancy between the observed mass removal in both laboratory aquifers at 0 days, which differs from numerical simulations (see Figures 4.7 and 4.8). However, estimated DCM biodegradation based on C and Cl stable isotope fractionation was similar for both aquifers at day 0 (see Chapter 3, Table 3.1), which suggests that both aquifers were comparable at the end of the incubation period.

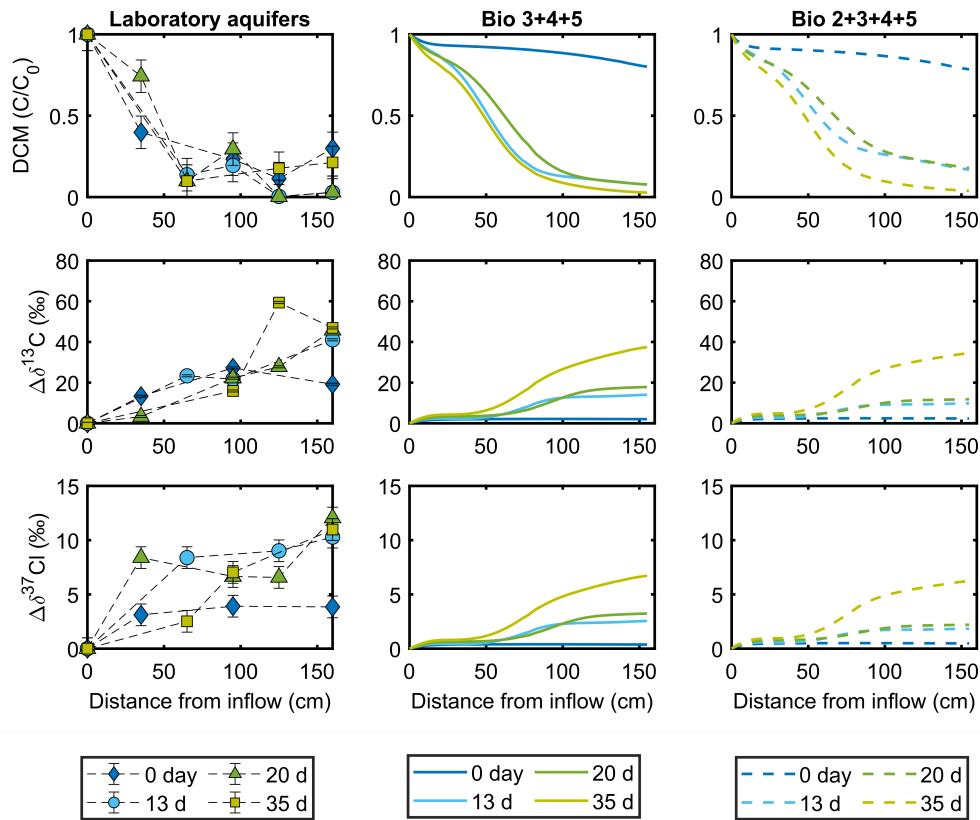


**Figure 4.8:** Experimental observations in laboratory aquifers (left panel) and numerical simulations for concomitant anaerobic DCM degradation by bacterial populations  $X_3$  (*D. formicoaceticum*) and  $X_4$  (*Ca. D. elyunquensis*) (middle panel; continuous lines), and in the presence of  $X_2$  (*Dehalobacter* sp.) (right panel; dashed lines). All simulations were carried out in the presence of a non-DCM degrader ( $X_5$ ) under transient conditions. Experimental observations and numerical simulations correspond to data at depth  $z=15$  cm and at different times: day 0 (diamonds, blue), day 13 (circles, light blue), day 20 (triangles, green) and day 35 (squares, light green).

Numerical results showed an increase in bacterial activity of  $X_5$  in the fluctuation zone coinciding with an increase in  $\text{CO}_2$  production. During the drainage periods,  $\text{O}_2$  diffused deeper into the underlying groundwater (Figure 4.3), resulting beneficial for DOC assimilation by bacterial population  $X_5$ , while maintaining  $\text{O}_2$ -depleted conditions during water table fluctuations, as observed in the laboratory aquifers (see SI of Chapter 3, Section A.4). This can be correlated with differences in oxygen fluxes between abiotic and biotic conditions (see Figure 4.3), as suggested previously (Jost et al., 2015b). Enhanced DOC assimilation in fluctuation zones has previously been suggested in soil column and microcosm experiments (Chimner and Cooper, 2003; Rezanezhad et al., 2014). It was suggested that oscillating redox conditions in this depth interval, together with a water saturation level on the order of 60%, possibly stimulates microbial respiratory activity and, hence, soil organic carbon turnover (Chimner and Cooper, 2003; Rezanezhad et al., 2014). Altogether, the numerical results underscore the importance of non-DCM degrading populations and the possibly indirect contribution to overall DCM degradation at contaminated sites, particularly for anaerobic DCM metabolisms requiring  $\text{CO}_2$ . Such decrease of DOC concentrations was evidenced in the laboratory aquifers over time and distance from inflow (see SI of Chapter 3; Section A.5, Figure A.3). For comparison, simulated evolution of all species is given for concomitant DCM degradation by bacterial populations  $X_3$  and  $X_4$  under steady-state (Figure 4.10 and SI, Section B.9) and transient conditions (Figure 4.11 and SI, Section B.9).

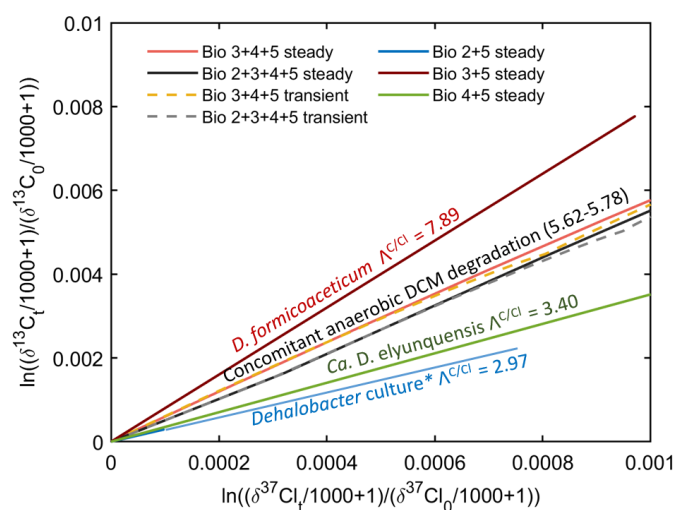


**Figure 4.9:** Numerical results of dual plot of  $\Delta^{13}\delta\text{C}$  versus  $\Delta^{37}\delta\text{Cl}$  for anaerobic DCM degradation. Continuous lines are related to DCM degradation by  $X_2$  (blue line, *Dehalobacter* sp.),  $X_3$  (red line, *Dehalobacterium formicoaceticum*) and  $X_4$  (green line, *Ca. D. elyunquensis*). Concomitant DCM degradation was simulated by bacterial populations  $X_3$  and  $X_4$ , with (gray lines) and without (orange lines) the presence of  $X_2$  under both steady-state (continuous lines) and transient conditions (dashed lines).

Though counterintuitive, the decrease in  $\text{CO}_2$  concentrations in the fluctuating zone evidenced the development of anaerobic bacterial populations  $X_3$  and  $X_4$ , while evolution of biomass  $X_2$  (iron-reducing) remained limiting (SI, Figure B.6). Overall, this coincides with the higher DCM mass removal under transient conditions compared to steady-state, providing a reasonable understanding of the observed processes in both laboratory aquifers. However, future laboratory flow-through experiments should consider a high-resolution monitoring of dissolved  $\text{CO}_2$  concentrations to examine anaerobic DCM degradation, and sustain our model-based hypotheses.

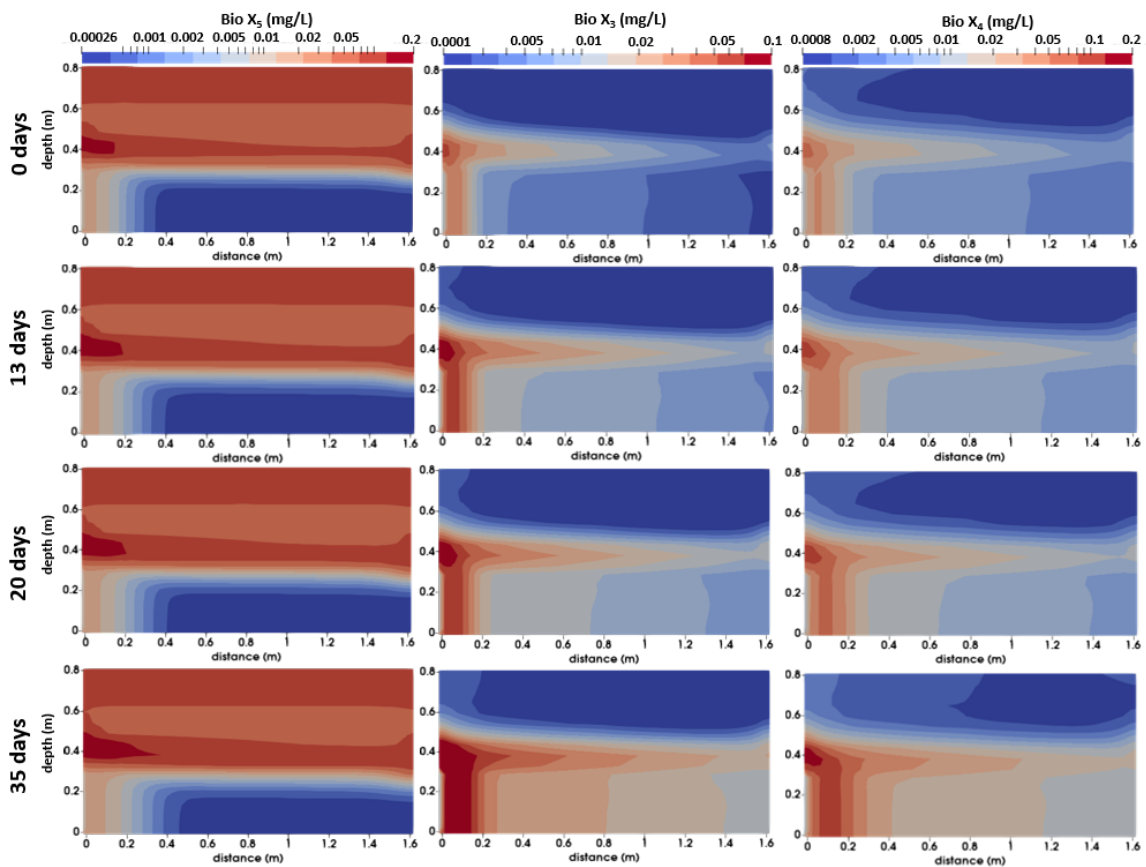


**Figure 4.10:** Simulated evolution (2D-domain) of biomass over time during concomitant DCM degradation by bacterial populations  $X_3$  (*D. formicoaceticum*) and  $X_4$  (*Ca. D. elyunquensis*) in the presence of a non-DCM degrader ( $X_5$ ) under steady-state conditions. The water table was positioned at 0.33 m.

Overall, numerical simulations showed that concomitant DCM biodegradation was dominant by bacterial populations  $X_3$  and  $X_4$  under both steady-state and transient conditions. This resulted in similar  $\Lambda^{\text{C/Cl}}$  for both conditions, which differs from experimental observations (Figure 4.9). Hence, further simulations testing differences in electrons availability could elucidate changes in biodegradation reactions over time and space (Van Breukelen, 2007), with the dom-

inance of one degradation pathway under transient conditions over one under steady-state. For instance, and in the context of concomitant DCM, water table fluctuations showed an increase in  $\text{CO}_2$  production due to DOC mineralization during drainage events, which could be a key driver of a distinct dominant DCM metabolism over steady-state conditions. Such differences could be correlated with changes in dominance of genera of the *Peptococcaceae* family under transient conditions, as evidenced in the laboratory aquifers (Chapter 3, Figure 3.5).

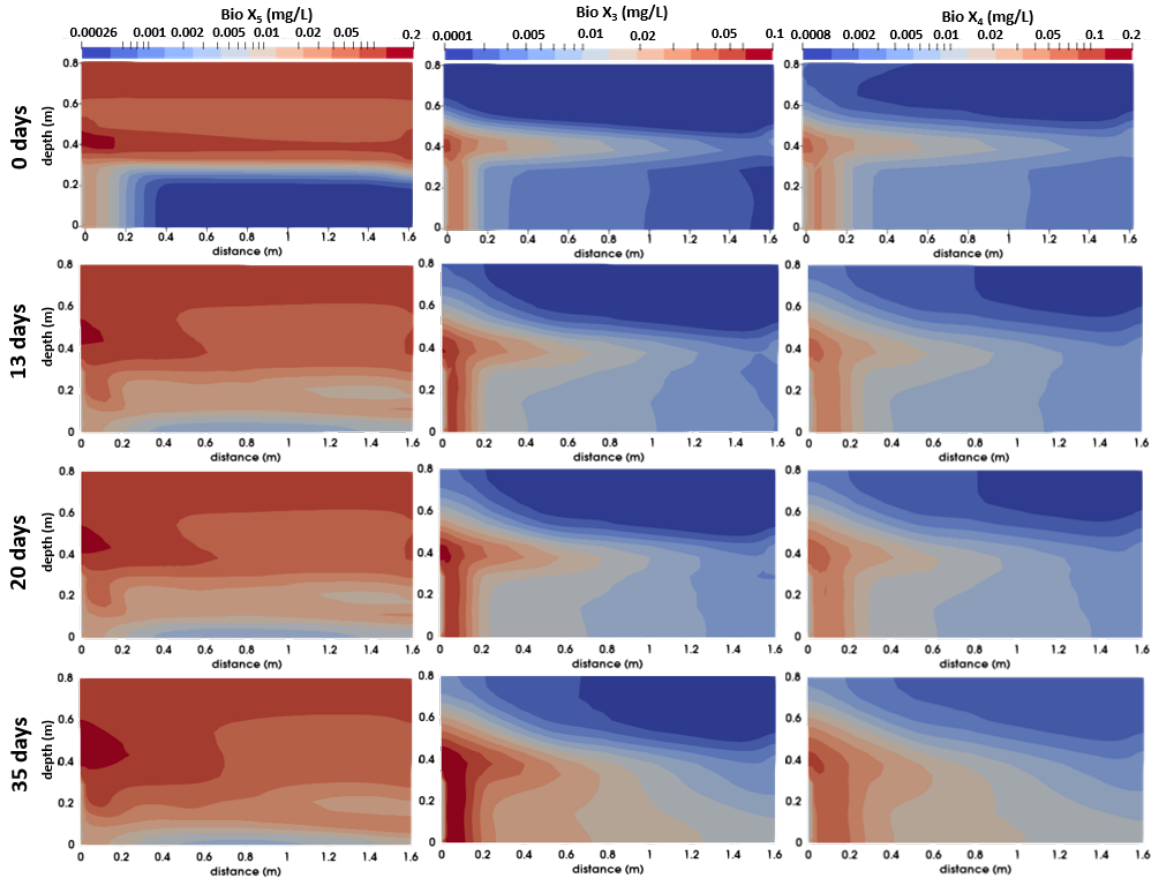


**Figure 4.11:** Simulated evolution (2D-domain) of biomass over time during concomitant DCM degradation by bacterial populations  $X_3$  (*D. formicoaceticum*) and  $X_4$  (*Ca. D. elyunquensis*) in the presence of a non-DCM degrader ( $X_5$ ) under transient conditions. The water table was positioned at 0.33 m, and lowered to 0.17 m during drainage events.

#### 4.5 Model limitations and future applications

The proposed mathematical formalism describing multi-phase flow and pathway-specific reaction rates with regard to DCM degradation proved suitable for shedding light on the numerous processes affecting reactive transport of dichloromethane under dynamic conditions. Though no attempts for model calibration have been done yet, results from numerical simulations well



captured the trends observed in the laboratory aquifers, as demonstrated previously (Hron et al., 2015). This indicates the ability of the proposed model to describe the strong relationships between transport and biodegradative processes under dynamic (transient) conditions, accounting for an evaluation strategy based on CSIA and pathway-specific reactions. Particularly, numerical simulations were able to reproduce the trends observed in laboratory aquifers subjected to steady-state and transient conditions, mirroring the large DCM mass removal accompanied by large C and Cl isotope fractionation.

Numerical results suggested that the contribution of non-DCM degraders on the overall DCM biodegradation was essential. Similarly, considerations on concomitant DCM degradation proved better at correlating with experimental observations, particularly for transient conditions. This highlights the importance of the whole bacterial dynamics with regard to natural attenuation of DCM in contaminated groundwater, rather than the enzymatic activity of a single bacterial population, and should be considered for future *in situ* assessments. In the future, an inverse modelling approach may improve the applicability of the model to obtain a more suitable parameterization, particularly for bacterial mediated processes. This can be further extended to a sensitivity analysis on parameters related to bacterial kinetics, fundamental for appropriate descriptions of bacterial developments during biodegradation reactions. Limitations on the experimental design of the laboratory aquifers were also encountered, restricting interpretations of DCM biodegradation to the saturated zone, while no monitoring of CO<sub>2</sub> and DCM transformation products were followed to support hypothesis on the possibly control of CO<sub>2</sub> fluxes to overall DCM dissipation under transient conditions. Moreover, anaerobic DCM degradation pathways and mechanisms are still poorly understood which calls for future studies to elucidate the possibility of concomitant anaerobic DCM degradation at contaminated sites. Finally, the model formalism presented on DCM degradation in dynamic hydrogeological systems, and based on an integrative experimental study, underscores the added value of RTMs in the evaluation of DCM natural attenuation at contaminated sites.

## References of Chapter 4

- Agostino, V., Lenic, A., Bardi, B., Rizzotto, V., Phan, A. N. T., Blank, L. M., and Rosenbaum, M. M. (2020). Electro-physiology of the facultative autotrophic bacterium *Desulfosporosinus orientis*. *Frontiers in Bioengineering and Biotechnology*, 8:14.
- Antelmi, M., Mazzon, P., Höhener, P., Marchesi, M., and Alberti, L. (2021). Evaluation of MNA in a chlorinated solvents-contaminated aquifer using reactive transport modeling coupled with isotopic fractionation analysis. *Water*, 13(21):2945.
- Badin, A., Braun, F., Halloran, L. J. S., Maillard, J., and Hunkeler, D. (2018). Modelling of C/Cl isotopic behaviour during chloroethene biotic reductive dechlorination: Capabilities and limitations of simplified and comprehensive models. *PLoS one*, 13:e0202416.
- Barry, D., Prommer, H., Miller, C., Engesgaard, P., Brun, A., and Zheng, C. (2002). Modelling the fate of oxidisable organic contaminants in groundwater. *Advances in Water Resources*, 25(8-12):945–983.
- Bauer, R. D., Maloszewski, P., Zhang, Y., Meckenstock, R. U., and Griebl, C. (2008). Mixing-controlled biodegradation in a toluene plume – Results from two-dimensional laboratory experiments. *Journal of Contaminant Hydrology*, 96(1):150–168.
- Blázquez-Pallí, N., Shouakar-Stash, O., Palau, J., Trueba-Santiso, A., Varias, J., Bosch, M., Soler, A., Vicent, T., Marco-Urrea, E., and Rosell, M. (2019). Use of dual element isotope analysis and microcosm studies to determine the origin and potential anaerobic biodegradation of dichloromethane in two multi-contaminated aquifers. *Science of The Total Environment*, 696:134066.
- Brooks, R. H. (1965). *Hydraulic properties of porous media*. Colorado State University.
- Chastanet, J., Côme, J.-M., Roupert, R. D. C., Schaefer, G., and Quintard, M. (2014). CubicM, un code de calcul pour simuler le devenir de polluants organiques dans le milieu souterrain. pages 1–4.
- Chen, G., Fisch, A. R., Gibson, C. M., Erin Mack, E., Seger, E. S., Campagna, S. R., and Löffler, F. E. (2020). Mineralization versus fermentation: evidence for two distinct anaerobic bacterial degradation pathways for dichloromethane. *The ISME Journal*, 14(4):959–970.
- Chen, G., Kleindienst, S., Griffiths, D. R., Mack, E. E., Seger, E. S., and Löffler, F. E. (2017). Mutualistic interaction between dichloromethane-and chloromethane-degrading bacteria in an anaerobic mixed culture. *Environmental microbiology*, 19(11):4784–4796.
- Chen, G., Shouakar-Stash, O., Phillips, E., Justicia-Leon, S. D., Gilevska, T., Sherwood Lollar, B., Mack, E. E., Seger, E. S., and Löffler, F. E. (2018). Dual carbon-chlorine isotope analysis indicates distinct anaerobic dichloromethane degradation pathways in two members of *Peptococcaceae*. *Environmental Science & Technology*, 52(15):8607–8616.

- Chimner, R. A. and Cooper, D. J. (2003). Influence of water table levels on CO<sub>2</sub> emissions in a Colorado subalpine fen: an in situ microcosm study. *Soil Biology and Biochemistry*, 35(3):345–351.
- Contois, D. E. (1959). Kinetics of bacterial growth: Relationship between population density and specific growth rate of continuous cultures. *Journal of General Microbiology*, 21(1):40–50.
- Coplen, T. B., Brand, W. A., Gehre, M., Gröning, M., Meijer, H. A. J., Toman, B., and Verkouteren, R. M. (2006). New guidelines for  $\delta^{13}\text{C}$  measurements. *Anal. Chem.*, 78(7):2439–2441.
- D’Affonseca, F., Prommer, H., Finkel, M., Blum, P., and Grathwohl, P. (2011). Modeling the long-term and transient evolution of biogeochemical and isotopic signatures in coal tar-contaminated aquifers. *Water Resources Research*, 47(5).
- Di Chiara Roupert, R. (2009). *Développement d’un code de calcul multiphasique multiconstituants*. PhD thesis, University of Strasbourg, Strasbourg, France.
- Di Chiara Roupert, R., Schäfer, G., Quintard, M., Marcoux, M., Chastanet, J., Côme, J.-M., and Duclos, Y. (2017). Multiphase multicomponent modelling of the NAPL transfer in the subsurface using method of lines.
- Eckert, D., Kürzinger, P., Bauer, R., Griebler, C., and Cirpka, O. A. (2015). Fringe-controlled biodegradation under dynamic conditions: Quasi 2-D flow-through experiments and reactive-transport modeling. *Journal of Contaminant Hydrology*, 172:100–111.
- Eckert, D., Qiu, S., Elsner, M., and Cirpka, O. A. (2013). Model complexity needed for quantitative analysis of high resolution isotope and concentration data from a toluene-pulse experiment. *Environmental Science & Technology*, 47(13):6900–6907.
- Eckert, D., Rolle, M., and Cirpka, O. A. (2012). Numerical simulation of isotope fractionation in steady-state bioreactive transport controlled by transverse mixing. *Journal of Contaminant Hydrology*, 140-141:95–106.
- Elsner, M. (2010). Stable isotope fractionation to investigate natural transformation mechanisms of organic contaminants: Principles, prospects and limitations. *Journal Environmental Monitoring*, 12(11):2005–2031.
- Geistlinger, H., Beckmann, A., and Lazik, D. (2005). Mass transfer between a multicomponent trapped gas phase and a mobile water phase: Experiment and theory. *Water Resources Research*, 41(11).
- Haberer, C. M., Rolle, M., Cirpka, O. A., and Grathwohl, P. (2012). Oxygen transfer in a fluctuating capillary fringe. *Vadose Zone Journal*, 11(3):vzj2011.0056.
- Hayoun, K., Geersens, E., Laczny, C. C., Halder, R., Lázaro Sánchez, C., Manna, A., Bringel, F., Ryckelynck, M., Wilmes, P., Muller, E. E. L., Alpha-Bazin, B., Armengaud, J., and Vuilleumier, S. (2020). Dichloromethane degradation pathway from unsequenced *Hyphomicrobium* sp. MC8b rapidly explored by pan-proteomics. *Microorganisms*, 8(12):1876.
- Hellal, J., Joulain, C., Urien, C., Ferreira, S., Denonfoux, J., Hermon, L., Vuilleumier, S., and Imfeld, G. (2021). Chlorinated ethene biodegradation and associated bacterial taxa in multi-polluted groundwater: Insights from biomolecular markers and stable isotope analysis. *Science of The Total Environment*, 763:142950.
- Heraty, L., Fuller, M., Huang, L., Abrajano, T., and Sturchio, N. (1999). Isotopic fractionation of carbon and chlorine by microbial degradation of dichloromethane. *Organic Geochemistry*, 30(8):793–799.
- Hermon, L., Denonfoux, J., Hellal, J., Joulain, C., Ferreira, S., Vuilleumier, S., and Imfeld, G. (2018). Dichloromethane biodegradation in multi-contaminated groundwater: Insights from biomolecular and compound-specific isotope analyses. *Water Research*, 142:217–226.

- Höhener, P. (2016). Simulating stable carbon and chlorine isotope ratios in dissolved chlorinated groundwater pollutants with BIOCHLOR-ISO. *Journal of Contaminant Hydrology*, 195:52–61.
- Holland, S. I., Edwards, R. J., Ertan, H., Wong, Y. K., Russell, T. L., Deshpande, N. P., Manefield, M. J., and Lee, M. (2019). Whole genome sequencing of a novel, dichloromethane-fermenting *Peptococcaceae* from an enrichment culture. *PeerJ*, 7:e7775.
- Holland, S. I., Ertan, H., Montgomery, K., Manefield, M. J., and Lee, M. (2021). Novel dichloromethane-fermenting bacteria in the *Peptococcaceae* family. *The ISME Journal*, 15:1709–1721.
- Holliger, C., Hahn, D., Harmsen, H., Ludwig, W., Schumacher, W., Tindall, B., Vazquez, F., Weiss, N., and Zehnder, A. J. B. (1998). *Dehalobacter restrictus* gen. nov. and sp. nov., a strictly anaerobic bacterium that reductively dechlorinates tetra- and trichloroethene in an anaerobic respiration. *Archives of Microbiology*, 169(4):313–321.
- Holocher, J., Peeters, F., Aeschbach-Hertig, W., Kinzelbach, W., and Kipfer, R. (2003). Kinetic model of gas bubble dissolution in groundwater and its implications for the dissolved gas composition. *Environmental Science & Technology*, 37(7):1337–1343.
- Höyng, D., Prommer, H., Blum, P., Grathwohl, P., and Mazo D’Affonseca, F. (2015). Evolution of carbon isotope signatures during reactive transport of hydrocarbons in heterogeneous aquifers. *Journal of Contaminant Hydrology*, 174:10–27.
- Hron, P., Jost, D., Bastian, P., Gallert, C., Winter, J., and Ippisch, O. (2015). Application of reactive transport modelling to growth and transport of microorganisms in the capillary fringe. *Vadose zone*, 14.
- Hunkeler, D., Meckenstock, R., and Sherwood Lollar, B. (2009a). A guide for assessing biodegradation and source identification of organic ground water contaminants using compound specific isotope analysis (CSIA). U.S. Environmental Protection Agency, Washington, D.C., EPA/600/R-08/148, page 82.
- Hunkeler, D., Van Breukelen, B. M., and Elsner, M. (2009b). Modeling chlorine isotope trends during sequential transformation of chlorinated ethenes. *Environmental Science & Technology*, 43(17):6750–6756.
- Jeannotat, S. and Hunkeler, D. (2013). Can soil gas VOCs be related to groundwater plumes based on their isotope signature? *Environmental Science & Technology*, 47(21):12115–12122.
- Jin, B., Nijenhuis, I., and Rolle, M. (2018). Simulation of dual carbon-bromine stable isotope fractionation during 1,2-dibromoethane degradation. *Isotopes in Environmental and Health Studies*, 54(4):418–434.
- Jost, D., Haberer, C. M., Grathwohl, P., Winter, J., and Gallert, C. (2015a). Oxygen transfer in a fluctuating capillary fringe: Impact of microbial respiratory activity. *Vadose Zone Journal*, 14(5):vzj2014.04.0039.
- Jost, D., Winter, J., and Gallert, C. (2015b). Noninvasive quantification of green fluorescent protein labeled *Escherichia coli* in a dynamic capillary fringe by fluorescence intensity. *Vadose Zone Journal*, 14(5):vzj2014.03.0028.
- Justicia-Leon, S. D., Ritalahti, K. M., Mack, E. E., and Löffler, F. E. (2012). Dichloromethane fermentation by a *Dehalobacter* sp. in an enrichment culture derived from pristine river sediment. *Applied and Environmental Microbiology*, 78(4):1288–1291.
- Kaufmann, R., Long, A., Bentley, H., and Davis, S. (1984). Natural chlorine isotope variations. *Nature*, 309(5966):338–340.

- Kleindienst, S., Chourey, K., Chen, G., Murdoch, R. W., Higgins, S. A., Iyer, R., Campagna, S. R., Mack, E. E., Seger, E. S., Hettich, R. L., and Löffler, F. E. (2019). Proteogenomics reveals novel reductive dehalogenases and methyltransferases expressed during anaerobic dichloromethane metabolism. *Appl Environ Microbiol*, 85(6).
- Kleindienst, S., Higgins, S. A., Tsementzi, D., Chen, G., Konstantinidis, K. T., Mack, E. E., and Löffler, F. E. (2017). '*Candidatus* dichloromethanomonas elyunquensis' gen. nov., sp. nov., a dichloromethane-degrading anaerobe of the *Peptococcaceae* family. *Systematic and Applied Microbiology*, 40(3):150–159.
- Kovárová-Kovar, K. and Egli, T. (1998). Growth kinetics of suspended microbial cells: From single-substrate-controlled growth to mixed-substrate kinetics. *Microbiology and molecular biology reviews*, 62(3):646–666.
- Kuder, T., Philp, R., Van Breukelen, B. M., Thoeument, H., and Vanderford, M. (2016). Integrated stable isotope – Reactive transport model approach for assessment of chlorinated solvent degradation. Technical report, University of Oklahoma Norman United States.
- Lee, M., Low, A., Zemb, O., Koenig, J., Michaelsen, A., and Manefield, M. (2012). Complete chloroform dechlorination by organochlorine respiration and fermentation: Microbial chloroform metabolism. *Environmental Microbiology*, 14(4):883–894.
- Lee, M., Wells, E., Wong, Y. K., Koenig, J., Adrian, L., Richnow, H. H., and Manefield, M. (2015). Relative contributions of *Dehalobacter* and zerovalent iron in the degradation of chlorinated methanes. *Environmental Science & Technology*, 49(7):4481–4489.
- Lueders, T. (2017). The ecology of anaerobic degraders of BTEX hydrocarbons in aquifers. *FEMS Microbiology Ecology*, 93(1):fiw220.
- Mägli, A., Messmer, M., and Leisinger, T. (1998). Metabolism of dichloromethane by the strict anaerobe *Dehalobacterium formicoaceticum*. *Applied and Environmental Microbiology*, 64(2):646–650.
- Mägli, A., Wendt, M., and Leisinger, T. (1996). Isolation and characterization of *Dehalobacterium formicoaceticum* gen. nov. sp. nov., a strictly anaerobic bacterium utilizing dichloromethane as source of carbon and energy. *Archives of Microbiology*, 166(2):101–108.
- Mardanov, A. V., Panova, I. A., Beletsky, A. V., Avakyan, M. R., Kadnikov, V. V., Antsiferov, D. V., Banks, D., Frank, Y. A., Pimenov, N. V., Ravin, N. V., and Karnachuk, O. V. (2016). Genomic insights into a new acidophilic, copper-resistant *Desulfosporosinus* isolate from the oxidized tailings area of an abandoned gold mine. *FEMS Microbiology Ecology*, 92(8):fiw111.
- McCarthy, K. A. and Johnson, R. L. (1993). Transport of volatile organic compounds across the capillary fringe. *Resources Research*, 29(6):1675–1683.
- Meckenstock, R. U., Elsner, M., Griebler, C., Lueders, T., Stumpp, C., Aamand, J., Agathos, S. N., Albrechtsen, H.-J., Bastiaens, L., Bjerg, P. L., Boon, N., Dejonghe, W., Huang, W. E., Schmidt, S. I., Smolders, E., Sorensen, S. R., Springael, D., and van Breukelen, B. M. (2015). Biodegradation: Updating the concepts of control for microbial cleanup in contaminated aquifers. *Environmental Science & Technology*, 49(12):7073–7081.
- Meile, C. and Scheibe, T. D. (2019). Reactive transport modeling of microbial dynamics. *Elements*, 15(2):111–116.
- Murdoch, R. W., Chen, G., Kara Murdoch, F., Mack, E. E., Villalobos Solis, M. I., Hettich, R. L., and Löffler, F. E. (2022). Identification and widespread environmental distribution of a gene cassette implicated in anaerobic dichloromethane degradation. *Global change biology*, 00:1–17.

- Ojeda, A. S., Phillips, E., and Sherwood Lollar, B. (2020). Multi-element (C, H, Cl, Br) stable isotope fractionation as a tool to investigate transformation processes for halogenated hydrocarbons. *Environmental Science: Processes & Impacts*, 22(3):567–582.
- Prommer, H., Anneser, B., Rolle, M., Einsiedl, F., and Griebler, C. (2009). Biogeochemical and isotopic gradients in a BTEX/PAH contaminant plume: Model-based interpretation of a high-resolution field data set. *Environmental Science & Technology*, 43(21):8206–8212.
- Pronk, G. J., Mellage, A., Milojevic, T., Smeaton, C. M., Engel, K., Neufeld, J. D., Rezanezhad, F., and Cappellen, P. V. (2020). Carbon turnover and microbial activity in an artificial soil under imposed cyclic drainage and imbibition. *Vadose Zone Journal*, 19(1):e20021.
- Ramel, F., Brasseur, G., Pieulle, L., Valette, O., Hirschler-Réa, A., Fardeau, M. L., and Dolla, A. (2015). Growth of the obligate anaerobe *Desulfovibrio vulgaris* Hildenborough under continuous low oxygen concentration sparging: Impact of the membrane-bound oxygen reductases. *PLOS ONE*, 10(4):e0123455.
- Rezanezhad, F., Couture, R.-M., Kovac, R., O'Connell, D., and Van Cappellen, P. (2014). Water table fluctuations and soil biogeochemistry: An experimental approach using an automated soil column system. *Journal of Hydrology*, 509:245–256.
- Rittmann, B. E. (2006). Microbial ecology to manage processes in environmental biotechnology. *Trends in Biotechnology*, 24(6):261–266.
- Rühle, F. A., von Netzer, F., Lueders, T., and Stumpp, C. (2015). Response of transport parameters and sediment microbiota to water table fluctuations in laboratory columns. *Vadose Zone Journal*, 14(5):vzj2014.09.0116.
- Seybold, C. A., Mersie, W., Huang, J., and McNamee, C. (2002). Soil redox, pH, temperature, and water-table patterns of a freshwater tidal wetland. *Wetlands*, 22(1):149–158.
- Speight, J. G. et al. (2005). *Lange's handbook of chemistry*, volume 1. McGraw-hill New York.
- Sun, F., Mellage, A., Gharasoo, M., Melsbach, A., Cao, X., Zimmermann, R., Griebler, C., Thullner, M., Cirpka, O. A., and Elsner, M. (2021). Mass-transfer-limited biodegradation at low concentrations – Evidence from reactive transport modeling of isotope profiles in a bench-scale aquifer. *Environmental Science & Technology*, 55(11):7386–7397.
- Trueba-Santiso, A., Fernández-Verdejo, D., Marco-Rius, I., Soder-Walz, J. M., Casabella, O., Vicent, T., and Marco-Urrea, E. (2020). Interspecies interaction and effect of co-contaminants in an anaerobic dichloromethane-degrading culture. *Chemosphere*, 240:124877.
- Trueba-Santiso, A., Parladé, E., Rosell, M., Lliros, M., Mortan, S. H., Martínez-Alonso, M., Gaju, N., Martín-González, L., Vicent, T., and Marco-Urrea, E. (2017). Molecular and carbon isotopic characterization of an anaerobic stable enrichment culture containing *Dehalobacterium* sp. during dichloromethane fermentation. *Science of The Total Environment*, 581:640–648.
- Van Breukelen, B. M. (2007). Extending the Rayleigh equation to allow competing isotope fractionating pathways to improve quantification of biodegradation. *Environmental Science & Technology*, 41(11):4004–4010.
- Van Breukelen, B. M., Hunkeler, D., and Volkerling, F. (2005). Quantification of sequential chlorinated ethene degradation by use of a reactive transport model incorporating isotope fractionation. *Environmental Science & Technology*, 39(11):4189–4197.

- Werner, D. and Höhener (2002). The influence of water table fluctuations on the volatilization of contaminants from groundwater. In: S. Thorton qnd S. Oswald (eds) *Groundwater quality: Natural and enhanced restoration of groundwater pollution (Proceedings of the groundwater quality 2001 conference held at Sheffield, UK, June 2001. IAHS PUBLICATION no. 275*, pages 213–218.
- Williams, M. and Oostrom, M. (2000). Oxygenation of anoxic water in a fluctuating water table system: an experimental and numerical study. *Journal of Hydrology*, 230(1):70–85.
- Wright, J., Kirchner, V., Bernard, W., Ulrich, N., McLimans, C., Campa, M. F., Hazen, T., Macbeth, T., Marabello, D., McDermott, J., Mackelprang, R., Roth, K., and Lamendella, R. (2017). Bacterial community dynamics in dichloromethane-contaminated groundwater undergoing natural attenuation. *Frontiers in Microbiology*, 8:2300.
- Yu, J., Cai, W., Cheng, Z., and Chen, J. (2014). Degradation of dichloromethane by an isolated strain *Pandoraea pnomenusa* and its performance in a biotrickling filter. *Journal of Environmental Sciences*, 26(5):1108–1117.

## Preface to Chapter 5

Groundwater quality is impacted by the ubiquitous presence of numerous micropollutants such as pesticides and pharmaceuticals. Removal of micropollutants from contaminated groundwater remains of major challenge due to their diffuse sources, persistence and toxicity. Similarly, their presence at low concentrations (sub- $\mu\text{g L}^{-1}$  range) is of concern due to their low bioavailability for microbial degradation.

Lessons learnt from legacy organic contaminants such as dichloromethane (DCM) (discussed in Chapter 3 and 4) can be taken to improve our understanding on micropollutants removal from subsurface environments. Here, however, stream-groundwater interactions represent a common entry pathway of micropollutants, due to their initial release in surface waters. **Chapter 5** presents an integrative study aiming at deciphering the reactive transport of a micropollutant mixture in laboratory aquifers mimicking lateral stream-to-groundwater flow interactions into oxygen rich areas of adjacent groundwater. Dynamic conditions were considered with regard to varying micropollutant exposure periods, representing variations in micropollutants inputs due to seasonal applications and hydrological events. This may have important implications on bacterial adaptations to long-term micropollutants exposure. The integration of ME-CSIA, biomolecular markers and conceptual RTMs may prove useful to derive a comprehensive framework to identify and quantify micropollutants degradation in contaminated aquifers.





# Chapter 5

## **Reactive transport of a micropollutant mixture in laboratory aquifers explored by CSIA, conceptual modeling and biomolecular markers**

Submitted to *Journal of Hazardous Materials*. Prieto-Espinoza, M., Di Chiara, R., Belfort, B., Weill, S., Imfeld, G. Reactive transport of a micropollutant mixture in laboratory aquifers explored by Compound-Specific Isotope Analysis (CSIA), biomolecular approaches and conceptual modeling.

## **Reactive transport of a micropollutant mixture in laboratory aquifers explored by Compound-Specific Isotope Analysis (CSIA), conceptual modeling and biomolecular markers**

### **Abstract**

Groundwater quality is of increasing concern due to the ubiquitous release of micropollutants, often originating from surface waters. Stream-groundwater interactions near agricultural and urban areas represent an important entry pathway of micropollutants into shallow aquifers. Here, we evaluate the biotransformation of a micropollutant mixture (i.e., caffeine, metformin, atrazine, terbutryn, *S*-metolachlor and metalaxyl) during stream-groundwater interactions dominated by lateral stream water flow to adjacent groundwater. We used an integrative approach including concentrations of micropollutants and transformation products (TPs), compound-specific isotope analysis ( $\delta^{13}\text{C}$  and  $\delta^{15}\text{N}$ ), sequencing of 16S rRNA gene amplicons and conceptual modeling. Duplicate laboratory aquifers (160 cm  $\times$  80 cm  $\times$  7 cm) were fed with stream water and subjected over 140 d to three successive periods of micropollutant exposure as pulse-like and constant injections under steady-state conditions. Atrazine, terbutryn, *S*-metolachlor and metalaxyl persisted ( $<10\%$  dissipation) in both aquifers during all periods. Metformin dissipation (up to 14%) was only observed from 90–140 d, suggesting enhanced degradation over time. In contrast, caffeine was dissipated ( $>90\%$ ) during all injection periods, agreeing with fast degradation rates ( $t_{1/2} < 3$  d) in parallel microcosm experiments and detection of TPs (theobromine and xanthine). Significant carbon stable isotope fractionation ( $\Delta\delta^{13}\text{C} \geq 6.6$  ‰) was observed for caffeine in both aquifers, whereas no enrichment in  $^{15}\text{N}$  occurred. A concentration dependence of caffeine biotransformation was further suggested by model simulations following Michaelis-Menten kinetics. Bacterial diversity varied and increased over time, suggesting long-term bacterial adaptation to micropollutant exposures. Altogether, our results highlight the variability of micropollutants degradation in aquifers subjected to a micropollutant mixture, and underscores the interest of an integrative approach to understand the interplay of subsurface hydrochemistry, bacterial adaptations and micropollutants biotransformation during stream-groundwater interactions.

## 5.1 Introduction

The ubiquitous release of micropollutants, typically in the  $\text{ng L}^{-1}$  to  $\mu\text{g L}^{-1}$  concentration range, results in the deterioration of water quality, aquatic life and human health (Barbosa et al., 2016; Schwarzenbach et al., 2010). Micropollutants cover a wide variety of substances such as pesticides, pharmaceuticals and consumer products. Pesticides are extensively used in agriculture to prevent and control harmful pests and crop yield losses worldwide (Damalas and Koutroubas, 2016). Pharmaceuticals and consumer products, however, are ubiquitously released into aquatic ecosystems, mainly from inefficient wastewater treatment facilities (WWTF) (Richardson and Kimura, 2016). The frequent and continuous release of micropollutants and their transformation products (TPs) results in their simultaneous presence as complex mixtures in both surface water (Bradley, 2021; Bradley et al., 2016; Hildebrandt et al., 2008), and groundwater (aus der Beek et al., 2016; Baran et al., 2021; Loos et al., 2010; Masoner et al., 2019; Seiler et al., 1999).

Natural attenuation in shallow aquifers relies on the ability of microorganisms to break down contaminants into less toxic chemicals (NRC, 2000). Micropollutants dissipation results from various biotic and/or abiotic transformation processes involving biological and chemical reactions, as well as non-degrading processes such as sorption or dilution (Fenner et al., 2013). Biodegradation mainly contributes to overall contaminant removal in aquifers (Fenner et al., 2013; Meckenstock et al., 2015). However, concentration measurements are generally not sufficient to infer the contribution of biodegradation to the overall micropollutant removal due to the simultaneous occurrence of both degradative and non-degradative processes. In this context, compound-specific isotope analysis (CSIA) may be used to evidence pollutant degradation by measuring changes of stable isotope ratios (e.g.,  $^{13}\text{C}/^{12}\text{C}$  or  $^{15}\text{N}/^{14}\text{N}$ ) of the remaining non-degraded molecules. This is due to kinetic isotope effects favoring the cleavage of molecules containing light isotopes compared to heavy isotopes. This results in an isotope fractionation effect in which the remaining contaminant is enriched in heavy isotopes (Elsner, 2010). The resulting change in isotope ratios may be related to micropollutant degradation extent, mechanisms and pathways, although micropollutant CSIA is an emerging field (Elsner and Imfeld, 2016).

In near-surface aquifers, the hyporheic zone (HZ), i.e., the transition zone between surface water and groundwater, is located beneath the stream bed and the two sides of the riparian zone (Zhang et al., 2017). The HZ represents a natural biogeochemical barrier against groundwater contamination (Boulton et al., 2010; Lewandowski et al., 2011). However, knowledge on the interplay of dynamic hydrological and biogeochemical conditions with respect to pol-

lutant transformation in the HZ is currently limited. Indeed, HZs can sustain micropollutants biotransformation particularly at the sediment-water interface (SWI) beneath the stream bed (Droz et al., 2021; Mechelke et al., 2020; Peter et al., 2019; Schaper et al., 2019). The reactivity of this zone is driven primarily by hydraulic residence times, surface-groundwater exchange, mass transfer rates, nutrient turnover and microbial diversity (Conant et al., 2019; Drouin et al., 2021; Peter et al., 2019; Posselt et al., 2020). Oxygen gradients are established across the HZ, while anoxic conditions are usually present at the bottom of the SWI, resulting in possibly lower micropollutants degradation rates (Droz et al., 2021), and thus their potential mobilization and accumulation in shallow groundwater (Hintze et al., 2020; Iker et al., 2010; Jakobsen et al., 2019; Lesser et al., 2018; Loos et al., 2010). In conditions where stream level is higher than the adjacent groundwater, e.g., due to seasonal hydrological changes (Winter et al., 1998), the losing streams may also laterally flow into groundwater (Ghysels et al., 2021; Winter et al., 1998) further mobilizing micropollutants into oxygen-rich zones in shallow aquifers (Chen and Chen, 2003; Derx et al., 2013; Hancock, 2002). This lateral transition zone represents a yet poorly understood highly dynamic mixing zone of stream-groundwater biogeochemical dynamics. As this area is often subject to seasonal variations in stream water level fluctuations and micropollutant inputs, aerobic biotransformation of micropollutants may be suggested.

Laboratory aquifers have proven advantageous to help unravelling the main drivers of micropollutants biotransformation under controlled conditions, while considering the spatial and temporal gradients usually formed across porous media (Bauer et al., 2008; Qiu et al., 2013; Schürner et al., 2016; Sun et al., 2021a). Recently, the use of CSIA in laboratory aquifers has shed light on micropollutant biotransformation, emphasizing the role of sorption and concentration dependence of micropollutant biotransformation (Schürner et al., 2016), diffusion and transverse-dispersion (Sun et al., 2021b), and mass-transfer limitations (Sun et al., 2021a). However, an integrative understanding of the dissipation of micropollutants mixtures and the long-term evolution of groundwater bacterial diversity in response to environmental perturbations at the stream-groundwater interface is yet required.

The present study aims to examine the reactive transport of a micropollutant mixture in laboratory aquifers fed with stream water mimicking stream-groundwater interactions dominated by lateral stream water flow to adjacent groundwater. Duplicate laboratory aquifers underwent a series of short- and long-term exposure periods (over 140 days), representing factors affecting pesticides trends such as seasonal applications and hydrological events (Baran et al., 2021; Chow et al., 2020), possibly affecting bacterial adaptations to variable micropollutants expo-

tures. Micropollutants and their TP concentration, C- and N-CSIA, and DNA analysis (i.e., 16S rRNA amplicons) were used to evaluate the contribution of micropollutants biotransformation of a mixture composed of the herbicides atrazine, terbutryn and *S*-metolachlor, the fungicide metalaxyl, the consumer product caffeine, and the anti-diabetic drug metformin, which may co-occur in surface and groundwater (Bradley, 2021; Lesser et al., 2018; Loos et al., 2010; Masoner et al., 2019). Concentrations and CSIA data were further interpreted using a parsimonious reactive transport model. In addition, parallel biotic and abiotic microcosms experiments were performed with stream water under oxic conditions to examine degradation potential and derive degradation kinetics of the micropollutant mixture.

## 5.2 Materials and methods

### 5.2.1 Stream water collection

Stream water was collected from the Souffel sub-catchment (3.6 km<sup>2</sup> out of 120 km<sup>2</sup> of total catchment area) located 30 km northeast of Strasbourg (Bas-Rhin, France; 48°40'09.4"N 7°33'51.5"E). With conventional agriculture accounting for 80% of the land use, of which 12% correspond to urban areas and 8% forests, the Souffel catchment is categorized as severely impacted by pesticide contamination. Corn and sugar beets are the main crops homogeneously cultivated over its surface area, receiving applications of *S*-metolachlor-containing herbicide products (Lefrancq et al., 2017; Lutz et al., 2017). *S*-metolachlor biodegradation in topsoil and stream water has been evidenced at the outlet of the Souffel and similar agricultural catchments (Alvarez-Zaldívar et al., 2018; Lefrancq et al., 2017). On the river sections downstream of the catchment area, discharges from the wastewater treatment plants temporarily cover the flows in the summer period (Droz, 2020).

For this study, freshwater was collected in three sterile 50 L stainless steel containers every two months from January to September 2020 and stored in a laboratory room at  $18 \pm 1$  °C until further use. For hydrochemical and bacterial diversity analyses, freshwater was collected in sterile 1 L glass bottles, transported on ice and stored immediately for further analysis. Total organic carbon was  $2.84 \pm 0.67$  mg L<sup>-1</sup> ( $n = 5$ ) and pH was  $7.1 \pm 0.2$  in Souffel stream water.

### 5.2.2 Micropollutant mixture

A detailed description of chemical reagents of the micropollutant mixture and corresponding TPs is provided in the Supporting Information (SI, Section C.1). The micropollutant mixture consisted of atrazine, caffeine, metalaxyl, *S*-metolachlor and terbutryn purchased from Sigma–

Aldrich (St: Louis, MO, USA; analytical grade purity: >99%). A stock solution containing a mixture of these chemicals was prepared in acetonitrile (ACN) at 5 g L<sup>-1</sup> and stored at -20 °C. Metformin was also purchased from Sigma-Aldrich (St: Louis, MO, USA; analytical grade purity: >99%) and prepared in water at 5 g L<sup>-1</sup> and stored at 4 °C. In addition, the following transformation products (TPs) were purchased from Sigma-Aldrich (St: Louis, MO, USA; analytical grade purity: >99%): desethylatrazine, deisopropylatrazine, hydroxy-atrazine, theobromine, paraxanthine, xanthine, carboxylic acid metalaxyl, demethylmetalaxyl, metolachlor ESA, metolachlor OXA, desethyl-terbutryn, desethyl-2-hydroxy-terbutryn, terbutryn-2-hydroxy, 1,3,5-triazine (terbutryn sulfoxide), and guanylurea. Stocks solutions were prepared in MeOH at 1 g L<sup>-1</sup> and stored at -20 °C.

### 5.2.3 Degradation kinetics experiment

Biodegradation microcosm experiments were performed to examine the dissipation potential of micropollutants in the stream water serving as inflow water of both laboratory aquifers. Biotic and abiotic microcosms were conducted under oxic conditions in a sacrificial mode at room temperature (20 ± 2°C) and in dark at natural pH (7.3 ± 0.4). Microcosms were prepared in 20 mL headspace vials crimped with butyl/PTFE caps (Interchim®) with a total volume of 15 mL of the micropollutant mixture. Stock solutions of the micropollutant mixture were spiked to reach final concentrations of 6 mg L<sup>-1</sup> per compound, representing the maximum concentrations established at the inflow of both laboratory aquifers and allowing C- and N-CSIA (Droz et al., 2021). The solution was stirred under sterile conditions until complete ACN evaporation. To maintain oxic conditions (4–9 ppm O<sub>2</sub>), limit water loss and avoid microbial contamination, a 0.2 µm PTFE syringe filter (Rotilabo®) was mounted on a syringe tip, which was stuck through the vial cap (Droz et al., 2021). All microcosms were kept under constant shaking (orbital shaker at 120 rpm). Biotic experiments were prepared in triplicates and sacrificed on days 0, 2, 5, 15, 50, 80, 100 and 200. Abiotic experiments (autoclaved triplicate solutions) and blanks were sacrificed at days 0, 5, 50 and 200. A 2 mL aliquot was used for hydrochemical analysis, 1 mL aliquot was collected to quantify metformin and TPs. The remaining solution (volume: 12 mL) was used for micropollutants quantification and C- and N-CSIA (i.e., δ<sup>13</sup>C and δ<sup>15</sup>N). Metformin CSIA was not performed in this study.

#### 5.2.4 Experimental setup and operation of laboratory aquifers

Experiments were conducted in two parallel laboratory aquifers with dimensions of 160 cm × 80 cm × 7 cm (length × height × width) and filled with sterile quartz sand (grain size: 0.4–0.6 mm; depth: 70 cm) (Figure 5.1). A detailed description of the experimental setup is provided in Section 2.3. Both aquifers were setup as duplicate and continuously fed in parallel with stream water (rate: 0.9 L d<sup>-1</sup>). The water table was positioned at 43 cm from the bottom. Each aquifer was connected to sterile 10 L reservoirs containing the inflow water which was kept under stirring (Figure 5.1). Oxic conditions were established by allowing atmospheric exchange from the top ports of the aquifers. The inflow water remained oxygenated throughout the experiments (8.6 mg L<sup>-1</sup>). The saturated zone (0–43 cm) was characterized by mean O<sub>2</sub> concentrations of 4.4 ± 0.8 mg L<sup>-1</sup>. Experiments were conducted in a temperature-controlled room at 18 ± 1 °C, and both aquifers were protected from light. A saline conservative tracer (NaCl) was injected to determine hydraulic retention times (1 L solution at 1 g L<sup>-1</sup>) (SI, Section C.2). The average pore water velocity was estimated as 0.08 m d<sup>-1</sup>.

After injection of the conservative tracer, aquifers were fed with stream water for 60 d (i.e., 2 pore water volumes) to ensure complete NaCl removal. An acclimation period was then established by injecting a pulse of the micropollutant mixture (1 L solution at 6 mg L<sup>-1</sup>) for 85 d to support adaptation of the bacterial community and favor micropollutant biodegradation (Poursat et al., 2019b; Prieto-Espinoza et al., 2021; Sun et al., 2021a). No samples were collected during the acclimation period. For the experiment, three consecutive injection periods were established in each aquifer over a lifespan of 140 d (Figure 5.1) to mimic punctual and chronic micropollutants emissions driven by hydrological events (Baran et al., 2021; Chow et al., 2020). At the beginning of the experiment (i.e., day 0; Figure 5.1), a first pulse injection of micropollutants was performed over a period of approximately 22 h (total volume: 1 L at ~6 mg L<sup>-1</sup> for each micropollutant). From days 40 to 61, a constant injection of the micropollutant mixture at 10 times lower concentrations (i.e., ~600 µg L<sup>-1</sup>) was conducted. Finally, a second pulse injection of the mixture was performed at day 93 (total volume: 1 L at ~6 mg L<sup>-1</sup>). Unspiked stream water fed the aquifers after each injection period (Figure 5.1) and until 220 d to flush out micropollutants prior to collection of core sand samples.



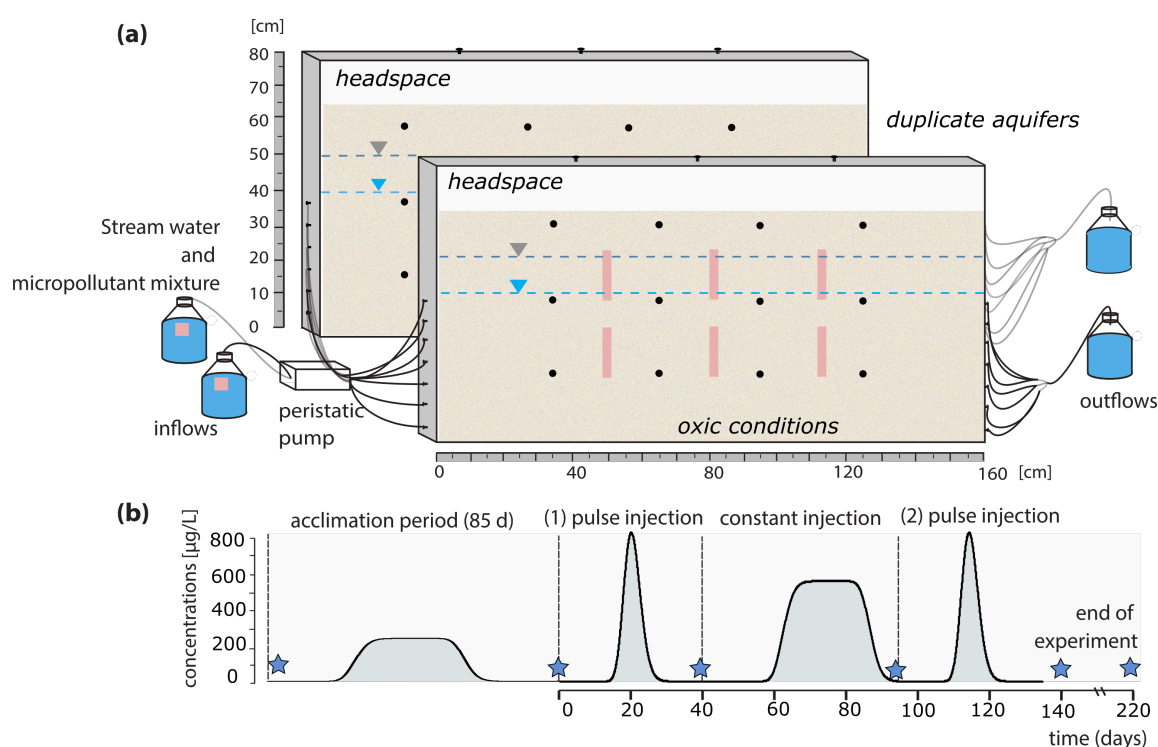


**Figure 5.1:** Laboratory aquifers receiving stream water and transient exposures of a micropollutant mixture. (a) Schematic overview of the laboratory aquifers, and (b) operation of the aquifers, including the acclimation period prior to the experiments, and subsequent micropollutants injection periods. Dotted lines represent micropollutants injections, followed by unspiked stream water. Breakthrough curves of the micropollutants were measured at the outflows (all ports,  $x=160$  cm). Stream-groundwater flows from left to right. Oxygen concentrations were followed across the porous media (pink rectangles). Bacterial dynamics were followed during the whole experiment (blue stars) from samples collected inside the aquifers (black circles) and outflows. Inflow and outflow bottles were kept sterile throughout the experiments.

### 5.2.5 Sampling procedure

For micropollutants and TPs concentrations, and CSIA (i.e.,  $\delta^{13}\text{C}$  and  $\delta^{15}\text{N}$ ), 1 L water was collected from the outlet reservoirs, immediately filtered ( $0.45\ \mu\text{m}$ ) and stored at  $4\ ^\circ\text{C}$  until further analysis. Sampling resolution during the pulse and constant injection periods was every 24 h and 48 h, respectively. For hydrochemical analysis, 30 mL water samples were collected every 5 d from inlet and outlet reservoirs. For DNA extraction, 200 mL were collected from inlet and outlet reservoirs at the beginning of the acclimation period, and during the experimental period at 0, 38, 90, 140 and 220 d (Figure 5.1). In addition, 2 depth-integrated pore water samples (volume: 10 mL) were collected from inside each aquifer at 45 cm (i.e., 35 cm and 65 cm horizontal sampling integration) and 105 cm (i.e., 95 cm and 125 cm horizontal sampling

integration) from the inflows, prior to the acclimation period and at 38, 140 and 220 d. Water samples were filtered through sterile 0.22  $\mu\text{m}$  membrane filters (Swinnex holder, 13 mm, Millipore, Bedford, USA) and stored at  $-20\text{ }^{\circ}\text{C}$  until DNA extraction. At the end of the experiments (220 d), 4 integrative sand cores were retrieved from each aquifer for DNA analysis at 45 cm and 105 cm distance from inflow and at depths of 15 cm and 45 cm. Each core subsample was thoroughly mixed and a subsample of 1 g of sand was used for DNA extraction.

## 5.2.6 Analytical methods

### 5.2.6.1 Hydrochemistry

Oxygen ( $\text{O}_2$ ) concentrations were monitored in situ by  $\text{O}_2$  sensitive optode foils (PreSens GmbH, Regensburg, Germany) located at the inlet reservoirs and across the aquifers (Figure 5.1). Redox potential (Eh), pH and electrical conductivity were monitored using laboratory probes (SCHOTT® Instruments). Major ions were measured by ion chromatography (Dionex ICS-5000, Thermo Scientific, USA). Total organic carbon (TOC), dissolved organic carbon (DOC) and dissolved inorganic carbon (DIC) were analyzed by a TOC analyzer (TOC-V-CPH Shimadzu, NF EN 1484).

### 5.2.6.2 Micropollutants extraction and quantification

Solid phase extraction (SPE) of pesticides and caffeine was carried out using SolEx C18 cartridges (1 g, Dionex®, CA, USA) and an AutoTrace 280 SPE system (Dionex®, CA, USA), following an in-house method described previously (Droz et al., 2021; Elsayed et al., 2014). A detailed description of micropollutants extraction and quantification methods is provided in the SI (Section C.3). All pesticides and caffeine were quantified by gas chromatography (GC, Trace 1300, Thermo Fisher Scientific) coupled with a mass spectrometer (MS, ISQ™, Thermo Scientific). Metformin was quantified by liquid chromatography (UHPLC, Ultimate 3000, Thermo Fisher Scientific) coupled with a tandem mass spectrometer (MS/MS, TSQ Quantiva, Thermo Fisher Scientific). Formation of TPs was quantified by LC-MS/MS for samples collected during the second injection period (90–140 d), as micropollutant dissipation mainly occurred during this period (see below).

### 5.2.6.3 Compound-specific isotope analysis

A detailed description of the analytical methods is provided in the SI (Section C.4). Stable carbon and nitrogen isotope composition of pesticides and caffeine was determined by gas

chromatography–combustion–isotope ratio mass spectrometry (GC–C–IRMS), with a gas chromatograph (Trace 1310) coupled via a GC/Conflow IV interface to an isotope ratio mass spectrometer (Delta V plus, Thermo Fisher Scientific). In-house standards were prepared daily and analyzed prior to sample measurements. Reproducibility of triplicate measurements was  $\leq 0.5\%$  ( $1\sigma$ ) for carbon and  $\leq 1\%$  ( $1\sigma$ ) for nitrogen within the linearity range (6–300 ng for C and 40–300 ng for N) (Droz et al., 2021). Carbon and nitrogen isotope ratios were reported in  $\delta$  notation as parts per thousand (‰) relative to the international reference material Vienna Pee Dee-Belemnite (V-PDB) (Coplen et al., 2006) and air standards, respectively. The average isotope value of the residual non-degraded fraction of the micropollutants was derived according to the Rayleigh equation (Elsner, 2010):

$$\ln \left( \frac{R_{t,E}}{R_{0,E}} \right) = \ln \left( \frac{c_t}{c_0} \right) \cdot \frac{\varepsilon_{bulk}^E}{1000} \quad (5.1)$$

where  $R_{t,E}/R_{0,E}$  is the isotope ratio of element  $E$  (i.e.  $^{13}\text{C}/^{12}\text{C}$  and  $^{15}\text{N}/^{14}\text{N}$ ), and  $c_t$  and  $c_0$  are the concentrations of a compound (i.e. DCM) at a given time ( $t$ ) and at the initial time ( $0$ ). Carbon and nitrogen isotopic composition are reported in delta notation ( $\delta^h\text{E}$ ) following  $\delta^h\text{E} = [(R_{\text{sample}}/R_{\text{standard}})-1] \times 1000$  (Elsner, 2010). Isotope enrichment factors ( $\varepsilon_{bulk}^E$ , in ‰) are obtained by least-squares linear regression without forcing the slope through the origin. The uncertainty corresponds to the 95% confidence interval (CI) and the error was determined using ordinary linear regression (Elsner et al., 2007).

#### 5.2.6.4 DNA extraction and sequencing

For both pore water and sand core samples, DNA was extracted using the DNeasy Power Water kit according to the manufacturer’s protocol (Qiagen, Hilden, Germany). Extracted DNA was quantified using Qubit fluorometric quantification with the Qubit dsDNA HS Assay kit (ThermoFisher Scientific, MA, USA). A detailed description of DNA sequencing is given in the SI (Section C.5). Multivariate statistical analysis of relative observed taxonomical units (OTU) abundance was performed with R (core Team, 2019). Non-metric multidimensional scaling (NMDS) based on Bray-Curtis dissimilarities of log-transformed data was performed to visualize dissimilarities between bacterial taxa (Hellal et al., 2020). Analysis of similarities (ANOSIM,  $n=31$  samples) based on Bray Curtis dissimilarities of samples was used to infer statistical differences between groups of community profiles (Torabi et al., 2020). Data sets obtained from Illumina sequencing were also used to compute  $\alpha$ -diversity indices and for rarefaction analysis (SI, Section C.5). In total, 1,861,511 high-quality sequences were obtained ( $n=31$  for pore

water  $n=8$  for sand samples). Rarefaction curves of diversity indices reached asymptotes with increasing sequencing depth, indicating sufficient sequencing efforts to capture the biodiversity extent of bacterial communities in all samples (SI, Section C.5).

### 5.2.7 Conceptual modeling

Since nitrogen isotope fractionation was not observed in this study, carbon isotope fractionation was only considered. The simple parsimonious reactive transport model considering equilibrium sorption can be described by (Eckert et al., 2013):

$$^{12}R \cdot \partial_t(^{12}c) + \mathbf{v} \cdot \nabla^{12}c = \nabla \cdot (\mathbf{D} \nabla^{12}c) + ^{12}r_{deg} \quad (5.2)$$

$$^{13}R \cdot \partial_t(^{13}c) + \mathbf{v} \cdot \nabla^{13}c = \nabla \cdot (\mathbf{D} \nabla^{13}c) + ^{13}r_{deg} \quad (5.3)$$

Here,  $c_{tot} = ^{12}c + ^{13}c$  (in  $\mu\text{g L}^{-1}$ ) is the total concentration of the micropollutant light ( $^{12}\text{C}$ ) and heavy ( $^{13}\text{C}$ ) isotopologues.  $R$  (-) is the retardation factor accounting for equilibrium sorption as  $R = 1 + \rho_b/n \cdot K_d$ , in which  $\rho_b$  ( $\text{kg L}^{-1}$ ) is the dry bulk density of the sediment,  $n$  is the porosity assumed as 0.37 (-), and  $K_d$  ( $\text{L kg}^{-1}$ ) is the linear distribution coefficient between water and sediment phases.  $\mathbf{v}$  ( $\text{m s}^{-1}$ ) is the average water velocity vector,  $\mathbf{D}$  ( $\text{m}^2 \text{s}^{-1}$ ) is the hydrodynamic dispersion tensor. The degradation rates  $r_{deg}$  ( $\mu\text{g L}^{-1}\text{s}^{-1}$ ) of the two most abundant light ( $^{12}\text{C}$ ) and heavy ( $^{13}\text{C}$ ) isotopologues assuming Michaelis-Menten kinetics (Breukelen and Prommer, 2008; Eckert et al., 2013) are given by:

$$^{12}r_{deg} = -^{12}r_{max} \frac{^{12}c}{^{12}K_m \left( \frac{^{12}c}{^{12}K_m} + \frac{^{13}c}{^{13}K_m} \right)} \quad (5.4)$$

$$^{13}r_{deg} = -^{13}r_{max} \frac{^{13}c \cdot \alpha_B}{^{13}K_m \left( \frac{^{12}c}{^{12}K_m} + \frac{^{13}c}{^{13}K_m} \right)} \quad (5.5)$$

where  $r_{max}$  is the maximum degradation rate and  $K_m$  is the half-saturation concentration ( $\mu\text{g L}^{-1}$ ) of the light ( $^{12}\text{C}$ ) and heavy ( $^{13}\text{C}$ ) isotopologues. To compute degradation rates of the isotopologues,  $K_m$  is assumed to be identical for both isotopologues, as suggested previously (Breukelen and Prommer, 2008; Eckert et al., 2013). The isotope fractionation factor  $\alpha_B$  (-) is thus defined as:

$$\alpha_B = \frac{{}^{13}r_{deg}/{}^{13}C}{{}^{12}r_{deg}/{}^{12}C} \quad (5.6)$$

Isotope fractionation by transverse dispersion was not here considered, since insignificant isotope effects by transverse dispersion have previously been shown for micropollutants reactive transport in flow-through aquifers (Schürner et al., 2016; Sun et al., 2021a). Although sorption is not expected to be significant in our aquifer's setup (clean quartz sand as solid matrix), isotope fractionation affected by equilibrium sorption was modeled considering that light isotopes tend to sorb slightly more than heavier isotopes (i.e.,  ${}^{12}K_d > {}^{13}K_d$ ) (Kopinke et al., 2005). Isotope fractionation affected by sorption is thus described as (Schürner et al., 2016):

$$\alpha_{sorp} = \frac{{}^{13}R - 1}{{}^{12}R - 1} = \frac{{}^{13}K_d}{{}^{12}K_d} \quad (5.7)$$

The breakthrough curve (BTC) of the conservative tracer was fitted to retrieve the average velocity  $\mathbf{v}$  and the longitudinal dispersion coefficient  $\mathbf{D}$ . A list of parameters and the fitting procedure are presented in the SI (Section C.6). Briefly, the coupled system of one-dimensional reactive-transport equations is solved in a fully implicit and fully coupled way using a cell-centered Finite Volume Method combining a Lax-Wendroff  $2^{nd}$  order scheme of the advective term for spatial discretization. All model parameters are assumed to be spatially uniform. Finally, isotope fractionation values associated with micropollutants biotransformation ( $\varepsilon_B$ , ‰) and sorption ( $\varepsilon_{sorp}$ , ‰) were estimated.

## 5.3 Results and discussion

### 5.3.1 Kinetics of micropollutants biotransformation in stream water

Microcosm experiments confirmed contrasted biotransformation potential of the selected micropollutants in the Souffel stream water. No significant changes in the hydrochemistry were observed in both biotic and abiotic conditions over time (SI, Section C.7). Under abiotic conditions, less than 10% of the initial mass dissipated after 200 d, corresponding to analytical uncertainties. This also indicates the occurrence of insignificant abiotic reactions such as hydrolysis (SI, Section C.7).

Under biotic conditions, caffeine rapidly dissipated ( $t_{1/2} = 3$  d; Figure 5.2), agreeing with previous studies showing rapid half-lives of caffeine ( $t_{1/2} < 4$  d) in river water microcosms (Lam et al., 2004; Nödler et al., 2014). Accordingly, caffeine  $\delta^{13}C$  values increased from  $-31.46 \pm$

0.60‰ up to  $-26.60 \pm 0.18$ ‰ (SI, Section C.8). The estimated  $\varepsilon_C$  value of caffeine of  $-1.1 \pm 0.3$ ‰ agreed with previous observations in a SWI batch experiment, where slight but significant fractionation ( $\Delta\delta^{13}\text{C} > 2$ ‰) occurred after  $>90\%$  of caffeine degradation ( $\varepsilon_C = -0.69 \pm 0.07$ ‰) (Droz, 2020). However, no changes in  $\delta^{15}\text{N}$  values were observed. Caffeine biodegradation via N-demethylation pathway has been suggested as the most common caffeine biodegradation pathway observed in at least 80% of the reported isolates characterized worldwide (Summers et al., 2015). Here, a sequential transformation of caffeine to theobromine to xanthine has been described (Dash and Gummadi, 2007; Yu et al., 2009). Indeed, the detection of theobromine and xanthine in biotic stream water microcosms further supports the likely occurrence of caffeine biodegradation via the N-demethylation pathway (SI, Section C.7).

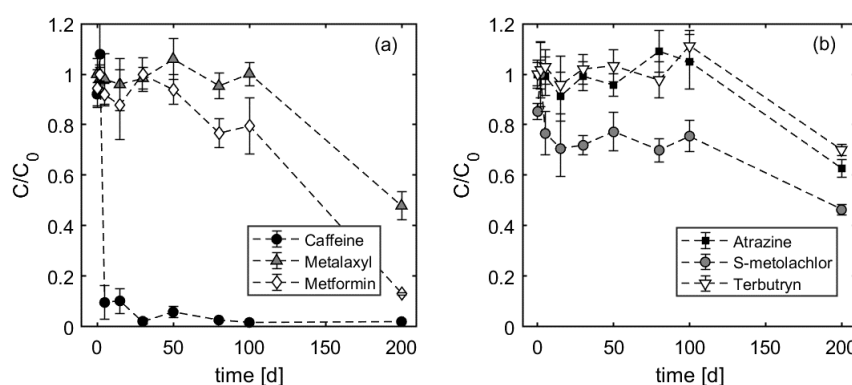


**Figure 5.2:** Dissipation of micropollutants in biotic stream water microcosms over time. (a) Caffeine, metalaxyl and metformin, and (b) atrazine, *S*-metolachlor and terbutryn. Error bars represent reproducibility of measurements ( $n=3$ ).

Contrastingly, *S*-metolachlor dissipated by 20% in the first 5 d, while overall dissipation was up to 60% after 200 d ( $t_{1/2} = 187$  d; Figure 5.2). This is in agreement with reported half-lives of *S*-metolachlor ranging from 56 to 182 d in agricultural soils and SWI microcosms (Droz et al., 2021; Torabi et al., 2020). Metformin and metalaxyl started dissipating after 50 d and 100 d, respectively, with estimated half-lives of 189 d and 147 d, respectively (Figure 5.2). Previous studies reported half-lives of metalaxyl ranging from 9 to 127 d in agricultural soils (Buerge et al., 2003), while metformin has been classified as a not readily biodegradable substance with half-lives ranging from 28 to 98 d in activated sludge (Straub et al., 2019). On the other hand, terbutryn and atrazine dissipated to up to 30% and 38% of their initial mass, respectively, at 200 d (Figure 5.2). Half-lives of atrazine and terbutryn, assuming pseudo-first order degradation, were estimated as 225 d and 290 d, respectively. This is in agreement with previous studies that reported long half-lives for terbutryn ( $t_{1/2} = 177$ –349 d) in groundwater microcosms under oxic

conditions (Talja et al., 2008). Carbon and nitrogen isotope fractionation of atrazine, terbutryn, metalaxyl and S-metolachlor were not observed after 200 d, mirroring their limited dissipation (<60%) (SI, Section C.8). However, TPs formation confirmed that biodegradation was the main dissipation process (SI, Section C.7). Overall, our results suggest the occurrence of a lag-phase of 50 d of metformin, and of 100 d for atrazine, terbutryn, and metalaxyl before slow biotransformation in stream water microcosms (Figure 5.2). Such lag-phase has also been observed for atrazine, metolachlor and alachlor degradation in biotic groundwater microcosms (Cavalier et al., 1991; Schwab et al., 2006), and may be attributed to early stages of bacterial adaptations to chemical exposure (Poursat et al., 2019b).

### 5.3.2 Micropollutants biotransformation in flow-through laboratory aquifers

Overall, the dynamics of hydrochemical conditions and micropollutant concentrations were similar in both aquifers. At the end of the acclimation period (i.e., 85 d prior to the experiments), background concentrations of micropollutants ranged from 1 to 10  $\mu\text{g L}^{-1}$  at the outlets. Hydrochemical conditions in both aquifers were constant over the whole experiment (SI, Section C.9). Mass recoveries of the micropollutants are provided in the SI (Section C.10).

*Caffeine* biotransformation occurred during all examined injection periods (0–140 d), and readily dissipated compared to other micropollutants (Figure 5.3, upper panel), in agreement with the fast caffeine biodegradation in the stream water microcosms (see Figure 5.2). Overall, caffeine has been previously demonstrated as a readily biodegradable substance in lysimeter experiments (Koroša et al., 2020) and river water microcosms (Lam et al., 2004; Nödler et al., 2014). Caffeine biodegradation was the main dissipation process as abiotic micropollutants biotransformation proved insignificant in stream water microcosms (see SI, Sections C.7 and C.8), and sorption is expected to be negligible due to low organic content (<0.01%) in the quartz sand matrix of the aquifers. Caffeine biodegradation was also supported by the detection of caffeine TPs, i.e., theobromine (up to 1460  $\mu\text{g L}^{-1}$ ) and xanthine (up to 328  $\mu\text{g L}^{-1}$ ), during the second injection period (SI, Section C.11). Fast caffeine dissipation may be associated with microorganisms adapted to regular and long periods of caffeine inputs into surface waters (Summers et al., 2015). At least 71 bacterial strains from many different habitats worldwide have been reported to be involved in caffeine biodegradation, possibly sustained by ancient metabolic pathways for methylxanthines still retained in some bacteria (Summers et al., 2015; Vega et al., 2021).

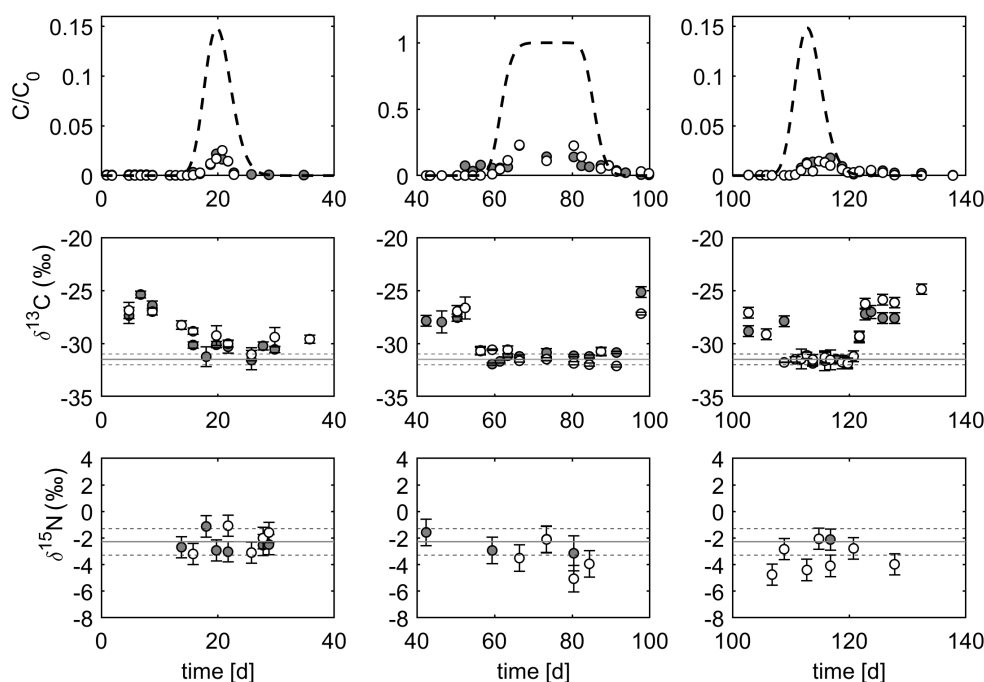


**Figure 5.3:** Caffeine concentrations (upper panel) and carbon ( $\delta^{13}\text{C}$ ) and nitrogen ( $\delta^{15}\text{N}$ ) isotope signatures (middle and lower panels) during the three injection periods of the micropollutant mixture: first pulse injection (0–40 d;  $C_0 \approx 6000 \mu\text{g L}^{-1}$ ), constant injection (40–90 d;  $C_0 \approx 600 \mu\text{g L}^{-1}$ ) and second pulse injection (90–140 d;  $C_0 \approx 6000 \mu\text{g L}^{-1}$ ). Full and empty symbols represent data sets from the duplicate aquifers. Dashed back lines represent the BTCs of the saline conservative tracer. Error bars represent the standard deviation of  $\delta^{13}\text{C}$  and  $\delta^{15}\text{N}$  ( $n=3$ ). Continuous horizontal lines represent caffeine EA values of carbon ( $-31.46 \pm 0.02 \text{‰}$ ) and nitrogen ( $-2.28 \pm 0.06 \text{‰}$ ) isotopes. Dashed horizontal lines represent the total uncertainty of carbon  $\pm 0.5 \text{‰}$  and nitrogen  $\pm 1 \text{‰}$ .

*Metformin* dissipation in both laboratory aquifers increased over time. During the first pulse injection (0–40 d), a similar *metformin* BTC was observed as the conservative tracer (SI, Section C.10). Similarly, during the constant injection period (40–90 d) no significant *metformin* dissipation was observed. In contrast, during the second pulse injection (90–140 d), only  $82 \pm 5 \%$  of the initial mass of *metformin* was recovered (SI, Section C.10). This indicates that *metformin* biodegradation in the aquifers occurred mostly from 90 to 140 d. *Metformin* biodegradation is also supported by observations in the freshwater microcosms (Figure 5.2) and the detection of guanylylurea (SI, Section C.11) as the main *metformin* TP in the aquifers (Poursat et al., 2019a). Overall, an increase in *metformin* dissipation over time suggests a gradual adaptation or increase of active bacterial degraders after the acclimation period and subsequent periods (from 0–90 d) of exposure to micropollutants. A similar adaptation has been suggested previously



in chemostat systems, where a 2-month pre-exposure period enhanced metformin degradation, correlating with an increase in bacterial community diversity, composition and activity (Dalmijn et al., 2021).

Contrastingly, *S-metolachlor* showed similar BTCs as those of the conservative tracer throughout the whole experiment (SI, Section C.10), suggesting limited *S-metolachlor* biodegradation. The limited *S-metolachlor* biodegradation in the laboratory aquifers also mirrored the slow *S-metolachlor* degradation kinetics after 100 days in the stream water microcosms (see Figure 5.2). This contradicts the idea that *S-metolachlor* degraders in the inflow stream water may be already adapted to long periods of *S-metolachlor* applications in the field (Droz, 2020). However, a previous study of oxic groundwater microcosms amended with a herbicide mixture (up to  $5 \mu\text{g L}^{-1}$ ) consisting of alachlor, metolachlor and propanil showed that metolachlor persisted during the first 12 months, while significant (up to 46%) biodegradation occurred only after 18 months (Cavalier et al., 1991). Minimal *S-metolachlor* degradation was also observed during the early stage (first 20 y) of a groundwater plume (concentrations:  $1\text{--}820 \mu\text{g L}^{-1}$ ) in an anaerobic fractured dolostone aquifer near an agrochemical facility (Parker et al., 2019). Overall, the persistence of *S-metolachlor* in laboratory aquifers indicates that long-term groundwater contamination by *S-metolachlor* may occur, even under oxic conditions during stream-groundwater interactions.

Similarly, *metalaxyl*, *atrazine* and *terbutryn* proved persistent in both aquifers. *Metalaxyl* dissipation was low to insignificant during all injection periods (SI, Section C.10). Mass recoveries were  $93 \pm 4\%$  during both pulses injections (0–40 d and 90–140 d), while during the constant injection period (40–90 d) *metalaxyl* concentrations followed those of *atrazine* and *terbutryn* (SI, Section C.10). *Atrazine* and *terbutryn* also showed similar BTCs as the saline conservative tracer (SI, Section C.10) during the first (0–40 d) and second (90–140 d) pulse injections. This indicates that these compounds were not significantly degraded or sorbed over time. Similarly, during the constant injection period (40–90 d), no mass depletion of *atrazine* and *terbutryn* was observed. Indeed, *atrazine* is a highly persistent substance and its accumulation in shallow groundwater has been proven even after decades of its ban in 1992 in Europe (Vonberg et al., 2014). Moreover, the persistence of the urban biocide *terbutryn* in both laboratory aquifers also suggests its potential accumulation in shallow groundwater from entry pathways such as leaching of facades and urban stormwater infiltration systems (Hensen et al., 2018). Overall, the absence of significant biodegradation of *metalaxyl*, *atrazine* and *terbutryn* in both laboratory aquifers is in agreement with observations from the stream water microcosms, where biotrans-

formation only occurred after 100 d (see Figure 5.2). However, detection of TPs of metalaxyl (demethylmetalaxyl), atrazine (deisopropylatrazine) and terbutryn (2-hydroxy-terbutryn) suggested that the low dissipation of these micropollutants (<10%) was mainly associated with degradation potential in the aquifers from 90 to 140 days (SI, Section C.11).

### 5.3.3 C and N isotope fractionation of micropollutants

Overall, insignificant stable isotope fractionation ( $\Delta\delta^{13}\text{C} < 2\text{‰}$  and  $\Delta\delta^{15}\text{N} < 2\text{‰}$ ) for atrazine, terbutryn, metalaxyl and *S*-metolachlor confirmed their limited biodegradation in both aquifers (SI, Section C.10). However,  $\delta^{13}\text{C}$  of caffeine featured a U-shaped trend during each injection period (Figure 5.3, middle panel), in particular during the second pulse injection (90–140 d). At low concentrations ( $< 20\text{ }\mu\text{g L}^{-1}$ ), i.e., at the front and tailing of the BTCs, significant enrichment in  $^{13}\text{C}$  of the non-degraded caffeine indicated the occurrence of caffeine biodegradation. In contrast, at peak concentrations,  $\delta^{13}\text{C}$  values were similar to the initial caffeine signature ( $\delta^{13}\text{C}_0 = -31.4 \pm 0.6\text{‰}$ ), although significant mass removal was evidenced (Figure 5.3, upper panel).

A concentration dependence following Michaelis-Menten kinetics has been associated with the U-shaped of  $\delta^{13}\text{C}$  values (Eckert et al., 2013; Schürner et al., 2016). This suggests that first-order kinetics may rather occur at low concentrations, given by the  $r_{max}$  and  $K_m$  parameters, followed by a transition to zero-order kinetics at peak concentrations. The role of Michaelis-Menten type kinetics has thus been suggested to exponentially increase isotopic shift at low concentrations, e.g., at a contaminant plume fringe or during a contaminant BTC (i.e., at front and tail) (Breukelen and Prommer, 2008). This agrees with the carbon isotopic shift observed for caffeine BTC (Figure C.10, middle panel). On the other hand, a similar stable isotope pattern was observed in a toluene pulse injection in a flow-through aquifer setup filled with natural sediment and groundwater (Eckert et al., 2013; Qiu et al., 2013). In the case of toluene in organic-rich sediments, the combination of both biodegradation and sorption resulted in U-shaped  $\delta^{13}\text{C}$  trends slightly skewed toward the tail of the BTC (Qiu et al., 2013). This is due to pollutant sorption to organic matter is assumed slightly stronger for the light than the heavy isotopologues, leading to faster breakthrough of the heavy isotopologues (i.e.,  $^{12}\text{K}_d > ^{13}\text{K}_d$  and  $^{14}\text{K}_d > ^{15}\text{K}_d$ ) (Kopinke et al., 2005; Schürner et al., 2016). This would result in an enrichment in  $^{13}\text{C}$  at the contaminant front, while the BTC of  $^{12}\text{C}$  isotopologues is expected to cause a counteracting effect of the  $^{13}\text{C}$  enriched signatures at the tail of the contaminant BTCs (Eckert et al., 2013; Schürner et al., 2016).

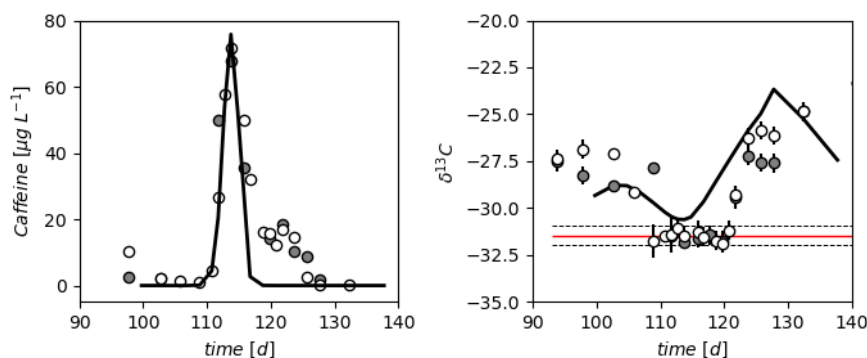


**Figure 5.4:** Simulated caffeine BTC (left) and carbon isotope fractionation (right;  $\delta^{13}\text{C}$ ) during the second pulse injection (90–140 d). Black lines represent simulated reactive transport of caffeine; symbols represent experimental observations of caffeine BTCs in two laboratory aquifers (in duplicates). Continuous horizontal line represent caffeine EA values of carbon ( $-31.46 \pm 0.02$  ‰) isotopes. Dashed horizontal lines represent the total uncertainty of carbon  $\pm 0.5$ ‰.

The parsimonious RT model allowed simulating the U-shaped trend of  $\delta^{13}\text{C}$  values from caffeine biotransformation data obtained in both aquifers after 90 d (i.e., second pulse injection). Simulations fitted with the caffeine BTC and  $\delta^{13}\text{C}$  values (Figure 5.4). The model confirmed that the U-shape  $\delta^{13}\text{C}$  trend was associated with a concentration dependence of caffeine biodegradation, coinciding with the increase in carbon isotope fractionation observed at the front and tail of the BTC. An  $\varepsilon_b$  value of  $-0.38 \pm 0.02$  ‰ was estimated from the RT model. Since  $\delta^{13}\text{C}$  values were similar to the initial  $\delta^{13}\text{C}$  at the caffeine peak (Figure 5.4), a lower mean caffeine  $\varepsilon_b$  is expected compared to that estimated from biotic stream water microcosms ( $\varepsilon_b = -1.1 \pm 0.3$  ‰, see SI, Section C.8). Furthermore, the Michaelis-Menten kinetics implemented in the model fitted the  $\delta^{13}\text{C}$  values (Figure 5.4). The effect of sorption on the U-shaped  $\delta^{13}\text{C}$  trend was negligible ( $\varepsilon_{sorp} = -0.05 \pm 0.002$  ‰), confirming the absence of significant caffeine sorption in the aquifers (Figures 5.3 and 5.4). Overall, the centered-like U-shaped  $\delta^{13}\text{C}$  trend observed during caffeine biodegradation in both laboratory aquifers suggested that Michaelis-Menten kinetics are better at representing realistic pollutant degradation behavior. Moreover, the possibly U-shaped  $\delta^{13}\text{C}$  trend during micropollutant biodegradation highlights the need for appropriate monitoring campaigns to capture isotopic shifts along BTCs in field scenarios, particularly for capturing possible stable isotope shifts during early micropollutants loading periods. This would further require an understanding of stream-groundwater flow interactions to properly predict micropollutants loadings (Hintze et al., 2020; Peralta-Maraver et al., 2018).

### 5.3.4 Gradual bacterial adaptations during transient exposures of a micropollutant mixture

A gradual increase in bacterial diversity was observed in both aquifers over time and according to the transient exposure periods (see Figure 5.1). NMDS ordination of the relative OTUs abundance showed that bacterial diversity mainly varied with exposure periods (SI, Section C.12). A first shift in bacterial diversity was observed from 0 to 38 days following the acclimation period and the first pulse injection of micropollutants (i.e., acute exposure at  $6 \text{ mg L}^{-1}$ ). This may be due to the pre-exposure of bacteria to micropollutants, possibly leading to a series of enzyme induction processes, and triggering pollutant biotransformation in the aquifers (Poursat et al., 2019b).

A second shift in bacterial diversity was observed from 90 to 140 d, following the constant and second pulse injection periods. This indicates that a distinct bacterial community diversity was developed after the chronic exposure at  $600 \text{ } \mu\text{g L}^{-1}$ , which may coincide with a high toxicity selective pressure of the micropollutant mixture for 21 consecutive days (SI, Section C.12). Hence, bacterial adaptation in aquifers may be driven by long-term exposure to the micropollutants, possibly generating changes at the community level or individual cells (e.g., by increasing competitive strains) to survive under adverse conditions (Kovářová-Kovar and Egli, 1998; Murínová and Dercová, 2014). A slight shift of the bacterial diversity was observed on day 220, while no micropollutant exposure occurred from 140 to 220 d. This suggests the establishment of a well-adapted bacterial community (SI, Section C.12). This idea is also supported by the gradual increase in species richness from 0 to 220 d, as emphasized by the increase in  $\alpha$ -diversity (SI, Section C.12).

Accordingly, the bacterial community composition also changed over time. Proteobacteria dominated in pore water samples during all exposure periods (Figure 5.5). However, the change in bacterial community composition (phylum level) after the first pulse injection (0–40 d) likely corresponds to a first community response associated with initial micropollutant exposure in both aquifers. The abundance of Actinobacteria, Bacteroidetes and Elusimicrobia phyla increased to up to 25%, 8% and 45%, respectively, after the chronic exposure period and the second pulse injection (90 to 140 d) (Figure 5.5). At the end of the experiments (at 220 d), Actinobacteria phylum remained as the second most abundant in pore water samples (up to 22%). This is in agreement with a previous study showing an increase in Actinobacteria phyla and associated genera in sediments of the hyporheic zone mimicked in river-simulating flumes (Posselt et al., 2020). Although the bacterial diversity did not vary spatially from the aquifer

inflow (SI, Section C.12), the bacterial community composition near the inflows ( $x=45$  cm; Figure 5.5) differed from that at the outflows ( $x = 160$  cm). This is likely due to the vicinity of the source zone of micropollutants (i.e., inflow) and thus higher exposure to micropollutants at the aquifer's inflow (Figure 5.5).

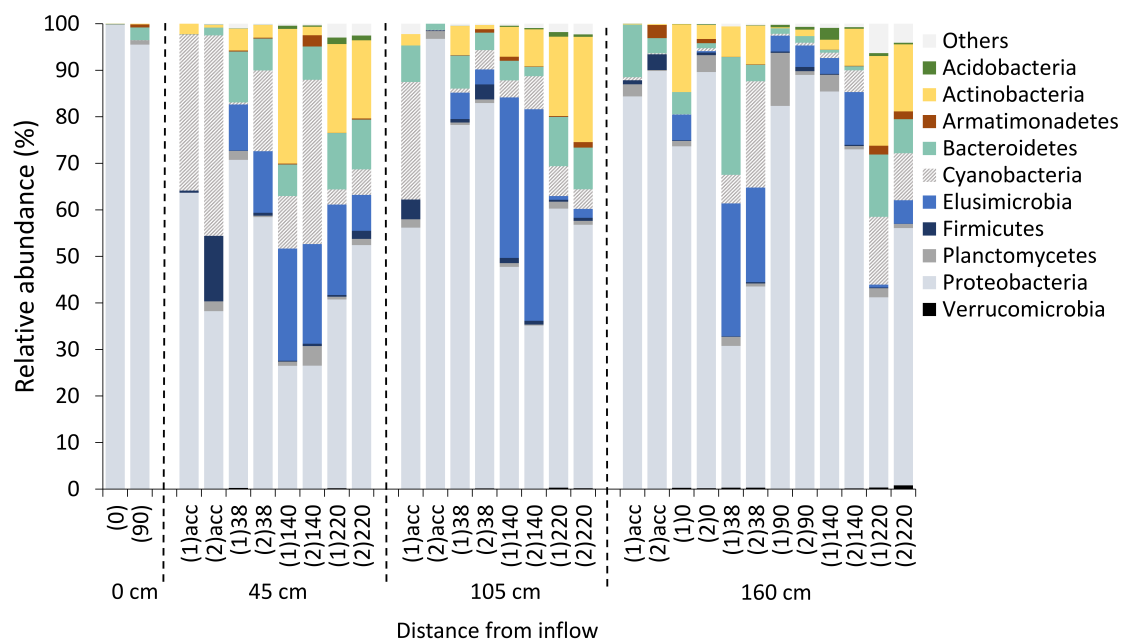


**Figure 5.5:** Relative abundance of bacterial phyla during transient exposure to the micropollutant mixture in laboratory aquifers. Labels in brackets represent samples collected from the duplicate laboratory aquifers. Samples were collected prior to the experiments (acc; acclimation period); after acclimation period (0 d), at the end of the first pulse injection (38 d), constant injection (90 d), and second injection periods (140 d). Samples were collected from inner samples of the aquifer at a distance of 45 cm and 105 cm from the inflow, as well as outlet samples ( $x=160$  cm). Samples at 220 d represent the end of the experiment.

The phylum Actinobacteria has been already associated with pesticide biodegradation and used for pollutant cleanup (Murínová and Dercová, 2014). For instance, *Arthrobacter* sp. and *Rhodococcus* sp. have been described for atrazine biodegradation in agricultural soils (Sagarkar et al., 2014), while their atrazine biodegradation capacity has also been evidenced in inoculated chemostats (Ehrl et al., 2019; Kundu et al., 2019). Although enhanced atrazine biodegradation was not observed in both aquifers, the increase in Actinobacteria (phylum level) suggests a gradual increase of competent bacteria degraders in the aquifers. This gradual increase in competent bacteria coincides with the lag-phase (up to 100 d) observed for most of the micropollutants in the stream water microcosm experiments (Figure 5.2). Our results thus suggests that bacterial tolerance and adaptation to long-term micropollutant exposure may have been established over

time (Figure 5.5), and coincides with the prevalence of a similar community composition in sand samples after 220 d (SI, Section C.13).

Although caffeine degradation has been associated with *Pseudomonas* strains (Summers et al., 2015), *Pseudomonas* taxa (genus level) accounted for <3% of the total sequences (SI, Section C.14). It is worth noting that 45% to 70% of the OTUs were not affiliated with some yet classified genera during the whole experiment (0–220 d). This indicates a wide array of yet unexplored taxa potentially involved in micropollutant degradation, notably for caffeine and metformin, and opens future research fields on the identification of micropollutants degrading taxa.

## 5.4 Conclusions

The integrative approach presented in this study, based on high resolution sampling from laboratory aquifers mimicking stream interactions with adjacent groundwater, may enable a robust assessment of *in situ* transformation of micropollutants in groundwater under varying micropollutants exposure periods (e.g., due to seasonal hydrological events). This study highlighted that biotransformation of micropollutants as chemical mixtures largely varies, independently on the acute or chronic level of exposure to micropollutants. For instance, caffeine biotransformation, evaluated with carbon and nitrogen CSIA and the TPs formation, was observed during all micropollutants injection periods. The carbon isotopic signatures of caffeine may be concentration-dependent, following Michaelis-Menten. In contrast, only moderate or negligible biotransformation of metformin, atrazine, terbutryn, S-metolachlor and metalaxyl occurred in the laboratory aquifers, emphasizing their potential persistence. CSIA of micropollutants can reinforce the evaluation of degradation or persistence of micropollutants and identify 'hot and cold periods' of *in situ* biotransformation for assessing natural attenuation of micropollutants during stream-groundwater interactions. However, the extension of ME-CSIA of micropollutants at low concentrations ( $\text{sub-}\mu\text{g L}^{-1}$ ) requires the pre-concentration of a sufficient mass of analyte while limiting the matrix effect. The integration of biomolecular markers, such as 16S rRNA, allowed to examine long-term acclimatation and adaptation of bacterial communities, and may be used as indicator of micropollutant biotransformation in groundwater. Taken together, these results highlight the relevance of integrative approaches based on DNA- and isotopic analysis data to improve the assessment of emerging pollutant in shallow groundwater connected to surface waters.

## **Acknowledgments**

I am grateful to Benoît Guyot, Eric Pernin and Colin Fournet for technical assistance in the laboratory, Dr. François Lehmann for help in mounting the laboratory aquifers and preliminary surveys, Dr. Boris Droz and Dr. Guillaume Droin for providing access to data recording of tracer experiments, and Dr. Jérémy Masbou for fruitful discussions.

## References of Chapter 5

- Alvarez-Zaldívar, P., Payraudeau, S., Meite, F., Masbou, J., and Imfeld, G. (2018). Pesticide degradation and export losses at the catchment scale: Insights from compound-specific isotope analysis (CSIA). *Water Research*, 139:198–207.
- aus der Beek, T., Weber, F.-A., Bergmann, A., Hickmann, S., Ebert, I., Hein, A., and Küster, A. (2016). Pharmaceuticals in the environment - global occurrences and perspectives. *Environmental Toxicology and Chemistry*, 35(4):823–835.
- Baran, N., Surdyk, N., and Auterives, C. (2021). Pesticides in groundwater at a national scale (France): Impact of regulations, molecular properties, uses, hydrogeology and climatic conditions. *Science of The Total Environment*, 791:148137.
- Barbosa, M. O., Moreira, N. F. F., Ribeiro, A. R., Pereira, M. F. R., and Silva, A. M. T. (2016). Occurrence and removal of organic micropollutants: An overview of the watch list of EU decision 2015/495. *Water Research*, 94:257–279.
- Bauer, R. D., Maloszewski, P., Zhang, Y., Meckenstock, R. U., and Griebler, C. (2008). Mixing-controlled biodegradation in a toluene plume – Results from two-dimensional laboratory experiments. *Journal of Contaminant Hydrology*, 96(1):150–168.
- Boulton, A. J., Datry, T., Kasahara, T., Mutz, M., and Stanford, J. A. (2010). Ecology and management of the hyporheic zone: stream-groundwater interactions of running waters and their floodplains. *Journal of the North American Benthological Society*, 29(1):26–40.
- Bradley, P. M. (2021). Multi-region assessment of chemical mixture exposures and predicted cumulative effects in USA Wadeable urban/agriculture-gradient streams. *Science of the Total Environment*, 773:145062.
- Bradley, P. M., Journey, C. A., Button, D. T., Carlisle, D. M., Clark, J. M., Mahler, B. J., Nakagaki, N., Qi, S. L., Waite, I. R., and VanMetre, P. C. (2016). Metformin and other pharmaceuticals widespread in Wadeable streams of the southeastern United States. *Environmental Science & Technology Letters*, 3(6):243–249.
- Breukelen, B. M. V. and Prommer, H. (2008). Beyond the Rayleigh equation: Reactive transport modeling of isotope fractionation effects to improve quantification of biodegradation. *Environmental Science & Technology*, 42(7):2457–2463.
- Buerge, I. J., Poiger, T., Müller, M. D., and Buser, H.-R. (2003). Enantioselective degradation of metalaxyl in soils: Chiral preference changes with soil pH. *Environmental Science & Technology*, 37(12):2668–2674.
- Cavalier, T. C., Lavy, T. L., and Mattice, J. D. (1991). Persistence of selected pesticides in ground-water samples. *Groundwater*, 29(2):225–231.
- Chen, X. and Chen, X. (2003). Stream water infiltration, bank storage, and storage zone changes due to stream-stage fluctuations. *Journal of Hydrology*, 280(1-4):246–264.



- Chow, R., Scheidegger, R., Doppler, T., Dietzel, A., Fenicia, F., and Stamm, C. (2020). A review of long-term pesticide monitoring studies to assess surface water quality trends. *Water Research X*, 9:100064.
- Conant, B., Robinson, C. E., Hinton, M. J., and Russell, H. A. J. (2019). A framework for conceptualizing groundwater-surface water interactions and identifying potential impacts on water quality, water quantity, and ecosystems. *Journal of Hydrology*, 574:609–627.
- Coplen, T. B., Brand, W. A., Gehre, M., Gröning, M., Meijer, H. A. J., Toman, B., and Verkouteren, R. M. (2006). New guidelines for  $\delta^{13}\text{C}$  measurements. *Analytical Chemistry*, 78(7):2439–2441.
- core Team, R. (2019). R: A language and environment for statistical computing, version 3.5.3. Place: Vienna, Austria.
- Dalmijn, J. A., Poursat, B. A. J., van Spanning, R. J. M., Brandt, B. W., de Voogt, P., and Parsons, J. R. (2021). Influence of short- and long-term exposure on the biodegradation capacity of activated sludge microbial communities in ready biodegradability tests. *Environmental Science: Water Research & Technology*, 7(1):107–121.
- Damalas, C. A. and Koutroubas, S. D. (2016). Farmers' exposure to pesticides: Toxicity types and ways of prevention. *Toxics*, 4(1):1.
- Dash, S. S. and Gummadi, S. N. (2007). Degradation kinetics of caffeine and related methylxanthines by induced cells of *Pseudomonas* sp. *Current Microbiology*, 55(1):56–60.
- Derx, J., Blaschke, A., Farnleitner, A., Pang, L., Blöschl, G., and Schijven, J. (2013). Effects of fluctuations in river water level on virus removal by bank filtration and aquifer passage – A scenario analysis. *Journal of Contaminant Hydrology*, 147:34–44.
- Drouin, G., Fahs, M., Droz, B., Younes, A., Imfeld, G., and Payraudeau, S. (2021). Pollutant dissipation at the sediment-water interface: A robust discrete continuum numerical model and recirculating laboratory experiments. *Water Resources Research*, 57(3).
- Droz, B. (2020). *Pesticides dissipation at the sediment-water interface: insight from compound-specific isotope analysis (CSIA)*. Doctoral thesis, University of Strasbourg.
- Droz, B., Drouin, G., Maurer, L., Villette, C., Payraudeau, S., and Imfeld, G. (2021). Phase transfer and biodegradation of pesticides in water-sediment systems explored by compound-specific isotope analysis and conceptual modeling. *Environmental Science & Technology*, 55(8):4720–4728.
- Eckert, D., Qiu, S., Elsner, M., and Cirpka, O. A. (2013). Model complexity needed for quantitative analysis of high resolution isotope and concentration data from a toluene-pulse experiment. *Environmental Science & Technology*, 47(13):6900–6907.
- Ehrl, B. N., Kundu, K., Gharasoo, M., Marozava, S., and Elsner, M. (2019). Rate-limiting mass transfer in micropollutant degradation revealed by isotope fractionation in chemostat. *Environ Sci Technol*, 53(3):1197–1205.
- Elsayed, O., Maillard, E., Vuilleumier, S., Nijenhuis, I., Richnow, H., and Imfeld, G. (2014). Using compound-specific isotope analysis to assess the degradation of chloroacetanilide herbicides in lab-scale wetlands. *Chemosphere*, 99:89–95.
- Elsner, M. (2010). Stable isotope fractionation to investigate natural transformation mechanisms of organic contaminants: Principles, prospects and limitations. *Journal Environmental Monitoring*, 12(11):2005–2031.
- Elsner, M. and Imfeld, G. (2016). Compound-specific isotope analysis (CSIA) of micropollutants in the environment – Current developments and future challenges. *Current Opinion in Biotechnology*, 41:60–72.

- Elsner, M., McKelvie, J., Lacrampe Couloume, G., and Sherwood Lollar, B. (2007). Insight into methyl *tert* -butyl ether (MTBE) stable isotope fractionation from abiotic reference experiments. *Environmental Science & Technology*, 41(16):5693–5700.
- Fenner, K., Canonica, S., Wackett, L. P., and Elsner, M. (2013). Evaluating pesticide degradation in the environment: Blind spots and emerging opportunities. *Science*, 341(6147):752–758.
- Ghysels, G., Anibas, C., Awol, H., Tolche, A., Schneidewind, U., and Huysmans, M. (2021). The significance of vertical and lateral groundwater-surface water exchange fluxes in riverbeds and riverbanks: Comparing 1D analytical flux estimates with 3D groundwater modelling. *Water*, 13(3):306.
- Hancock, P. J. (2002). Human impacts on the stream-groundwater exchange zone. *Environmental Management*, 29(6):763–781.
- Hellal, J., Joulain, C., Urien, C., Ferreira, S., Denonfoux, J., Hermon, L., Vuilleumier, S., and Imfeld, G. (2020). Chlorinated ethene biodegradation and associated bacterial taxa in multi-polluted groundwater: Insights from biomolecular markers and stable isotope analysis. *Science of The Total Environment*, page 142950.
- Hensen, B., Lange, J., Jackisch, N., Zieger, F., Olsson, O., and Kümmerer, K. (2018). Entry of biocides and their transformation products into groundwater via urban stormwater infiltration systems. *Water Research*, 144:413–423.
- Hildebrandt, A., Guillaumon, M., Lacorte, S., Tauler, R., and Barceló, D. (2008). Impact of pesticides used in agriculture and vineyards to surface and groundwater quality (North Spain). *Water Research*, 42(13):3315–3326.
- Hintze, S., Glauser, G., and Hunkeler, D. (2020). Influence of surface water - groundwater interactions on the spatial distribution of pesticide metabolites in groundwater. *Science of The Total Environment*, 733:139109.
- Iker, B. C., Kambesis, P., Oehrle, S. A., Groves, C., and Barton, H. A. (2010). Microbial atrazine breakdown in a karst groundwater system and its effect on ecosystem energetics. *Journal of Environmental Quality*, 39(2):509–518.
- Jakobsen, R., Hinsby, K., Aamand, J., van der Keur, P., Kidmose, J., Purtschert, R., Jurgens, B., Sültenfuss, J., and Albers, C. N. (2019). History and sources of co-occurring pesticides in an abstraction well unraveled by age distributions of depth-specific groundwater samples. *Environmental Science & Technology*.
- Kopinke, F.-D., Georgi, A., Voskamp, M., and Richnow, H. H. (2005). Carbon isotope fractionation of organic contaminants due to retardation on humic substances: Implications for natural attenuation studies in aquifers. *Environmental Science & Technology*, 39(16):6052–6062.
- Koroša, A., Brenčič, M., and Mali, N. (2020). Estimating the transport parameters of propyphenazone, caffeine and carbamazepine by means of a tracer experiment in a coarse-gravel unsaturated zone. *Water Research*, 175:115680.
- Kovárová-Kovar, K. and Egli, T. (1998). Growth kinetics of suspended microbial cells: From single-substrate-controlled growth to mixed-substrate kinetics. *Microbiology and Molecular Biology Reviews*, 62(3):646–666.
- Kundu, K., Marozava, S., Ehrl, B., Merl-Pham, J., Griebler, C., and Elsner, M. (2019). Defining lower limits of biodegradation: atrazine degradation regulated by mass transfer and maintenance demand in *Arthrobacter aurescens* TC1. *The ISME Journal*, 13(9):2236–2251.
- Lam, M. W., Young, C. J., Brain, R. A., Johnson, D. J., Hanson, M. A., Wilson, C. J., Richards, S. M., Solomon, K. R., and Mabury, S. A. (2004). Aquatic persistence of eight pharmaceuticals in a microcosm study. *Environmental Toxicology and Chemistry*, 23(6):1431–1440.

- Lefrancq, M., Payraudeau, S., Guyot, B., Millet, M., and Imfeld, G. (2017). Degradation and transport of the chiral herbicide *S*-metolachlor at the catchment scale: Combining observation scales and analytical approaches. *Environmental Science & Technology*, 51(22):13231–13240.
- Lesser, L. E., Mora, A., Moreau, C., Mahlke, J., Hernández-Antonio, A., Ramírez, A. I., and Barrios-Piña, H. (2018). Survey of 218 organic contaminants in groundwater derived from the world's largest untreated wastewater irrigation system: Mezquital Valley, Mexico. *Chemosphere*, 198:510–521.
- Lewandowski, J., Putschew, A., Schwesig, D., Neumann, C., and Radke, M. (2011). Fate of organic micropollutants in the hyporheic zone of a eutrophic lowland stream: Results of a preliminary field study. *Science of The Total Environment*, 409(10):1824–1835.
- Loos, R., Locoro, G., Comero, S., Contini, S., Schwesig, D., Werres, F., Balsaa, P., Gans, O., Weiss, S., Blaha, L., Bolchi, M., and Gawlik, B. M. (2010). Pan-european survey on the occurrence of selected polar organic persistent pollutants in ground water. *Water Research*, 44(14):4115–4126.
- Lutz, S. R., Velde, Y. v. d., Elsayed, O. F., Imfeld, G., Lefrancq, M., Payraudeau, S., and van Breukelen, B. M. (2017). Pesticide fate on catchment scale: conceptual modelling of stream CSIA data. *Hydrology and Earth System Sciences*, 21(10):5243–5261.
- Masoner, J. R., Kolpin, D. W., Cozzarelli, I. M., Barber, L. B., Burden, D. S., Foreman, W. T., Forshay, K. J., Furlong, E. T., Groves, J. F., Hladik, M. L., Hopton, M. E., Jaeschke, J. B., Keefe, S. H., Krabbenhoft, D. P., Lowrance, R., Romanok, K. M., Rus, D. L., Selbig, W. R., Williams, B. H., and Bradley, P. M. (2019). Urban stormwater: An overlooked pathway of extensive mixed contaminants to surface and groundwaters in the United States. *Environmental Science & Technology*, 53(17):10070–10081.
- Meichelke, J., Rust, D., Jaeger, A., and Hollender, J. (2020). Enantiomeric fractionation during biotransformation of chiral pharmaceuticals in recirculating water-sediment test flumes. *Environmental Science & Technology*, 54(12):7291–7301.
- Meckenstock, R. U., Elsner, M., Griebler, C., Lueders, T., Stumpp, C., Aamand, J., Agathos, S. N., Albrechtsen, H.-J., Bastiaens, L., Bjerg, P. L., Boon, N., Dejonghe, W., Huang, W. E., Schmidt, S. I., Smolders, E., Sorensen, S. R., Springael, D., and van Breukelen, B. M. (2015). Biodegradation: Updating the concepts of control for microbial cleanup in contaminated aquifers. *Environmental Science & Technology*, 49(12):7073–7081.
- Murínová, S. and Dercová, K. (2014). Response mechanisms of bacterial degraders to environmental contaminants on the level of cell walls and cytoplasmic membrane. *International Journal of Microbiology*, 2014:1–16.
- Nödler, K., Tsakiri, M., and Licha, T. (2014). The impact of different proportions of a treated effluent on the biotransformation of selected micro-contaminants in river water microcosms. *International journal of environmental research and public health*, 11(10):10390–10405.
- NRC (2000). *Natural Attenuation for Groundwater Remediation*. National Research Council. National Academies Press.
- Parker, B. L., Bairos, K., Maldaner, C. H., Chapman, S. W., Turner, C. M., Burns, L. S., Plett, J., Carter, R., and Cherry, J. A. (2019). Metolachlor dense non-aqueous phase liquid source conditions and plume attenuation in a dolostone water supply aquifer. *Geological Society, London, Special Publications*, 479(1):207–236.
- Peralta-Maraver, I., Reiss, J., and Robertson, A. L. (2018). Interplay of hydrology, community ecology and pollutant attenuation in the hyporheic zone. *Science of The Total Environment*, 610-611:267–275.

- Peter, K. T., Herzog, S., Tian, Z., Wu, C., McCray, J. E., Lynch, K., and Kolodziej, E. P. (2019). Evaluating emerging organic contaminant removal in an engineered hyporheic zone using high resolution mass spectrometry. *Water Research*, 150:140–152.
- Posselt, M., Mechelke, J., Rutere, C., Coll, C., Jaeger, A., Raza, M., Meinikmann, K., Krause, S., Sobek, A., Lewandowski, J., Horn, M. A., Hollender, J., and Benskin, J. P. (2020). Bacterial diversity controls transformation of wastewater-derived organic contaminants in river-simulating flumes. *Environmental Science & Technology*, 54(9):5467–5479.
- Poursat, B. A. J., van Spanning, R. J. M., Braster, M., Helmus, R., de Voogt, P., and Parsons, J. R. (2019a). Biodegradation of metformin and its transformation product, guanyurea, by natural and exposed microbial communities. *Ecotoxicology and Environmental Safety*, 182:109414.
- Poursat, B. A. J., van Spanning, R. J. M., de Voogt, P., and Parsons, J. R. (2019b). Implications of microbial adaptation for the assessment of environmental persistence of chemicals. *Critical Reviews in Environmental Science & Technology*, 49(23):2220–2255.
- Prieto-Espinoza, M., Weill, S., Belfort, B., Muller, E. E., Masbou, J., Lehmann, F., Vuilleumier, S., and Imfeld, G. (2021). Water table fluctuations affect dichloromethane biodegradation in lab-scale aquifers contaminated with organohalides. *Water Research*, 203:117530.
- Qiu, S., Eckert, D., Cirpka, O. A., Huenniger, M., Knappett, P., Maloszewski, P., Meckenstock, R. U., Griebler, C., and Elsner, M. (2013). Direct experimental evidence of non-first order degradation kinetics and sorption-induced isotopic fractionation in a mesoscale aquifer:  $^{13}\text{C}/^{12}\text{C}$  analysis of a transient toluene pulse. *Environmental Science & Technology*, 47(13):6892–6899.
- Richardson, S. D. and Kimura, S. Y. (2016). Water analysis: Emerging contaminants and current issues. *Analytical Chemistry*, 88(1):546–582.
- Sagarkar, S., Nousiainen, A., Shaligram, S., Björklöf, K., Lindström, K., Jorgensen, K. S., and Kapley, A. (2014). Soil mesocosm studies on atrazine bioremediation. *Journal of Environmental Management*, 139:208–216.
- Schaper, J. L., Posselt, M., Bouchez, C., Jaeger, A., Nuetzmann, G., Putschew, A., Singer, G., and Lewandowski, J. (2019). Fate of trace organic compounds in the hyporheic zone: Influence of retardation, the benthic biolayer, and organic carbon. *Environmental Science & Technology*, 53(8):4224–4234.
- Schürner, H. K. V., Maier, M. P., Eckert, D., Brejcha, R., Neumann, C.-C., Stumpp, C., Cirpka, O. A., and Elsner, M. (2016). Compound-specific stable isotope fractionation of pesticides and pharmaceuticals in a mesoscale aquifer model. *Environmental Science & Technology*, 50(11):5729–5739.
- Schwab, A. P., Splichal, P. A., and Banks, M. K. (2006). Persistence of atrazine and alachlor in ground water aquifers and soil. *Water, Air, Soil & Pollution*, 171(1):203–235.
- Schwarzenbach, R. P., Egli, T., Hofstetter, T. B., von Gunten, U., and Wehrli, B. (2010). Global water pollution and human health. *Annual Review of Environment and Resources*, 35(1):109–136.
- Seiler, R. L., Zugg, S. D., Thomas, J. M., and Howcroft, D. L. (1999). Caffeine and pharmaceuticals as indicators of waste water contamination in wells. *Groundwater*, 37(3):405–410.
- Straub, J. O., Caldwell, D. J., Davidson, T., D'Aco, V., Kappler, K., Robinson, P. F., Simon-Hettich, B., and Tell, J. (2019). Environmental risk assessment of metformin and its transformation product guanyurea. I. Environmental fate. *Chemosphere*, 216:844–854.

- Summers, R. M., Mohanty, S. K., Gopishetty, S., and Subramanian, M. (2015). Genetic characterization of caffeine degradation by bacteria and its potential applications. *Microbial Biotechnology*, 8(3):369–378.
- Sun, F., Melage, A., Gharasoo, M., Melsbach, A., Cao, X., Zimmermann, R., Griebler, C., Thullner, M., Cirpka, O. A., and Elsner, M. (2021a). Mass-transfer-limited biodegradation at low concentrations - evidence from reactive transport modeling of isotope profiles in a bench-scale aquifer. *Environmental Science & Technology*, 55(11):7386–7397.
- Sun, F., Peters, J., Thullner, M., Cirpka, O. A., and Elsner, M. (2021b). Magnitude of diffusion- and transverse dispersion-induced isotope fractionation of organic compounds in aqueous systems. *Environmental Science & Technology*, 55(8):4772–4782.
- Talja, K. M., Kaukonen, S., Kilpi-Koski, J., Malin, I., Kairesalo, T., Romantschuk, M., Tuominen, J., and Kontro, M. H. (2008). Atrazine and terbutryn degradation in deposits from groundwater environment within the boreal region in Lahti, Finland. *Journal of Agricultural and Food Chemistry*, 56(24):11962–11968.
- Torabi, E., Wiegert, C., Guyot, B., Vuilleumier, S., and Imfeld, G. (2020). Dissipation of S-metolachlor and butachlor in agricultural soils and responses of bacterial communities: Insights from compound-specific isotope and biomolecular analyses. *Journal of Environmental Sciences*, 92:163–175.
- Vega, F. E., Emche, S., Shao, J., Simpkins, A., Summers, R. M., Mock, M. B., Ebert, D., Infante, F., Aoki, S., and Maul, J. E. (2021). Cultivation and genome sequencing of bacteria isolated from the coffee berry borer (*Hypothenemus hampei*), with emphasis on the role of caffeine degradation. *Frontiers in Microbiology*, 12:644768.
- Vonberg, D., Vanderborght, J., Cremer, N., Pütz, T., Herbst, M., and Vereecken, H. (2014). 20 years of long-term atrazine monitoring in a shallow aquifer in western Germany. *Water Research*, 50:294–306.
- Winter, T., Harvey, J. W., Franke, O., and Alley, W. (1998). Ground water and surface water a single resource. Circular, U.S. Geological Survey. Series: Circular.
- Yu, C. L., Louie, T. M., Summers, R., Kale, Y., Gopishetty, S., and Subramanian, M. (2009). Two distinct pathways for metabolism of theophylline and caffeine are coexpressed in *Pseudomonas putida* CBB5. *Journal of bacteriology*, 191(14):4624–4632.
- Zhang, Y., Wang, J., Yang, P., and Xie, S. (2017). Movement of lateral hyporheic flow between stream and groundwater. *Science China Earth Sciences*, 60(11):2033–2040.

# Chapter 6

## General conclusions and perspectives

The overall goal of this PhD thesis was to improve the understanding of dynamic environmental conditions on the natural attenuation of organic pollutants in contaminated aquifers. Particularly, this thesis focused on the reactive transport of dichloromethane (DCM), representing point-source contamination of legacy chlorinated industrial contaminants (Chapters 3 and 4), and a micropollutant mixture representing diffuse contamination from seasonal pesticide applications and/or inefficient waste release from WWTF (Chapter 5). The main motivation of this thesis is that monitored natural attenuation of organic contaminants in groundwater is today recognized as a cost-effective and sustainable strategy for the detoxification of contaminated aquifers (NRC, 2000). Indeed, biodegradation is widely recognized as a key dissipation process determining the fate of pollutants in groundwater. However, hydrogeological systems are often subjected to dynamic environmental conditions, such as water table fluctuations and/or stream-groundwater interactions, possibly affecting *in situ* biodegradation. The underlying hypothesis of this thesis is that the interplay of dynamic hydrochemical and biological conditions may exert a powerful control on pollutant degradation extent and pathways.

Globally, this thesis addressed the following research questions: (i) How are hydrogeochemical conditions evolving in aquifers subjected to dynamic condition (e.g., water table fluctuations)? (ii) What is the role of transition zones, such as the capillary fringe and hyporheic zone, to limit or enhance pollutants biodegradation? (iii) What is the link between the diversity and composition of bacterial communities and biodegradation under dynamic hydrogeochemical conditions? (iv) How do rates and dissipation pathways evolve along with hydrogeochemical and bacterial dynamics? (v) What is the most relevant (simple, reliable and mechanistic) reaction scheme to be designed to model the transport and dissipation of organic pollutants in aquifers? and (vi) Can the dissipation of these pollutants be reliably predicted to evaluate reactive transport and ultimately the potential for remediation of a polluted aquifer?

Overall, the general methodology used in this thesis, relying on an integrative approach combining analytical, microbiological and modeling methods, proved useful to bridge the gap on the effect of varying environmental conditions on pollutant biodegradation. This thesis generated several relevant outcomes. In Chapter 3, it was evidenced that water table fluctuations affected DCM biodegradation in laboratory aquifers. Here, dynamics of hydrochemical and bacterial community diversity and composition varied according to transient conditions compared to steady-state. Enhanced DCM degradation was observed under transient conditions, and stable isotope composition of DCM evidenced distinct DCM degradation pathways according to transient and steady-state conditions. Complementarily, numerical simulations showed a

distinct evolution of hydrochemical conditions and bacterial populations associated with DCM degradation, and consistently showed that water table fluctuations enhanced DCM degradation, in line with experimental observations (Chapter 4). Here, higher metabolic activity of a bacterial population assimilating DOC and producing CO<sub>2</sub> across the fluctuation zone was suggested. In turn, DOC turnover across the fluctuation zone likely enhanced metabolic activity of specific anaerobic DCM bacterial populations dependent on CO<sub>2</sub> availability (Chen et al., 2020). Similarly, the integrative approach presented in this thesis also showed its potential use for assessing the natural attenuation of micropollutants during stream-groundwater interactions (Chapter 5). Here, dynamic conditions were associated with varying micropollutants exposures representing variations of seasonal pesticides applications and hydrological events. Indeed, biodegradation capacity of the laboratory aquifers was shown based on concentration measurements of parent compounds and TPs, evidence of isotope fraction and changes in bacterial community diversity and composition according to variations in micropollutant exposures.

Altogether, this thesis highlights the relevance of using integrative approaches to define a comprehensive framework for the assessment of natural attenuation of organic contaminants in dynamic hydrogeological conditions. In the following, the potentials and limitations of assessing the natural attenuation of DCM and micropollutants in laboratory aquifers under dynamic conditions are further discussed (Section 6.1). The interest of using an integrative approach to improve natural attenuation of organic contaminants in groundwater is provided in Section 6.2, and the perspectives on the use of integrative RTMs are discussed in Section 6.3. Finally, future experimental and conceptual developments are proposed to evaluate natural attenuation of DCM and micropollutants in aquifers, including groundwater-surface water transition zones (Section 6.4).

## **6.1 Natural attenuation of DCM and micropollutants in laboratory aquifers under dynamic conditions**

Globally, the reactive transport of DCM and micropollutants was examined in two laboratory aquifers fed with groundwater or stream water, respectively. Here, the use of laboratory aquifers allowed for near-natural representations of field scenarios, where the effect of dynamic environmental conditions is easier to control compared to field conditions. In this context, the evolution of *in situ* hydrochemical and bacterial dynamics was examined through high spatial and temporal resolution, allowing a detailed *in situ* characterization of the laboratory aquifers. The use of natural groundwater or stream water feeding the laboratory aquifers, further allowed investigat-



ing the dynamics of *endogenous* conditions and processes. However, the design of the laboratory aquifers was rather restricted to investigations of reactive transport processes in the saturated zone. Hence, diffusive fluxes across the unsaturated zone were not possible to examine due to insufficient sampling ports across the aquifer's depth, which constitutes a major limitation of this approach.

This thesis followed an integrative approach including pollutant concentration measurements, hydrochemical and bacterial analysis, ME-CSIA, and reactive transport modeling. **Assessing natural attenuation of organic contaminants** requires multiple lines of evidence of *in situ* degradation processes. Ideally, this may include (i) a thorough hydrogeochemical characterization of the site, (ii) evidence of the degradation extent and pathways using stable isotopes, and (iii) a possible identification of bacterial populations associated with the degradation of the target pollutant over space and time (Hunkeler et al., 2009; NRC, 2000). Additionally, reactive transport modeling enables evaluation and prediction of the natural attenuation of contaminants in hydrogeological systems, by accounting for the physical and chemical processes involved and by integrating CSIA and/or biomolecular information (e.g., Badin et al. (2018); Kuder et al. (2016); Van Breukelen et al. (2005)). The integrative approach used in this thesis was thus adapted to the intrinsic characteristic of the investigated organic contaminants, accounting for dynamic environmental conditions.

### 6.1.1 Water table fluctuations affect DCM degradation

In the case of **dichloromethane**, laboratory aquifers were fed with anoxic DCM contaminated groundwater from a well-characterized former industrial site. Here, a focus was given on the effect of **water table fluctuations**, which may affect hydrochemical conditions, bacterial dynamics, and in turn, pollutants biodegradation extent and pathways. Particularly, dynamic conditions are of interest across the fluctuation zone and the capillary fringe, suggested as potential hotspots for natural attenuation of organic contaminants (Pronk et al., 2020). In **Chapter 3**, it was shown that environmental dynamics such as water table fluctuations, which are often excluded from laboratory degradation experiments and results interpretation, significantly affect *in situ* DCM biodegradation. Indeed, DCM biodegradation was more pronounced under transient conditions (i.e., induced by water table fluctuations; B=95%) compared to steady-state conditions (i.e., static water table; B=42%). Based on C and Cl isotopes, dual C-Cl isotope analysis suggested the prevalence of distinct anaerobic DCM degradation pathways associated with steady-state ( $\Lambda^{C/Cl} = 1.92 \pm 0.30$ ) and transient conditions ( $\Lambda^{C/Cl} = 3.58 \pm 0.42$ ). This was in

line with the prevailing iron-reducing conditions observed in both laboratory aquifers. Water table fluctuations also caused gradual changes in redox conditions and oxygen levels, particularly after drainage events; however, the system returned to (initial) equilibrium shortly after imbibition events. Most importantly, this study shows that high-resolution monitoring of the evolution of hydrochemical conditions over time and along the flow path provides detailed information on the established *in situ* conditions under both steady-state and transient conditions.

A specificity of this study is that bacterial diversity and distribution of DCM-associated taxa was examined in parallel of hydrochemical monitoring, and proved similar under both conditions. Interestingly, responses to water table fluctuations resulted in different bacterial community composition dominated by bacteria from the *Peptococcaceae* family, in particular *Desulfosporosinus* sp. The co-occurrence of bacteria from these taxa points to possible concomitant DCM degradation pathways at contaminated sites (Blázquez-Pallí et al., 2019; Hermon et al., 2018; Wright et al., 2017). This idea was further supported by a possible gene cassette implicated in anaerobic DCM degradation by known DCM degraders of the *Peptococcaceae* family (Murdoch et al., 2022). Future studies addressing concomitant anaerobic DCM degradation are needed to improve interpretations on the often enrichment of several bacterial taxa at DCM contaminated sites, often belonging to the *Peptococcaceae* family (Blázquez-Pallí et al., 2019; Hermon et al., 2018; Wright et al., 2017). Taken together, this study highlights that monitoring of hydrochemical species and the targeted contaminant, together with a high-resolution follow-up of stable isotope signatures of contaminant and associated bacterial diversity, ultimately provide a robust framework to evaluate natural attenuation of chlorinated solvents, such as DCM, in dynamic hydrogeological systems.

The use of ME-CSIA and biomolecular approaches presented in Chapter 3 underscored that fundamental research on dynamics of environmental conditions, such as water table fluctuations, are still needed to improve bioremediation strategies at contaminated sites. To this end, an original **multi-phase flow RTM** was proposed in **Chapter 4** to improve our understanding of the main drivers of anaerobic DCM biodegradation during water table fluctuations. A mathematical formalism was developed for **multi-component reactive transport processes** in saturated and unsaturated porous media, including the capillary fringe. The presented model was also developed on the basis of **concomitant DCM degradation** according to four distinct pathway-specific reaction rates. Due to lack of evidence of aerobic DCM degradation in the laboratory aquifers, model simulations were restricted to anaerobic DCM metabolisms, which simplified the procedure. The description of DCM degradation pathways by the chosen modeled bacterial

populations was based on available C and/or Cl CSIA. This allows a quantitative description of DCM biodegradation under the different tested conditions (e.g., steady-state vs. transient, degradation by individual bacteria or concomitantly). In addition, a bacterial population associated with dissolved organic carbon (DOC) assimilation was included, thus representing a broad bacterial community composition. All modeled simulations were based on experimental results presented in Chapter 3, so that simulated times and initial and boundary conditions mirrored experimental observations. Due to numerous processes and variables considered in this study, and thus the high computational demand, no automated calibration was attempted for the reactive transport simulations yet. Future and long-term developments with regard to model calibration and inverse modeling approaches may enable better characterization of the proposed reactive transport scheme and chosen parameters, particularly for bacterial kinetics. Nevertheless, the adopted strategy for the first evaluation of the model proved useful to identify, quantify and examine bacterial processes associated with DCM degradation under steady-state and transient conditions.

Numerical results presented in Chapter 4 suggested that the contribution of non-DCM degraders on the overall DCM biodegradation was essential, correlating with higher DOC turnover upon water table fluctuations (Chapter 4). Indeed, numerical results pointed to the increase in CO<sub>2</sub> production across the fluctuation zone due to oxygen and ferric iron utilization during DOC assimilation. This, in turn, resulted in an increase in anaerobic DCM metabolisms by those DCM degraders dependent on CO<sub>2</sub> (Chen et al., 2020). This was also supported by previous studies evidencing higher carbon turnover upon water table fluctuations, coinciding with higher metabolic activity (Jost et al., 2015; Pronk et al., 2020; Rezanezhad et al., 2014). Although the lack of CO<sub>2</sub> monitoring in the laboratory aquifers underscores some limitations of the experimental design, the presented numerical results may provide insights into the main drivers for the shift in DCM degradation pathways under transient conditions. A simple experimental setup such as up-flow column experiments under anoxic conditions may be used to examine and compare the role of CO<sub>2</sub> availability and fluxes during anaerobic DCM biodegradation under transient and steady-state conditions. Moreover, experimental descriptions of interspecies metabolic networks with regard to concomitant anaerobic DCM degradation are further needed to validate the proposed model and should remain as a short-term perspective.

Most importantly, numerical results highlighted the importance of the whole bacterial dynamics regarding natural attenuation of DCM in groundwater, rather than the enzymatic activity of a single bacterial population during water table fluctuations. Simulations of concomitant

anaerobic DCM degradation proved better at correlating with experimental observations, particularly for transient conditions. These results underscored the need for fundamental investigations of concomitant anaerobic DCM degradation. In this context, microcosms experiments inoculated with various DCM-degrading isolates or consortiums may provide an opportunity to examine concomitant anaerobic DCM degradation (Chen et al., 2017; Hermon et al., 2019; Trueba-Santiso et al., 2020), and sustain the enrichment of several anaerobic bacterial taxa at DCM contaminated sites. However, results from steady-state simulations were more difficult to correlate with experimental observations, particularly for C and Cl isotope signatures. The simulated extent of DCM degradation under steady-state conditions largely differed from the low  $\Lambda^{C/Cl}$  values obtained experimentally. This suggests that unidentified bacterial strains from the *Peptococcaceae* family may be implicated. In this context, future studies such as enrichment culture techniques of the groundwater and sand collected from the laboratory aquifers, could reveal hints on the possible specific taxa implicated in anaerobic DCM degradation under steady-state conditions.

Overall, this study paves the road for future studies to elucidate (i) the possibility of concomitant anaerobic DCM degradation at contaminated sites, and (ii) the role of CO<sub>2</sub> availability upon water table fluctuations to enhance (or inhibit) anaerobic DCM degradation. Finally, although the presented formalism was dedicated to DCM, a generic formulation can be obtained from this model providing its extension to other chlorinated compounds (i.e., Cl-VOCs). This may include (i) implementations of a description of sequential reductive dechlorination of the CEs family (e.g., Badin et al. (2018); Kuder et al. (2016); Van Breukelen et al. (2005)), (ii) implementation of bacterial populations implicated in CEs degradation described by C- and Cl-CSIA data, and (iii) the multi-phase flow framework proposed in the CubicM model scheme (see Chapter 4). Altogether, the flexible model used in this study provides a comprehensive understanding of concomitant contaminant biodegradation under dynamic hydrogeological systems, and showed its potential use for assessment of natural attenuation of DCM at contaminated sites.

### 6.1.2 Varying micropollutant exposures during stream-groundwater interactions

The ubiquitous release of micropollutants into surface and groundwater has urged for improved environmental studies representing more realistic field conditions. Current research issues in the field of micropollutant transformation include (i) how the contribution of degradative processes can be evaluated *in situ*, and (ii) what are the factors controlling micropollutant biotransformation even at trace concentrations. **Stream-groundwater interactions** represent a common entry

pathway of **micropollutants**, due to their initial release in surface waters. The integrative approach used for examining degradation of legacy organic contaminants such as dichloromethane (DCM) (discussed in Chapter 3 and 4) can be taken to improve our understanding on micropollutants removal from subsurface environments. **Chapter 5** presented an integrative study aiming at deciphering micropollutants degradation in laboratory aquifers mimicking stream flow to adjacent groundwater. This lateral transition zone represents a yet poorly understood highly dynamic mixing zone of stream-groundwater biogeochemical dynamics. As this area is often subject to seasonal variations in stream water level fluctuations and micropollutant inputs, aerobic biotransformation of micropollutants may be suggested. The investigated micropollutants included a mixture composed of the herbicides atrazine, terbutryn and *S*-metolachlor, the fungicide metalaxyl, the consumer product caffeine, and the anti-diabetic drug metformin, whose co-occurrence has been evidence in surface and groundwater (Lesser et al., 2018; Loos et al., 2010).

Dynamic conditions were considered with regards to **varying micropollutant exposure periods**, representing variations in micropollutants inputs due to **seasonal applications and hydrological events**. This may have important implications on bacterial adaptations to long-term micropollutants exposure. Overall, the integration of ME-CSIA, biomolecular markers and conceptual RTMs proved relevant to derive a comprehensive framework to identify and quantify micropollutants degradation in contaminated aquifers. The results presented in Chapter 5 highlighted that biotransformation of micropollutants as chemical mixtures largely varied, independently on the acute or chronic level of exposure to micropollutants. Particularly, caffeine biotransformation was observed during all micropollutants injection periods based on isotope signatures and formation of TPs, such as theobromine and xanthine. The conceptual model developed in Chapter 5 showed that caffeine isotopic signatures were associated with a possibly concentration dependence following Michaelis-Menten, in agreement with previous studies (Sun et al., 2021). This suggested that a conceptual framework such as that proposed in Chapter 5, and elsewhere (Eckert et al., 2013), was sufficient to describe and predict the reactive transport of micropollutants in groundwater. This may allow to predict and target the 'hot periods' for *in situ* high resolution sampling and monitoring of micropollutants in stream-groundwater transition zones. In contrast, only moderate or negligible biotransformation of metformin, atrazine, terbutryn, *S*-metolachlor and metalaxyl occurred in the laboratory aquifers, emphasizing their potential persistence and possible risks of long-term groundwater contamination.

Altogether, the integrative approach of the natural attenuation of micropollutants in shal-

low groundwater connected to surface waters underscored its relevance for future applications of high-resolution monitoring at the lateral transition zones to adjacent groundwater. Because caffeine degradation proved relevant at low concentration ranges ( $<20 \mu\text{g L}^{-1}$ ), questions remain on the limit of concentrations for the occurrence of bioavailability effects. Although this study relied on high concentration levels (up to  $6 \text{ mg L}^{-1}$ ) for the experimental design, allowing ME-CSIA evaluation, future studies on bioavailability limitations should be considered to understand the fate of the investigated micropollutants at lower concentration levels (e.g.,  $<1 \mu\text{g L}^{-1}$ ), and the effect of micropollutant mixtures on their persistence. Indeed, recent studies are reporting the presence of chemical-contaminant mixtures in surface water in urban/agricultural catchment areas, highlighting that to date biological effects of micropollutants are less well understood (Baran et al., 2021; Bradley et al., 2021; Lesser et al., 2018). The integration of biomolecular markers such as 16S rRNA further enabled to examine the possibly long-term adaptation of bacterial communities and suggesting their potential use as indicators of micropollutants biotransformation in groundwater.

## **6.2 Integrative approaches to improve natural attenuation of organic contaminants in groundwater**

Integrative approaches, as those implemented in this thesis, need to provide a flexible framework for their applicability to a wide range of contaminants and associated sources. However, potentials and limitations of the presented integrative approach were encountered throughout this thesis.

ME-CSIA (i.e., following the changes in stable isotope ratios of two or more elements) was a primary line of evidence to evaluate biodegradation extent and pathways of the investigated contaminants (i.e., DCM and the micropollutant mixture). Generally, CSIA is a well-recognized tool for the identification and quantification of degradative processes at contaminated sites. The use of ME-CSIA may allow for a stronger line of evidence of the extent and pathways of *in situ* degradation. This was particularly evident for legacy contaminants such as DCM (Chapter 3 and 4) compared to micropollutants (Chapter 5). The estimation of isotope fractionation values (e.g.,  $\varepsilon_{\text{C}}$ ) from reference laboratory experiments under controlled conditions (e.g., a degradative process occurring under a specific redox condition) represent a basis for qualifying and quantifying *in situ* degradation. For instance, it allowed estimating the extent of biodegradation of DCM described in Chapter 3. However, the reference isotope fractionation values should be carefully selected prior interpreting *in situ* biodegradative processes in the field. It is thus essential that

such isotope fractionation values correspond to the established hydrochemical conditions *in situ* and the prevailing degradation pathway, as documented in Chapter 3. Most importantly, the multi-phase reactive transport model presented in Chapter 4 relied on pathway-specific reaction rates of DCM based on available C- and/or Cl-data. In this context, the high-resolution monitoring of *in situ* hydrochemical conditions, along with the evolution of isotope signatures and bacterial diversity results, oriented the appropriate selection of reported  $\varepsilon$  values with respect to DCM degradation.

Along with CSIA, the integration of biomolecular approaches such as 16S rRNA gene has well proven the potential for a more robust characterization of *in situ* conditions. Globally, the integration of high-resolution hydrochemical analysis, ME-CSIA and biomolecular approaches proved advantageous throughout this thesis to provide robust evidence of the natural attenuation of DCM and micropollutants in laboratory aquifers. Notably, the state of the art of the biodegradation of Cl-VOCs (e.g., such as DCM; Chapters 3 and 4) *versus* micropollutants (Chapter 5) differs greatly. For instance, over the last 30 decades, knowledge on DCM degradation pathways has been increasingly reported (Chen et al., 2020, 2018; Hermon et al., 2018; Kleindienst et al., 2019; Mägli et al., 1998; Torgonskaya et al., 2019). Recently, the advance of biomolecular approaches, including proteogenomics, allowed for better characterization of DCM metabolisms of isolates or enriched cultures. To date, CSIA has been able to pinpoint the mechanisms of DCM biodegradation. The combination of CSIA and biomolecular markers provides a good integrative framework for teasing apart distinct DCM degradation pathways and mechanisms. With such information, interpretations of *in situ* DCM biodegradation in the laboratory aquifers were possible, coinciding with identification of taxa potentially associated with DCM biodegradation such as those belonging to the *Peptococcaceae* family (Chapter 3). This included taxa associated with *Dehalobacter*, *Dehalobacterium* and *Desulfosporosinus* spp. Additionally, the isotope signatures observed in both laboratory aquifers also correlated with the established iron-reducing conditions and the reported isotope fractionation values for anaerobic DCM degradation (Chapter 3).

It is also relevant to mention that in the case of DCM, both aquifers were fed with contaminated groundwater from a well-characterized former industrial site. This allowed to operate the systems under near-natural settings and monitor DCM biodegradative processes under controlled conditions, as opposed to groundwater monitoring in the field. The laboratory aquifers also allowed to obtain detailed insights from the evolution of hydrochemical conditions over time and along the flow path, as well as the evolution of stable isotopes (i.e.,  $^{13}\text{C}/^{12}\text{C}$  and

$^{37}\text{Cl}/^{35}\text{Cl}$ ) and bacterial diversity and composition. Thanks to previous studies on the characterization of the DCM contaminated site based on CSIA and biomolecular markers (Hellal et al., 2021; Hermon et al., 2018), comparisons between laboratory and field observations could be established. These comparisons highlighted that laboratory aquifers operated under near-natural conditions are valuable experimental setups to investigate reactive transport processes mimicking hydrogeological systems.

Contrastingly, knowledge on degradation mechanisms and pathways of micropollutants in groundwater is less understood. First, a vast number of studies largely focus on examining the fate and transport of micropollutants in surface water and soils. Here, relevant degradative processes include hydrolysis, photolysis and biotic transformation, and CSIA may allow teasing apart such micropollutant degradation pathways (Elsner and Imfeld, 2016). Thus, several micropollutants, such as atrazine, metalaxyl, and *S*-metolachlor, have been documented for both abiotic and biotic transformation in surface waters and soils, providing important information on their degradation rates, half-lives and/or stable isotope fractionation values, particularly for C and N (e.g., Drouin et al. (2021); Droz et al. (2021); Ehrl et al. (2018); Masbou et al. (2018a,b)). However, when it comes to groundwater contamination, micropollutant biodegradation is rather relevant at transition zones between surface waters and groundwater such as the hyporheic zone. In addition to the classical methods to evidence micropollutant degradation, such as monitoring concentrations and formations of TPs, the recent use of CSIA and biomolecular methods have improved our understanding of reactive transport of micropollutants in the hyporheic zone (Droz et al., 2021; Jaeger et al., 2021; Posselt et al., 2020). However, the fate of micropollutants on the lateral hyporheic zone adjacent to groundwater is yet poorly understood, which calls for future studies addressing the fate of micropollutants in this highly dynamic transition zones. This thesis did not focus on field evidence of the hydrological processes involved during stream-groundwater interactions at the Souffel catchment from which stream water was collected (Chapter 5). However, it was demonstrated in Chapter 5 that micropollutant degradation can occur across this lateral transition zone, underscoring the interest of integrative studies to elucidate micropollutants biotransformation in the lateral hyporheic zone.

Particularly, the bacterial community response with respect to micropollutant exposure showed gradual temporal changes (Chapter 5). Compared to the biomolecular information obtained with respect to DCM biodegradation (Chapter 3), it is clear that known bacterial isolates associated with micropollutant degradation are less known than bacteria involved in chlorinated solvent degradation. This severely limits the interpretation of *in situ* degradative processes and



definition of remediation strategies with regard to micropollutants. However, understanding adaptive mechanisms at the bacterial community level in response to micropollutant exposure provides a genuine basis of the current stage of the contaminated aquifer, and the possible effect on micropollutant degradation. It has been suggested that degradation of micropollutants may rather occur during co-metabolism, where enzymes may no longer be harbored by a single microorganism only, but may be distributed over a bacterial community (Fenner et al., 2021). In this context, the increasing use of biomolecular approaches, with sustained evidence of its relevance along with CSIA applications, opens an opportunity for (i) exploring the wide range of the yet unclassified taxa associated with micropollutant degradation, and (ii) understanding bacterial community responses to micropollutants exposure. This may include soil, river water, and groundwater samples with historical evidence of micropollutant exposure periods. Moreover, the often presence of micropollutants at low concentrations ( $<1 \mu\text{g L}^{-1}$ ) further advocates for integrative studies addressing the effect of low bioavailability on micropollutant degradation, particularly in transition zones between surface water and groundwater, and its effect on stable isotope fractionation (e.g., due to rate-limiting steps).

Finally, applications of ME-CSIA of micropollutants for *in situ* interpretations of contaminated aquifers is still challenging compared to legacy contaminants such as DCM. Studies addressing micropollutant degradation in microcosm enable evidencing degradative processes using CSIA, but lacking characterization of the possible microorganisms involved (e.g., Droz et al. (2021); Masbou et al. (2018b)). In this context, fundamental studies are needed to provide more information on the possible microorganisms involved, mechanisms and pathways of micropollutants biotransformation. Here, ME-CSIA may become advantageous for further environmental investigations of micropollutants degradation in groundwater transition zones.

### **6.3 Toward improved reactive transport models to predict *in situ* natural attenuation at contaminated sites**

Reactive transport modeling is a powerful tool for monitoring and quantifying the natural attenuation of organic contaminants in aquifers. Generally, the outputs obtained from model simulations may provide a robust understanding of the underlying processes affecting reactive transport in porous media. Parameter estimations of lumped variables, such as degradation rates, are often obtained from fitting experimental data, thus providing a quantitative description of biodegradative process. The integration of CSIA in RTMs brought forward a powerful concept to explore key controlling processes affecting biodegradation in aquifers. Developments of 1-D

RTMs have proven sufficient to correlate the evolution of isotope signatures and depletion of the target contaminant based on experimental observations. In Chapter 5, a simple 1-D numerical reactive scheme could capture the reactive transport of caffeine in the laboratory aquifers. First, a saline tracer test allowed to obtain transport parameters such as average velocity and longitudinal dispersion. Although the reactive scheme was restricted to longitudinal dispersion along the flow line, it proved sufficient for fitting the caffeine BTC and carbon isotope signatures. The fitting procedure of the reactive scheme was based on computing caffeine degradation rates following Michaelis-Menten, the half-saturation of caffeine, and the isotope fraction values. The latter was restricted to C isotope fractionation due no evidence of N fractionation over the whole experiment. Thus, experimental observations were well described by the implemented 1-D numerical model, agreeing with caffeine dissipation and evolution of carbon isotope signatures. Caffeine model simulations further provided a robust line of evidence of the likely biodegradation dependence on substrate concentrations. This correlated with the U-shaped  $\delta^{13}\text{C}$  trend observed in both laboratory aquifers, suggesting that carbon isotope fractionation was affected throughout the BTC and according to Michaelis-Menten kinetics, as suggested previously (Eckert et al., 2013; Schürner et al., 2016; Sun et al., 2021). This brings forward the implications of monitoring *in situ* micropollutants degradation, and the relevance for accurate predictions of micropollutants inputs into groundwater, e.g., by following seasonal applications and hydrological events at the catchment scale, to capture isotope signatures along a micropollutant BTC.

Simulating dynamic conditions, such as water table fluctuations, require reactive transport schemes capable of coupling the numerous physical and chemical processes affecting pollutant fate in groundwater. Hence, numerical developments of multi-phase flow were needed to fully represent the interplay of such processes under dynamic conditions, as presented in Chapter 4. Here, mass exchange across the capillary fringe was possible with the development of a multi-phase and multi-component framework, particularly to capture DCM volatilization and  $\text{O}_2$  diffusion upon water table fluctuations. Given that evidence of possible concomitant DCM degradation was documented in Chapter 3, the numerical model was developed to include a broad range of bacterial populations, providing available descriptions with C- and/or Cl- CSIA. One of the assets of the model presented in Chapter 4 is the detail description of the reactive scheme, including (i) products specific to a DCM degradation pathway, (ii) evolution of key redox species such as  $\text{O}_2$ , ferric iron and  $\text{CO}_2$ , (iii) evolution of C and Cl isotope ratios of the 6 DCM isotopologues, and (iv) biomass evolution of distinct modeled bacterial populations representing the complex interspecies interactions often overlooked at contaminated sites. Nu-

merical results presented in Chapter 4 showed that the proposed reactive scheme was capable of capturing the main trends observed in the laboratory aquifers (Chapter 3). This supports that concomitant DCM degradation should be considered for assessment of DCM degradation at contaminated sites, and that numerical simulations can further shed light on the possible 'hot and cold periods' for DCM biodegradation during water table fluctuations. To date, such reactive scheme could not be implemented for micropollutants biotransformation in aquifers.

In Chapter 4, it was also evidenced that many factors are linked to DCM degradation, notably growth rates and the availability of redox species. In addition, simulating evolution of biomass required assumptions on the percentage of assimilation of the substrate to biomass growth and energy metabolism (Rittmann, 2006). In the presented multi-phase flow RTM, it was assumed that all bacterial populations assimilated 50% DCM or DOC for their growth, independently on the type of reaction. However, biomass yield differs among redox reactions and microorganisms and should be considered in reactive schemes (Rittmann, 2006), which is often not well documented. A sensitivity analysis of the model implemented in Chapter 4 could provide insights regarding the effect of biomass growth among distinct microorganisms during DCM biodegradation. Another aspect of the proposed reactive scheme was the introduction of maintenance factors, which may provide a proper description of bacterial kinetics. The numerical results presented in Chapter 4, however, assumed negligible maintenance factors due to a lack of reported values for DCM. Nevertheless, introduction of maintenance factors has been suggested to account for the fact that bacterial cells may need substrate for other purposes than grow (Kovářová-Kovar and Egli, 1998), particularly when thriving at low substrate concentrations (Egli, 2010; Ehrl et al., 2018). However, determining maintenance factors, homologous as with estimating growth rates, it would require appropriate chemostat experiments, which requires future considerations for describing DCM degradation reactions. Finally, various transport processes are also implicated in the evolution of contaminants, redox species and biomass, further controlling biodegradative processes. This may include (i) transverse dispersion, particularly for plume evolution upon water table fluctuations, (ii) the tortuosity flow which can be affected by entrapped air upon water table fluctuations (Klenk and Grathwohl, 2002), and (iii) the kinetic mass transfer coefficient by volatilization (Hron et al., 2015).

Thus, the interplay of transport and reactive processes upon dynamic environmental conditions in hydrogeological systems require a comprehensive and holistic approach for the developing of appropriate reactive schemes. These reactive schemes may include simulations of (i) the bacteria present in the community, (ii) the metabolic pathways that each bacterium can

carry out, (iii) evidence of their active metabolism by following changes in stable isotope ratios and hydrochemical species, and (iv) the inter-relationships among the members of the community and between their environment (i.e., fluctuating vs. static water table) (VanBriesen and Rittmann, 2000). Such integrative model developments may thus pave the way to provide a more robust prediction of the natural attenuation of organic contaminants in groundwater.

## 6.4 Implications and perspectives

The methodology used in this thesis showed that integrative approaches are useful for better description of reactive transport processes. This encompasses a thorough description of *in situ* hydrochemical conditions, contaminant concentrations and evolution of stable isotopes, and bacterial dynamics. The use of laboratory aquifers also enabled for near-natural representations of hydrogeological systems, while dynamic conditions were able to be examined under controlled events. However, the experimental setup in the laboratory aquifers faced some shortcomings.

First, although a high-resolution sampling over time and across the sand compartment was established in all experiments, the laboratory aquifers did not enable examining reactive transport processes in high resolution depth. Only 3 sampling points covered the depth of the sand compartments, which is insufficient for describing the mass exchange from the saturated zone to the unsaturated zone. Particularly, this depth resolution was not sufficient to capture the evolution of diffusive species across the unsaturated zone such as oxygen and DCM (Chapter 3). Consequently, the numerical simulations presented in Chapter 4 still require for a calibration approach. Oxygen levels can indeed be followed across vertical profiles; however, DCM concentration measurements across the capillary fringe and unsaturated zone are lacking, which hampers accurate calibration of the model with regard to DCM volatilization. While this may be an obstacle for a good model calibration, numerical simulations of multi-phase and multi-component transport processes can be compared with other model outputs, such as COMSOL® multi-physics, to validate the model framework for DCM volatilization and oxygen diffusion. In addition, and as a long-term perspective, a global sensitivity analysis of key transport and reactive parameters (see Section 6.3) is still needed, and may pay the way to define key parameters for a possible inverse modeling approach of the CubicM model (Chapter 4).

Second, the integration of CSIA and biomolecular approaches provided a robust line of evidence of the degradation of DCM (Chapter 3) and micropollutants (Chapter 5) in the laboratory aquifers. Indeed, explorations based on RNA content in groundwater may be suitable to iden-

tify the active populations or the expressed pathways (meta-transcriptomics). However, RNA explorations from field studies require large volumes of groundwater samples of >50 L (Lopez-Fernandez et al., 2019; Yamamoto et al., 2019). In our study, the limited volume of interstitial groundwater (volume: 2–10 mL) and the relatively low amount of nucleic acids initially recovered from our set-up did not allow the performance of RNA analyses. High-throughput DNA sequencing of the 16S rRNA gene, nevertheless, provides information about groundwater bacterial community composition and structure, allowing bacterial taxonomical classification and ecological metrics calculations, such as diversity analysis (e.g., Hellal et al. (2021); Torabi et al. (2020); Trueba-Santiso et al. (2017); Wright et al. (2017)). For instance, Chapter 3 was able to show that bacterial community dynamics were different in aquifers under steady-state conditions compared to transient conditions, and was further correlated with CSIA data suggesting distinct DCM degradation pathways. This was evidenced by the occurrence of taxa previously linked with anaerobic DCM degradation, and distinct C and Cl isotope signatures. However, future studies should address possible concomitant anaerobic DCM degradation in microcosms experiments to examine why enrichment of distinct potentially associated DCM degraders often occurs at contaminated sites. Moreover, further experiments are needed to further unravel the effect of water table fluctuations on distinct DCM degradation pathways. For instance, available anaerobic biomarkers, such as the proposed *mec* gene cassette (Murdoch et al., 2022), may elucidate differences in active metabolisms relative to static and transient conditions. This may be examined in column experiments or laboratory aquifers inoculated with contaminant groundwater and *endogenous* microorganisms. Further questions may be here addressed in long-term experiments such as (i) what is the effect of water saturation on DCM degradation during a low water table? (ii) what is the shortest transient drying/wetting period that could drive/enhance DCM degradation? and (iii) what is the role of CO<sub>2</sub> fluxes and associated metabolic processes of other organic substrates on direct or indirect DCM biodegradation?

In the case of micropollutants (Chapter 5), high-throughput DNA sequencing of the 16S rRNA gene also provided evidence of the gradual changes of the bacterial community composition along varying micropollutant exposure periods. Contrastingly, these gradual changes were likely associated with the selective toxicity pressure that micropollutants exerted over the bacterial community rather than enhance micropollutants degradation. Future studies focusing on understanding the bacterial community in response to micropollutant perturbations will continue to provide valuable information on the fate of micropollutants in subsurface environments. Particularly, the fate of micropollutants across transition zones such as the hyporheic

zone are still of utmost need to define their ultimately mobilization to shallow groundwater. For instance, microcosms experiments may provide a good experimental framework to examine pollutant biodegradation kinetics under varying conditions such as (i) distinct redox species, including oxic and anoxic conditions, (ii) the selective pressure of individual micropollutants, and as chemical mixtures, on the bacterial dynamics and thus degradation kinetics, and (iii) alternating oxic and anoxic conditions in biodegradation experiments to elucidate dynamics in the HZ. These microcosm experiments may be scaled up to column experiments or laboratory aquifers to include flow-through effects on overall micropollutant dissipation processes.

Altogether, the results presented in this thesis highlighted the effect of dynamic environmental conditions on the degradation of DCM and micropollutants in laboratory aquifers. The use of an integrative approaches may pave the way toward more specific and adapted remediation strategies in dynamic hydrogeological systems. Finally, while the proposed integrative approach in this study may proof useful to evidence pollutant biodegradation at contaminated sites, limitations of monitored natural attenuation should also be considered. This may include the definition of active remediation strategies when sensible targets are endangered, such as drinking water supply wells (Antelmi et al., 2021).

## References of Chapter 6

- Antelmi, M., Mazzon, P., Höhener, P., Marchesi, M., and Alberti, L. (2021). Evaluation of MNA in a chlorinated solvents-contaminated aquifer using reactive transport modeling coupled with isotopic fractionation analysis. *Water*, 13(21):2945.
- Badin, A., Braun, F., Halloran, L. J. S., Maillard, J., and Hunkeler, D. (2018). Modelling of C/Cl isotopic behaviour during chloroethene biotic reductive dechlorination: Capabilities and limitations of simplified and comprehensive models. *PloS one*, 13(8):e0202416.
- Baran, N., Surdyk, N., and Auterives, C. (2021). Pesticides in groundwater at a national scale (France): Impact of regulations, molecular properties, uses, hydrogeology and climatic conditions. *Science of The Total Environment*, 791:148137.
- Blázquez-Pallí, N., Shouakar-Stash, O., Palau, J., Trueba-Santiso, A., Varias, J., Bosch, M., Soler, A., Vicent, T., Marco-Urrea, E., and Rosell, M. (2019). Use of dual element isotope analysis and microcosm studies to determine the origin and potential anaerobic biodegradation of dichloromethane in two multi-contaminated aquifers. *Science of The Total Environment*, 696:134066.
- Bradley, P. M., Journey, C. A., Romanok, K. M., Breitmeyer, S. E., Button, D. T., Carlisle, D. M., Huffman, B. J., Mahler, B. J., Nowell, L. H., Qi, S. L., et al. (2021). Multi-region assessment of chemical mixture exposures and predicted cumulative effects in USA wadeable urban/agriculture-gradient streams. *Science of the Total Environment*, 773:145062.
- Chen, G., Fisch, A. R., Gibson, C. M., Erin Mack, E., Seger, E. S., Campagna, S. R., and Löffler, F. E. (2020). Mineralization versus fermentation: Evidence for two distinct anaerobic bacterial degradation pathways for dichloromethane. *The ISME Journal*, 14(4):959–970.
- Chen, G., Kleindienst, S., Griffiths, D. R., Mack, E. E., Seger, E. S., and Löffler, F. E. (2017). Mutualistic interaction between dichloromethane-and chloromethane-degrading bacteria in an anaerobic mixed culture. *Environmental Microbiology*, 19(11):4784–4796.
- Chen, G., Shouakar-Stash, O., Phillips, E., Justicia-Leon, S. D., Gilevska, T., Sherwood Lollar, B., Mack, E. E., Seger, E. S., and Löffler, F. E. (2018). Dual carbon-chlorine isotope analysis indicates distinct anaerobic dichloromethane degradation pathways in two members of *Peptococcaceae*. *Environmental Science & Technology*, 52(15):8607–8616.
- Drouin, G., Droz, B., Leresche, F., Payraudeau, S., Masbou, J., and Imfeld, G. (2021). Direct and indirect photodegradation of atrazine and s-metolachlor in agriculturally impacted surface water and associated C and N isotope fractionation. *Environmental Science: Processes & Impacts*, 23(11):1791–1802.
- Droz, B., Drouin, G., Maurer, L., Villette, C., Payraudeau, S., and Imfeld, G. (2021). Phase transfer and biodegra-

- dation of pesticides in water-sediment systems explored by compound-specific isotope analysis and conceptual modeling. *Environmental Science & Technology*, 55(8):4720–4728.
- Eckert, D., Qiu, S., Elsner, M., and Cirpka, O. A. (2013). Model complexity needed for quantitative analysis of high resolution isotope and concentration data from a toluene-pulse experiment. *Environmental Science & Technology*, 47(13):6900–6907.
- Egli, T. (2010). How to live at very low substrate concentration. *Water Research*, 44(17):4826–4837.
- Ehrl, B. N., Gharasoo, M., and Elsner, M. (2018). Isotope fractionation pinpoints membrane permeability as a barrier to atrazine biodegradation in gram-negative *Polaromonas* sp. Nea-C. *Environmental Science & Technology*, 52(7):4137–4144.
- Elsner, M. and Imfeld, G. (2016). Compound-specific isotope analysis (CSIA) of micropollutants in the environment – Current developments and future challenges. *Current Opinion in Biotechnology*, 41:60–72.
- Fenner, K., Elsner, M., Lueders, T., McLachlan, M. S., Wackett, L. P., Zimmermann, M., and Drewes, J. E. (2021). Methodological advances to study contaminant biotransformation: New prospects for understanding and reducing environmental persistence? *ACS ES&T Water*, 1(7):1541–1554.
- Hellal, J., Joulain, C., Urien, C., Ferreira, S., Denonfoux, J., Hermon, L., Vuilleumier, S., and Imfeld, G. (2021). Chlorinated ethene biodegradation and associated bacterial taxa in multi-polluted groundwater: Insights from biomolecular markers and stable isotope analysis. *Science of The Total Environment*, 763:142950.
- Hermon, L., Denonfoux, J., Hellal, J., Joulain, C., Ferreira, S., Vuilleumier, S., and Imfeld, G. (2018). Dichloromethane biodegradation in multi-contaminated groundwater: Insights from biomolecular and compound-specific isotope analyses. *Water Research*, 142:217–226.
- Hermon, L., Hellal, J., Denonfoux, J., Vuilleumier, S., Imfeld, G., Urien, C., Ferreira, S., and Joulain, C. (2019). Functional genes and bacterial communities during organohalide respiration of chloroethenes in microcosms of multi-contaminated groundwater. *Frontiers in Microbiology*, 10:89.
- Hron, P., Jost, D., Bastian, P., Gallert, C., Winter, J., and Ippisch, O. (2015). Application of reactive transport modeling to growth and transport of microorganisms in the capillary fringe. *Vadose Zone Journal*, 14(5).
- Hunkeler, D., Meckenstock, R., and Sherwood Lollar, B. (2009). A guide for assessing biodegradation and source identification of organic ground water contaminants using compound specific isotope analysis (CSIA). *U.S. Environmental Protection Agency, Washington, D.C., EPA/600/R-08/148*, pages 1–82.
- Jaeger, A., Posselt, M., Schaper, J. L., Betterle, A., Rutere, C., Coll, C., Mechelke, J., Raza, M., Meinikmann, K., Portmann, A., Blaen, P. J., Horn, M. A., Krause, S., and Lewandowski, J. (2021). Transformation of organic micropollutants along hyporheic flow in bedforms of river-simulating flumes. *Scientific Reports*, 11(1):13034.
- Jost, D., Haberer, C. M., Grathwohl, P., Winter, J., and Gallert, C. (2015). Oxygen transfer in a fluctuating capillary fringe: Impact of microbial respiratory activity. *Vadose Zone Journal*, 14(5):vzj2014.04.0039.
- Kleindienst, S., Chourey, K., Chen, G., Murdoch, R. W., Higgins, S. A., Iyer, R., Campagna, S. R., Mack, E. E., Seger, E. S., Hettich, R. L., and Löffler, F. E. (2019). Proteogenomics reveals novel reductive dehalogenases and methyltransferases expressed during anaerobic dichloromethane metabolism. *Applied Environmental Microbiology*, 85(6):e02768–18.
- Klenk, I. and Grathwohl, P. (2002). Transverse vertical dispersion in groundwater and the capillary fringe. *Journal of Contaminant Hydrology*, 58(1):111–128.



- Kovárová-Kovar, K. and Egli, T. (1998). Growth kinetics of suspended microbial cells: From single-substrate-controlled growth to mixed-substrate kinetics. *Microbiology and molecular biology reviews*, 62(3):646–666.
- Kuder, T., Philp, R., Van Breukelen, B. M., Thoeument, H., and Vanderford, M. (2016). Integrated stable isotope – Reactive transport model approach for assessment of chlorinated solvent degradation. Technical report, University of Oklahoma Norman United States.
- Lesser, L. E., Mora, A., Moreau, C., Mahlke, J., Hernández-Antonio, A., Ramírez, A. I., and Barrios-Piña, H. (2018). Survey of 218 organic contaminants in groundwater derived from the world’s largest untreated wastewater irrigation system: Mezquital Valley, Mexico. *Chemosphere*, 198:510–521.
- Loos, R., Locoro, G., Comero, S., Contini, S., Schwesig, D., Werres, F., Balsaa, P., Gans, O., Weiss, S., Blaha, L., Bolchi, M., and Gawlik, B. M. (2010). Pan-european survey on the occurrence of selected polar organic persistent pollutants in ground water. *Water Research*, 44(14):4115–4126.
- Lopez-Fernandez, M., Broman, E., Simone, D., Bertilsson, S., and Dopson, M. (2019). Statistical analysis of community RNA transcripts between organic carbon and geogas-fed continental deep biosphere groundwaters. *mBio*, 10(4).
- Mägli, A., Messmer, M., and Leisinger, T. (1998). Metabolism of dichloromethane by the strict anaerobe *Dehalobacterium formicoaceticum*. *Applied and Environmental Microbiology*, 64(2):646–650.
- Masbou, J., Drouin, G., Payraudeau, S., and Imfeld, G. (2018a). Carbon and nitrogen stable isotope fractionation during abiotic hydrolysis of pesticides. *Chemosphere*, 213:368–376.
- Masbou, J., Meite, F., Guyot, B., and Imfeld, G. (2018b). Enantiomer-specific stable carbon isotope analysis (ESIA) to evaluate degradation of the chiral fungicide metalaxyl in soils. *Journal of Hazardous Materials*, 353:99–107.
- Murdoch, R. W., Chen, G., Kara Murdoch, F., Mack, E. E., Villalobos Solis, M. I., Hettich, R. L., and Löffler, F. E. (2022). Identification and widespread environmental distribution of a gene cassette implicated in anaerobic dichloromethane degradation. *Global change biology*, 00:1–17.
- NRC (2000). *Natural Attenuation for Groundwater Remediation*. National Research Council. National Academies Press.
- Posselt, M., Mechelke, J., Rutere, C., Coll, C., Jaeger, A., Raza, M., Meinikmann, K., Krause, S., Sobek, A., Lewandowski, J., Horn, M. A., Hollender, J., and Benskin, J. P. (2020). Bacterial diversity controls transformation of wastewater-derived organic contaminants in river-simulating flumes. *Environmental Science & Technology*, 54(9):5467–5479.
- Pronk, G. J., Mellage, A., Milojevic, T., Smeaton, C. M., Engel, K., Neufeld, J. D., Rezanezhad, F., and Cappellen, P. V. (2020). Carbon turnover and microbial activity in an artificial soil under imposed cyclic drainage and imbibition. *Vadose Zone Journal*, 19(1):e20021.
- Rezanezhad, F., Couture, R.-M., Kovac, R., O’Connell, D., and Van Cappellen, P. (2014). Water table fluctuations and soil biogeochemistry: An experimental approach using an automated soil column system. *Journal of Hydrology*, 509:245–256.
- Rittmann, B. E. (2006). Microbial ecology to manage processes in environmental biotechnology. *Trends in Biotechnology*, 24(6):261–266.
- Schürner, H. K. V., Maier, M. P., Eckert, D., Brejcha, R., Neumann, C.-C., Stumpp, C., Cirpka, O. A., and Elsner, M. (2016). Compound-specific stable isotope fractionation of pesticides and pharmaceuticals in a mesoscale aquifer model. *Environmental Science & Technology*, 50(11):5729–5739.

- Sun, F., Mellage, A., Gharasoo, M., Melsbach, A., Cao, X., Zimmermann, R., Griebler, C., Thullner, M., Cirpka, O. A., and Elsner, M. (2021). Mass-transfer-limited biodegradation at low concentrations – Evidence from reactive transport modeling of isotope profiles in a bench-scale aquifer. *Environmental Science & Technology*, 55(11):7386–7397.
- Torabi, E., Wiegert, C., Guyot, B., Vuilleumier, S., and Imfeld, G. (2020). Dissipation of s-metolachlor and butachlor in agricultural soils and responses of bacterial communities: Insights from compound-specific isotope and biomolecular analyses. *Journal of Environmental Sciences*, 92:163–175.
- Torgonskaya, M. L., Zyakun, A. M., Trotsenko, Y. A., Laurinavichius, K. S., Kümmel, S., Vuilleumier, S., and Richnow, H. H. (2019). Individual stages of bacterial dichloromethane degradation mapped by carbon and chlorine stable isotope analysis. *Journal of Environmental Sciences*, 78:147–160.
- Trueba-Santiso, A., Fernández-Verdejo, D., Marco-Rius, I., Soder-Walz, J. M., Casabella, O., Vicent, T., and Marco-Urrea, E. (2020). Interspecies interaction and effect of co-contaminants in an anaerobic dichloromethane-degrading culture. *Chemosphere*, 240:124877.
- Trueba-Santiso, A., Parladé, E., Rosell, M., Lliros, M., Mortan, S. H., Martínez-Alonso, M., Gaju, N., Martín-González, L., Vicent, T., and Marco-Urrea, E. (2017). Molecular and carbon isotopic characterization of an anaerobic stable enrichment culture containing *Dehalobacterium* sp. during dichloromethane fermentation. *Science of The Total Environment*, 581-582:640–648.
- Van Breukelen, B. M., Hunkeler, D., and Volkerling, F. (2005). Quantification of sequential chlorinated ethene degradation by use of a reactive transport model incorporating isotope fractionation. *Environmental Science & Technology*, 39(11):4189–4197.
- VanBriesen, J. M. and Rittmann, B. E. (2000). Mathematical description of microbiological reactions involving intermediates. *Biotechnology and Bioengineering*, 67(1):35–52.
- Wright, J., Kirchner, V., Bernard, W., Ulrich, N., McLimans, C., Campa, M. F., Hazen, T., Macbeth, T., Marabello, D., McDermott, J., Mackelprang, R., Roth, K., and Lamendella, R. (2017). Bacterial community dynamics in dichloromethane-contaminated groundwater undergoing natural attenuation. *Frontiers in Microbiology*, 8:2300.
- Yamamoto, K., Hackley, K. C., Kelly, W. R., Panno, S. V., Sekiguchi, Y., Sanford, R. A., Liu, W.-T., Kamagata, Y., and Tamaki, H. (2019). Diversity and geochemical community assembly processes of the living rare biosphere in a sand-and-gravel aquifer ecosystem in the midwestern united states. *Scientific Reports*, 9(1):13484.



# **Appendix A**

## **Supporting information of Chapter 3**

## A.1 Grounwater collection

The supplied groundwater was collected from the industrial site of Thermeroil (Varennese-Grand, Saône-et-Loire, France; GPS coordinates, 46.701141 N, 4.843919 E). Groundwater was collected from well Pz28 which is located at the source zone of the DNAPL plume (Hermon et al., 2018). Groundwater was stored in three 50 L tanks (Walther Pilot, Wuppertal, Germany) and kept at constant N<sub>2</sub>-flux to maintain anoxic conditions. In the laboratory, the 50 L tanks were stored in a temperature-controlled room at 18 ± 1 °C until further analysis.

## A.2 Quantification of VOCs

For DCM, *cis*-DCE and VC concentration measurements, 200 µL of headspace samples were analyzed in a gas chromatograph (GC, Trace 1300, Thermo Fisher Scientific) coupled with a mass spectrometer (MS, ISQ™, Thermo Fisher Scientific) and equipped with a DB-624 (30 m × 0.32 mm ID, 1.80 µm film thickness) and a flame ionization detector (FID). Helium was used as the carrier gas with a flow rate of 1.5 mL min<sup>-1</sup>. Sampling was automated using a headspace autosampler (TriPlus RHS™, Thermo Fisher Scientific), and headspace equilibrium was reached by 3 min agitation at 70 °C temperature. The GC injector and detector were set at 240 °C and 250 °C, respectively. Headspace samples were injected through a split/splitless injector (split ratio 1:300). The initial oven temperature (35 °C) was held for 3 minutes, then ramped at 10 °C/min to 115 °C followed by an increase to 260 °C at a ramping rate of 30 °C min<sup>-1</sup>. DCM calibration curves were prepared similarly as the aqueous samples, with the same standard and NaCl ratio (1:1) and headspace volume. Detection limits (DLs) and quantification limits (QLs) were 1 and 64 µg/L, respectively.

## A.3 Compound Specific Isotope Analysis (CSIA) of VOCs

### A.3.1 Cl-CSIA analysis of DCM

Dichloromethane δ<sup>37</sup>Cl values were obtained by GC-qMS measurements. A summary of used GC-qMS parameters can be found in Table A1. The chlorine isotope composition of DCM was based on the two most abundant fragment ion peaks [<sup>35</sup>Cl<sup>12</sup>C<sub>1</sub>H<sub>2</sub>]<sup>+</sup> (m/z 49) and [<sup>37</sup>Cl<sup>12</sup>C<sub>1</sub>H<sub>2</sub>]<sup>+</sup> (m/z 51) (Heckel et al., 2017; Jin et al., 2011). To convert delta values relative to the international reference Standard Mean Ocean Chloride (SMOC), a two-point calibration was performed with two external standards of DCM from Sigma Aldrich (DCM<sub>#1</sub>) and VWR (DCM<sub>#2</sub>) suppliers. The external DCM standards (DCM<sub>#1</sub> = 3.68 ± 0.10‰ and DCM<sub>#2</sub> = -3.35 ± 0.12‰,

n=17) were characterized at the Isotope Tracer Technologies Inc., Waterloo, Canada by IRMS after conversion to  $\text{CH}_3\text{Cl}$  (Holt et al., 1997). The two standards were also analyzed at the Departament de Mineralogia, Petrologia i Geologia Aplicada (Barcelona, Spain) by GC-qMS. A shift of  $\Delta\delta^{37}\text{Cl} = 7.2 \pm 0.6\text{‰}$  (n=10) was derive between the two standards, validating previous measurements.

These external standards were placed into daily measurement sequences in the following way. At the beginning of a session, six injections of the first standard and six injections of the second standard were performed at different DCM concentrations. This resulted in a series of amplitudes for evaluation of the linearity of the method. Duplicate measurements of both standards were introduced after every ten sample injections to evaluate drift. The measurement sequence was concluded by duplicate measurements of both standards with the same concentration and headspace volumes. All samples were injected 6 times and bracketed with six injections of DCM<sub>#1</sub> standard. Typical reproducibility of six injections was 0.5‰ (1 $\sigma$ ) within the tested linearity range (0.5–20 mg L<sup>-1</sup>). Values for external standards (after amplitude and drift correction) were plotted against their values on the SMOC scale and sample measurements were evaluated using the intercept and the slope of this regression.

**Table A.1:** Setup of GC-qMS for chlorine isotope analysis.

Instrument manufacturer	Thermo Fisher Scientific
GC	Trace 1300 (Thermo Fisher Scientific)
qMs	ISQ (Thermo Fisher Scientific)
m/z	49 & 51 <sup>a</sup>
EI (eV)	70
Dwell time (msec)	60
Flow (mL min <sup>-1</sup> )	1.5
Split	10
Column	DB-624 (30m, 0.32 mm inside diameter, 1.80 $\mu\text{m}$ film thickness, Agilent) Thermo Fisher Scientific
Temperature program	Start at 50 °C (2 min), 20 °C min <sup>-1</sup> to 230 °C (0.5 min)
Injection temperature	240 °C
Injection technique	Automated HS
Injection vial	20 mL (18 mL headspace + 2 mL liquid)
Agitator temperature	70
Autosampler	TriPlus RSH (Thermo Fisher Scientific)
Peak integration	Xcalibur <sup>®</sup> standard method
Software	Xcalibur <sup>®</sup> Software - Thermo Fisher Scientific
Concentration range	0.5 to 20 mg L <sup>-1</sup>
Calibration slope	1.00 $\pm$ 0.02

<sup>a</sup> Most abundant fragments of DCM.

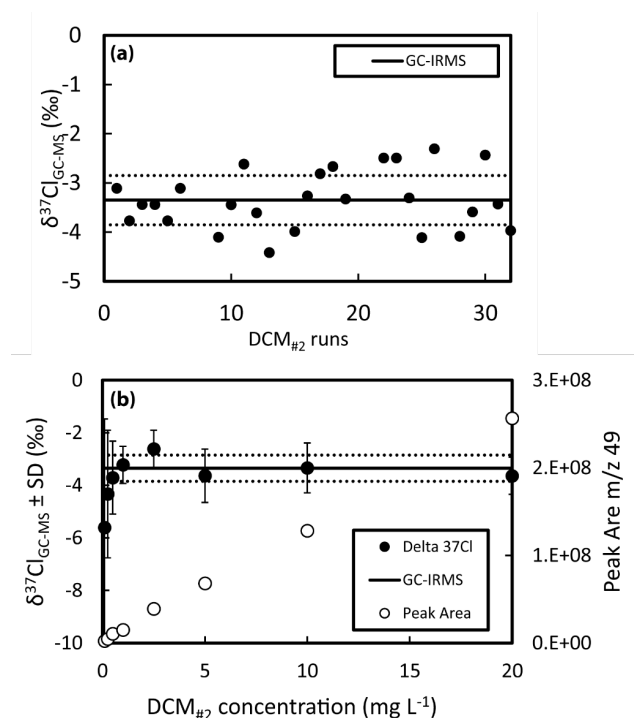


**Figure A.1:** Results of the DCM  $\delta^{37}\text{Cl}$  GCq-MS validation protocol. (a) Long term reproducibility of DCM<sub>#2</sub> standards run over the analytical sessions (concentration range: 1–20 mg L<sup>-1</sup>). For comparison, DCM<sub>#2</sub>  $\delta^{37}\text{Cl}$  GC-IRMS consensus mean (black line) associated with typical 0.5‰ uncertainties (dashed lines) have been added to the plot. (b) DCM<sub>#2</sub> amount dependence on  $\delta^{37}\text{Cl}$  GC-qMS measurement within the linearity test. Racketing standard DCM<sub>#1</sub> was kept at 10 mg L<sup>-1</sup> and only DCM<sub>#2</sub> concentration varied. For comparison, DCM<sub>#2</sub>  $\delta^{37}\text{Cl}$  GC-IRMS consensus mean (black line) associated with typical 0.5‰ uncertainties (dashed lines) have been added to the plot.

### A.3.2 C-CSIA analysis of DCM, cis-DCE and VC

Stable carbon isotope composition of DCM was determined by gas chromatography–combustion–isotope ratio mass spectrometry (GC-C-IRMS). The GC-C-IRMS system consisted of a gas chromatograph (Trace 1310, ThermoFisher Scientific) coupled via a GC/Conflow IV interface to an isotope ratio mass spectrometer (DeltaV plus, ThermoFisher Scientific). The oxidation furnace of the interface was set to a temperature of 1000 °C. A DB-624 column (60 m × 0.25 mm ID, 1.40 μm film thickness) was used for chromatographic separation at a flow rate of 1.5 mL min<sup>-1</sup>, with helium as the carrier gas. The column was held at 35 °C for 6 min, heated at a rate of 5 °C min<sup>-1</sup> to 115 °C and held for 7 min, then up to 130 °C at 10 °C min<sup>-1</sup>, then heated at 20 °C min<sup>-1</sup> up to 220 °C and held for 2 min. Headspace samples (250–500 μL) were injected using a CTC PAL GC autosampler into a split/splitless injector operated in splitless or split mode (7 to 30) at 250°C.

The  $\delta^{13}\text{C}$  values were calibrated using a three-point calibration of international reference materials AIEA600, USGS40, and USGS41 ( $\sigma < 0.05\text{‰}$ ). Reproducibility of triplicate measurements was  $\leq 0.2\text{‰}$  ( $1\sigma$ ) within the linearity range of the instrument (5–200 ng of carbon injected on column). A DCM and BTEX standard of known isotopic composition was measured every nine injections for quality control. Carbon isotope ratios were reported in  $\delta$  notation as parts per thousand [‰] relative to the international reference material Vienna Pee Dee-Belemnite (V-PDB) (Coplen et al., 2006).



#### A.4 Oxygen evolution under transient and steady-state conditions

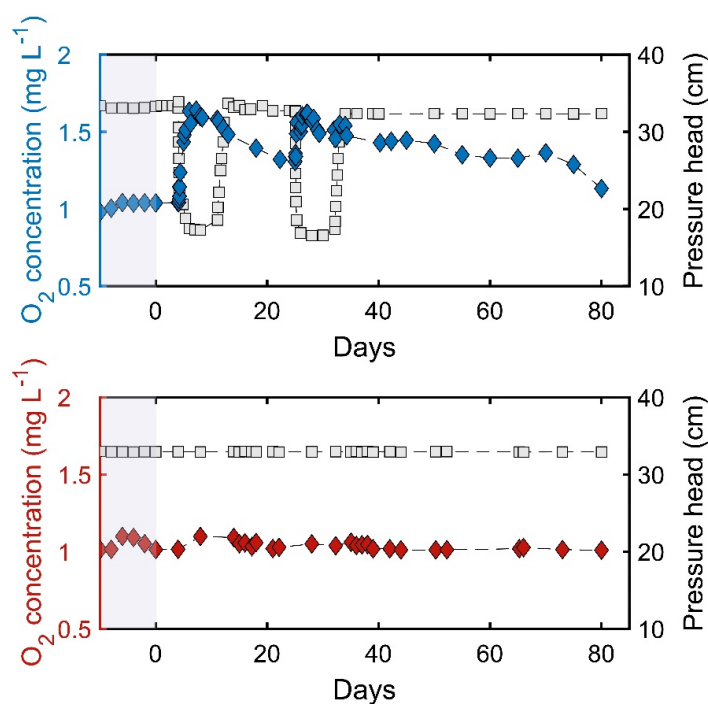


**Figure A.2:** Oxygen concentrations (diamonds) *versus* pressure head (squares) under transient (top blue) and steady-state (bottom red) conditions at depth 25 cm from the bottom. Observation points cover the experimental phase from 0 to 80 days. Grey zones represent the end of the incubation period. Error of measurement:  $\pm 0.4 \text{ mg L}^{-1}$ . Inflow groundwater concentrations:  $0.7 \pm 0.4 \text{ mg L}^{-1}$ .

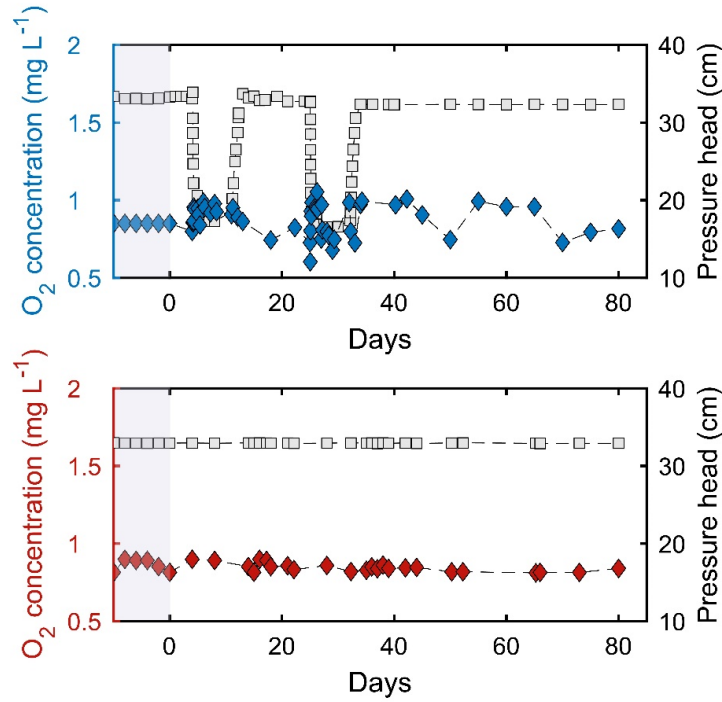


**Figure A.3:** Oxygen concentrations (diamonds) *versus* pressure head (squares) under transient (top blue) and steady-state (bottom red) conditions at depth 10 cm from the bottom. Observation points cover the experimental phase from 0 to 80 days. Grey zones represent the end of the incubation period. Error of measurement:  $\pm 0.4 \text{ mg L}^{-1}$ . Inflow groundwater concentrations:  $0.7 \pm 0.4 \text{ mg L}^{-1}$ .

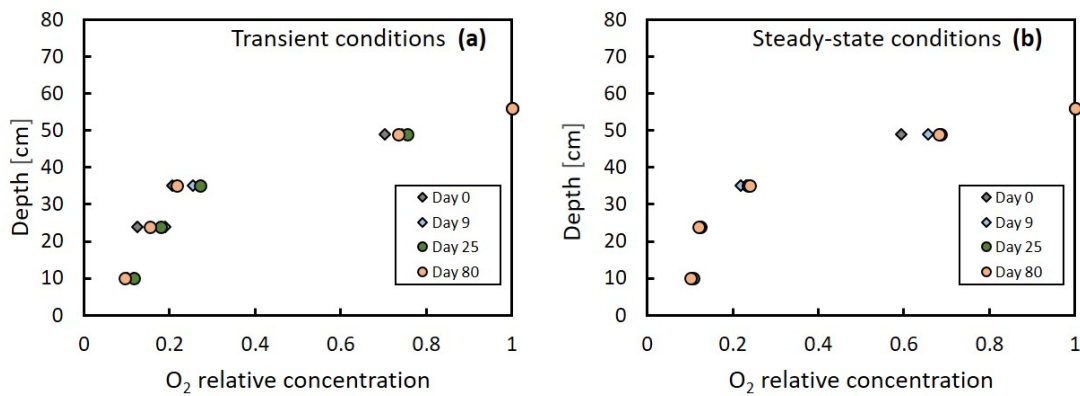


**Figure A.4:** Relative oxygen concentration *versus* depth under transient (a) and steady-state (b) conditions at  $x=65 \text{ cm}$  from the inflow. Observation points cover the experimental phase from 0 to 80 days. Error of measurement:  $\pm 0.4 \text{ mg L}^{-1}$ . The initial water table was position at 33 cm from the bottom. During water table fluctuations, the water table was dropped to 17 cm.

## A.5 Hydrochemical evolution

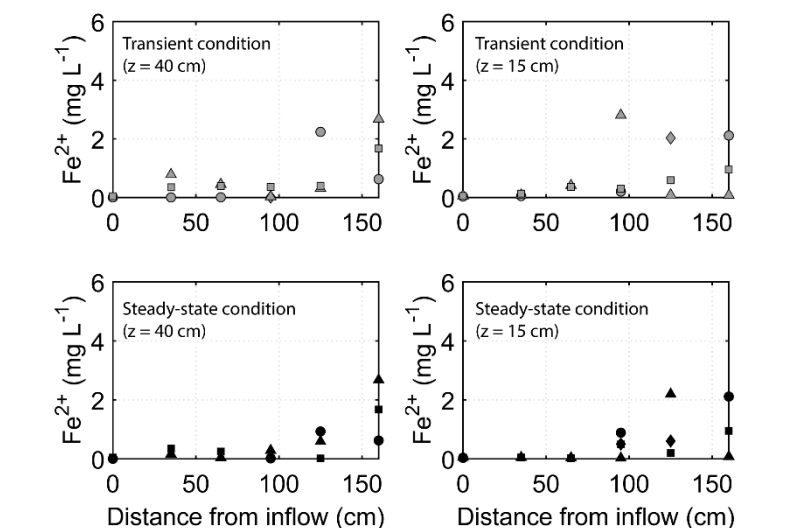


**Figure A.5:** Evolution of  $\text{Fe}^{2+}$  concentrations along the flow path in aquifers under steady-state and transient conditions. Symbols represent measured values over distance from inflow and during the investigated period: day 0 (diamonds), day 13 (circles), day 20 (triangles) and day 35 (squares).

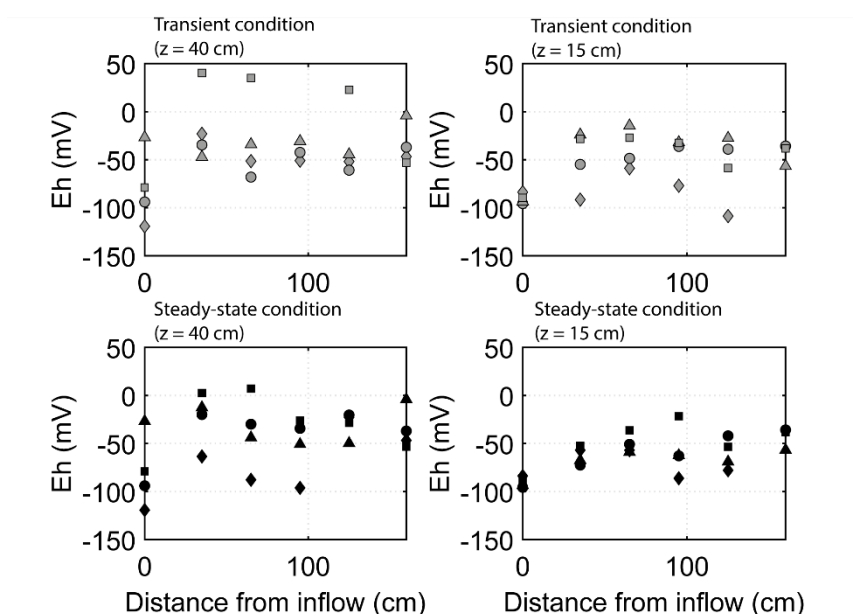


**Figure A.6:** Evolution of Eh values along the flow path in aquifers under steady-state and transient conditions. Symbols represent measured values over distance from inflow and during the investigated period: day 0 (diamonds), day 13 (circles), day 20 (triangles) and day 35 (squares).

**Table A.2:** Hydrochemistry of lab-scale aquifers fed with spiked-DCM groundwater under transient and steady-state conditions. Data represent incubation period (inc, n=10), first water table fluctuation (day 0-13, n=20), second water table fluctuation (day 20–35, n=20) and end of the experiment (day 80, n=10). The reported values correspond to mean values of measurements taken at each sampling event from sampling ports located at the inlets, outlets, and depths 15 cm and 40 from the bottom. Reported values for supplied groundwater correspond to the day of sample collection (n=3).

Parameter	Units	Groundwater	Aquifer 1: Transient condition (days)				Aquifer 2: Steady-state condition (days)			
			inc <sup>a</sup>	0-13	20-35	80	inc	0-13	20-35	80
pH	-	6.7±0.2	6.9 <sup>b</sup> ±0.1 <sup>c</sup>	6.8±0.2	7.1±0.2	6.9±0.2	6.7±0.1	7.0±0.2	7.2±0.1	6.9±0.2
Redox	mV	-170±96	-74±37	-53±27	-8±40	-35±16	-98±28	-55±37	-43±20	-50±25
Elec. Cond.	mS cm <sup>-1</sup>	2.1±1.0	0.7±0.1	0.8±0.3	1.1±0.3	0.9±0.1	0.7±0.1	0.8±0.1	0.9±0.1	0.9±0.1
Cl <sup>-</sup>	mg L <sup>-1</sup>	450±2	103±30	145±29	135±23	155±36	103±10	130±32	142±64	153±34
NO <sub>3</sub> <sup>-</sup>	mg L <sup>-1</sup>	1.9±0.1	<L.Q.	0.5±0.1	0.4±0.1	0.4±0.1	<L.Q.	0.5±0.1	0.3±0.1	<L.Q.
NO <sub>2</sub> <sup>-</sup>	mg L <sup>-1</sup>	<L.Q. <sup>d</sup>	<L.Q.	<L.Q.	<L.Q.	<L.Q.	<L.Q.	<L.Q.	<L.Q.	<L.Q.
Mn <sup>2+</sup>	mg L <sup>-1</sup>	161±0.8	37±1.0	34±4.0	28±5.3	33±5.0	37±4.0	34±4.3	29±3.2	35±4.0
Total Fe	mg L <sup>-1</sup>	-	0.4±0.2	1.4±1.3	0.7±0.8	0.5±0.6	0.6±0.4	1.3±1.2	1.1±1.1	0.5±0.5
Fe <sup>2+</sup>	mg L <sup>-1</sup>	14±6	0.5±0.3	0.6±0.8	0.6±0.8	0.5±0.5	0.3±0.2	1.2±0.8	0.6±0.8	0.3±0.3
SO <sub>4</sub> <sup>2-</sup>	mg L <sup>-1</sup>	68±10	0.9±0.4	0.8±0.3	0.7±0.3	1.1±0.7	1.1±0.5	0.8±0.2	0.5±0.3	0.8±0.1

<sup>a</sup> Total incubation period of 70 days prior to experiments. Data within the incubation period corresponds to sample collection at day 35.

<sup>b</sup> Mean values of n measurements.

<sup>c</sup> Standard deviation ( $\sigma$ ) of the mean values of n measurements.

<sup>d</sup> Below limit of quantification.

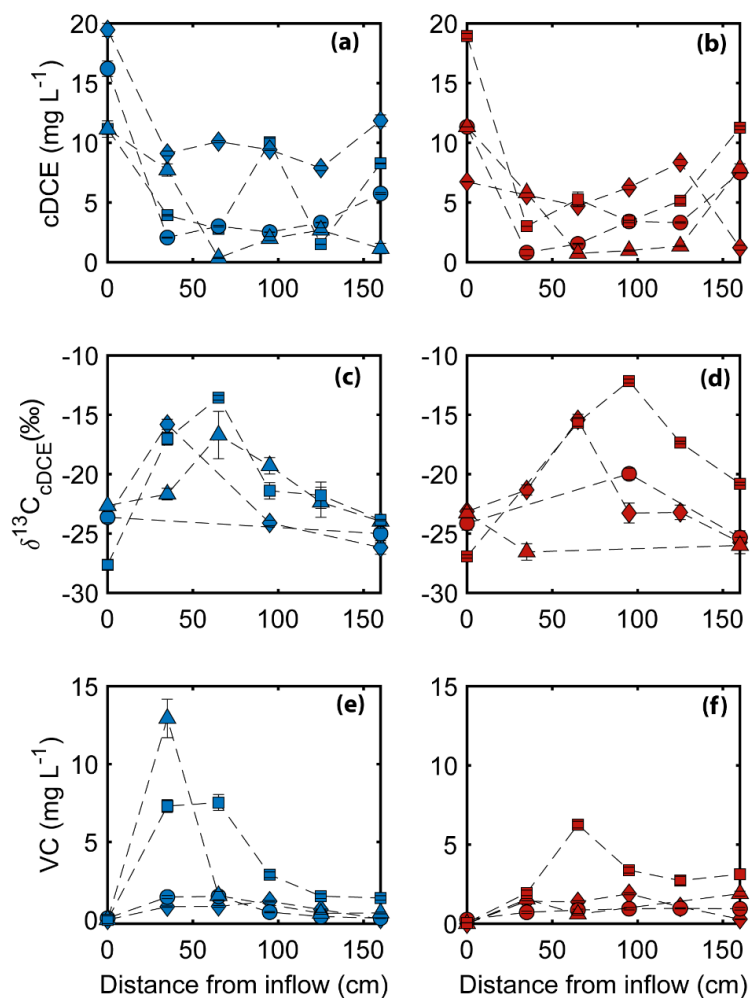
**Table A.3:** Total organic carbon (TOC), non-purgeable organic carbon (NPOC) and inorganic carbon (IC) in lab-scale aquifers fed with spiked-DCM ground-water under transient and steady-state conditions. Data represent incubation period (inc), first water table fluctuation (day 0-13), second water table fluctuation (day 20-35) and end of the experiment (day 80). Values correspond to samples collected from inlet and outlet reservoirs only (n=2).

Parameter	Units	Sample	Aquifer 1: Transient condition				Aquifer 2: Steady-state condition			
			inc <sup>a</sup>	0-13	20-35	80	inc	0-13	20-35	80
TOC	mg L <sup>-1</sup>	inlet	118 <sup>b</sup> ±15 <sup>c</sup>	110±11	80±13	98±12	76±5	99±6	78±17	90±12
		outlet	106±13	73±30	63±9	52±15	85±6	78±7	73±8	75±7
NPOC	mg L <sup>-1</sup>	inlet	118±14	120±21	100±6	100±11	100±11	107±6	89±10	96±8
		outlet	106±11	88±16	75±3	61±7	88±5	83±2	84±10	76±5
IC	mg L <sup>-1</sup>	inlet	56±5	60±7	60±3	50±5	64±3	57±3	65±2	56±4
		outlet	51±5	28±5	23±7	25±6	48±4	41±8	36±5	21±6

<sup>a</sup> Total incubation period of 70 days prior to experiments. Data within the incubation period corresponds to sample collection at day 35.

<sup>b</sup> Mean values of n measurements.

<sup>c</sup> Standard deviation ( $\sigma$ ) of the mean values of n measurements.

A.6 Concentrations and carbon isotope composition of *cis*-DCE and VC

**Figure A.7:** Concentrations and carbon isotope composition of *cis*-DCE and VC under transient (blue) and steady-state (red) conditions. Symbols represent measured values over distance from inflow and during the investigated period: day 0 (diamonds), day 13 (circles), day 20 (triangles) and day 35 (squares). Transformation of *cis*-DCE occurred in both aquifers. The newly formed VC (VC not detected at the inflow) was systematically lighter compared to *cis*-DCE with  $\delta^{13}\text{C}$  values ranging from  $-43.56 \pm 0.43\text{‰}$  to  $-35.7 \pm 0.40\text{‰}$  ( $n=20$ ).

### A.7 Rayleigh plots of DCM degradation under transient and steady-state conditions

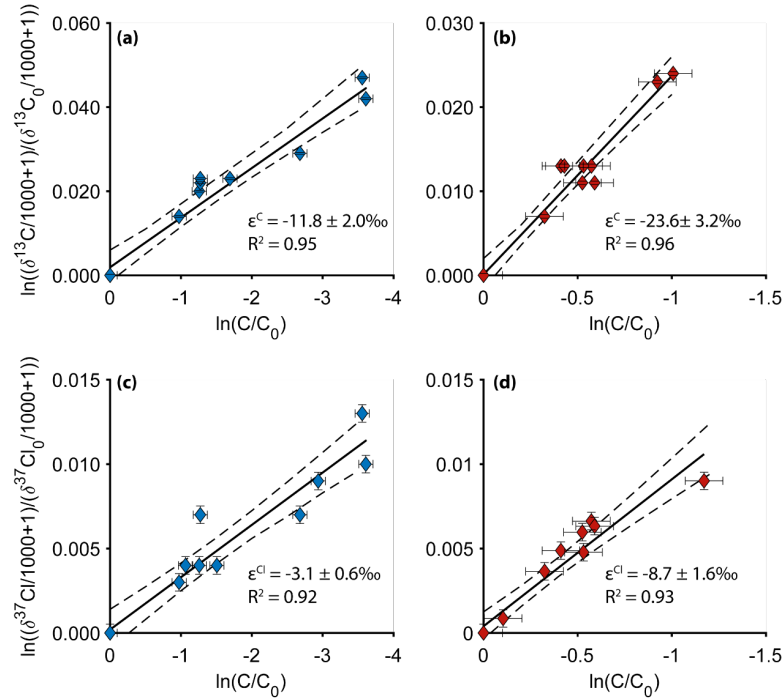


**Figure A.8:** Rayleigh plots of carbon (a, b) and chlorine (c, d) isotope ratios vs. residual DCM fraction for DCM degradation in the saturated zone of laboratory aquifers under  $\text{O}_2$ -depleted conditions from day 0 to 35. Blue: DCM degradation under transient conditions; red: DCM degradation under steady-state conditions. Carbon and chlorine isotope fractionation values ( $\epsilon_{\text{bulk}}^{\text{C}}$  and  $\epsilon_{\text{bulk}}^{\text{Cl}}$ ) were obtained from the slope of the linear regression using the Rayleigh model. Error bars represent total uncertainty of isotope ratios. Dashed lines represent the 95% confidence of interval (C.I.).

## A.8 State of the art of proposed DCM pathways and stoichiometry reactions based on stable isotope analysis

**Table A.4:** Proposed DCM degradation pathways and stoichiometry reactions based on stable isotopes.<sup>a</sup>

Experiments	$\varepsilon_C$	$\varepsilon_{Cl}$	$\Lambda^{C/Cl}$	Degradation pathway	Degradation reaction	Source
<b>Aerobic cultures</b>						
<i>Hyphomicrobium</i> sp. strain MC8b	-42.4 <sup>b</sup>	-3.8 <sup>c</sup>	11.2 <sup>b,c</sup>	Glutathione S-transferase	$CH_2Cl_2 + GSH + H_2O \rightarrow CH_2O + 2 HCl + GSH$	(Heraty et al., 1999) (Hayoun et al., 2020)
<i>Methylobacterium extorquens</i> DM4 <sup>d</sup>	-71±2.0	-7.0±0.4	9.5±0.54	Glutathione S-transferase	$CH_2Cl_2 + GSH + H_2O \rightarrow CH_2O + 2 HCl + GSH$	(Torgonskaya et al., 2019)
<b>Anaerobic cultures</b>						
<i>Dehalobacterium formicoaceticum</i>	-42.4 ± 0.7	-5.3 ± 0.1	7.89 ± 0.12	Fermentation harboring WLP	$3CH_2Cl_2 + H_2O + CO_2 \rightarrow 2HCOO^- + CH_3COO^- + 9H^+ + 6Cl^-$	(Chen et al., 2020, 2018)
Mixed culture containing <i>Dehalobacterium</i> sp.	-31 ± 3	-5.2 ± 0.6	5.9 ± 0.3	Fermentation <sup>e</sup>	n.a.	(Blázquez-Pallí et al., 2019)
Consortium RM harboring <i>Ca. Dichloromethanomonas elyunquensis</i>	-18.3 ± 0.2	-5.2 ± 0.1	3.40 ± 0.03	Mineralization (acetogenesis required) <sup>f</sup>	$CH_2Cl_2 + 2H_2O \rightarrow CO_2 + 2H_2 + 2Cl^- + 2H^+$ $4H_2 + 2CO_2 \rightarrow CH_3COO^- + H^+$	(Chen et al., 2020, 2018)
<i>Ca. Formimonas warabiya</i> strain DCMF	n.a. <sup>g</sup>	n.a.	n.a.	Fermentation harboring WLP	$CH_2Cl_2 + 2H_2O \rightarrow CH_3COO^- + H^+ + 4Cl^-$	(Holland et al., 2021)
<b>Laboratory aquifers<sup>h</sup></b>						
Transient conditions	-11.8 ± 2.0	-3.1 ± 0.6	3.58 ± 0.42	Prevailing anaerobic		This study
Steady-state conditions	-23.5 ± 2.1	-8.7 ± 1.6	1.92 ± 0.30	Prevailing anaerobic	n.a.	This study

<sup>a</sup> Uncertainties of  $\varepsilon$  and  $\Lambda$  values correspond to the 95% confidence interval (CI).

<sup>b</sup> Uncertainties were not provided by the author

<sup>c</sup>  $\Lambda^{C/Cl}$  values were calculated based on reported  $\varepsilon_C$  and  $\varepsilon_{Cl}$  data by the referenced authors.

<sup>d</sup> *M. extorquens* DM4 cell suspensions: average from "low and high density".

<sup>e</sup> Indication of fermentation pathways with formate and acetate as end products (Trueba-Santiso et al., 2017).

<sup>f</sup> DCM mineralization by *Ca. D. elyunquensis* requires the presence of  $H_2$ -consuming partner populations.

<sup>g</sup> n.a.: values were not analyzed/derived.

<sup>h</sup> This study.



## A.9 Rarefaction curves for pore water and sand OTUs and bacterial diversity

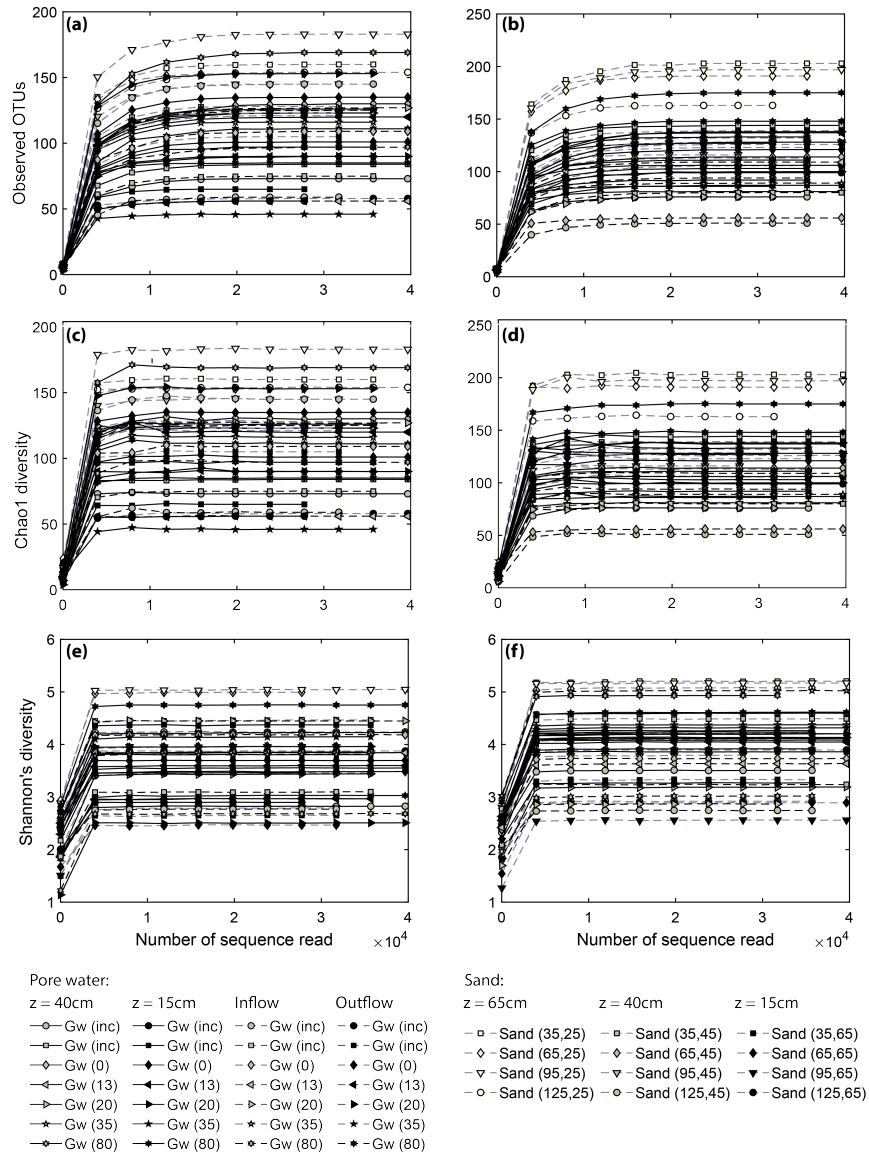


**Figure A.9:** Rarefaction curves based on OTUs (a, b),  $S_{\text{chao1}}$  diversity (c, d) and Shannon diversity (e, f) from pore water (Gw) and sand samples under transient (left) and steady-state (right) conditions. Numbers indicated in parenthesis: sand (coordinates x, y) and Gw (in days). Depth is from the bottom of the aquifers.

## A.10 Relative abundance of bacterial communities in pore water samples

### Transient conditions

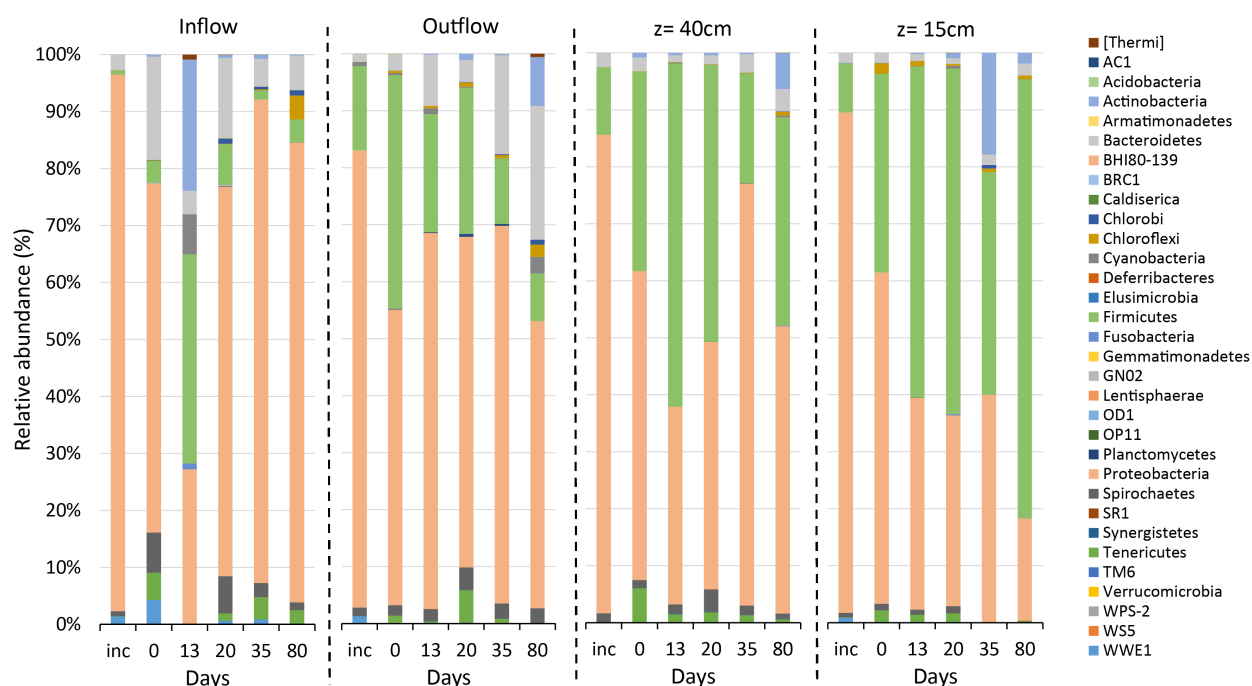


**Figure A.10:** Relative abundance of bacterial phyla in pore water samples over time in a DCM contaminated lab-scale aquifer under transient conditions. Sampling event within the incubation period (inc) corresponds to 35 days prior to the experiments.

## Steady-state conditions

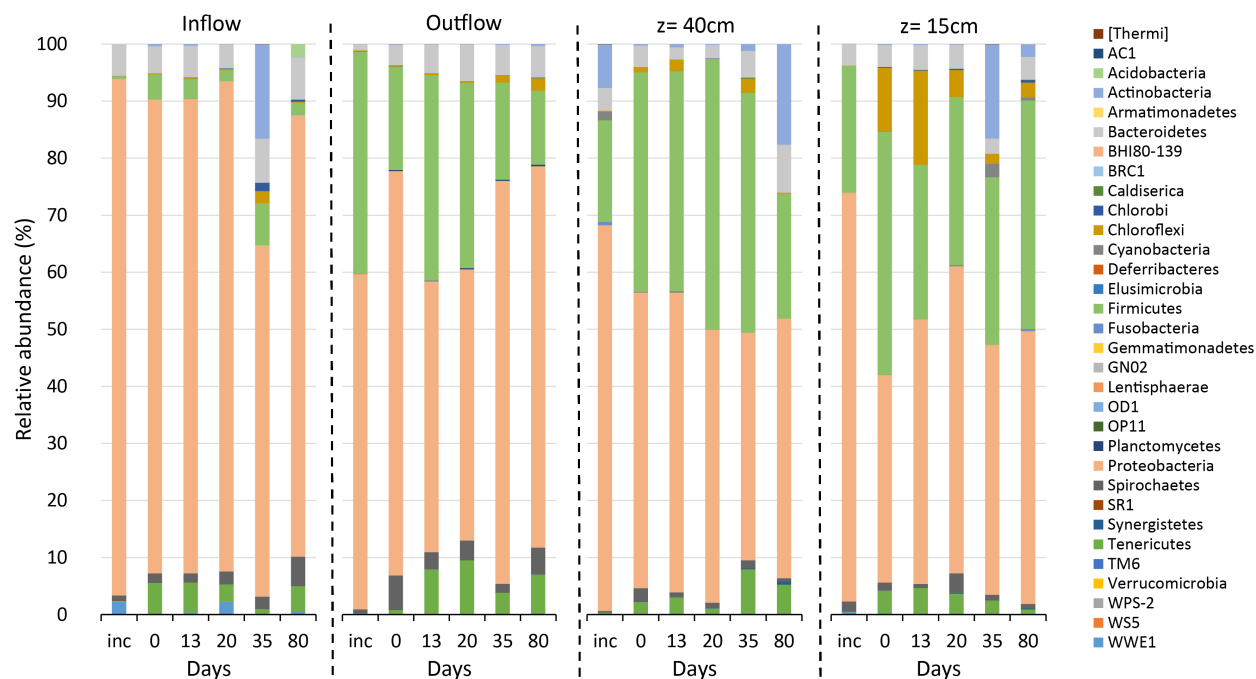


**Figure A.11:** Relative abundance of bacterial phyla in pore water samples over time in a DCM contaminated lab-scale aquifer under steady-state conditions. Sampling event within the incubation period (inc) corresponds to 35 days prior to the experiments.

### A.11 Relative abundance of bacterial communities in sand samples

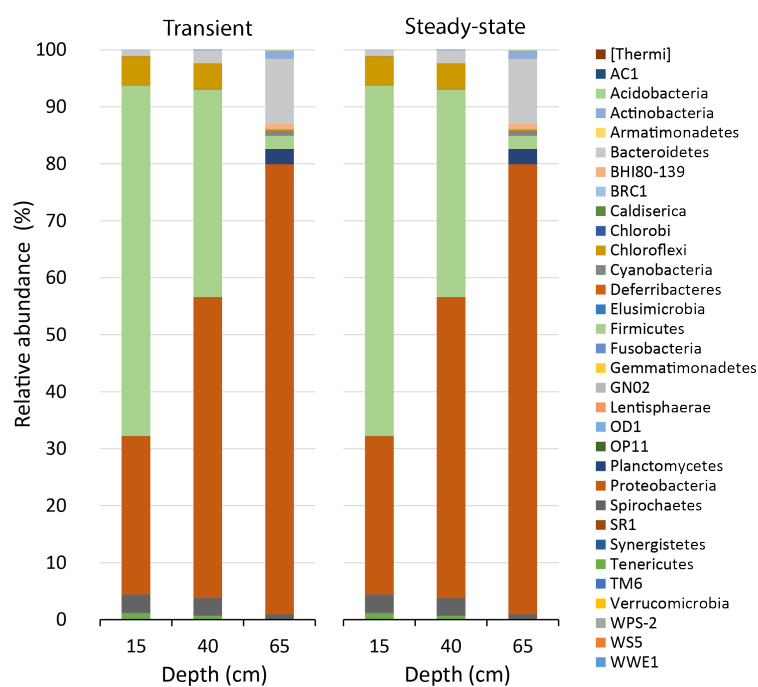


**Figure A.12:** Relative abundance of bacterial phyla in sand samples at day 88 (end of experiment), and at depths of 15, 40 and 65 cm representing anoxic zone, capillary fringe and oxic zone, respectively.

## References of Appendix A

- Blázquez-Pallí, N., Shouakar-Stash, O., Palau, J., Trueba-Santiso, A., Varias, J., Bosch, M., Soler, A., Vicent, T., Marco-Urrea, E., and Rosell, M. (2019). Use of dual element isotope analysis and microcosm studies to determine the origin and potential anaerobic biodegradation of dichloromethane in two multi-contaminated aquifers. *Science of The Total Environment*, 696:134066.
- Chen, G., Fisch, A. R., Gibson, C. M., Erin Mack, E., Seger, E. S., Campagna, S. R., and Löffler, F. E. (2020). Mineralization versus fermentation: evidence for two distinct anaerobic bacterial degradation pathways for dichloromethane. *The ISME Journal*, 14(4):959–970.
- Chen, G., Shouakar-Stash, O., Phillips, E., Justicia-Leon, S. D., Gilevska, T., Sherwood Lollar, B., Mack, E. E., Seger, E. S., and Löffler, F. E. (2018). Dual carbon-chlorine isotope analysis indicates distinct anaerobic dichloromethane degradation pathways in two members of *Peptococcaceae*. *Environmental Science & Technology*, 52(15):8607–8616.
- Coplen, T. B., Brand, W. A., Gehre, M., Gröning, M., Meijer, H. A. J., Toman, B., and Verkouteren, R. M. (2006). New guidelines for  $\delta^{13}\text{C}$  measurements. *Analytical Chemistry*, 78(7):2439–2441.
- Hayoun, K., Geersens, E., Laczny, C. C., Halder, R., Lázaro Sánchez, C., Manna, A., Bringel, F., Ryckelynck, M., Wilmes, P., Muller, E. E. L., Alpha-Bazin, B., Armengaud, J., and Vuilleumier, S. (2020). Dichloromethane degradation pathway from unsequenced *Hyphomicrobium* sp. MC8b rapidly explored by pan-proteomics. *Microorganisms*, 8(12):1876.
- Heckel, B., Rodríguez-Fernández, D., Torrentó, C., Meyer, A., Palau, J., Domenech, C., Rosell, M., Soler, A., Hunkeler, D., and Elsner, M. (2017). Compound-specific chlorine isotope analysis of tetrachloromethane and trichloromethane by gas chromatography-isotope ratio mass spectrometry vs gas chromatography-quadrupole mass spectrometry: Method development and evaluation of precision and trueness. *Analytical Chemistry*, 89(6):3411–3420.
- Heraty, L., Fuller, M., Huang, L., Abrajano, T., and Sturchio, N. (1999). Isotopic fractionation of carbon and chlorine by microbial degradation of dichloromethane. *Organic Geochemistry*, 30(8):793–799.
- Hermon, L., Denonfoux, J., Hellal, J., Joulain, C., Ferreira, S., Vuilleumier, S., and Imfeld, G. (2018). Dichloromethane biodegradation in multi-contaminated groundwater: Insights from biomolecular and compound-specific isotope analyses. *Water Research*, 142:217–226.
- Holland, S. I., Ertan, H., Manefield, M. J., and Lee, M. (2021). A novel, dichloromethane-fermenting bacterium in the *Peptococcaceae* family, *Candidatus formamonas warabiya*, gen. nov. sp. nov. *The ISME journal*, 5(6):1709–1721.
- Jin, B., Laskov, C., Rolle, M., and Haderlein, S. B. (2011). Chlorine isotope analysis of organic contaminants using GC-qMS: Method optimization and comparison of different evaluation schemes. *Environmental Science and Technology*, 45(12):5279–5286.

- Torgonskaya, M. L., Zyakun, A. M., Trotsenko, Y. A., Laurinavichius, K. S., Kümmel, S., Vuilleumier, S., and Richnow, H. H. (2019). Individual stages of bacterial dichloromethane degradation mapped by carbon and chlorine stable isotope analysis. *Journal of Environmental Sciences*, 78:147–160.



# Appendix **B**

## Supporting information of Chapter 4



## B.1 Mathematical model for two phase flow

### B.1.1 Mass-momentum conservation equations for the capillary fringe

Due to capillary effects, averaged pressure fields of each phase are not equal, therefore, a macro-scale capillary pressure  $p_c$  depending on the water saturation  $s_w$  is defined:

$$p_c = p_n - p_w \quad (\text{B.1})$$

where  $p_n$  is the pressure of the non-wetting phase and  $p_w$  the pressure of the wetting phase in Pa. The  $p_c$  values are usually obtained from correlation model for example Brooks-Corey or Van Genuchten models.

Introducing capillary pressure in water mass-momentum equation gives:

$$\begin{cases} -\phi \frac{\partial S_w}{\partial t} + \nabla \cdot \left( -\frac{kr_n(s_w)}{\mu_n} \mathbf{K}_s \cdot (\nabla p_n - \rho_n \mathbf{g}) \right) = Q_n \\ \phi \frac{\partial S_w}{\partial t} + \nabla \cdot \left( -\frac{kr_w(s_w)}{\mu_w} \mathbf{K}_s \cdot (\nabla p_n - \nabla p_c(s_w) - \rho_w \mathbf{g}) \right) = Q_w \end{cases} \quad (\text{B.2})$$

where  $p_n$  is the non-wetting (air  $n = g$ ) pressure and  $s_w$  wetting pressure (water) are the system variables.

### B.1.2 Fractional gas/water flow formulation

The mass conservation equations are reformulated into a pressure-saturation system of equation, the pressure equation in  $p_n$  is obtained by summing the two previous equations. The relative phase mobility  $\lambda_\alpha$  is introduced :

$$\lambda_\alpha = \frac{kr_\alpha(s_w)}{\mu_\alpha} \quad (\text{B.3})$$

The capillary pressure only depends on water saturation, thus  $\nabla p_c$  can be written as:

$$\nabla p_c = \frac{dp_c}{dS_w} \nabla S_w = p'_c(s_w) \nabla S_w \quad (\text{B.4})$$

which allows to reformulate the non-wetting phase pressure in Poisson-type equation:

$$\nabla \cdot \left( \lambda_t \nabla p_g \right) = -\nabla \cdot \left( \bar{\rho} \mathbf{g} - \lambda_g p'_c \nabla S_w \right) + Q_w + Q_g \quad (\text{B.5})$$

where  $\bar{\rho} = \lambda_w \rho_w + \lambda_g \rho_g$  in  $\text{kg/m}^3$  is the total mass density and  $\lambda_t = \lambda_w + \lambda_n$  is the total phase mobility and the saturation equation:

$$\phi \frac{\partial S_w}{\partial t} + \nabla \cdot \left( -\lambda_w \nabla p_g + \lambda_w \rho_w \mathbf{g} + \lambda_g p'_c \nabla S_w \right) = Q_w \quad (\text{B.6})$$

Pressure gradient, gravity and capillary pressure are computed on face of the computational grid using a cell-centered-to-face-centered interpolation and involving a face weighting factor. The values of  $\phi$  are known at the control volume centroids  $c_1$  and  $c_2$ , and are to be used to compute the value of  $\phi$  at the interface  $f$ . A simple linear interpolation will result in the following formula:

$$\phi \Big|_f = W_f \phi_{c_1} + (1 - W_f) \phi_{c_2} \text{ and } W_f = \frac{\mathbf{d}_{c_1 f} \cdot \mathbf{n}_f}{\mathbf{d}_{c_1 f} \cdot \mathbf{n}_f + \mathbf{d}_{f c_2} \cdot \mathbf{n}_f} \quad (\text{B.7})$$

with  $\mathbf{n}_f$  the outward normal unit vector of face  $f$  and  $\mathbf{d}_{cf}$  the tangential vector from node  $c$  to center of face  $f$ . Therefore, fluxes are written:

$$\phi_p \Big|_f = \lambda_t \Big|_f \nabla p_n \cdot \mathbf{n}_f ||f|| \quad (\text{B.8})$$

$$\phi_g \Big|_f = \bar{\rho} \Big|_f \mathbf{g} \cdot \mathbf{n}_f ||f|| \quad (\text{B.9})$$

$$\phi_c \Big|_f = \lambda_w \Big|_f \left( p'_c \nabla S_w \right) \Big|_f \cdot \mathbf{n}_f ||f|| \quad (\text{B.10})$$

where  $||f||$  is the length/area of the face. The global flux is computed as follows:

$$\phi \Big|_f = \phi_p \Big|_f + \phi_g \Big|_f + \phi_c \Big|_f \quad (\text{B.11})$$

and the flux of wetting phase  $w$  can be expressed as:

$$\phi_w \Big|_f = \left( \frac{\lambda_w}{\lambda_t} \phi_p \right) \Big|_f + \left( \frac{\lambda_w \rho_w}{\bar{\rho}} \phi_g \right) \Big|_f + \phi_c \Big|_f \quad (\text{B.12})$$

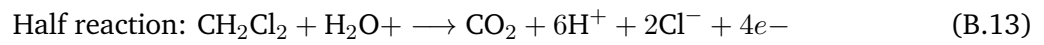
**Table B.1:** Flow parameters according to Brooks-corey model.

Type	value	unity	variation	remark
$\phi$	0.37	-		porosity
$K_{xx}$	$4 \times 10^{-11}$	$\text{m}^2$		isotropic permeability tensor $x$
$K_{yy}$	$4 \times 10^{-11}$	$\text{m}^2$		isotropic permeability tensor $y$
$K_{xy}$	0	$\text{m}^2$		isotropic permeability tensor $xy$
$\mu_w$	$1.308 \times 10^{-3}$	Pa s		dynamic viscosity of water
$\mu_g$	$1 \times 10^{-5}$	Pa s		dynamic viscosity of gas Kim et al. (2019)
$s_w^{\min}$	0.001	-		minimal water saturation (numerical)
$s_w^{\max}$	0.999	-		maximal water saturation (numerical)
$s_{wr}$	0.087	-		irreducible saturation of phase $w$
$\lambda$	2	-		Brooks-Corey pore size distribution index
$p_d$	1850.	Pa		Brooks-Corey entry pressure
$\rho_w$	1000.	$\text{kg}/\text{m}^3$		water mass density
$\rho_g$	1.225	$\text{kg}/\text{m}^3$	1 – 1.3	Gas mass density

## B.2 Stoichiometry of pathway-specific degradation reactions of DCM

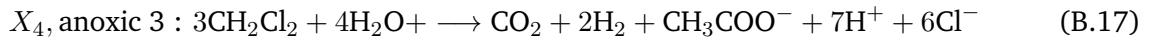
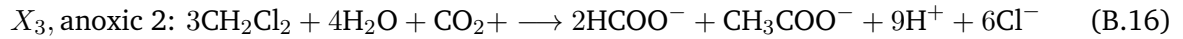
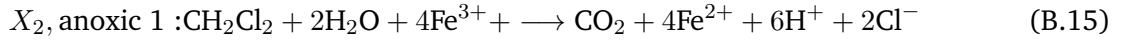
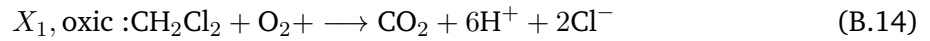
When microbial activity is coupled to biomass growth, the overall stoichiometry of the reaction is altered due to transfer of electrons during chemical reactions. Substrate utilization for both energy and growth metabolism is assumed, where biomass is considered in a simplified chemical form of  $C_5H_7O_2N$  (Rittmann, 2006).

Consider the mineralization of dichloromethane (DCM) under oxic and anoxic conditions, with DCM as the sole carbon source.

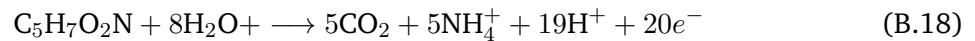


Balanced stoichiometry reactions of energy metabolism can thus be described according to distinct electron acceptors.

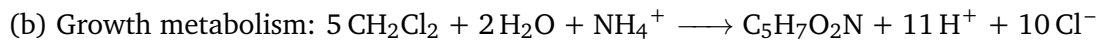
(a) Energy metabolisms for all DCM bacterial populations can be described as:



Oxidation of biomass  $C_5H_7O_2N$  can be described as (Rittmann, 2006):



Balancing the half reactions (B.13) and (B.18) leads to the growth metabolism reaction equation:



Stoichiometric reaction (b) shows that 5 moles of DCM are required to produce 1 mol of biomass ( $C_5H_7O_2N$ ). In other words, the specific yield may be expressed as  $0.2 [mol_{bio}/mol_{DCM}]$ . Let's now assume that 50% of DCM is assimilated (incorporated in the biomass) and the rest is degraded. Thus, the specific yield needs to be multiplied by a factor of 0.5 which results in  $11.3 [g_{bio}/mol_{DCM}]$  ( $C_5H_7O_2N$  molar mass: 113 g/mol).

The total growth reaction for producing 11.3 [g,bio/mol,DCM] is:  $f \cdot \text{equations}(a) + \text{equation}(b)$  (VanBriesen and Rittmann, 2000). The term  $f$  denotes a factor used to obtain a linear combination of both energy and growth metabolisms meeting the yield of the reaction. Factor  $f$  can be computed using equation B.19.

$$f = \frac{1 - Y * f_g}{Y * f_e} \quad (\text{B.19})$$

where  $f_g$  is the ratio of moles of DCM consumed to produce 1 g of biomass during growth metabolism, and  $f_e$  is the ratio of moles of DCM consumed during energy metabolism. The factor  $f$  is used to obtain the linear combination of both metabolisms and obtain the total growth reaction. For bacterial populations  $X_1$ ,  $X_2$ ,  $X_{5,ox}$  and  $X_{5_a,nox}$ ,  $f$  was calculated as 0.044, and for bacterial populations  $X_3$  and  $X_4$  as 0.015.

### B.3 Numerical resolution

The numerical resolution of the multi-phase flow, multi-processes cubicM model was developed at the Institut Terre et Environnement de Strasbourg, France (CubicM model; Dr. Raphaël Di Chiara) (Chastanet et al., 2014; Di Chiara Roupert, 2009; Di Chiara Roupert et al., 2017). The flow is solved by an IMPES scheme (IMplicit in gas Pressure and Euler Explicit in water Saturation) with a finite volume discretization centered on the nodes (CVFE). The linear solver for the gas phase is a preconditioned conjugate gradient (PCG, diagonal preconditioning based on a DIC incomplete Cholesky decomposition, symmetric matrix, abs tol  $1e^{-12}$ ). The gas is assumed to be incompressible and the density does not change with the phase composition, the  $\rho_g$  gradient is neglected. A Courant criterion is imposed for saturation (0.5) which can be declined with other criteria (Coats), allowing higher time steps ( $\sim 2.7$  sec) for the explicit resolution of water saturation and taking into account capillary diffusion and gravity effects. Following the Method Of Line (MOL) framework, the transport (non-symmetric matrix) is solved with a large-scale preconditioned differential-algebraic solver using a Krylov method (DASPK) (Brown et al., 1994) and performing an adaptive time-step strategy based on interpolation of previous time solutions (BDF scheme). A possible option would be to freeze the flow and solve the transport faster (larger BDF time step).

A linear solver for non-symmetric matrix is used PBicCGstab (preconditioned and stabilized Bi conj gradient) with a diagonal preconditioning (incomplete LU decomposition, DILU). A variant called cubicMIsotopFoam integrating a distributed parallelization is implemented (PStream library of OpenFoam 9 solver, Weller et al. (1998)) to handle massively parallel cases. Finally, the whole code is now integrated in a user interface coded in python (3.10.2) and based on the QT 15.2 library, initially coded with DISLIN (Michels, 1998).

**Adaptative time step strategy:** To avoid sudden and too large increases of the time-step which could lead to numerical instabilities, an optimal time step is computed as the minimum between transport  $\Delta t_{trans}$  (based on truncation error) and flow ( $\Delta t_{flow}$ ) processes based on CFL criterion:

$$\Delta t_{flow} = \min(\min(c_{\Delta t}, 1 + 0.1c_{\Delta t}), 1.2) \Delta t_{last} \text{ and } c_{\Delta t} = \frac{CFL_{max}}{CFL} \quad (B.20)$$

$$\text{with } CFL = \max_{\forall cells} \left[ \frac{\Delta t}{\phi \mathcal{V}_{cell}} \left( \frac{\partial p_c}{\partial s_w} K \frac{\lambda_w \lambda_g}{\lambda_w + \lambda_g} \sum_f^{\mathcal{N}_f} \mathcal{T}_f + \frac{\partial f_w}{\partial s_w} \sum_f^{\mathcal{N}_f} \phi_f \right) \right] \quad (B.21)$$

where  $\phi_f$  is the total flux at face  $f$ ,  $\mathcal{N}_f$  is the total number of face of a given cell,  $f_w = \lambda_w / (\lambda_w + \lambda_g)$  is the water fractional flux,  $\mathcal{T}_f = K_f ||S_f|| / \Delta x_f$  is the transmissivity of the face  $f$ ,  $\Delta x_f$

is the distance between the centers of two neighboring cells,  $K_f$  is the interpolated intrinsic permeability at face  $f$  (linear) and  $\mathbf{S}_f = \mathbf{n}_f ||f||$  is the oriented outward scale vector. The constant  $\text{CFL}_{\max}$  is fixed to 0.75.

## B.4 Parameters used for all test cases

All parameters are listed in Tables B.2 and B.3.

**Table B.2:** Parameter set for all test cases (no calibration is done from experiment), index  $j$  is referred to  $j$ th-isotopologue of DCM. (Part 1)

Type	value	unity	remark
$T$	21	°C	experiment
$\alpha_l$	0.05	m	estimated
$\alpha_t$	0.0005	m	estimated
$s_s = 1 - \phi$	63%	—	solid fraction
$D_{w,j}^{mol}$	$7.2 \times 10^{-10}$	$m^2/s$	$j = DCM_j$
$D_{w,i}^{mol}$	$2.2 \times 10^{-9}$	$m^2/s$	$i = CO_2, O_2$
$D_{w,i}^{mol}$	$1 \times 10^{-10}$	$m^2/s$	$i = Fe, Cl, acetate, formate, DOC$
$D_{g,j}^{mol}$	$1.0 \times 10^{-6}$	$m^2/s$	$j = DCM_j$
$D_{g,O_2}^{mol}$	$2.2 \times 10^{-5}$	$m^2/s$	Hron et al. (2015)
$D_{g,CO_2}^{mol}$	$1.35 \times 10^{-5}$	$m^2/s$	Hron et al. (2015)
$\Gamma_{volat,j}$	$1.16 \times 10^{-6}$	1/s	calibrated
$\Gamma_{volat,i}$	$1. \times 10^{-7}$	1/s	calibrated, $i = CO_2, O_2$
$v_w$	0.233	m/d	simulated
$C_j^{eq}$	13.2	g/L	Kim et al. (2019); Yaws (1999)
$C_{O_2}^{eq}$	$8.26 \times 10^{-3}$	g/L	Kim et al. (2019); Yaws (1999)
$C_{CO_2}^{eq}$	$6.06 \times 10^{-4}$	g/L	Kim et al. (2019); Yaws (1999)
$M_{mol,j}$	84.9331	g/mol	constant
$M_{mol,O_2}$	32	g/mol	constant
$M_{mol,CO_2}$	44	g/mol	constant
$M_{mol,Cl}$	35.45	g/mol	constant
$M_{mol,Fe}$	55.84	g/mol	constant
$M_{mol,DOC}$	30	g/mol	constant
$M_{mol,HCO_2^-}$	45	g/mol	constant
$M_{mol,C_2H_3O_2^-}$	59	g/mol	constant
$p_{O_2}^{vap}$	19184	Pa	estimated
$p_{CO_2}^{vap}$	78123	Pa	estimated
$p_j^{vap}$	4740	Pa	Kim et al. (2019); Yaws (1999)

**Table B.3:** Parameter set for all test cases (no calibration is done from experiment), index  $j$  is referred to  $j$ th-isotopologue of DCM. (Part 2)

Type	value	unity	remark
$\gamma_j$	1	—	activity of $j$
$H_{k,j}^{cc}$	$8.49 \times 10^{-2}$	—	EPA data base at 21°C
$m_{bact}$	$5 \times 10^{-13}$	g	From Hron et al. (2015)
$\psi_\kappa$	[0 : 1]	—	see Equation (4.25)
$Y_{X_k/j}$	0.133	$g_{bio}/g_j$	see Section 4.2.6
$E_{O_2/j}$	0.188	$g_{O_2}/g_j$	see Section 4.2.6
$E_{Fe/j}$	3.72	$g_{Fe}/g_j$	see Section 4.2.6
$E_{CO_2,K_3/j}$	0.078	$g_{CO_2}/g_j$	see Section 4.2.6
$E_{CO_2,K_4/j}$	0.088	$g_{CO_2}/g_j$	see Section 4.2.6
$E_{O_2/DOC}$	0.533	$g_{O_2}/g_{DOC}$	see Section 4.2.6
$E_{Fe/DOC}$	1.31	$g_{Fe}/g_{DOC}$	see Section 4.2.6
$\Upsilon_{CO_2/j}^{1,2}$	0.965	$g_{CO_2}/g_{bio}$	see Section 4.2.6
$\Upsilon_{Cl-/j}^\kappa$	0.835	$g_{Cl-}/g_{bio}$	see Section 4.2.6
$\Upsilon_{HCO_2^-/j}^3$	0.525	$g_{HCO_2^-}/g_j$	see Section 4.2.6
$\Upsilon_{C_2H_3O_2^-/j}^3$	0.104	$g_{C_2H_3O_2^-}/g_j$	see Section 4.2.6
$\Upsilon_{C_2H_3O_2^-/j}^4$	0.118	$g_{C_2H_3O_2^-}/g_j$	see Section 4.2.6
$\Upsilon_{CO_2/DOC}^{ox,an}$	0.733	$g_{CO_2}/g_{DOC}$	see Section 4.2.6
$\mu_{max}^{ox,1}$	$1 \times 10^{-6}$	1/s	Hron et al. (2015)
$\mu_{max}^{ox,5}$	$1 \times 10^{-5}$	1/s	Hron et al. (2015); Rolle et al. (2010)
$\mu_{max}^{an,2,3,4}$	$1 \times 10^{-6}$	1/s	Hron et al. (2015); Rolle et al. (2010)
$\mu_{max}^{an,5}$	$1 \times 10^{-7}$	1/s	Hron et al. (2015); Rolle et al. (2010)
$m_{O_2,Fe,CO_2}$	0.003	—	see Hron et al. (2015)
$k_\kappa^{dec}$	$2.31 \times 10^{-9}$	1/s	see Hron et al. (2015)
$k_\kappa^{att}$	$3 \times 10^{-4}$	1/s	see Hron et al. (2015)
$k_\kappa^{det}$	$6.2 \times 10^{-6}$	1/s	see Hron et al. (2015)
$c_s^{max}$	$1.6 \times 10^8$	cells/mL	see Hron et al. (2015)
$B_{DOC}$	1.8	—	see Hron et al. (2015)
$B_{DCM}^{ox}$	1.8	—	see Hron et al. (2015)
$B_{DCM}^{an,2,3,4}$	3.	—	see Hron et al. (2015)
$B_{O_2,Fe,CO_2}$	0.019	—	see Hron et al. (2015)
$m_{O_2,Fe,^3CO_2,^4CO_2}$	0	—	-



**Table B.4:** Pathway-specific reaction rates of DCM carbon-chlorine isotopologues for  $\varepsilon_C^\kappa = -42.4\text{‰}$  and  $\varepsilon_{Cl}^\kappa = -3.8\text{‰}$  in oxic condition ( $\kappa = 1$ ) following Glutathione S-transferase pathway and mediated by *Hyphomicrobium* sp. strain MC8b with  $\Lambda^{C/Cl} = 11.2$  (see Heraty et al. (1999).)

DCM $j$ th isotopologue	Carbon $^{12}\text{C}$	$^{13}\text{C}$ ( $= a_j$ )	Chlorine $^{35}\text{Cl}$	$^{37}\text{Cl}$ ( $= b_j$ )	Abundance $A_j$ %	$\kappa$ -AKIE	$\kappa$ -rate $\alpha_j$
1 : $\text{CCl}_2$	1	0	2	0	56.7744	1	1
2 : $^{13}\text{CCl}_2$	0	1	2	0	0.6379	1.04428	0.95760
3 : $\text{CCl} - ^{37}\text{Cl}$	1	0	1	1	36.3090	1.00381	0.99620
4 : $^{13}\text{CCl} - ^{37}\text{Cl}$	0	1	1	1	0.4080	1.04826	0.95396
5 : $\text{C}^{37}\text{Cl}_2$	1	0	0	2	5.8052	1.00764	0.99241
6 : $^{13}\text{C}^{37}\text{Cl}_2$	0	1	0	2	0.6052	1.05226	0.95034

**Table B.5:** Pathway-specific reaction rates of DCM carbon-chlorine isotopologues for  $\varepsilon_C^\kappa = -15.5\text{‰}$  and  $\varepsilon_{Cl}^\kappa = -5.2\text{‰}$  (assumed) under anoxic iron-reducing condition ( $\kappa = 2$ ) mediated by *Dehalobacter* sp. with  $\Lambda^{C/Cl} = 2.98$  (see Lee et al. (2015).)

DCM $j$ th isotopologue	Carbon $^{12}\text{C}$	$^{13}\text{C}$ ( $= a_j$ )	Chlorine $^{35}\text{Cl}$	$^{37}\text{Cl}$ ( $= b_j$ )	Abundance $A_j$ %	$\kappa$ -AKIE	$\kappa$ -rate $\alpha_j$
1 : $\text{CCl}_2$	1	0	2	0	56.7744	1	1
2 : $^{13}\text{CCl}_2$	0	1	2	0	0.6379	1.02407	0.9845
3 : $\text{CCl} - ^{37}\text{Cl}$	1	0	1	1	36.3090	1.00523	0.99480
4 : $^{13}\text{CCl} - ^{37}\text{Cl}$	0	1	1	1	0.4080	1.02942	0.97938
5 : $\text{C}^{37}\text{Cl}_2$	1	0	0	2	5.8052	1.01048	0.98963
6 : $^{13}\text{C}^{37}\text{Cl}_2$	0	1	0	2	0.6052	1.03480	0.97423

**Table B.6:** Pathway-specific reaction rates of DCM carbon-chlorine isotopologues for  $\varepsilon_C^\kappa = -42.4\text{‰}$  and  $\varepsilon_{Cl}^\kappa = -5.3\text{‰}$  in anoxic condition ( $\kappa = 3$ ) mediated by *Dehalobacterium formicoaceticum* following the WLP with  $\Lambda^{C/Cl} = 7.89 \pm 0.12$  (see Chen et al. (2018); Kleindienst et al. (2019).)

DCM $j$ th isotopologue	Carbon $^{12}\text{C}$	$^{13}\text{C}$ ( $= a_j$ )	Chlorine $^{35}\text{Cl}$	$^{37}\text{Cl}$ ( $= b_j$ )	Abundance $A_j$ %	$\kappa$ -AKIE	$\kappa$ -rate $\alpha_j$
1 : $\text{CCl}_2$	1	0	2	0	56.7744	1	1
2 : $^{13}\text{CCl}_2$	0	1	2	0	0.6379	1.04427	0.95760
3 : $\text{CCl} - ^{37}\text{Cl}$	1	0	1	1	36.3090	1.00533	0.99470
4 : $^{13}\text{CCl} - ^{37}\text{Cl}$	0	1	1	1	0.4080	1.04984	0.95252
5 : $\text{C}^{37}\text{Cl}_2$	1	0	0	2	5.8052	1.01068	0.98943
6 : $^{13}\text{C}^{37}\text{Cl}_2$	0	1	0	2	0.6052	1.05544	0.94748

**Table B.7:** Pathway-specific reaction rates of DCM carbon-chlorine isotopologues for  $\varepsilon_C^\kappa = -18.3\text{‰}$  and  $\varepsilon_{Cl}^\kappa = -5.2\text{‰}$  in anoxic condition ( $\kappa = 4$ ) mediated by *Ca. Dichloromethanomonas elyunquensis* following the WLP with  $\Lambda^{C/Cl} = 3.40 \pm 0.03$  (see Chen et al. (2018); Kleindienst et al. (2019)).

DCM $j$ th isotopologue	Carbon $^{12}\text{C}$	$^{13}\text{C}$ ( $= a_j$ )	Chlorine $^{35}\text{Cl}$	$^{37}\text{Cl}$ ( $= b_j$ )	Abundance $A_j$ %	$\kappa$ -AKIE	$\kappa$ -rate $\alpha_j$
1 : $\text{CCl}_2$	1	0	2	0	56.7744	1	1
2 : $^{13}\text{CCl}_2$	0	1	2	0	0.6379	1.01864	0.98170
3 : $\text{CCl} - ^{37}\text{Cl}$	1	0	1	1	36.3090	1.00523	0.99480
4 : $^{13}\text{CCl} - ^{37}\text{Cl}$	0	1	1	1	0.4080	1.02397	0.97660
5 : $\text{C}^{37}\text{Cl}_2$	1	0	0	2	5.8052	1.01048	0.98963
6 : $^{13}\text{C}^{37}\text{Cl}_2$	0	1	0	2	0.6052	1.02932	0.97152

## B.5 DCM gas phase concentrations

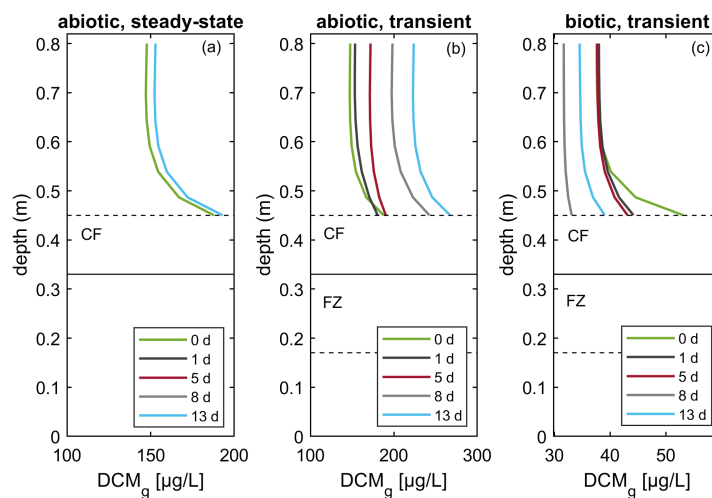


**Figure B.1:** Evolution of DCM gas-phase concentrations during one water table fluctuation cycle (0–13 days) in (a) abiotic transport case under steady-state conditions, (b) abiotic transport case under transient conditions, and (c) biotic case (test case 3) under transient conditions. Continuous horizontal line shows the position of the water table and dashed lines represented the upper part of the capillary fringe (CF) and the position of the water table after one drainage event (fluctuation zone, FZ).

## B.6 Anaerobic DCM degradation by individual bacterial populations

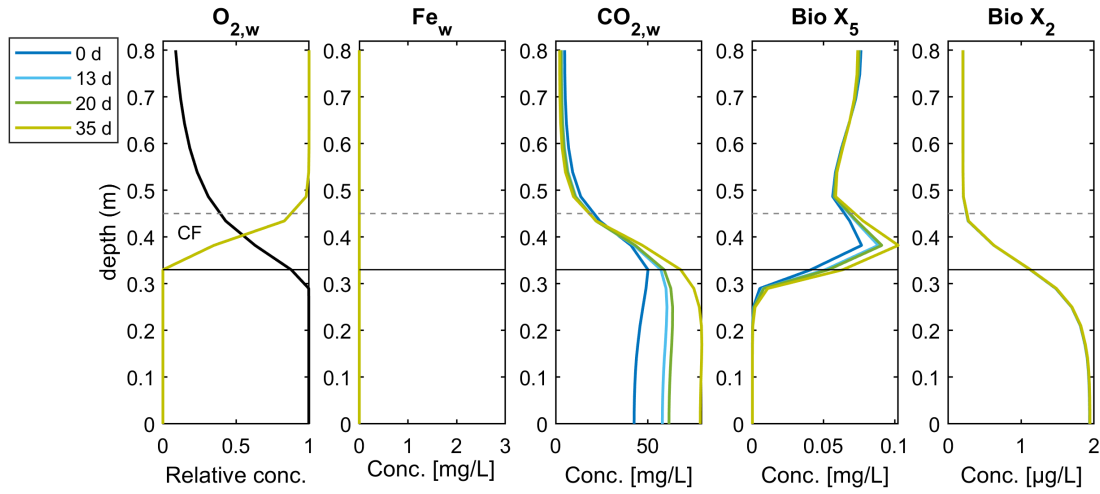


**Figure B.2:** DCM degradation by bacterial population  $X_2$  (*Dehalobacter* sp.) in the presence of a non-DCM degrader ( $X_5$ ) under steady-state conditions. Evolution of  $O_2$ , ferric iron and  $CO_2$ , and bacterial populations  $X_5$  and  $X_2$ . In addition to oxygen vertical profile (left), the gravimetric saturation (in black) is given. Horizontal line is the position of the water table. Dashed line is the upper boundary of the capillary fringe.

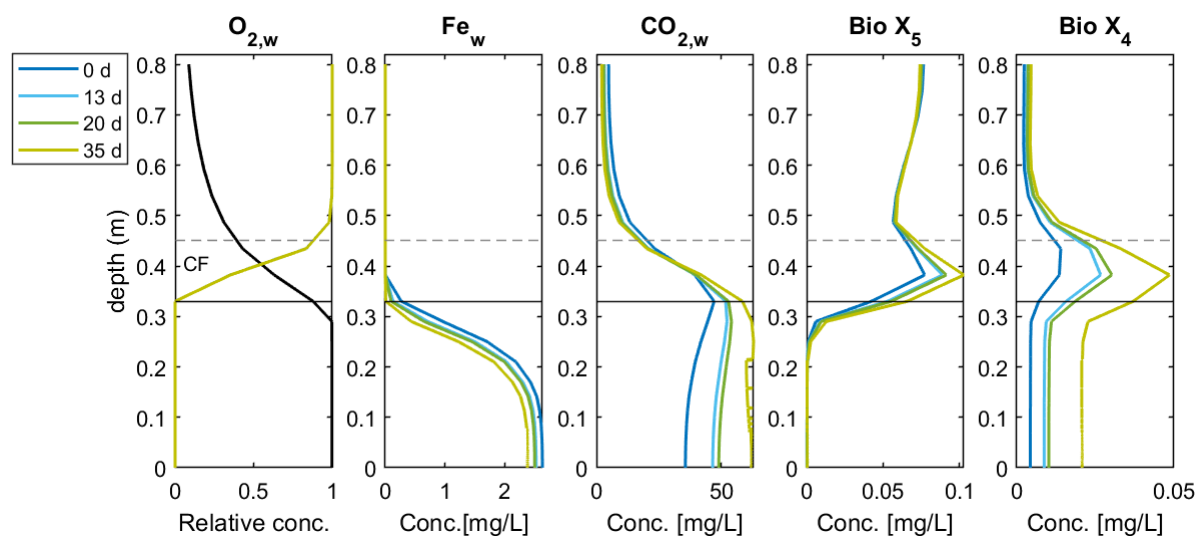


**Figure B.3:** DCM degradation by bacterial population  $X_4$  (*Ca D. elyunquensis*) of a non-DCM degrader ( $X_5$ ) under steady-state conditions. Evolution of  $O_2$ , ferric iron and  $CO_2$ , and bacterial populations  $X_5$  and  $X_4$ . In addition to oxygen vertical profile (left), the gravimetric saturation (in black) is given. Horizontal line is the position of the water table. Dashed line is the upper boundary of the capillary fringe.

### B.7 Concomitant DCM degradation under steady-state conditions

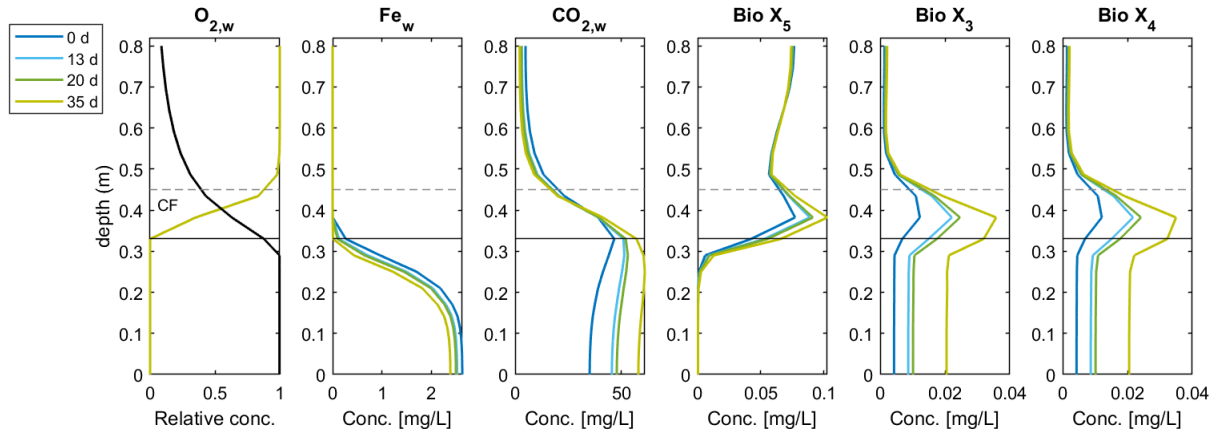


**Figure B.4:** Concomitant DCM degradation by bacterial populations  $X_3$  (*D. formicoaceticum*) and  $X_4$  (*Ca. D. elyunquensis*) in the presence of a non-DCM degrader ( $X_5$ ) under steady-state conditions. Evolution of  $O_2$ , ferric iron and  $CO_2$ , and bacterial populations  $X_5$ ,  $X_3$  and  $X_4$ . In addition to oxygen vertical profile (left), the gravimetric saturation (in black) is given. Horizontal line is the position of the water table. Dashed line is the upper boundary of the capillary fringe (CF).

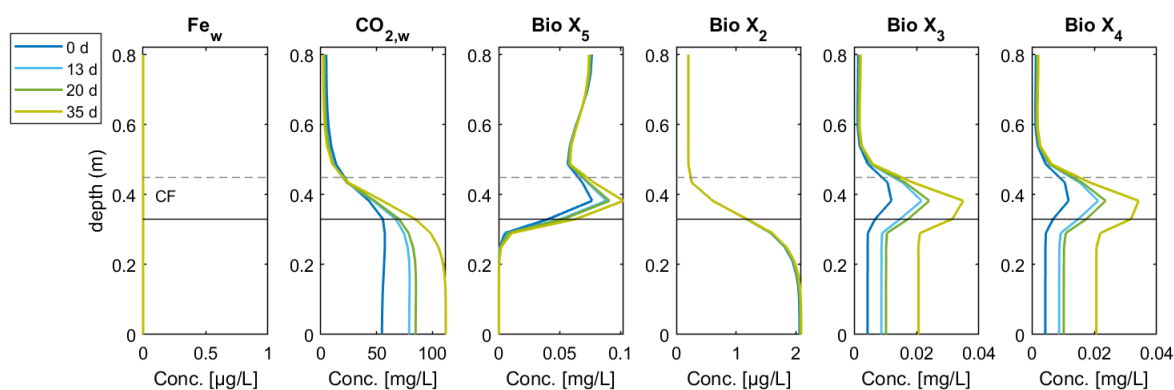


**Figure B.5:** Concomitant DCM degradation by bacterial populations  $X_2$  (*Dehalobacter* sp.),  $X_3$  (*D. formicoaceticum*) and  $X_4$  (*Ca. D. elyunquensis*) in the presence of a non-DCM degrader ( $X_5$ ) under steady-state conditions. Evolution of ferric iron, CO<sub>2</sub>, and bacterial populations  $X_5$ ,  $X_2$ ,  $X_3$  and  $X_4$ . Horizontal line is the position of the water table. Dashed line is the upper boundary of the capillary fringe (CF).

## B.8 Concomitant DCM degradation under transient conditions

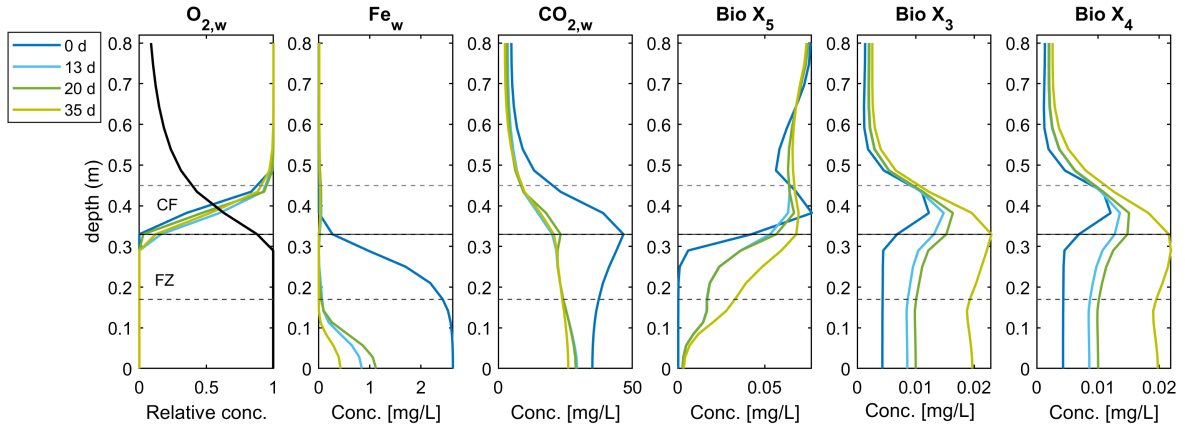


**Figure B.6:** Concomitant DCM degradation by bacterial populations  $X_3$  (*D. formicoaceticum*) and  $X_4$  (*Ca. D. elyunquensis*) in the presence of a non-DCM degrader ( $X_5$ ) under transient conditions. Evolution of  $O_2$ , ferric iron and  $CO_2$ , and bacterial populations  $X_5$ ,  $X_3$  and  $X_4$ . In addition to oxygen vertical profile (left), the gravimetric saturation (in black) is given. Horizontal line is the position of the water table. Dashed line is the upper boundary of the capillary fringe (CF). Lower dashed line is the position of the water table after drainage periods, representing the fluctuation zone (FZ).



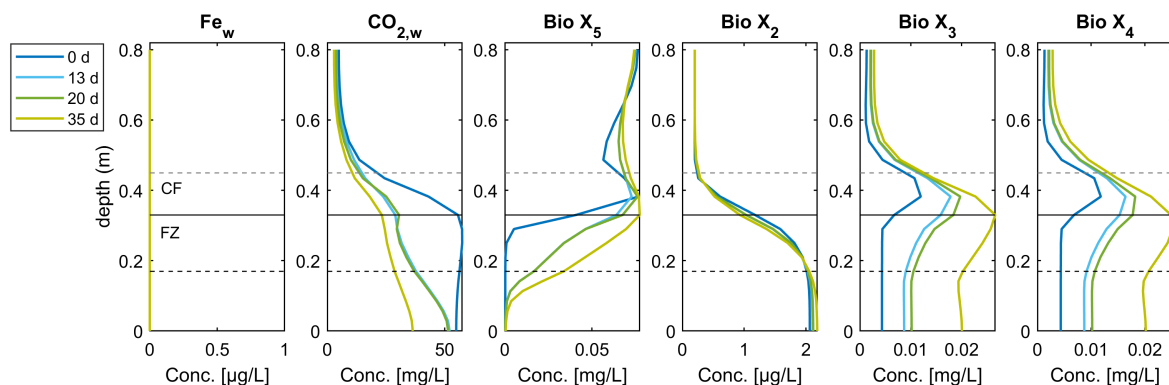


**Figure B.7:** Concomitant DCM degradation by bacterial populations  $X_2$  (*Dehalobacter* sp.),  $X_3$  (*D. formicoaceticum*) and  $X_4$  (*Ca. D. elyunquensis*) in the presence of a non-DCM degrader ( $X_5$ ) under transient conditions. Evolution of ferric iron,  $\text{CO}_2$ , and bacterial populations  $X_5$ ,  $X_2$ ,  $X_3$  and  $X_4$ . Horizontal line is the position of the water table. Dashed line is the upper boundary of the capillary fringe (CF). Lower dashed line is the position of the water table after drainage periods, representing the fluctuation zone (FZ).

**B.9 Simulated evolution (2D-domain) of concomitant DCM degradation by bacterial populations  $X_3$  (*D. formicoaceticum*) and  $X_4$  (*Ca. D. elyunquensis*) in the presence of a non-DCM degrader ( $X_5$ )**

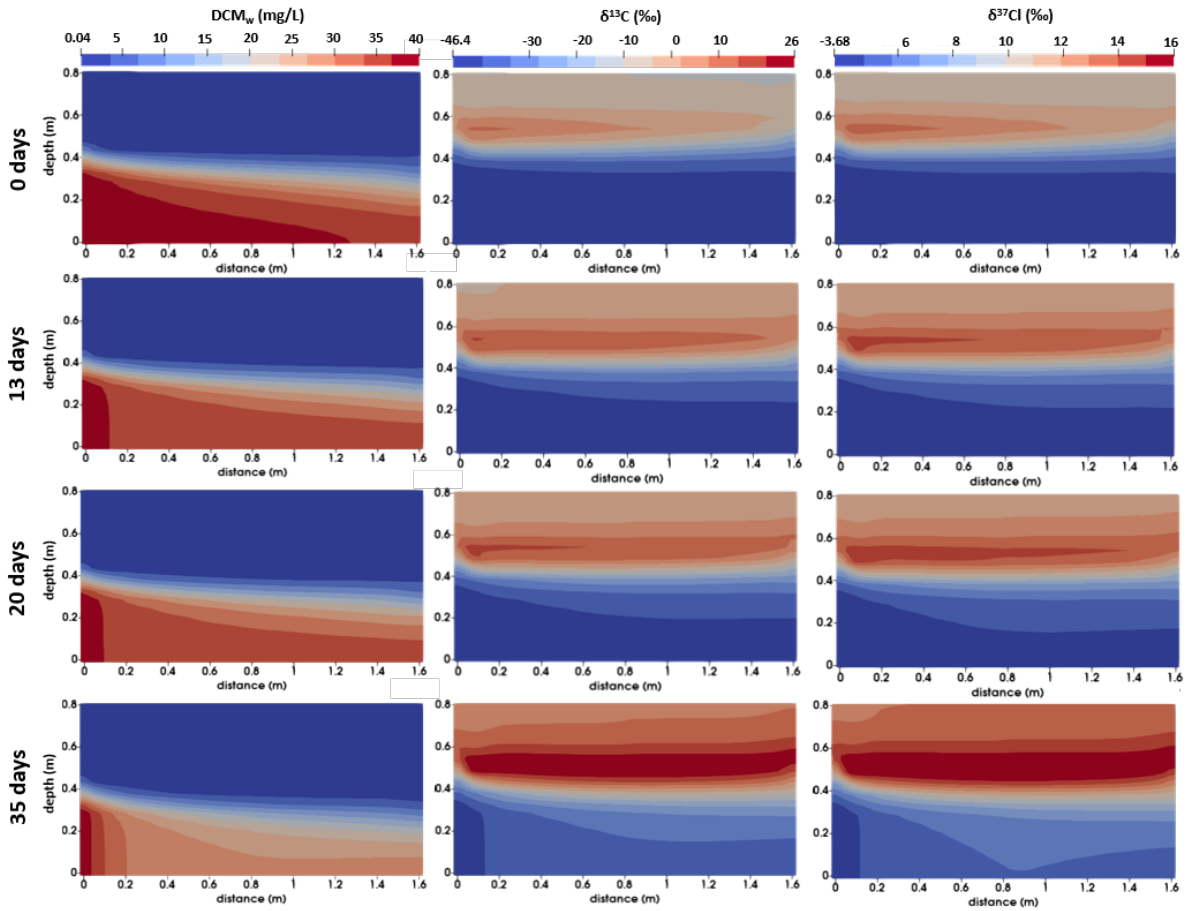


**Figure B.8:** Simulated evolution (2D-domain) of concomitant DCM degradation by bacterial populations  $X_3$  (*D. formicoaceticum*) and  $X_4$  (*Ca. D. elyunquensis*) in the presence of a non-DCM degrader ( $X_5$ ) under steady-state conditions. Evolution of DCM in water, and carbon and chlorine isotope ratios over time. The water table was positioned at 0.33 m from the bottom.

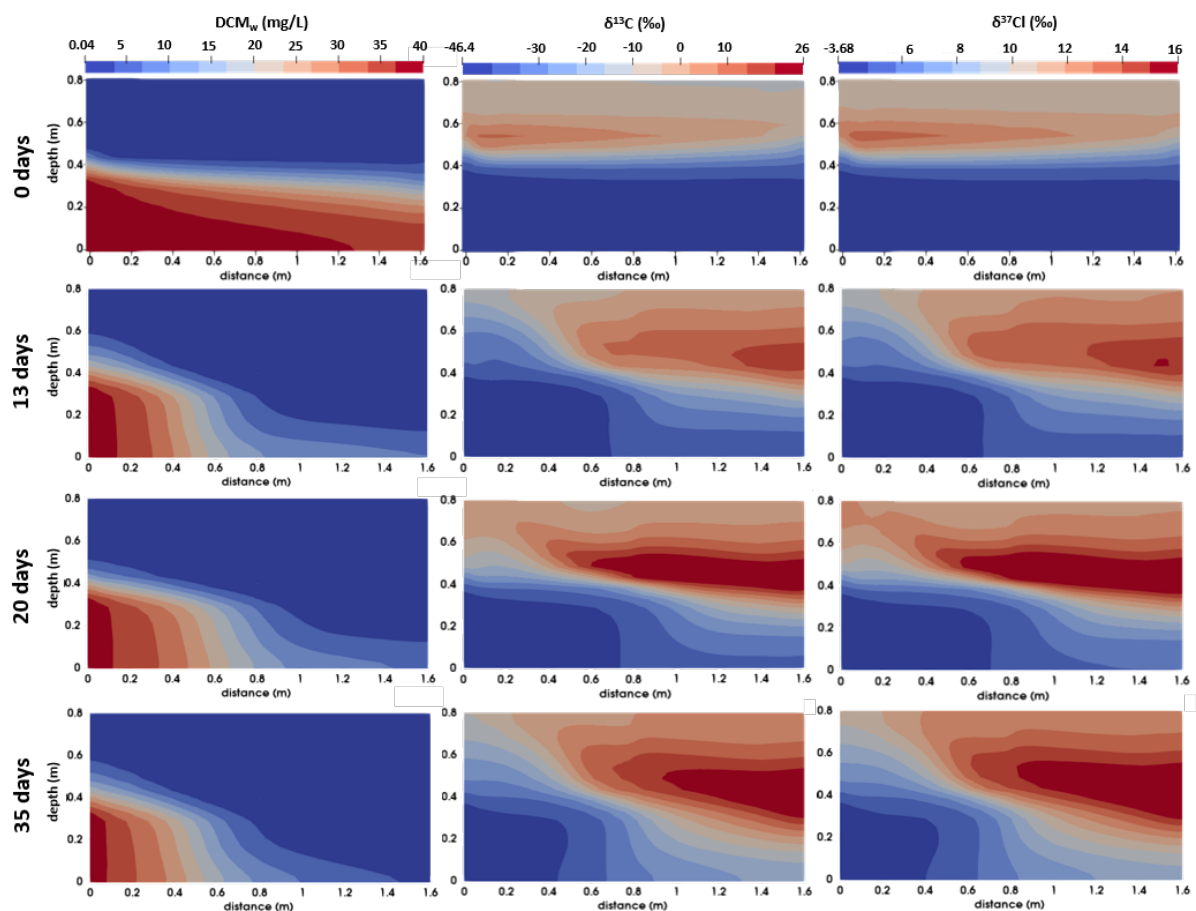


**Figure B.9:** Simulated evolution (2D-domain) of concomitant DCM degradation by bacterial populations  $X_3$  (*D. formicoaceticum*) and  $X_4$  (*Ca. D. elyunquensis*) in the presence of a non-DCM degrader ( $X_5$ ) under transient conditions. Evolution of DCM in water, and carbon and chlorine isotope ratios over time. The water table was positioned at 0.33 m from the bottom, and lowered to 0.17 m during drainage events.

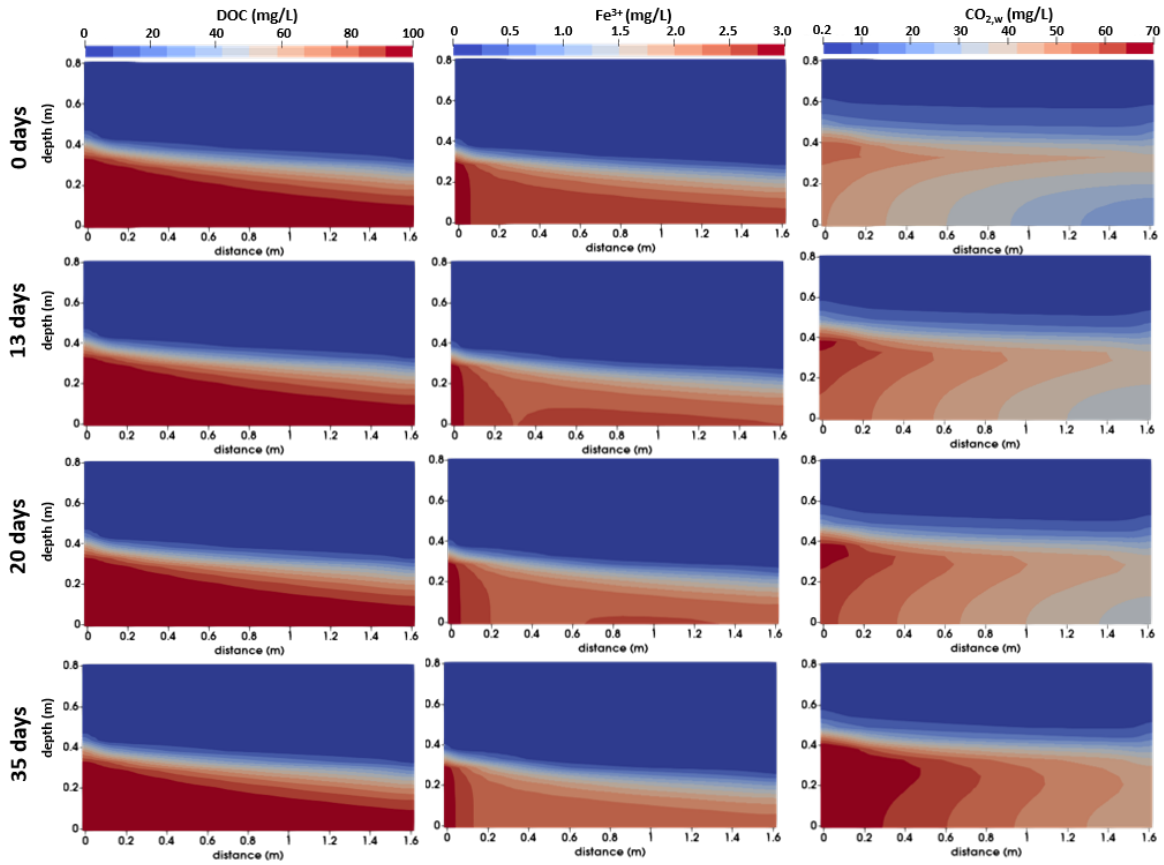


**Figure B.10:** Simulated evolution (2D-domain) of concomitant DCM degradation by bacterial populations  $X_3$  (*D. formicoaceticum*) and  $X_4$  (*Ca. D. elyunquensis*) in the presence of a non-DCM degrader ( $X_5$ ) under steady-state conditions. Evolution of DOC, ferric iron and  $\text{CO}_2$  over time. The water table was positioned at 0.33 m.

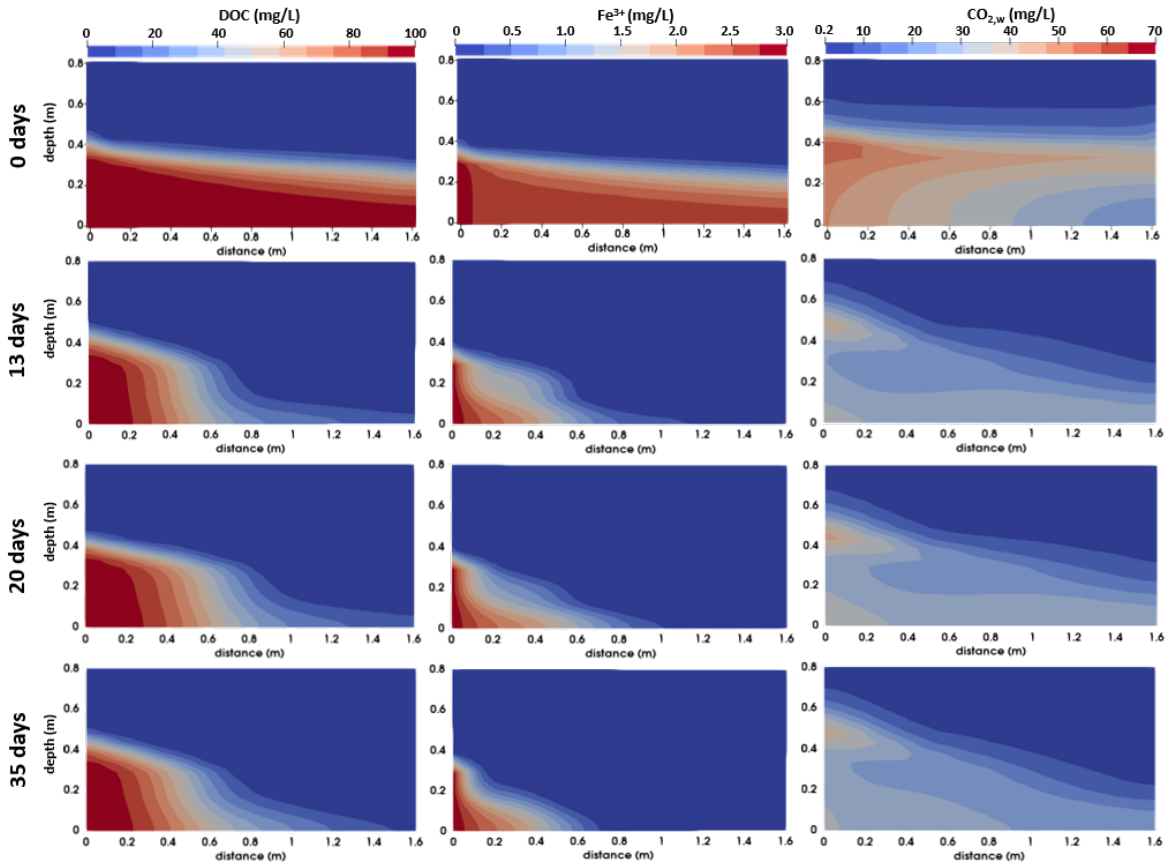


**Figure B.11:** Simulated evolution (2D-domain) of concomitant DCM degradation by bacterial populations  $X_3$  (*D. formicoaceticum*) and  $X_4$  (*Ca. D. elyunquensis*) in the presence of a non-DCM degrader ( $X_5$ ) under transient conditions. Evolution of DOC, ferric iron and  $\text{CO}_2$  over time. The water table was positioned at 0.33 m, and lowered to 0.17 m during drainage events.

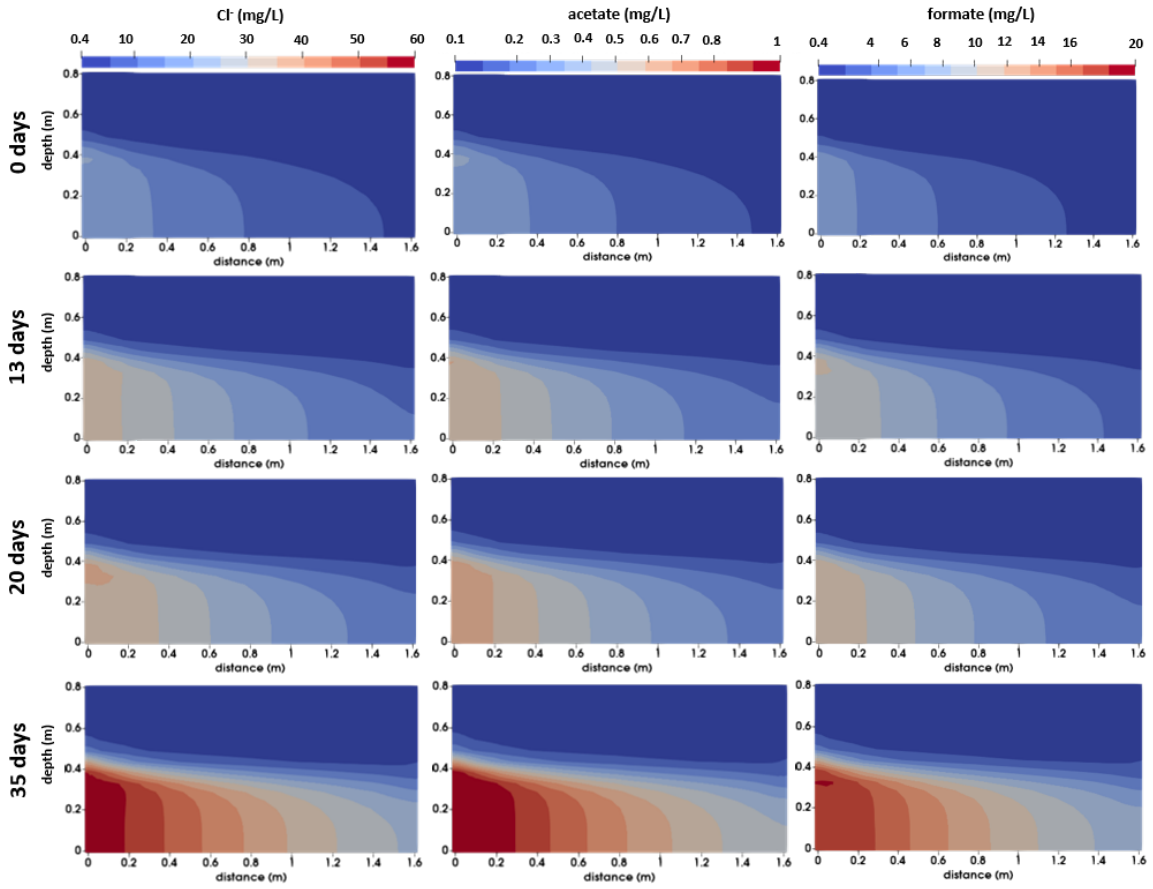


**Figure B.12:** Simulated evolution (2D-domain) of concomitant DCM degradation by bacterial populations  $X_3$  (*D. formicoaceticum*) and  $X_4$  (*Ca. D. elyunquensis*) in the presence of a non-DCM degrader ( $X_5$ ) under steady-state conditions. Evolution of  $\text{Cl}^-$ , acetate and formate over time. The water table was positioned at 0.33 m.

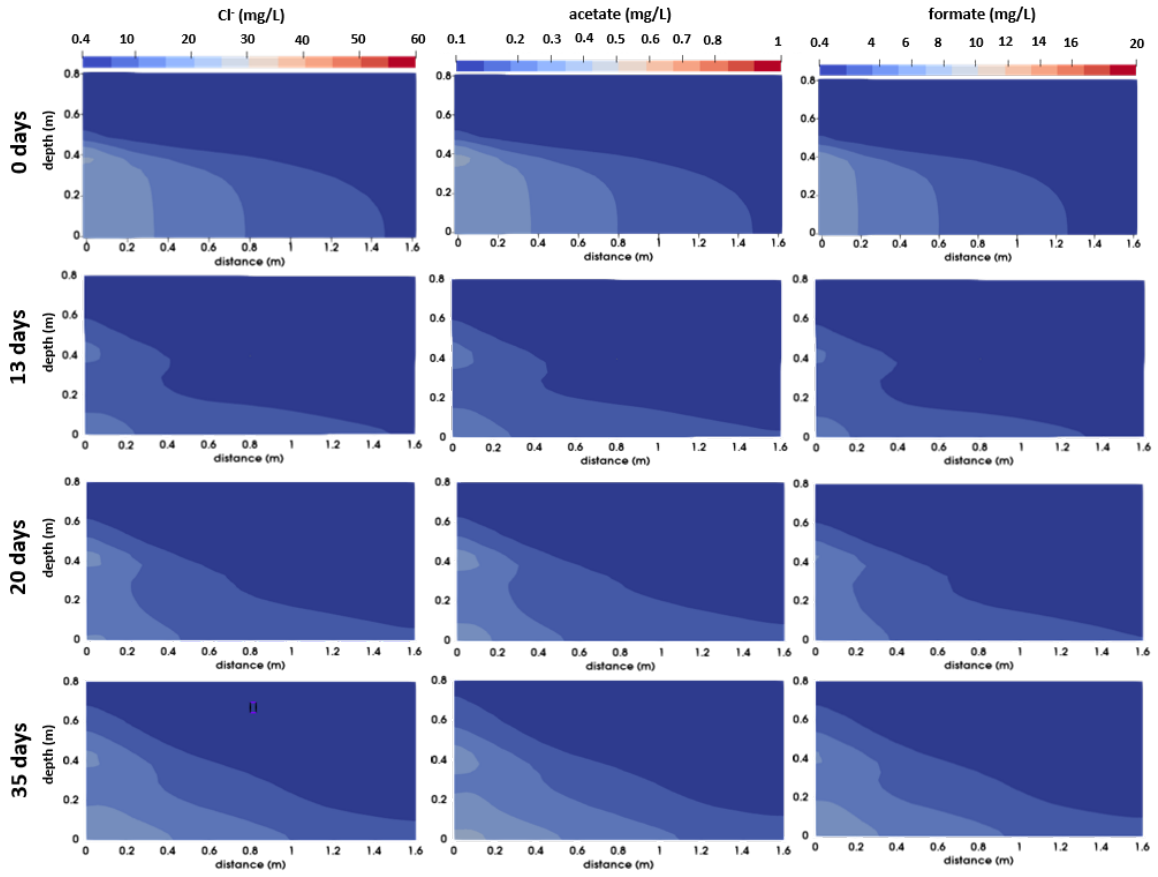


**Figure B.13:** Simulated evolution (2D-domain) of concomitant DCM degradation by bacterial populations  $X_3$  (*D. formicoaceticum*) and  $X_4$  (*Ca. D. elyunquensis*) in the presence of a non-DCM degrader ( $X_5$ ) under transient conditions. Evolution of  $\text{Cl}^-$ , acetate and formate over time. The water table was positioned at 0.33 m, and lowered to 0.17 m during drainage events.

## References of Appendix B

- Brown, P. N., Hindmarsh, A. C., and Petzold, L. R. (1994). Using krylov methods in the solution of large-scale differential-algebraic systems. *SIAM Journal on Scientific Computing*, 15(6):1467–1488.
- Chastanet, J., Côme, J.-M., Roupert, R. D. C., Schaefer, G., and Quintard, M. (2014). Cubicm, un code de calcul pour simuler le devenir de polluants organiques dans le milieu souterrain.
- Chen, G., Shouakar-Stash, O., Phillips, E., Justicia-Leon, S. D., Gilevska, T., Sherwood Lollar, B., Mack, E. E., Seger, E. S., and Löffler, F. E. (2018). Dual carbon-chlorine isotope analysis indicates distinct anaerobic dichloromethane degradation pathways in two members of *Peptococcaceae*. *Environmental Science and Technology*, 52(15):8607–8616.
- Di Chiara Roupert, R. (2009). *Développement d'un code de calcul multiphasique multiconstituants*. PhD thesis, University of Strasbourg, Strasbourg, France.
- Di Chiara Roupert, R., Schäfer, G., Quintard, M., Marcoux, M., Chastanet, J., Côme, J.-M., and Duclos, Y. (2017). Multiphase multicomponent modelling of the napl transfer in the subsurface using method of lines.
- Heraty, L., Fuller, M., Huang, L., Abrajano, T., and Sturchio, N. (1999). Isotopic fractionation of carbon and chlorine by microbial degradation of dichloromethane. *Organic Geochemistry*, 30(8):793–799.
- Hron, P., Jost, D., Bastian, P., Gallert, C., Winter, J., and Ippisch, O. (2015). Application of reactive transport modeling to growth and transport of microorganisms in the capillary fringe. *Vadose Zone Journal*, 14(5).
- Kim, S., Chen, J., Cheng, T., Gindulyte, A., He, J., He, S., Li, Q., Shoemaker, B. A., Thiessen, P. A., Yu, B., et al. (2019). PubChem 2019 update: improved access to chemical data. *Nucleic acids research*, 47(D1):D1102–D1109.
- Kleindienst, S., Chourey, K., Chen, G., Murdoch, R. W., Higgins, S. A., Iyer, R., Campagna, S. R., Mack, E. E., Seger, E. S., Hettich, R. L., and Löffler, F. E. (2019). Proteogenomics reveals novel reductive dehalogenases and methyltransferases expressed during anaerobic dichloromethane metabolism. *Applied and Environmental Microbiology*, 85(6).
- Lee, M., Wells, E., Wong, Y. K., Koenig, J., Adrian, L., Richnow, H. H., and Manefield, M. (2015). Relative contributions of *Dehalobacter* and zerovalent iron in the degradation of chlorinated methanes. *Environmental Science and Technology*, 49(7):4481–4489.
- Michels, H. (1998). *DISLIN manual*. Max-Planck-Institut für Aeronomie, Katlenburg-Lindau.
- Rittmann, B. E. (2006). Microbial ecology to manage processes in environmental biotechnology. *TRENDS in Biotechnology*, 24(6):261–266.
- Rolle, M., Chiogna, G., Bauer, R., Griebler, C., and Grathwohl, P. (2010). Isotopic fractionation by transverse dispersion: Flow-through microcosms and reactive transport modeling study. *Environmental science & technology*, 44(16):6167–6173.



## *References of Appendix B*

---

- VanBriesen, J. M. and Rittmann, B. E. (2000). Mathematical description of microbiological reactions involving intermediates. *Biotechnology and Bioengineering*, 67(1):35–52.
- Weller, H. G., Tabor, G., Jasak, H., and Fureby, C. (1998). A tensorial approach to computational continuum mechanics using object-oriented techniques. *Computers in physics*, 12(6):620–631.
- Yaws, C. L. (1999). *Chemical properties handbook: physical, thermodynamic, environmental, transport, safety and health related properties for organic and inorganic chemicals*. McGraw-Hill. 779.

# **Appendix**

# **C**

## **Supporting information of Chapter 5**

### C.1 Chemical reagents of the micropollutant mixture and transformation products

**Micropollutant mixture:** atrazine (6-chloro-4-N-ethyl-2-N-propan-2-yl-1,3,5-triazine-2,4-diamine), caffeine (1,3,7-trimethylpurine-2,6-dione), metalaxyl (methyl 2-(N-(2-methoxyacetyl)-2,6-dimethyl-anilino)propanoate), S-metolachlor (2-chloro-N-(2-ethyl-6-methylphenyl)-N-[(2S)-1-methoxypropan-2-yl]acetamide), metolachlor-d11, terbutryn (2-N-tert-butyl-4-N-ethyl-6-methylsulfanyl-1,3,5-triazine-2,4-diamine), and metformin (3-(diaminomethylidene)-1,1-dimethylguanidine) were purchased in highest available purity (>99%; Sigma-Aldrich, St. Louis, USA).

**Commercially available transformation products of micropollutant mixture:**

2-hydroxy-atrazine (HA; 2-(ethylamino)-6-(propan-2-ylamino)-1H-1,3,5-triazin-4-one), desethyl-atrazine (DEA; 6-chloro-2-N-propan-2-yl-1,3,5-triazine-2,4-diamine), deisopropylatrazine (DIA; 6-chloro-2-N-ethyl-1,3,5-triazine-2,4-diamine), carboxylic acid metalaxyl (2-((1-Carboxyethyl)(methoxyacetyl)amino)-3-methylbenzoic acid), demethylmetalaxyl (N-(2,6-Dimethylphenyl)-N-(methoxyacetyl)alanine), S-metolachlor ethanesulfonic acid (MET ESA; sodium 2-((2-ethyl-6-methylphenyl)(1-methoxy-2-propanyl)amino)-2-oxoethanesulfonate), S-metolachlor oxanilic acid (MET OXA; 2-(2-ethylN-(1-methoxypropan-2-yl)-6-methylanilino)-2-oxoacetic acid), and guanylurea (diaminomethylideneurea) were purchased in A.C.S-grade reagents (>98%) from Sigma-Aldrich (USA). Desethyl-terbutryn (2-N-tert-butyl-6-methylsulfanyl-1,3,5-triazine-2,4-diamine), 2-hydroxy-terbutryn (6-(tert-butylamino)-4-(ethylamino)-1H-1,3,5-triazin-2-one), terbutryn sulfoxide (N2-(1,1-Dimethylethyl)-N4-ethyl-6-(methylsulfinyl)-1,3,5-triazine-2,4-diamine), desethyl-2-hydroxy-terbutryn (6-amino-4-(tert-butylamino)-1H-1,3,5-triazin-2-one) were purchased in highest available purity (>99%) from TechLab (Metz, France). Theobromine (3,7-dimethylpurine-2,6-dione), paraxanthine (1,7-dimethyl-3H-purine-2,6-dione) and xanthine (3,7-dihydropurine-2,6-dione) were purchased from HPC Standards GmbH (Cunnersdorf, Germany).

## C.2 Saline conservative tracer

Prior to the saline (NaCl) tracer injection, both laboratory aquifers were continuously flushed with milliQ water for at least two pore volumes. A pulse of the saline tracer (concentration:  $1 \text{ g L}^{-1}$ , volume:  $1 \text{ L}$ ) took place at the established flow rate of  $0.9 \text{ L d}^{-1}$ . NaCl concentrations were measured based on observed electrical conductivity values at the outflows using a flow-through conductivity cell (WTW™ Tetra-Con™ DU/T; cell constant:  $0.778 \text{ cm}^{-1}$ ) connected with a DuraProbe 4-Electrode conductivity cell. This electrical conductivity (EC) cell is suitable for extensive measuring series and online data acquisition. Electrical conductivity was recorded using an the Multi 340i Handheld multimeter (pH/Cond, WTW™) at sampling frequency of 30 seconds, and data acquisition was done via a code developed in R (core Team, 2019). The EC cells were calibrated prior to the experiments (calibration range:  $20\text{--}200 \text{ mg L}^{-1}$ ). During the flushing period with milliQ water prior to the experiments, EC values were recorded to obtain background concentrations. The pulse injection of the conservative tracer took place once stable background concentrations were observed over time. Finally, the measured EC values (in  $\mu\text{S cm}^{-1}$ ) were corrected by subtracting the background EC values, and finally converted to dissolved NaCl concentrations using a previously established linear relationship.

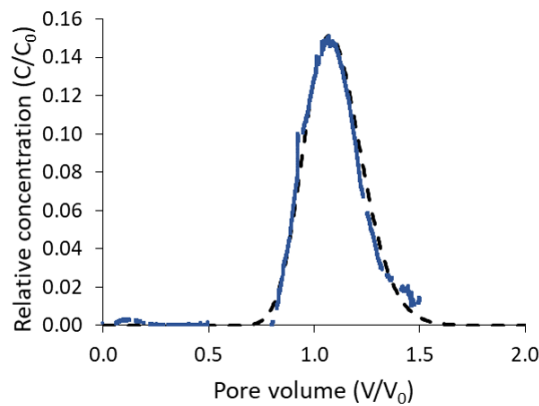


**Figure C.1:** Measured saline (NaCl) conservative tracer BTC (blue) in a laboratory aquifer (dimensions:  $160 \text{ cm} \times 80 \text{ cm} \times 7 \text{ cm}$ ). Dashed line represents one-dimensional fitted model.

### C.3 Micropollutants extraction and quantification measurements

#### Solid-phase extraction

Solid phase extraction (SPE) of atrazine, caffeine, metalaxyl, terbutryn and S-metolachlor was carried out using SolEx C18 cartridges (1 g, Dionex®, CA, USA) and an AutoTrace 280 SPE system (Dionex®, CA, USA), following an in-house method (Droz et al., 2021; Elsayed et al., 2014). Briefly, the extraction cartridge was conditioned by washing successively with ethanol (5 mL), acetonitrile (5 mL), and deionized water (10 mL). Sample was loaded on the cartridge and dried under nitrogen flux for 10 min. Micropollutants were eluted by 5 mL of ethylacetate, followed by 5 mL of acetonitrile. The extracts were dried under nitrogen stream at room temperature, and then re-suspended into acetonitrile up to 0.5 mL by vortexing to collect residues on the glassware. Samples were stored at -20 °C until further analysis. Extraction efficiency of all micropollutants was determined elsewhere (Droz et al., 2021).

#### Quantification by GC-MS

Atrazine, caffeine, metalaxyl, terbutryn and S-metolachlor were quantified using a gas chromatograph (GC, Trace 1300, Thermo Fisher Scientific) coupled with a mass spectrometer (MS, ISQTM, Thermo Fisher Scientific) equipped with a TG-5MS column (30 m × 0.25 mm ID, 0.25 µm film thickness, Thermo Fischer Scientific). The sample (1.5 µL) and the standard Metolachlor-d11 (1 µL at 300 µg L<sup>-1</sup>) were injected together via a split/splitless injector in splitless mode at 280 °C with helium as carrier gas at a 1.5 mL min<sup>-1</sup> flow rate. The GC oven program was set to a ramp mode: 2 min hold time at 50 °C, heating at 30 °C min<sup>-1</sup> to 160 °C, then heating at 4 °C min<sup>-1</sup> to 220 °C, then heating at 30 °C min<sup>-1</sup> to 300 °C followed by a 1 min hold time at 300 °C. The MS transfer line and source were heated at 320 °C. Eluted micropollutants were identified by their specific masses in a selective ion mode (SIM). Detection limits (DLs) and quantification limits (QLs) were below 8 and 45 µg L<sup>-1</sup>, respectively. Dilution of samples was required to be within the measurement range (1–500 µg L<sup>-1</sup>).

#### Quantification by LC-MS/MS

Metformin and transformation products of the micropollutant mixture (see Table S1) were quantified using an Ultra High Performance Liquid Chromatography (UHPLC, Ultimate 3000, Thermo Fisher Scientific) coupled with a triple quadrupole mass spectrometer (MS/MS, TSQ Quantiva, Thermo Fisher Scientific) equipped with a Accucore aQ C18 column (100 × 2.1 mm, 2.6 µm

granulometry, Thermo Fischer Scientific). The column and autosampler temperatures were 20 °C and 9 °C, respectively. The sample (10  $\mu$ L) containing internal standard Alachlor-d13 ( $\mu$ g L<sup>-1</sup>) were injected with a ACC-3000 autosampler (Ultimate 3000, Thermo Fisher Scientific). LC-grade water and methanol, both acidified with 0.1% and 0.05% formic acid, respectively, were used as eluents for the chromatographic gradient at a flow rate of 0.3 mL min<sup>-1</sup> (10% to 95% methanol in 8 min, 90% methanol for 1 min, 90% to 10% methanol in 1 min, and 10% methanol for 3 min). The MS/MS was operated at an ionization voltage of 1500V (in positive mode) and 2000 V (in negative mode), CID gas at 1.5 mTorr and vaporizing temperature of 300 °C. Precursors and fragments ions were acquired in multi reaction mode (MRM). The screened masses are shown in Table S1.

**Table C.1:** Mass spectrometry parameters for quantification of transformation products of the micropollutant mixture and parent compound metformin by LC–MS/MS.

Analytes	Formula	Parent compound	Molecular mass [g/mol]	Fragment masses [m/z]	Collision energies [mV]	Polarity
Metformin	C <sub>4</sub> H <sub>11</sub> N <sub>5</sub>	-	129.16	71/62	22/14	+
Theobromine	C <sub>7</sub> H <sub>8</sub> N <sub>4</sub> O <sub>2</sub>	Caffeine	180.16	163/85	18/17	+
Xanthine	C <sub>5</sub> H <sub>4</sub> N <sub>4</sub> O <sub>2</sub>	Caffeine	152.11	110.08/136	18/18	+
Paraxanthine	C <sub>7</sub> H <sub>8</sub> N <sub>4</sub> O <sub>2</sub>	Caffeine	180.16	124/69	20/31	+
Guanyllurea	C <sub>2</sub> H <sub>6</sub> N <sub>4</sub> O	Metformin	102.1	60/86	13/10	+
Carboxylicacid metalaxyl	C <sub>14</sub> H <sub>17</sub> NO <sub>6</sub>	Metalaxyl	295.29	250/160	11/23	+
Dimethylmetalaxyl	C <sub>14</sub> H <sub>19</sub> NO <sub>6</sub>	Metalaxyl	265.3	220/160	13/22	+
S-met ethanesulfonic acid	C <sub>15</sub> H <sub>23</sub> NO <sub>5</sub> S	S-metolachlor	329.4	121/135	23/28	-
S-met oxanilic acid	C <sub>15</sub> H <sub>21</sub> NO <sub>4</sub>	S-metolachlor	279.33	206/174	11/16	-
2-hydroxyatrazine	C <sub>8</sub> H <sub>15</sub> N <sub>5</sub> O	Atrazine	197.24	156/86	18/23	+
Desethylatrazine	C <sub>6</sub> H <sub>10</sub> ClN <sub>5</sub>	Atrazine	187.63	146/104	17/25	+
Deisopropylatrazine	C <sub>5</sub> H <sub>8</sub> ClN <sub>5</sub>	Atrazine	173.6	104/132	23/18	+
Terbutryn sulfoxide	C <sub>10</sub> H <sub>19</sub> N <sub>5</sub> OS	Terbutryn	257.36	184/156	18/20	+
Desethyl-2-hydroxy-terbutryn	C <sub>7</sub> H <sub>13</sub> N <sub>5</sub> O	Terbutryn	183.21	128/86	15/24	+
2-hydroxy-terbutryn	C <sub>9</sub> H <sub>17</sub> N <sub>5</sub> O	Terbutryn	211.26	156/86	16/25	+
Desethyl-terbutryn	C <sub>8</sub> H <sub>15</sub> N <sub>5</sub> S	Terbutryn	213.31	110/157.98	26/18	+
Alachlor D13	C <sub>14</sub> H <sub>7</sub> D <sub>13</sub> ClNO <sub>2</sub>	Internal standard	282.85	251/173	10/21	+

#### C.4 Compound-specific isotope analysis (CSIA) of micropollutants

Carbon ( $\delta^{13}\text{C}$ ) and nitrogen ( $\delta^{15}\text{N}$ ) analyses of atrazine, caffeine, metalaxyl, terbutryn and *S*-metolachlor were performed by gas chromatography–combustion–isotope ratio mass spectrometry (GC–C–IRMS). The GC–C–IRMS system consisted of a GC (TRACE<sup>TM</sup> Ultra) followed by a GC combustion interface (IsoLink/Conflow IV) and an isotope ratio mass spectrometer (DeltaV, both from Thermo Fischer Scientific). Samples (1–3  $\mu\text{L}$ ) were injected via a split/splitless injector in splitless mode at 250 °C with helium as carrier gas at a 1.5 mL min<sup>-1</sup> flow rate into a TG–5MS column (60 m  $\times$  0.25 mm ID, 0.25  $\mu\text{m}$  film thickness). For carbon, GC oven was held at 50 °C for 2 min, heated at a rate of 20 °C min<sup>-1</sup> to 150 °C, then up to 242 °C at 5 °C min<sup>-1</sup>, and then heated at 30 °C min<sup>-1</sup> to 310 °C and held for 1 min. For nitrogen, the oven was held at 50 °C for 1 min, heated at a rate of 20 °C min<sup>-1</sup> to 150 °C, then up to 300 °C at 10 °C min<sup>-1</sup> and held at 300 °C for 4 min. For both elements, target compounds were combusted to the analyte gases ( $\text{CO}_2$  and  $\text{N}_2$ ) in a single combined reactor (P/N 1255321, NiO tube/CuO–NiO, Thermo) operated at 1000 °C and re-oxidized for 60 min with continuous  $\text{O}_2$  stream after passing 100 and 30 samples for C and N, respectively. For nitrogen, liquid  $\text{N}_2$  was used for cryogenic trapping of  $\text{CO}_2$ . The MS transfer line and source were heated at 320 °C.

To control the quality of the measurements, a BTEX standard (Benzene, Toluene, Ethylbenzene and *o*-Xylene 15 mL of each in 50 mL of *n*-Pentane) and an international reference material AIEA600 (Caffeine; 150 mg L<sup>-1</sup> in acetone) were measured between a series of measurements for C and N, respectively. In addition, an in-house standard mixture of the micropollutants was measured every 9 and 4 samples injections for C and N, respectively. Reproducibility of triplicate measurements was  $\leq 0.5\text{‰}$  ( $1\sigma$ ) for carbon and  $\leq 1\text{‰}$  ( $1\sigma$ ) nitrogen within the linearity range (6–300 ng for C and 40–300 ng for N) (Droz et al., 2021). Carbon and nitrogen isotope ratios were reported in  $\delta$  notation as parts per thousand (‰) relative to the international reference material Vienna Pee Dee-Belemnite (V-PDB) (Coplen et al., 2006) and air standards, respectively. Pure solid powders of atrazine, caffeine, metalaxyl, terbutryn and *S*-metolachlor were measured as the reference isotope signatures by elemental analyzer IRMS (Flash EA IsoLink<sup>TM</sup> CN IRMS, Thermo Fisher Scientific).

### C.5 DNA extraction and rarefaction curves

For both pore water and sand core samples, DNA was extracted using the DNeasy Power Water kit according to the manufacturer's protocol (Qiagen, Hilden, Germany). Extracted DNA was quantified using Qubit fluorometric quantification with the Qubit dsDNA HS Assay kit (ThermoFischer Scientific, MA, USA). The V4-V5 hypervariable region of the 16S rRNA gene was PCR amplified by an optimized and standardized amplicon library preparation protocol (Metabiote<sup>®</sup>, GenoScreen, Lille, France), including a positive (mock community) and negative (blank) control (Hermon et al., 2018). Libraries were sequenced by paired-end Illumina MiSeq 2x250 bases. Demultiplexing and trimming was followed by paired read assembly (minimum overlap 30 nt, minimum identity of 97%), resulting in a total of 1,861,511 sequences. Denoising, chimera checking, generation of operational taxonomic units (OTUs), taxonomic classification using Greengenes (v13.8 as reference), and alpha-diversity metrics were performed using a custom-scripted bioinformatics pipeline of GenoScreen (see Hermon et al. (2018)). Analysis of similarities (ANOSIM,  $n=31$  samples) based on Bray Curtis dissimilarities of samples was used to infer statistical differences between groups of community profiles (Torabi et al., 2020). Datasets obtained from Illumina sequencing were also used to compute  $\alpha$ -diversity indices and for rarefaction analysis. Estimation of  $\alpha$ -diversity indices included (i) observed OTUs, (ii) Shannon's diversity index ( $H'$ ), which provides an estimate of community heterogeneity, and increases with increasing heterogeneity, and (iii) the  $S_{\text{chao1}}$  richness estimate which provides an estimate of the number of total OTUs in the sample, based on the number of detected OTUs represented by singletons and doubletons (Hellal et al., 2020).



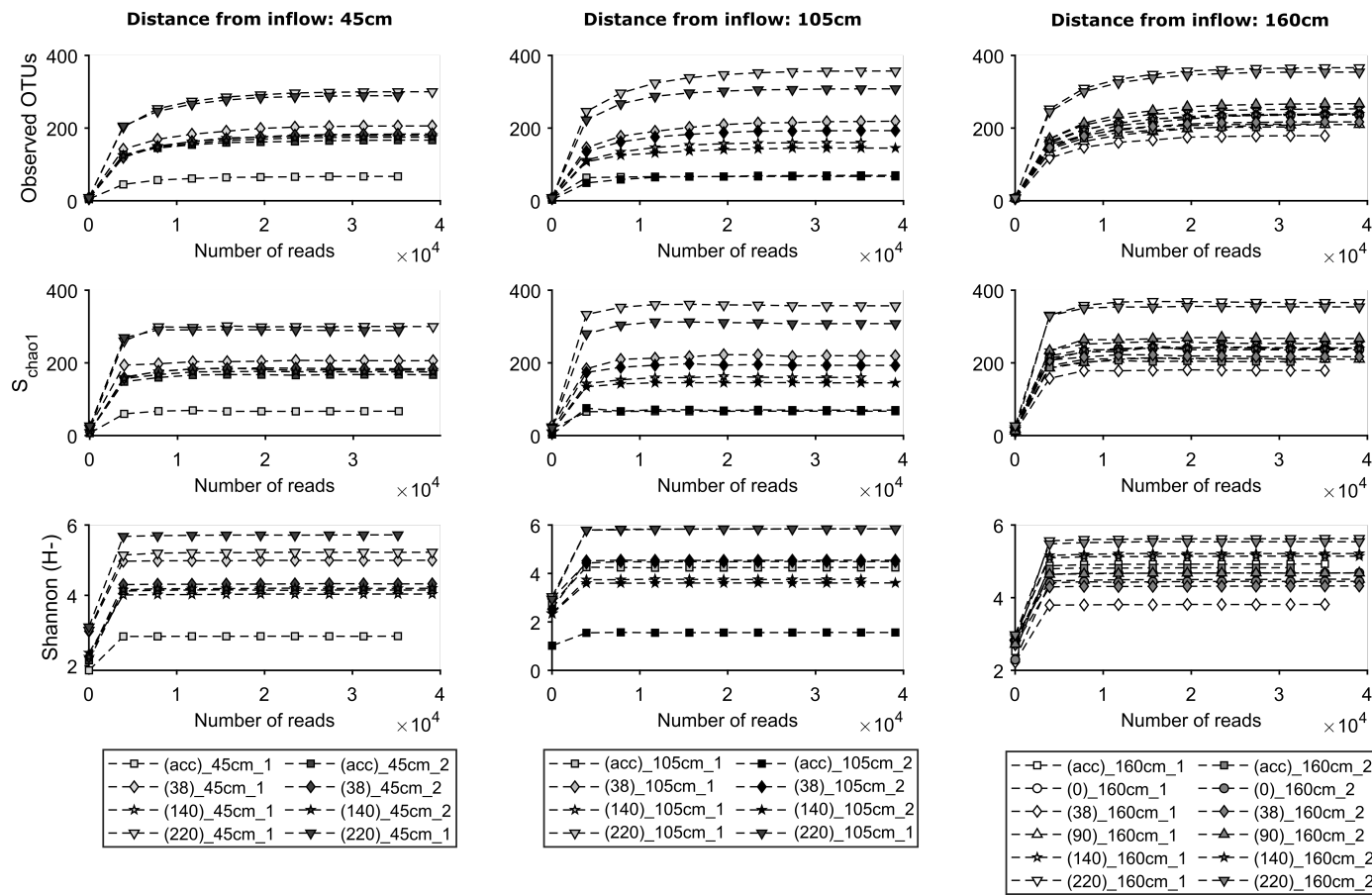


**Figure C.2:** Rarefaction curves based on observed OTUs (top),  $S_{chao1}$  diversity (middle) and Shannon diversity (bottom) from integrative water samples collected at 45 cm, 105 cm and 160 cm (outflow) distance from inflow. Numbers indicated in parenthesis represent samples collected during the acclimation period (acc; 85 d prior to experiments), and at 0, 38, 90, 140 and 220 days.

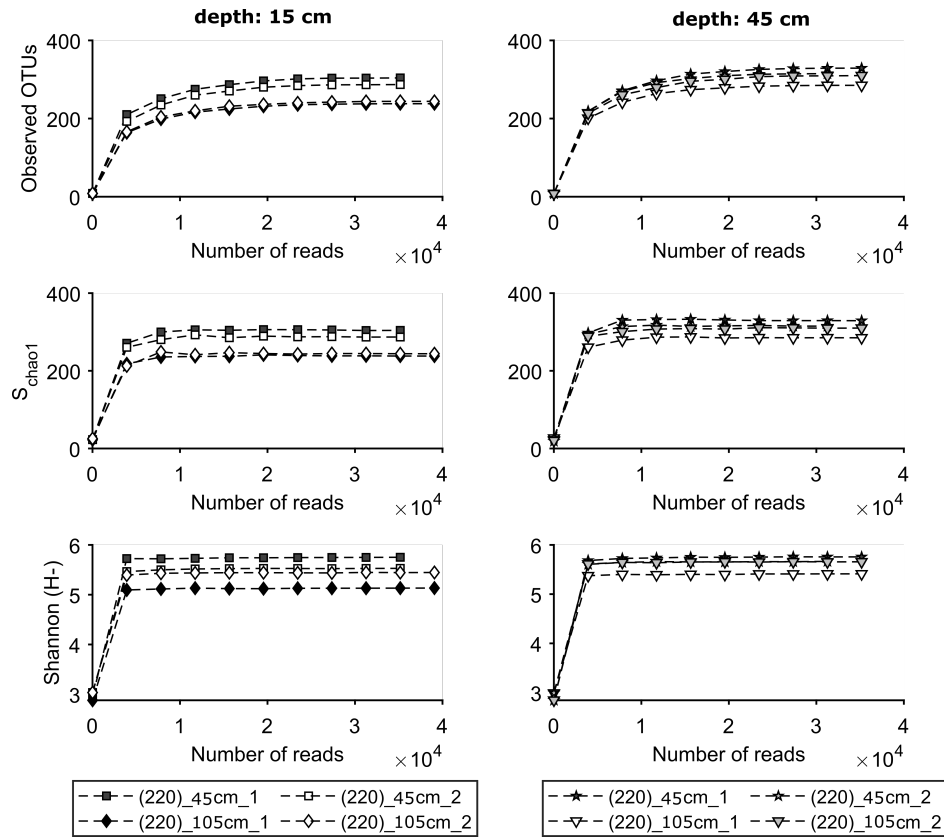


**Figure C.3:** Rarefaction curves based on observed OTUs (top),  $S_{\text{chao1}}$  diversity (middle) and Shannon diversity (bottom) from integrative sand samples collected at 45 cm and 105 cm distance from inflow, and at 15 cm and 45 cm depth (from bottom to top of the aquifers). Numbers indicated in parenthesis represent samples collected at the end of the experiments corresponding to 220 days.

## C.6 Simple parsimonious reactive transport model

The reactive transport system is solved in a fully implicit and fully coupled way. Instead of a first-order upstream scheme, the hyperbolic (advective) part of the transport equation is treated numerically using a second-order Lax-Wendroff scheme (Lax and Wendroff, 1960; LeVeque and Leveque, 1992), the rest of the terms are treated using cell-centered description (Laplacian, reactive terms). The treatment of the temporal derivatives is performed by a Method Of Lines (fifth-order BDF scheme in time, Ascher and Petzold (1998)) allowing an adaptive time step while preserving the order of the spatial schemes. The absolute tolerance is fixed at  $10^{-12}$  (relative tolerance at  $10^{-6}$ ). In order to preserve satisfactory balance between numerical accuracy (tolerances) and computational costs (CPU time efficiency), the MOL solver increases the time step when the solution tends to a stationary regime and drastically reduces it at the sharp front neighborhood. The last spatial temporal derivative is linearly extrapolated on the base of the two previous adjacent cell terms. The Python (3.7.10) `solve-ivp` method present in the SciPy package (Virtanen et al., 2020) is used as time solver. The whole 'microP' project is carried out in an JupyterLab (3.0.16) environment.

**Table C.2:** Estimated parameters from fitted caffeine BTCs.

parameter	unit	value
$n$	-	0.37
$v$	m s	$9.26 \times 10^{-7}$
$\rho_b$	kg L <sup>-1</sup>	2.64
$D$	m <sup>2</sup> s <sup>-1</sup>	$9.98 \times 10^{-9}$
$^{12}r_{\max}$	mg L <sup>-1</sup> s <sup>-1</sup>	$5.50 \times 10^{-10}$
$K_m$	mg L <sup>-1</sup>	$9.7 \times 10^{-5}$
$^{12}K_d$	L mg <sup>-1</sup>	$3.26 \times 10^{-5}$
$\varepsilon_b$	‰	-0.40
$\varepsilon_{\text{sorp}}$	‰	-0.06

## C.7 Microcosms experiments

### Hydrochemistry of microcosms experiments

**Table C.3:** Hydrochemistry of stream water microcosm experiments under oxic conditions. Abiotic (sterile) and biotic (non-sterile) experiments were spiked with a micropollutant mixture (concentration: 6 mg L<sup>-1</sup>) at 0 d. Controls received no sterilization and spiking of the mixture. Data represent abiotic and biotic samples collected over time. The reported values correspond to mean values of triplicate measurements taken at each sampling event, with the corresponding standard deviation.

Condition	days	pH	Redox mV	Elec. Cond. mS cm <sup>-1</sup>	NH <sub>4</sub> <sup>+</sup> mg L <sup>-1</sup>	Na <sup>+</sup> mg L <sup>-1</sup>	K <sup>+</sup> mg L <sup>-1</sup>	Mn <sup>2+</sup> mg L <sup>-1</sup>	Ca <sup>2+</sup> mg L <sup>-1</sup>	Cl <sup>-</sup> mg L <sup>-1</sup>	NO <sub>3</sub> <sup>-</sup> mg L <sup>-1</sup>	SO <sub>4</sub> <sup>2-</sup> mg L <sup>-1</sup>
Abiotic	0	6.9±0.1	123±10	1.1±0.1	<Q.L.a	17.4±0.7	22.6±6.0	44.4±0.1	71.9±1.6	54.2±5.9	67.5±0.6	223±0.8
	5	7.1±0.2	130±10	0.9±0.1	<Q.L.	14.6±0.4	9.4±2.0	43.9±1.3	70.6±1.8	41.1±1.6	66.7±0.6	222±0.5
	50	7.1±0.2	128±10	1.1±0.1	<0.1	14.9±0.6	25.0±4.3	43.7±0.9	71.0±3.4	57.2±2.8	62.0±0.8	222±2.7
	200	6.9±0.2	127±10	1.1±0.1	<0.1	15.6±0.8	8.3±0.3	43.9±2.0	69.5±0.3	39.4±1.4	62.9±1.1	211±4.9
Biotic	0	7.6±0.2	135±10	1.1±0.1	<Q.L.	14.0±0.2	13.9±6.0	46.7±0.6	174±2.5	42.8±5.9	60.9±0.6	215±1.9
	2	7.3±0.2	145±10	0.9±0.1	<Q.L.	13.5±0.1	14.5±2.0	46.8±0.3	178±0.9	43.7±1.6	61.2±0.6	217±1.1
	5	7.0±0.1	131±10	1.1±0.1	<0.1	14.0±0.5	17.3±4.3	46.5±0.3	148±25	46.5±2.8	58.9±0.8	216±1.4
	15	7.1±0.1	128±10	1.1±0.1	<0.1	14.8±1.5	8.4±0.3	44.5±0.8	67.2±9.0	37.8±1.4	60.3±1.1	212±1.7
	30	7.1±0.2	126±10	1.1±0.1	<Q.L.	13.5±0.2	6.4±6.0	43.5±1.3	59.9±9.3	35.5±5.9	40.9±18	212±0.5
	50	7.3±0.2	153±10	0.9±0.1	<Q.L.	13.6±0.1	14.7±2.0	43.3±1.0	42.6±1.0	44.8±1.6	47.7±10	214±1.2
	80	7.1±0.1	126±10	1.1±0.1	<0.1	13.5±0.2	25.7±4.3	41.9±0.5	23.5±6.0	46.7±15	39.0±10	209±0.6
	100	7.2±0.1	126±10	1.1±0.1	<0.1	13.8±0.2	8.3±0.3	43.0±2.7	22.6±1.2	51.8±22	26.4±2.1	211±2.0
	200	7.1±0.2	135±10	1.1±0.1	<0.1	13.8±0.1	4.3±0.3	36.5±0.3	13.3±2.6	37.1±1.4	20.8±2.0	204±2.4
Controls	0	7.1±0.2	123±10	1.1±0.1	<Q.L.	14.2±1.2	14.0±2.5	47.1±0.6	176.9±1.8	42.2±1.6	62.8±0.7	217±1.5
	5	7.0±0.2	130±10	0.9±0.1	<Q.L.	13.5±0.3	6.4±0.3	47.3±0.6	176.9±0.7	34.4±0.3	63.4±0.2	215±1.1
	50	7.0±0.1	128±10	1.1±0.1	0.3±0.1	13.8±0.1	7.3±0.7	47.1±0.5	140.3±16	50.9±14	62.8±0.2	218±1.2
	200	7.1±0.1	127±10	1.1±0.1	<Q.L	14.2±0.3	8.3±0.3	45.9±0.1	66.0±0.4	37.0±0.5	63.9±0.	209±0.5

## Evolution of micropollutants concentrations in abiotic experiments under oxic conditions

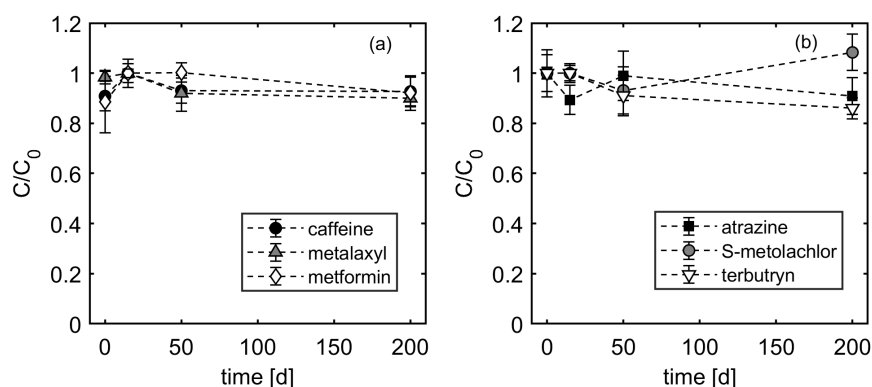


**Figure C.4:** Relative concentrations ( $C/C_0$ ) of a micropollutant mixture consisting of (a) caffeine, metalaxyl and metformin, and (b) atrazine, S-metolachlor and terbutryn in abiotic microcosm experiments as a function of time (d). Error bars correspond to standard error ( $n \leq 3$ ).

## Evolution of transformation products in biotic experiments under oxic conditions

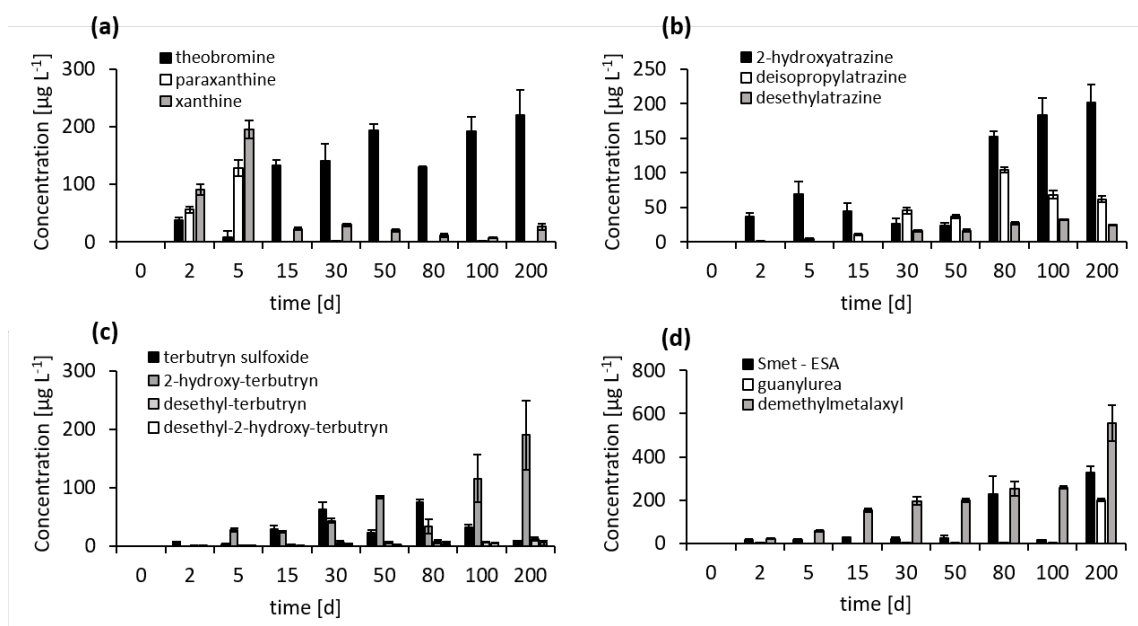


**Figure C.5:** Concentrations of (a) caffeine, (b) atrazine, (c) terbutryn and (d) S-metolachlor, metformin and metalaxyl transformation products in biotic microcosm experiments as a function of time. Error bars correspond to standard error ( $n \leq 3$ ).

## C.8 Carbon and nitrogen isotope fractionation in microcosm experiments

**Table C.4:** Carbon ( $\delta^{13}\text{C}$ ) and nitrogen isotope ( $\delta^{15}\text{N}$ ) fractionation in freshwater microcosm experiments under oxic conditions. Abiotic (sterile) and biotic (non-sterile) experiments were spiked with a micropollutant mixture (concentration:  $6 \text{ mg L}^{-1}$ ) at 0 d. Controls received no sterilization and spiking of the mixture. Data represent abiotic and biotic samples collected over time ( $n=3$ ). The reported values correspond to mean values of triplicate measurements taken at each sampling event. Reproducibility of triplicate measurements was  $\leq 0.5\text{‰}$  ( $1\sigma$ ) for carbon and  $\leq 1\text{‰}$  ( $1\sigma$ ) nitrogen.

Condition	Abiotic (0-200 d)		Biotic (0-200d)		EA (n=3)		Standard (n=15)	
	$\Delta\delta^{13}\text{C}$ (‰)	$\Delta\delta^{15}\text{N}$ (‰)	$\Delta\delta^{13}\text{C}$ (‰)	$\Delta\delta^{15}\text{N}$ (‰)	$\delta^{13}\text{C}$ (‰)	$\delta^{15}\text{N}$ (‰)	$\delta^{13}\text{C}$ (‰)	$\delta^{15}\text{N}$ (‰)
atrazine	<0.5	<1.0	<0.5	<1.0	$-25.92 \pm 0.01$	$0.18 \pm 0.09$	$-26.79 \pm 0.38$	$0.27 \pm 0.95$
caffeine	<0.5	<1.0	4.86	<1.0	$-31.40 \pm 0.02$	$-2.28 \pm 0.06$	$-31.46 \pm 0.32$	$-2.38 \pm 0.35$
metalaxyl	<0.5	<1.0	0.71	<1.0	$-29.12 \pm 0.05$	$-2.17 \pm 0.44$	$-30.55 \pm 0.44$	$-0.90 \pm 0.58$
terbutryn	<0.5	<1.0	0.55	<1.0	$-30.16 \pm 0.03$	$-3.14 \pm 0.08$	$-30.16 \pm 0.40$	$-2.61 \pm 0.62$
S-metolachlor	<0.5	<1.0	<0.5	<1.0	$-30.36 \pm 0.03$	$-1.41 \pm 0.47$	$-30.69 \pm 0.40$	$-1.04 \pm 0.58$

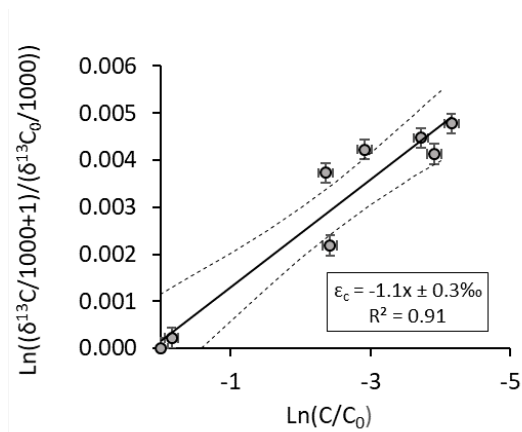


**Figure C.6:** Rayleigh plots of carbon isotope ratios vs. residual caffeine fraction in biotic freshwater microcosm experiments under oxic conditions. Carbon isotope fractionation value ( $\epsilon_{bulk}^C$ ) was obtained from the slope of the linear regression using the Rayleigh model. Error bars represent total uncertainty of isotope ratios. Dashed lines represent the 95% confidence of interval (C.I.).

## C.9 Hydrochemistry of laboratory aquifers

**Table C.5:** Hydrochemistry of outflow samples (x=160 cm) in laboratory aquifers under oxic conditions. Sampling days correspond to first pulse injection (0–40 d), the constant injection (40–90 d) and second pulse injection (90–140 d).

days	NH <sub>4</sub> <sup>+</sup> mg L <sup>-1</sup>	Na <sup>+</sup>	K <sup>+</sup>	Mn <sup>2+</sup> mg L <sup>-1</sup>	Ca <sup>2+</sup>	Cl <sup>-</sup>	NO <sub>3</sub> <sup>-</sup> mg L <sup>-1</sup>	SO <sub>4</sub> <sup>2-</sup>	NPOC	IC mg L <sup>-1</sup>	TOC
<b>Aquifer 1</b>											
0	2.5	12.3	6.2	39.7	137.3	31	53.8	193.4	8.1	70.1	-
10	1.8	13.1	6.4	42.9	119.1	35.9	59.4	206.2	8.9	53.9	5
20	5.3	12	5.7	44.4	109.9	34.2	54.5	197.2	1.1	68.8	3.2
30	2.4	11.2	5.5	44.2	132	34.3	60.7	195.1	2.5	92.6	3.6
40	0.9	10.8	5.4	45.4	139.3	34.4	65.9	194.7	2.7	90.8	3
50	1.2	10.7	5.1	44.5	136.2	33.6	65	193.3	4.4	29.4	4.1
60	16	11.4	5.4	44.7	111.4	35.4	26.9	192.2	5.8	69.5	3.1
70	25.5	10.9	5.4	40	103.5	33.7	6	191.4	11	65.8	3.8
80	26.7	11.4	5.7	43.7	98.8	35.1	2.5	200	13.6	63.9	8.1
90	6.3	10.5	4.9	44.8	144.1	31.5	51.6	212.4	4.1	67.4	2.7
100	5.6	14.3	4.4	46.1	160.2	31.8	60.4	212.8	2.6	72.1	2.3
110	1.1	15.4	5.2	46.3	168.4	31.2	67.9	213.6	7.5	68.2	2.2
120	2.6	15.7	6.2	47.1	122.6	31.3	54.4	210.9	3	63.8	2.3
130	9.7	14.2	6.5	46.7	128.7	36.4	26.5	224.8	6.2	78.6	3
140	22.5	18.9	6.3	45.2	87.1	34.8	14.9	223.3	3.3	42.4	3.3
<b>Aquifer 2 (duplicate)</b>											
0	2.5	12.2	6	38.7	145.1	31.2	53.6	187	10.2	68	-
10	1	12.9	6.8	43.7	145.9	33.2	60.8	203.9	4.2	69.3	3.9
20	3.8	11.9	5.9	44.8	136.7	33.9	54.9	195	3.9	99	4
30	3.5	11.3	5.6	42.8	141.2	33.4	60	191.2	3.1	94.4	4.4
40	1.5	10.8	5.4	43.3	135.4	33.7	64.2	189.7	3	97.9	3.5
50	1	10.6	5.1	44.7	124.9	33.5	65.4	192.9	4	71.6	3.1
60	5	11.5	6.3	45.6	110.8	35.4	49.4	191.3	4.2	37.2	3
70	28.8	11.1	5.5	41.7	115	34.7	8	193.4	8.4	71.8	5
80	19.9	11.3	5.5	42.1	121.7	35.3	26	193.9	5.4	68.3	4.9
90	5.2	10.5	5	44.6	118.9	31.8	55	211.9	3	50.1	2.8
100	0.7	15.7	5.1	46	173.7	31.4	63.2	214.3	2.6	73.4	1.7
110	0.7	16	5.3	45.9	171.9	31.3	65.2	214.7	6.8	77.2	5.3
120	0.1	10.5	5.6	43.7	156.8	32.7	64.6	211.4	2.3	82.4	2.1
130	35.3	16.8	8.1	50.9	131.2	35.8	20.7	222.1	36.7	90	12.8
140	28.3	16	5.6	46.6	112.5	36.5	17.1	223.2	6.5	67.8	3.8

### C.10 BTCs and carbon and nitrogen isotopes of a micropollutant mixture in laboratory aquifers

**Table C.6:** Mass recovery of a micropollutant mixture from outflow samples ( $x=160$  cm) in laboratory aquifers under oxic conditions. Recoveries (in %) correspond to average data of both aquifers for the first pulse (0–40 d), constant (40–90 d) and second pulse injections (90–140 d). Recoveries of the outflows correspond to the total merging of several flow paths in the systems.

Micropollutant mixture	Pulse injection 1 0–40 d	Constant injection 40–90 d	Pulse injection 2 90–140 d
caffeine (%)	$12 \pm 5$	$13 \pm 1$	$13 \pm 1$
metformin (%)	$99 \pm 2$	$97 \pm 4$	$82 \pm 6$
atrazine (%)	$99 \pm 2$	$97 \pm 3$	$94 \pm 2$
metalaxyl (%)	$97 \pm 6$	$97 \pm 6$	$93 \pm 5$
terbutryn (%)	$99 \pm 1$	$98 \pm 4$	$94 \pm 10$
<i>S</i> -metolachlor (%)	$96 \pm 1$	$98 \pm 3$	$95 \pm 7$



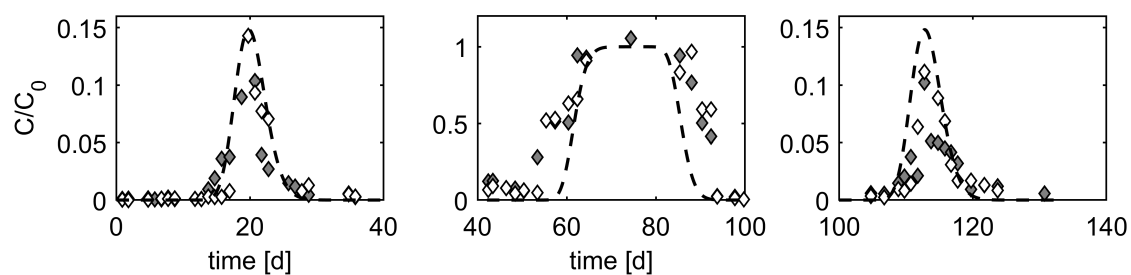


**Figure C.7:** Metformin concentrations during transient injections of a micropollutant mixture over time: first pulse injection (0–40 d;  $C_0 \approx 6000 \mu\text{g L}^{-1}$ ), constant injection (40–90 d;  $C_0 \approx 600 \mu\text{g L}^{-1}$ ) and second pulse injection (90–140 d;  $C_0 \approx 6000 \mu\text{g L}^{-1}$ ). Full and empty symbols represent data sets from duplicate aquifers. Dashed back lines represent the BTCs of the saline conservative tracer.

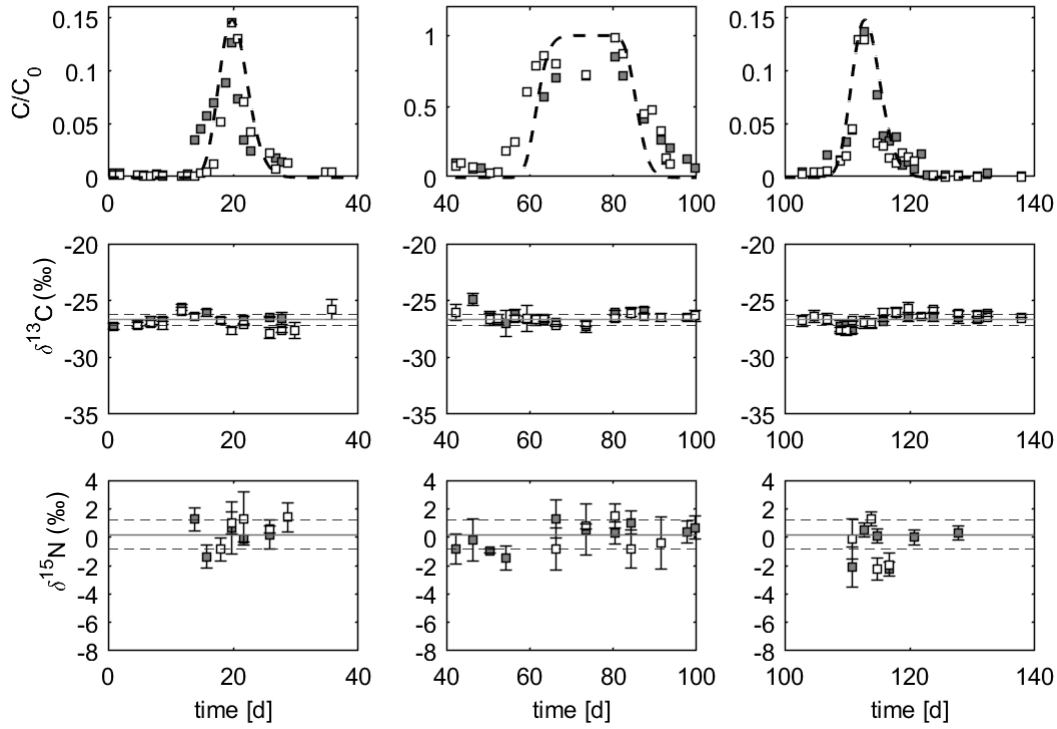


**Figure C.8:** Atrazine concentrations (upper panel), and carbon and nitrogen isotope values (middle and lower panels, respectively) during transient injections of a micropollutant mixture over time: first pulse injection (0–40 d;  $C_0 \approx 6000 \mu\text{g L}^{-1}$ ), constant injection (40–90 d;  $C_0 \approx 600 \mu\text{g L}^{-1}$ ) and second pulse injection (90–140 d;  $C_0 \approx 6000 \mu\text{g L}^{-1}$ ). Full and empty symbols represent data sets from duplicate aquifers. Dashed back lines represent the BTCs of the saline conservative tracer. Error bars represent the standard error of carbon and isotope values of triplicate measurements. Continuous horizontal lines represent atrazine EA values of carbon ( $-25.92 \pm 0.01$ ‰) and nitrogen ( $0.18 \pm 0.09$ ‰) isotopes. Dashed horizontal lines represent the total uncertainty of carbon  $\pm 0.5$ ‰ and nitrogen  $\pm 1$ ‰.

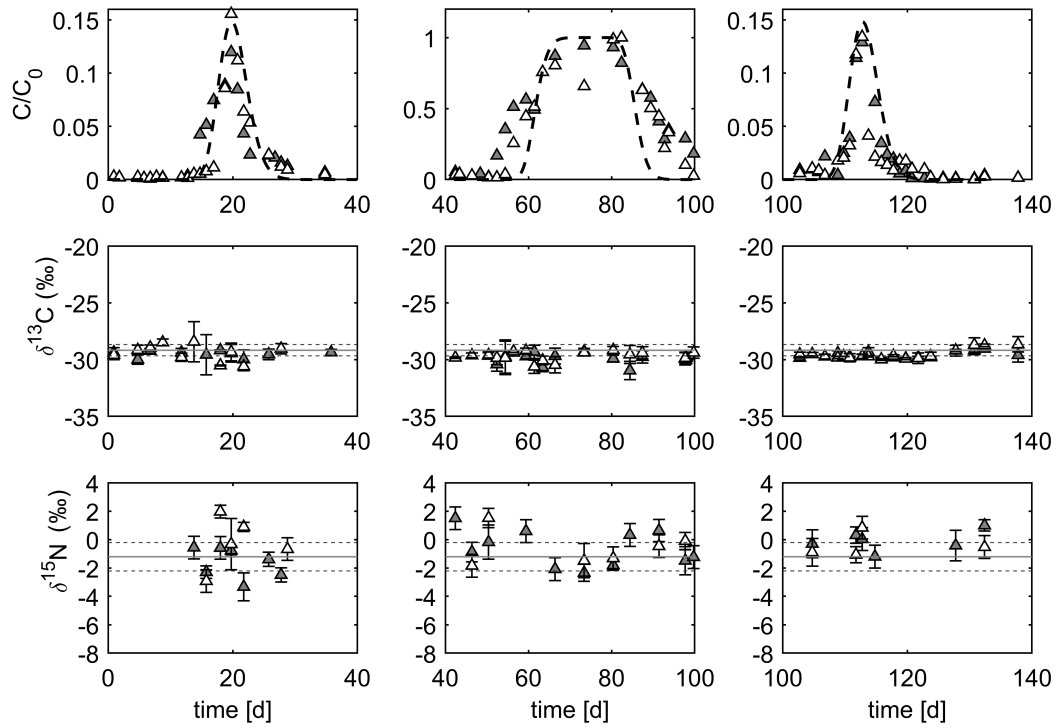


**Figure C.9:** Metalaxyl concentrations (upper panel), and carbon and nitrogen isotope values (middle and lower panels, respectively) during transient injections of a micropollutant mixture over time: first pulse injection (0–40 d;  $C_0 \approx 6000 \mu\text{g L}^{-1}$ ), constant injection (40–90 d;  $C_0 \approx 600 \mu\text{g L}^{-1}$ ) and second pulse injection (90–140 d;  $C_0 \approx 6000 \mu\text{g L}^{-1}$ ). Full and empty symbols represent data sets from duplicate aquifers. Dashed back lines represent the BTCs of the saline conservative tracer. Error bars represent the standard error of carbon and isotope values of triplicate measurements. Continuous horizontal lines represent atrazine EA values of carbon ( $-29.12 \pm 0.05\text{‰}$ ) and nitrogen ( $-2.17 \pm 0.44\text{‰}$ ) isotopes. Dashed horizontal lines represent the total uncertainty of carbon  $\pm 0.5\text{‰}$  and nitrogen  $\pm 1\text{‰}$ .

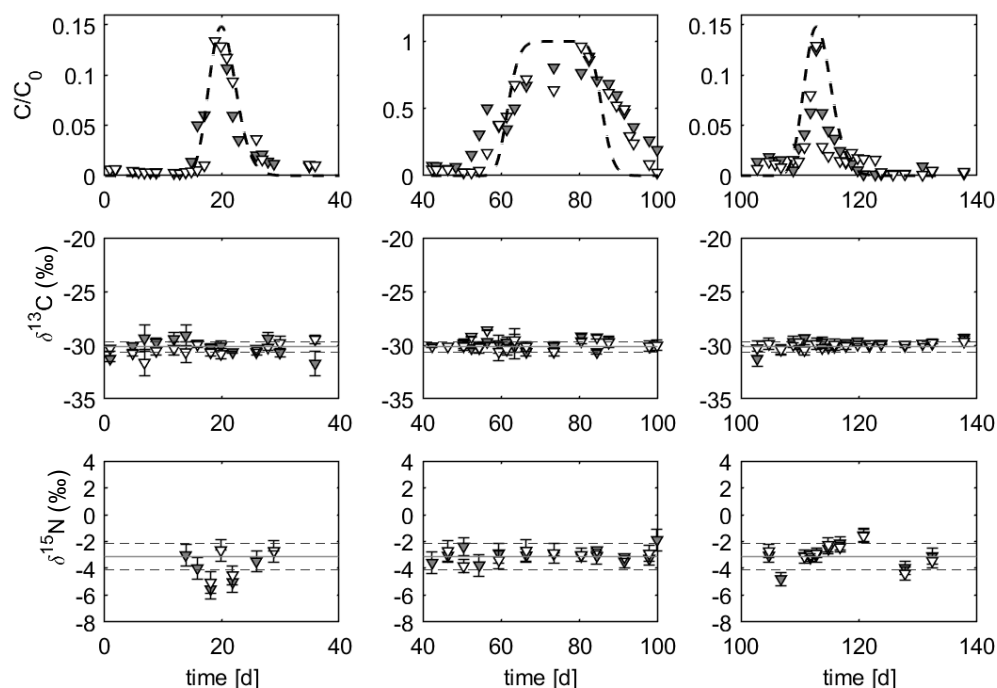


**Figure C.10:** Terbutryn concentrations (upper panel), and carbon and nitrogen isotope values (middle and lower panels, respectively) during transient injections of a micropollutant mixture over time: first pulse injection (0–40 d;  $C_0 \approx 6000 \mu\text{g L}^{-1}$ ), constant injection (40–90 d;  $C_0 \approx 600 \mu\text{g L}^{-1}$ ) and second pulse injection (90–140 d;  $C_0 \approx 6000 \mu\text{g L}^{-1}$ ). Full and empty symbols represent data sets from duplicate aquifers. Dashed back lines represent the BTCs of the saline conservative tracer. Error bars represent the standard error of carbon and isotope values of triplicate measurements. Continuous horizontal lines represent atrazine EA values of carbon ( $-30.16 \pm 0.02‰$ ) and nitrogen ( $-3.14 \pm 0.08‰$ ) isotopes. Dashed horizontal lines represent the total uncertainty of carbon  $\pm 0.5‰$  and nitrogen  $\pm 1‰$ .

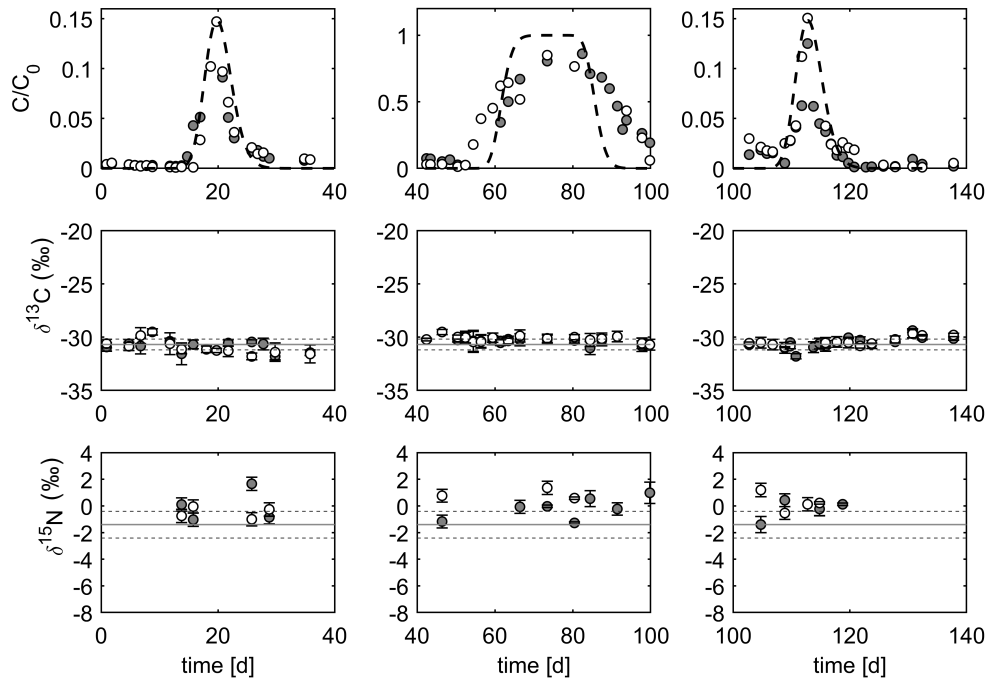


**Figure C.11:** *S*-metolachlor concentrations (upper panel), and carbon and nitrogen isotope values (middle and lower panels, respectively) during transient injections of a micropollutant mixture over time: first pulse injection (0–40 d;  $C_0 \approx 6000 \mu\text{g L}^{-1}$ ), constant injection (40–90 d;  $C_0 \approx 600 \mu\text{g L}^{-1}$ ) and second pulse injection (90–140 d;  $C_0 \approx 6000 \mu\text{g L}^{-1}$ ). Full and empty symbols represent data sets from duplicate aquifers. Dashed back lines represent the BTCs of the saline conservative tracer. Error bars represent the standard error of carbon and isotope values of triplicate measurements. Continuous horizontal lines represent atrazine EA values of carbon ( $-30.36 \pm 0.03\text{‰}$ ) and nitrogen ( $-1.41 \pm 0.47\text{‰}$ ) isotopes. Dashed horizontal lines represent the total uncertainty of carbon  $\pm 0.5\text{‰}$  and nitrogen  $\pm 1\text{‰}$ .

## C.11 BTCs of transformation products in laboratory aquifers

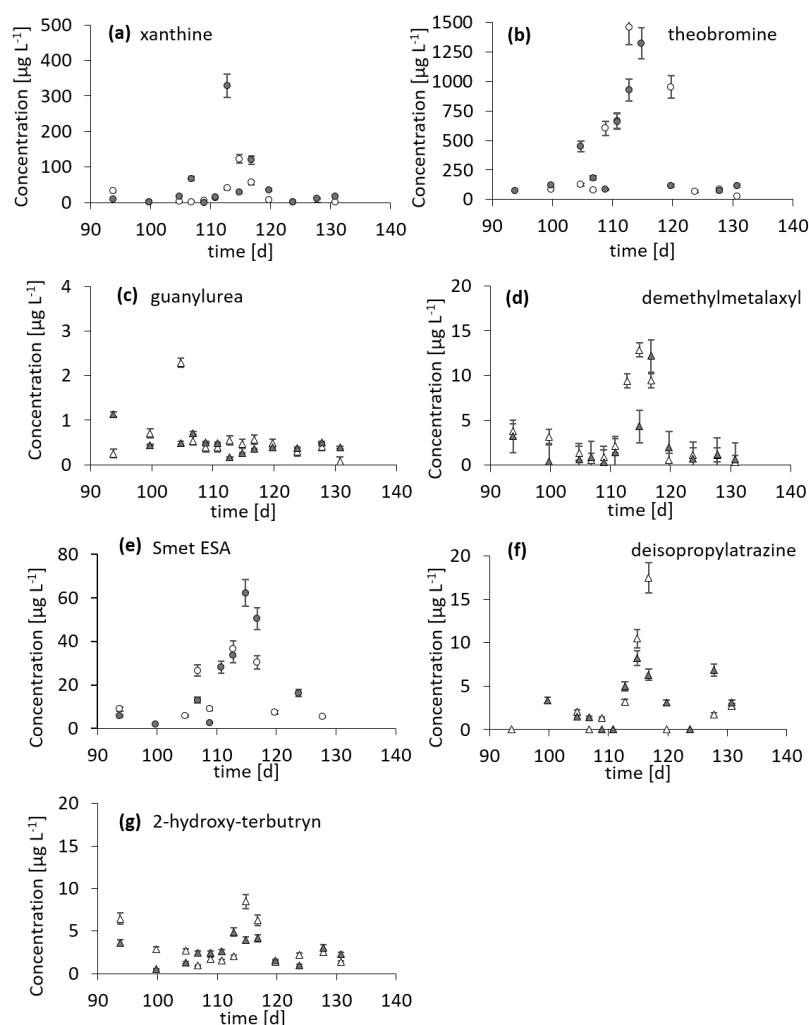


**Figure C.12:** Observed transformation products of caffeine (a, b), metformin (c), metalaxyl (d), S-metolachlor (e), atrazine (f) and terbutryn (g) biotransformation in laboratory aquifers receiving stream water during the second injection period (90–140 d). Error bars correspond to standard error ( $n \leq 3$ ).

## C.12 Changes in bacterial diversity

### Non-metric dimensional scaling (NMDS)

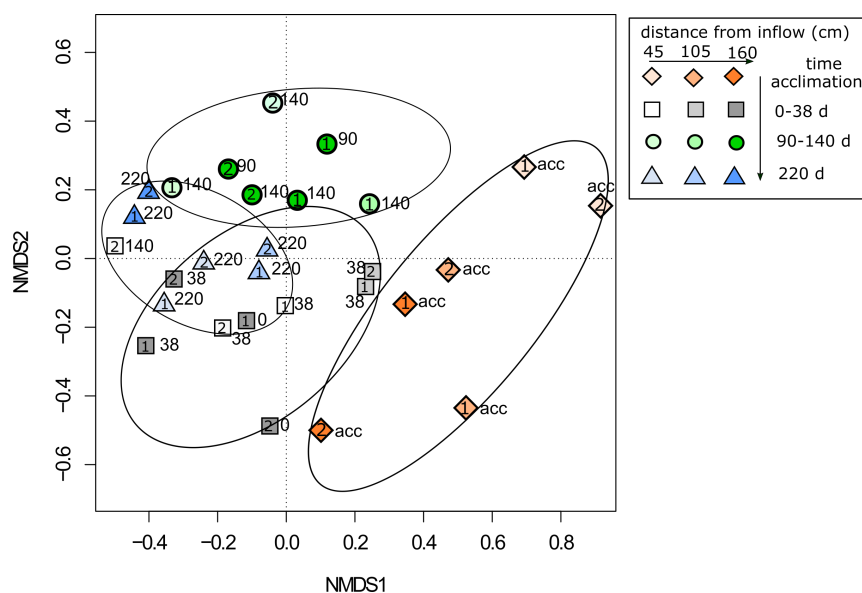


**Figure C.13:** NMDS ordination plot of bacterial diversity profiles from pore water over time in duplicate aquifers. Numbers inside the symbols represent sample collected from one of the duplicate aquifers. Numbers next to symbols represent sampling before the acclimation period (acc), and at 0, 38, 90, 140 and 220 days. Plot stress: 0.17%. Statistically different clusters (ANOSIM,  $p < 0.05$ ) were associated with exposure of micropollutants over time before the acclimation period, from 0 to 38 days, from 90 to 140 days, and at 220 days (end of the experiment).

## Bacterial diversity indices

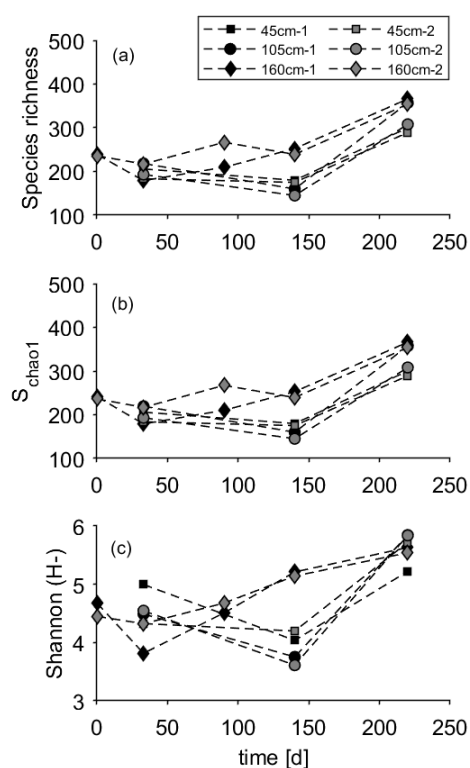


**Figure C.14:** Changes in bacterial diversity indices over time in laboratory aquifers exposed to a micropollutant mixture. First pulse injection (0–40 d;  $C_0 \approx 6000 \mu\text{g L}^{-1}$ ), constant injection (40–90 d;  $C_0 \approx 600 \mu\text{g L}^{-1}$ ) and second pulse injection (90–140 d;  $C_0 \approx 6000 \mu\text{g L}^{-1}$ ). Black and gray symbols represent data sets from duplicate aquifers.



### C.13 Relative abundance of phyla in sand samples

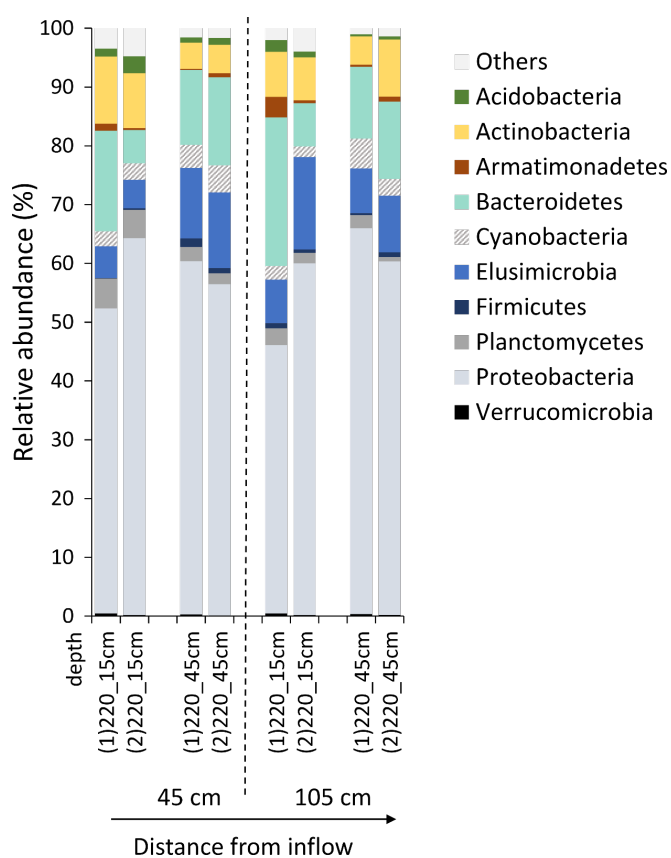


**Figure C.15:** Relative abundance of bacterial phyla in sand samples at day 220 (end of experiment), with increasing distance from inflow and at depths of 15 cm and 45 cm. Numbers in parenthesis represent samples from duplicate laboratory aquifers.

### C.14 Relative abundance of genera in pore water samples

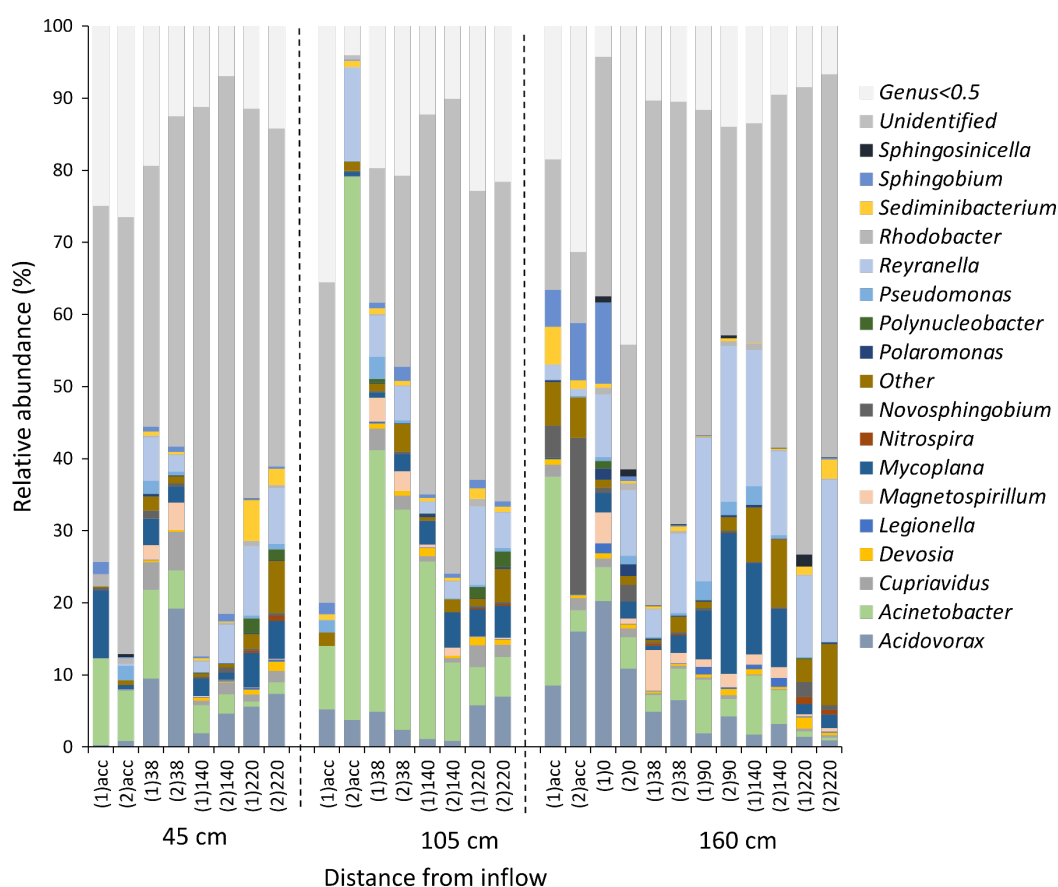


**Figure C.16:** Relative abundance of bacterial genera from pore water samples over time and with increasing distance from inflow. Numbers in parenthesis represent samples from duplicate laboratory aquifers. Samples were collected prior to the experiments (acc; acclimation period); after acclimation period (0 d), at the end of the first pulse injection (38 d), constant injection (90 d), and second injection periods (140 d). Samples at 220 d represent the end of the experiment. Samples were collected from inner samples of the aquifers at a distance of 45 cm and 105 cm from the inflow, as well as outlet samples ( $x=160$  cm).

## References of Appendix C

- Ascher, U. M. and Petzold, L. R. (1998). *Computer methods for ordinary differential equations and differential-algebraic equations*, volume 61. Siam.
- core Team, R. (2019). R: A language and environment for statistical computing, version 3.5.3. Place: Vienna, Austria.
- Droz, B., Drouin, G., Maurer, L., Villette, C., Payraudeau, S., and Imfeld, G. (2021). Phase transfer and biodegradation of pesticides in water-sediment systems explored by compound-specific isotope analysis and conceptual modeling. *Environmental Science and Technology*, 55(8):4720–4728.
- Elsayed, O., Maillard, E., Vuilleumier, S., Nijenhuis, I., Richnow, H., and Imfeld, G. (2014). Using compound-specific isotope analysis to assess the degradation of chloroacetanilide herbicides in lab-scale wetlands. *Chemosphere*, 99:89–95.
- Hellal, J., Joulain, C., Urien, C., Ferreira, S., Denonfoux, J., Hermon, L., Vuilleumier, S., and Imfeld, G. (2020). Chlorinated ethene biodegradation and associated bacterial taxa in multi-polluted groundwater: Insights from biomolecular markers and stable isotope analysis. *Science of The Total Environment*, 763:142950.
- Hermon, L., Denonfoux, J., Hellal, J., Joulain, C., Ferreira, S., Vuilleumier, S., and Imfeld, G. (2018). Dichloromethane biodegradation in multi-contaminated groundwater: Insights from biomolecular and compound-specific isotope analyses. *Water Research*, 142:217–226.
- Lax, P. and Wendroff, B. (1960). Systems of conservation laws. *Communications on Pure and Applied Mathematics*, 13(2):217–237.
- LeVeque, R. J. and LeVeque, R. J. (1992). *Numerical methods for conservation laws*, volume 214. Springer.
- Virtanen, P., Gommers, R., Oliphant, T. E., Haberland, M., Reddy, T., Cournapeau, D., Burovski, E., Peterson, P., Weckesser, W., Bright, J., et al. (2020). Scipy 1.0: fundamental algorithms for scientific computing in python. *Nature methods*, 17(3):261–272.



## Résumé

La qualité des eaux souterraines est une préoccupation croissante en raison de l'omniprésence et du transfert de nombreuses polluants dans les environnements de sub-surface. Bien que la biodégradation soit un processus majeur pour l'élimination des polluants organiques dans les aquifères, l'interaction entre les conditions hydrogéochimiques dynamiques, la diversité bactérienne et la dissipation des contaminants est encore mal comprise. Dans cette étude, nous avons examiné le transport réactif du dichlorométhane (DCM) et d'un mélange de micropolluants dans deux aquifères de laboratoire dans des conditions quasi-naturelles et dynamiques, associées respectivement aux fluctuations de la nappe phréatique et aux interactions entre le cours d'eau et les eaux souterraines. Une approche intégrative a été utilisée pour examiner les processus de transport réactif, incluant la surveillance hydrochimique à haute résolution, l'analyse isotopique spécifique de plusieurs éléments (ME-CSIA), les marqueurs biomoléculaires (séquençage du gène de l'ARNr 16S) et la modélisation numérique. Les résultats ont montré que les fluctuations de la nappe phréatique influencent les taux de dégradation et les voies de transformation du DCM, en lien avec les conditions hydrogéochimiques. Cela suggère que les fluctuations de la nappe phréatique peuvent affecter la dégradation *in situ* du DCM. Cette étude a également mis en évidence que la biotransformation d'un mélange de micropolluants varie largement, indépendamment du niveau d'exposition aigu ou chronique aux micropolluants, mettant en évidence une possible adaptation à long terme des communautés bactériennes au cours des interactions entre les eaux de surface et les eaux souterraines. En perspective, des approches intégratives tenant compte des conditions hydrogéologiques et biogéochimiques dynamiques pourraient améliorer l'évaluation de l'atténuation naturelle des polluants organiques dans les eaux souterraines.

**Mots clés :** contamination des eaux souterraines, dynamique hydrogéochimique, ME-CSIA, dynamique microbienne, modélisation numérique

## Abstract

Groundwater quality is of increasing concern due to the ubiquitous release of many substances in subsurface environments. Although biodegradation is a major process for the removal of organic pollutants in aquifers, the interplay of dynamic hydrogeochemical conditions, bacterial diversity and contaminant dissipation is yet poorly understood. In this study, we examined the reactive transport of dichloromethane (DCM) and a micropollutant mixture in two laboratory aquifers under near-natural settings and dynamic conditions, associated with fluctuations in the water table and stream-groundwater interactions, respectively. An integrative approach was used to examine reactive transport processes, including high-resolution hydrochemical monitoring, compound-specific isotope analysis of multiple elements (ME-CSIA), biomolecular markers (16S rRNA gene sequencing) and numerical modeling. Results evidenced that water table fluctuations affected the extent of DCM degradation and the DCM transformation pathways. This suggests that water table fluctuations can affect *in situ* DCM degradation, depending on hydrogeochemical conditions. This study also highlighted that biotransformation of micropollutants as chemical mixtures largely varies, independently on the acute or chronic level of exposure to micropollutants, and evidenced possibly long-term adaptation of bacterial communities during stream-groundwater interactions. In the future, integrative approaches accounting for dynamic hydrogeological and biogeochemical conditions may improve the assessment of natural attenuation of organic pollutants in groundwater.

**Keywords:** groundwater contamination, hydrogeochemical dynamics, ME-CSIA, microbial dynamics, numerical modeling